BioMed Research International

Imaging Infection and Inflammation

Guest Editors: Alberto Signore, Andor W. J. M. Glaudemans, Filippo Galli, and François Rouzet

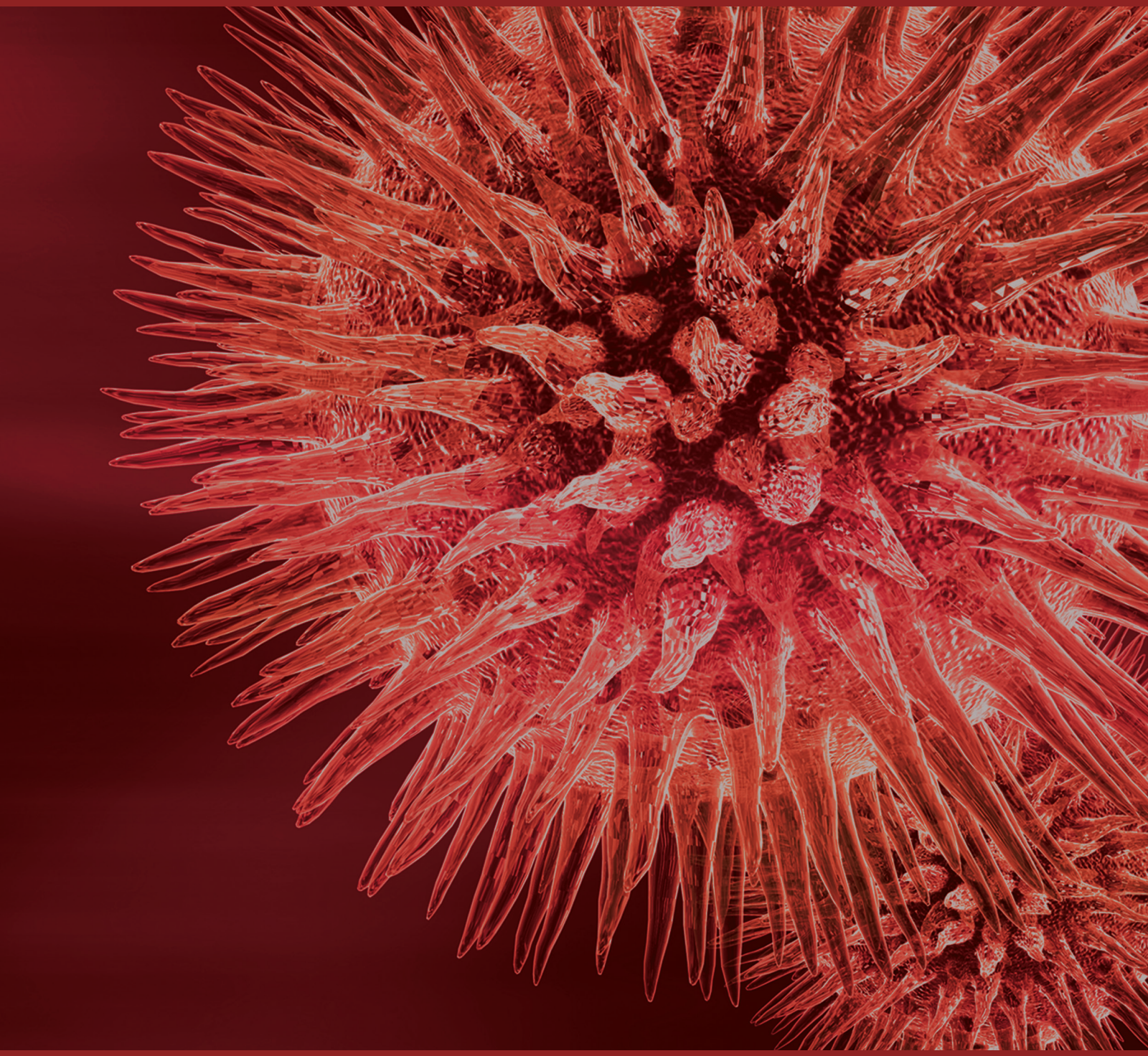

Imaging Infection and Inflammation

BioMed Research International

Imaging Infection and Inflammation

Guest Editors: Alberto Signore, Andor W. J. M. Glaudemans, Filippo Galli, and François Rouzet

Contents

Imaging Infection and Inflammation, Alberto Signore, Andor W. J. M. Glaudemans, Filippo Galli, and François Rouzet
Volume 2015, Article ID 615150, 3 pages

***In Vivo* Evaluation of TNF-Alpha in the Lungs of Patients Affected by Sarcoidosis**, Filippo Galli, Tiziana Lanzolla, Vittorio Pietrangeli, Gaurav Malviya, Alberto Ricci, Pierdonato Bruno, Paola Ragni, Francesco Scopinaro, Salvatore Mariotta, and Alberto Signore
Volume 2015, Article ID 401341, 7 pages

Large-Vessel Vasculitis: Interobserver Agreement and Diagnostic Accuracy of ^{18}F-FDG-PET/CT, K. D. F. Lensen, E. F. I. Comans, A. E. Voskuyl, C. J. van der Laken, E. Brouwer, A. T. Zwijnenburg, L. M. Pereira Arias-Bouda, A. W. J. M. Glaudemans, R. H. J. A. Slart, and Y. M. Smulders
Volume 2015, Article ID 914692, 8 pages

Sustained Macrophage Infiltration upon Multiple Intra-Articular Injections: An Improved Rat Model of Rheumatoid Arthritis for PET Guided Therapy Evaluation, Durga M. S. H. Chandrupatla, Karin Weijers, Yoony Y. J. Gent, Inge de Greeuw, Adriaan A. Lammertsma, Gerrit Jansen, Conny J. van der Laken, and Carla F. M. Molthoff
Volume 2015, Article ID 509295, 11 pages

Imaging Atherosclerosis with Hybrid Positron Emission Tomography/Magnetic Resonance Imaging, Rasmus Sejersten Ripa and Andreas Kjær
Volume 2015, Article ID 914516, 8 pages

Synthesis, ^{68}Ga-Radiolabeling, and Preliminary *In Vivo* Assessment of a Depsipeptide-Derived Compound as a Potential PET/CT Infection Imaging Agent, Botshelo B. Mokaleng, Thomas Ebenhan, Suhas Ramesh, Thavendran Govender, Hendrik G. Kruger, Raveen Parboosing, Puja P. Hazari, Anil K. Mishra, Biljana Marjanovic-Painter, Jan R. Zeevaart, and Mike M. Sathekge
Volume 2015, Article ID 284354, 12 pages

Nuclear Medicine in Diagnosis of Prosthetic Valve Endocarditis: An Update, Maria Musso and Nicola Petrosillo
Volume 2015, Article ID 127325, 7 pages

The Longitudinal Assessment of Osteomyelitis Development by Molecular Imaging in a Rabbit Model, Jim C. E. Odekerken, Geert H. I. M. Walenkamp, Boudewijn T. Brans, Tim J. M. Welting, and Jacobus J. C. Arts
Volume 2014, Article ID 424652, 10 pages

Giant Cell Arteritis: A Systematic Review of the Qualitative and Semiquantitative Methods to Assess Vasculitis with 18F-Fluorodeoxyglucose Positron Emission Tomography, Cristina Puppo, Michela Massollo, Francesco Paparo, Dario Camellino, Arnoldo Piccardo, Mehrdad Shoushtari Zadeh Naseri, Giampiero Villavecchia, Gian Andrea Rollandi, and Marco Amedeo Cimmino
Volume 2014, Article ID 574248, 11 pages

Assessment of Cardiac Sarcoidosis with Advanced Imaging Modalities, Makoto Orii, Toshio Imanishi, and Takashi Akasaka
Volume 2014, Article ID 897956, 15 pages

Antimicrobial Peptides: Their Role as Infection-Selective Tracers for Molecular Imaging, Thomas Ebenhan, Olivier Gheysens, Hendrick Gert Kruger, Jan Rijn Zeevaart, and Mike Machaba Sathekge
Volume 2014, Article ID 867381, 15 pages

^{18}F-Fluorodeoxyglucose Positron Emission Tomography/CT Scanning in Diagnosing Vascular Prosthetic Graft Infection, Ben R. Saleem, Robert A. Pol, Riemer H. J. A. Slart, Michel M. P. J. Reijnen, and Clark J. Zeebregts
Volume 2014, Article ID 471971, 8 pages

Hepatosplenic Sarcoidosis: Contrast-Enhanced Ultrasound Findings and Implications for Clinical Practice, Claudio Tana, Christoph F. Dietrich, and Cosima Schiavone
Volume 2014, Article ID 926203, 8 pages

The Role of ^{18}F-FDG PET/CT in Large-Vessel Vasculitis: Appropriateness of Current Classification Criteria?, H. Balink, R. J. Bennink, B. L. F. van Eck-Smit, and H. J. Verberne
Volume 2014, Article ID 687608, 13 pages

Hindawi Publishing Corporation
BioMed Research International
Volume 2015, Article ID 615150, 3 pages
http://dx.doi.org/10.1155/2015/615150

Editorial

Imaging Infection and Inflammation

Alberto Signore,[1,2] Andor W. J. M. Glaudemans,[2] Filippo Galli,[1,2] and François Rouzet[3]

[1]*Nuclear Medicine Unit, Department of Medical-Surgical Sciences and Translational Medicine, Faculty of Medicine and Psychology, Ospedale S. Andrea, "Sapienza" University, Via di Grottarossa 1035, 00189 Roma, Italy*
[2]*Department of Nuclear Medicine and Molecular Imaging, University Medical Center Groningen University of Groningen, Hanzeplein 1, 9700 RB Groningen, Netherlands*
[3]*Nuclear Medicine Department, Bichat-Claude Bernard Hospital and Paris Diderot University, 46 Rue Henri Huchard, 75018 Paris, France*

Correspondence should be addressed to Alberto Signore; alberto.signore@uniroma1.it

Received 25 November 2014; Accepted 25 November 2014

Infectious and inflammatory diseases are a heterogeneous class of diseases encompassing many different clinical conditions and may be classified into infection, acute inflammation, and chronic inflammation. These diseases can affect multiple organs (systemic) or can be localized in one specific organ and are often relapsing and invalidating and may require life-long treatment [1].

Clinicians often struggle with questions in patients dealing with presumed or established infectious and inflammatory disorders. Often they are not well-recognized and when recognized many questions remain: Is there an infectious focus or an inflammatory sign? What are the size and the extent of the lesion? Is this the only lesion in the body or are there infectious metastases? When can the treatment be stopped or should it be switched or continued?

It is very important for the clinician to distinguish between an infection and sterile inflammation. If possible, it may lead to major changes in the treatment of the patients. The recent progress in our understanding and knowledge of the pathophysiology of many infectious and inflammatory diseases has led to the development of several new and specific radiopharmaceuticals in order to meet clinical demand [2–4]. We also learned that, with some radiopharmaceuticals, the lack of specificity can be overcome by applying a particular imaging acquisition protocol (as it is for white-blood-cell scan in prosthetic joint infections) [5] or by using combination of two radiopharmaceuticals (as it is for imaging diabetic foot infection in patients with Charcot joint) [6].

Nowadays, the goal is to identify the type of the disease and the cells and mediators that are involved in the process [7–10].

Diagnosis and characterization of the infectious or inflammatory processes are most often performed with conventional radiology and biochemical tests. Radiological techniques show anatomical changes. These changes, however, usually occur in a late and chronic stage of the disease, thereby leading to a delayed diagnosis and therapy. Nuclear medicine imaging techniques detect biological and biochemical changes in the earliest phase of the diseases, thereby allowing the clinician not only to promptly identify the infective or inflammatory focus but also to establish the best therapeutic approach for patients. The recent availability of many innovative molecules, such as monoclonal antibodies and analogues of growth and signaling factors, offers to nuclear medicine physicians a wide spectrum of promising radiopharmaceuticals as markers for different pathological events.

The development of hybrid camera techniques, such as PET/CT and SPECT/CT, led to a new area of imaging, in which the best of both anatomical and pathophysiological techniques are combined, leading to higher specificities and diagnostic accuracies [11]. The very recent development of combined PET/MRI camera systems may bring this diagnostic accuracy to an even higher level, especially in inflammatory cases, since MRI offers better soft tissue contrast information than CT [12].

This special issue consists of both invited review articles and original research papers from experts from all over the world in the booming field of infectious and inflammatory diseases. The focus of this special issue is to highlight existing imaging techniques and their current position in specific infectious and inflammatory diseases, to share new possibilities in new hybrid camera systems, to identify common patterns for nuclear medicine and radiological diagnosis of infectious and inflammatory diseases, to present new cellular and animal models for preclinical research, and to share the development and testing of novel radiopharmaceuticals in the field.

Infection and Inflammation of the Cardiovascular System. Diagnosing infections and inflammation of the cardiovascular system is a rapidly growing area in which nuclear medicine techniques play an important role. Several papers on this topic are published in this special issue dealing with vasculitis, vascular prosthetic graft infection, atherosclerosis, and endocarditis.

H. Balink et al. present an overview of the use of ^{18}F-FDG-PET/CT in large vessel vasculitis. They claim that there is a substantial under diagnosis of large vessel vasculitis and that ^{18}F-FDG-PET/CT may shed a new light on the classification of giant cell arteritis and Takayasu arteritis, thereby strengthening the idea that both diseases are more likely to be different expressions of a common histopathological entity.

C. Puppo et al. provide a systematic review including 19 original articles with a total of 442 patients with giant cell arteritis. They describe all the different qualitative, semiquantitative, and combined methods that have been proposed for assessing the presence and grading of the severity of the vascular inflammation. Qualitative methods are less sensitive but more specific than semiquantitative methods. Among the semiquantitative approaches, the aortic-to-blood pool uptake ratio of the aortic arch seems to be the most accurate method.

K. J. Lensen et al. evaluated several qualitative/visual analysis methods in this setting and looked at the best interobserver agreement between six nuclear medicine physicians of both academic and peripheral/general hospitals. They found the highest interobserver agreement when vascular wall ^{18}F-FDG uptake higher than liver uptake was used as a diagnostic criterion. Agreement was also good without predefined methods, the so-called first impression. They highlighted that standardization of image assessment promotes interobserver agreement.

The paper by B. R. Saleem et al. deals with the same problem of which interpretation criterion should be used but this time in vascular prosthetic graft infections (VPGI). No clear guidelines exist on this area and the interpretation by a visual grading scale is considered to be too subjective. Based on literature they suggest that a linear, diffuse, and homogeneous uptake should not be regarded as an infection, whereas focal or heterogeneous uptake with a projection over the vessel on CT is highly suggestive of infection.

To the opinion of the guest editors, ^{18}F-FDG-PET/CT should routinely be used in the imaging of vasculitis and in vascular graft infection, both for diagnosis and for therapy evaluation. Of course it is of invaluable importance that we all follow the same procedures in acquisition protocols and interpretation criteria to make comparison between literature results possible and to start multicenter prospective trials to finally make this technique a new standard in diagnostic and therapy evaluating flow charts.

R. S. Ripa and A. Kjaer share with us the initial experiences with simultaneous PET/MRI for atherosclerosis imaging. They give a short summary of current relevant clinical applications of PET and MRI in the setting of atherosclerosis and discuss future potential vascular applications exploiting the unique combination of PET and MRI.

M. Musso and N. Petrosillo performed a review of the literature to assess the available evidence on the role of nuclear medicine techniques in the diagnosis of prosthetic valve endocarditis. Both ^{18}F-FDG-PET/CT and ^{99m}Tc-HMPAO labelled white blood cells with SPECT/CT have demonstrated to be effective imaging methods that maybe can be used to increase the sensitivity of the Duke criteria and can identify important complications in the course of prosthetic valve endocarditis, including perivalvular abscesses and metastatic septic embolization.

Sarcoidosis. Sarcoidosis is a granulomatous disease that usually affects multiple organs. The presence of cardiac involvement is associated with adverse events such as heart failure, arrhythmias and sudden cardiac death, and an overall poor outcome. Early diagnosis and treatment is critically important. Therefore, M. Orii et al. provide us an overview of the epidemiology, etiology, histological findings, and clinical features of sarcoidosis. In this paper, they introduce advanced imaging methods including ^{18}F-FDG-PET and cardiac MRI as reliable diagnostic modalities for cardiac sarcoidosis. Hepatosplenic involvement of sarcoidosis often shows a benign course but portal hypertension and loss of liver function may occur. Therefore, a correct evaluation of these organs represents an important step in patients with sarcoidosis. The role of conventional imaging, such as CT and MRI in the assessment of hepatosplenic sarcoidosis, is well-established, by revealing organ enlargement, multiple discrete nodules, and lymphadenopathy. C. Tana et al. describe in their review contrast-enhanced ultrasound findings in liver and spleen involvement and share with us evidence from the literature and cases from their own experience.

Preclinical Research. Preclinical research is of invaluable importance to continue look for new radiopharmaceuticals and better use of existing radiopharmaceuticals to improve the diagnostic possibilities. J. C. E. Odekerken et al. focused on the longitudinal assessment of a nonimplant related osteomyelitis by introducing an intramedullary tibial infection with *S. aureus* in NZW rabbits. The development of the infection was assessed by microPET at consecutive time points using ^{18}F-FDG as an infection tracer. Indeed, the intramedullary contamination of the rabbit tibia resulted in osteomyelitis, so osteomyelitis in the rabbit can be induced without the use of an implant or sclerosing agent as was used in earlier studies. From all parameters used, the diagnostic

value of ^{18}F-FDG micro PET was the most versatile to assess the presence of an orthopaedic infection in this animal model.

D. M. Chandrupatla et al. made modifications in a rat model of rheumatoid arthritis (RA) to widen the therapeutic window for PET-guided evaluation of novel anti-RA agents. They induced arthritis in the right knee of Wistar rats and gave, after immunization, one or more intra-articular methylated bovine serum albumin injections over time in the right knee. Besides many other analyses, they found increased ^{18}F-FDG and ^{11}C-PK11195 accumulation in arthritic knees as compared to contralateral normal knees, which was confirmed in *ex vivo* tissue distribution studies. This model will offer excellent opportunities for repeated PET studies to monitor progression of disease and efficacy of novel therapeutic agents for RA in the same animal.

Antimicrobial peptides are a heterogeneous class of compounds found in a variety of organisms including humans. The ability of these peptides to accumulate at sites of infection combined with the minimal host's cytotoxicity makes these peptides potential radiopharmaceuticals to allow noninvasive whole-body examination for detection of occult infection. An overview of all the existing peptides and the strategy, design, and utilization of these peptides is given by T. Ebenhan et al.

B. Mokaleng et al. report TBIA101, an antimicrobial peptide derivate that was conjugated to DOTA and radiolabelled with ^{68}Ga for an *in vitro* and *in vivo* infection imaging using *Escherischia coli*-bearing mice by targeting bacterial lipopolysaccharides with PET/CT. ^{68}Ga-DOTA-TBIA101-PET detected *E. coli*-infected muscle tissue > noninfected thighs > forearm muscles > background in the same animal. Normalization of the infected thigh muscle to reference tissue showed a ratio of 3.0 ± 0.8 compared to a ratio of 2.3 ± 0.6 in the identical healthy tissue. These findings warrant further preclinical imaging studies of greater depth.

Tailored Radiopharmaceuticals. Nuclear medicine techniques may play a crucial role by providing objective biomarkers for personalized medicine. These techniques offer the unique possibility to target cells and molecules that are involved for histological characterization, selection of patients for targeted therapy, therapy response prediction, and therapy response follow-up. Research in this field must be encouraged and supported.

The paper from F. Galli et al. is a nice example of this important concept. Recently, the use of anti-tumor necrosis factor alpha (anti-TNFα) agents has been introduced for therapy of chronic and refractory sarcoidosis with controversial results. Therefore, ^{99m}Tc-labelled infliximab was used to study the expression of TNFα in sarcoid lesions and to evaluate its role as a predictive marker of response to therapy. The results were, however, slightly disappointing. A low correlation was found between target-to-background ratios and BAL results in patients that were despite positive at ^{18}F-FDG-PET. The authors concluded that in this study 10 patients had a low presence of TNFα. The concept that this anti-TNFα scintigraphy is a good tool for the selection of patients to be treated with anti-TNFα drugs is an important one since our techniques can reveal if this expensive therapy will be successful in the individual patient. So maybe the 10 patients scanned should not be treated with anti-TNFα drugs; however, to conclude this further investigation is warranted.

Alberto Signore
Andor W. J. M. Glaudemans
Filippo Galli
François Rouzet

References

[1] A. Signore and A. W. J. M. Glaudemans, "The molecular imaging approach to image infections and inflammation by nuclear medicine techniques," *Annals of Nuclear Medicine*, vol. 25, no. 10, pp. 681–700, 2011.

[2] V. Kumar and D. K. Boddeti, "^{68}Ga-radiopharmaceuticals for PET imaging of infection and inflammation," *Recent Results in Cancer Research*, vol. 194, pp. 189–219, 2013.

[3] A. W. J. M. Glaudemans, F. Galli, M. Pacilio, and A. Signore, "Leukocyte and bacteria imaging in prosthetic joint infection," *European Cells and Materials*, vol. 25, pp. 61–77, 2012.

[4] A. W. Glaudemans, E. F. de Vries, F. Galli, R. A. Dierckx, R. H. Slart, and A. Signore, "The use of ^{18}F-FDG-PET/CT for diagnosis and treatment monitoring of inflammatory and infectious diseases," *Clinical and Developmental Immunology*, vol. 2013, Article ID 623036, 14 pages, 2013.

[5] P. Erba, A. W. Glaudemans, N. C. Veltman et al., "Image acquisition and interpretation criteria for 99mTc-HMPAO-labelled white blood cell scintigraphy: results of a multicentre study," *European Journal of Nuclear Medicine and Molecular Imaging*, vol. 41, pp. 615–623, 2014.

[6] C. J. Palestro and C. Love, "Nuclear medicine and diabetic foot infections," *Seminars in Nuclear Medicine*, vol. 39, no. 1, pp. 52–65, 2009.

[7] F. Galli, S. Histed, and O. Aras, "NK cell imaging by in vitro and in vivo labelling approaches," *The Quarterly Journal of Nuclear Medicine and Molecular Imaging*, vol. 58, no. 3, pp. 276–283, 2014.

[8] V. Iodice, B. Laganà, C. Lauri et al., "Imaging B lymphocytes in autoimmune inflammatory diseases," *The Quarterly Journal of Nuclear Medicine and Molecular Imaging*, vol. 58, no. 3, pp. 258–268, 2014.

[9] G. Malviya, F. Galli, I. Sonni, and A. Signore, "Imaging T-lymphocytes in inflammatory diseases: a nuclear medicine approach," *The Quarterly Journal of Nuclear Medicine and Molecular Imaging*, vol. 58, no. 3, pp. 237–257, 2014.

[10] C. van de Wiele, M. Sathekge, and A. Maes, "Targeting monocytes and macrophages by means of SPECT and PET," *The Quarterly Journal of Nuclear Medicine and Molecular Imaging*, vol. 58, no. 3, pp. 269–275, 2014.

[11] S. Navalkissoor, E. Nowosinska, G. Gnanasegaran, and J. R. Buscombe, "Single-photon emission computed tomography-computed tomography in imaging infection," *Nuclear Medicine Communications*, vol. 34, no. 4, pp. 283–290, 2013.

[12] A. W. J. M. Glaudemans, A. M. Quintero, and A. Signore, "PET/MRI in infectious and inflammatory diseases: will it be a useful improvement?" *European Journal of Nuclear Medicine and Molecular Imaging*, vol. 39, no. 5, pp. 745–749, 2012.

Hindawi Publishing Corporation
BioMed Research International
Volume 2015, Article ID 401341, 7 pages
http://dx.doi.org/10.1155/2015/401341

Research Article

In Vivo Evaluation of TNF-Alpha in the Lungs of Patients Affected by Sarcoidosis

Filippo Galli,[1] Tiziana Lanzolla,[1] Vittorio Pietrangeli,[2] Gaurav Malviya,[1] Alberto Ricci,[2] Pierdonato Bruno,[2] Paola Ragni,[1] Francesco Scopinaro,[1] Salvatore Mariotta,[2] and Alberto Signore[1]

[1]*Nuclear Medicine Unit, Department of Medical-Surgical Sciences and Translational Medicine, Faculty of Medicine and Psychology, Ospedale S. Andrea, "Sapienza" University of Rome, Via di Grottarossa 1035, 00189 Roma, Italy*
[2]*Pneumology Unit, Department of Clinical and Molecular Medicine, Faculty of Medicine and Psychology, Ospedale S. Andrea, "Sapienza" University of Rome, Via di Grottarossa 1035, 00189 Roma, Italy*

Correspondence should be addressed to Alberto Signore; alberto.signore@uniroma1.it

Received 7 June 2014; Revised 9 August 2014; Accepted 11 August 2014

Academic Editor: Andor Glaudemans

Introduction. Sarcoidosis is a multisystemic granulomatous disorder characterized by multiple noncaseating granulomas involving intrathoracic lymph nodes and lung parenchyma. Recently, the use of anti-tumor necrosis factor alpha (anti-TNFα) agents has been introduced for therapy of chronic and refractory sarcoidosis with controversial results. Infliximab (Remicade) is a chimeric monoclonal antibody (mAb) that recognizes and binds TNFα, neutralizing its biological effects. In the present study, ^{99m}Tc labelled infliximab was used to study the expression of TNFα in sarcoid lesions and to evaluate its role as a predictive marker in response to therapy with Remicade. *Material and Methods*. A total of 10 patients with newly diagnosed sarcoidosis were enrolled together with 10 control patients affected by rheumatoid arthritis. All patients were studied by planar imaging of the chest with ^{99m}Tc-infliximab at 6 h and 24 h and total body [^{18}F]-FDG PET/CT. Regions of interest were drawn over the lungs and the right arm and target-to-background ratios were analysed for ^{99m}Tc-infliximab. SUV_{mean} and SUV_{max} were calculated over lungs for FDG. *Results and Discussion*. Image analysis showed low correlation between *T/B* ratios and BAL results in patients despite positivity at [^{18}F]-FDG PET. *Conclusion*. In conclusion, patients with newly diagnosed pulmonary sarcoidosis, with FDG-PET and BAL positivity, showed a negative ^{99m}Tc-infliximab scintigraphy.

1. Introduction

Sarcoidosis is a multisystemic granulomatous disorder characterized by multiple noncaseating granulomas involving intrathoracic lymph nodes and lung parenchyma. Inflammatory lesions can occur also in other organs like eyes and skin and, although less frequently, also in liver, spleen, extrathoracic lymph nodes, salivary glands, heart, nervous system, bones, and muscles. Even if its aetiology is still unknown, the role of cell-mediated immunity in the formation and in the maintenance of typical granulomas has been clarified [1, 2]. For this reason immunosuppressive therapy remains the gold standard for treatment and in particular corticosteroid are used as a first line therapy [3]. However, serious side effects of steroid therapy and the loss of long-term efficacy of this treatment have led researchers to use new drugs. Recently, the use of anti-tumor necrosis factor alpha (anti-TNFα) agents has been introduced for therapy of chronic and refractory sarcoidosis [4–6]. TNFα is an important cytokine released by alveolar activated macrophages, implicated in the development of granulomas. Infliximab (Remicade) is a chimeric monoclonal antibody (mAb) that recognizes and binds TNFα, neutralizing its biological effects [7]. However, the effectiveness of such therapy is still uncertain and under investigation [8]. It is indeed not well known if TNFα is sufficiently present in sarcoid lesions to play a relevant biological role despite the fact that its presence in BAL has been shown to correlate with the severity of alveolitis [9].

Nevertheless, which patient and which lesion have high levels of TNFα and may respond to anti-TNFα therapy is difficult to ascertain. In this view, the assessment of TNFα in sarcoid lesions by a noninvasive technique could be important to strengthen the hypothesis behind the use of anti-TNFα drugs and to select patients that could respond to therapy. Currently there are no specific diagnostic tools to directly evaluate the presence of anti-TNFα in sarcoid lesions but several methods have been reported for measuring disease activity. Chest X-ray and pulmonary function tests (spirometry), the measurement of serum angiotensin-converting-enzyme (ACE) levels and ^{67}Ga-citrate scintigraphy, and bronchoalveolar lavage (BAL) with evaluation of $CD4^+$ and $CD8^+$ lymphocytes have all been and still are used as surrogate markers of diseases activity [10, 11]. In particular, [^{18}F]-Fluoro-2-deoxy-D-glucose PET/CT ([^{18}F]-FDG PET/CT) has been shown to be of high clinical value for evaluation of disease activity and extent and for therapy follow-up [12–15].

In the present study, we have used ^{99m}Technetium (^{99m}Tc) labelled infliximab in patients with newly diagnosed sarcoidosis for noninvasive *in vivo* scintigraphic evaluation of the presence of TNFα in pulmonary and lymph nodal sarcoid lesions. Patients were also studied by [^{18}F]-FDG PET/CT and BAL with lymphocyte phenotyping for complete evaluation of disease activity.

2. Patients and Methods

2.1. Patients and Diagnosis. Study design included 20 patients with newly diagnosed sarcoidosis at stages II-III to be prospectively recruited for [^{18}F]-FDG-PET/CT and ^{99m}Tc-infliximab scintigraphy and 10 control subjects (patients without sarcoidosis but affected by rheumatoid arthritis (RA) to evaluate disease activity in joints). After enrolling all controls (7 females and 3 males, mean age 54 ± 10 years) and 10 sarcoidosis patients (8 females and 2 males, mean age 55 ± 8 years) we performed an interim analysis and decided to stop recruitment, based on results. Sarcoidosis patients were symptomatic and presented respiratory symptoms of the disease, without involvement of specific organs but lungs, thoracic and extrathoracic lymph nodes. They were also subjected to a standard assessment that included history and physical examination, with particular attention to respiratory disorders, blood test with peripheral blood counts and lymphocytes count ratio, and X-ray examination of the chest, including X-ray and high-resolution CT, bronchoscopy with bronchoalveolar lavage and bronchial biopsy, and analysis of BAL with lymphocytes immune-phenotyping (2 patients refused to perform the BAL). The diagnosis of sarcoidosis was performed using histological demonstration of the presence of the typical noncaseating granulomas; other diseases such as Wegener's granulomatosis, tuberculosis, aspergillosis, and neoplastic diseases were excluded for each patient. None of enrolled patients had previously been treated with corticosteroid therapy or immunosuppressive drugs. The study was approved by the local medical ethical committee and each patient expressed written informed consensus.

2.2. [^{18}F]-FDG PET/CT. Within 2 months from clinical diagnosis of sarcoidosis, a [^{18}F]-FDG PET/CT was performed after fasting for at least 6 h before the intravenous injection of [^{18}F]-FDG and with a serum glucose level lower than 160 mg/dL. Diazepam (5 mg) was administered to reduce muscle activity and activation of the brown fat. The activity of [^{18}F]-FDG to be administered was calculated for each patient according to the following formula [(weight in Kg/10 × 37 MBq) + 1]. The PET scan was performed with hybrid PET/CT Gemini (Philips, NL). Imaging acquisition started 60 minutes after the radiopharmaceutical injection from the upper thigh to the head, with a preliminary low-dose unenhanced CT scan (16 slice, 100 mAs) followed by PET imaging (2.5 min per bed position, 3D mode, matrix). Images were reconstructed with CT data by common iterative algorithm (OSEM, ordered subset expectation maximization, 2 iterations, 28 subsets) to obtain attenuation corrected images and anatomical mapping on functional images. [^{18}F]-FDG PET/CT images were visually analysed and disease activity was assessed separately in the mediastinum, hilum, lung parenchyma, extrapulmonary lymph nodes, even with obvious evaluation of liver, spleen, bone marrow, bones, and joints, in order to highlight a possible involvement of these organs. Each site was scored either positive or negative (positive = [^{18}F]-FDG uptake higher than background; negative = [^{18}F]-FDG uptake lower or equal to background). The semiquantitative analysis was based on the analysis of standardized uptake value (SUV) evaluated as SUV_{max} and SUV_{mean}, obtained by drawing regions of interest (ROIs) on transaxial sections of lung parenchyma at the level of the 3rd, 5th, and 7th thoracic vertebral body. The SUV values obtained were then compared with those obtained in the control population.

2.3. ^{99m}Tc-Infliximab Scintigraphy. The mAb infliximab was radiolabelled as previously described [16]. Briefly, 200 μL of $^{99m}TcO_4^-$ (666 MBq) was added to 200 μL of reduced mAb (200 mg/mL) followed by 7 μL of methylene diphosphonate (MDP). After 10 minutes of incubation at room temperature, quality controls were performed by instant thin layer chromatography (ITLC). Silica gel strips and 0.9% NaCl solution were used, respectively, as stationary and mobile phase for labelling efficiency determination. Albumin precoated silica gel strips and H_2O : EtOH : NH_3 (5 : 3 : 1) solution were used for colloids evaluation.

Within 1 week from the PET/CT scan, all patients performed a scintigraphic study with radiolabelled anti-TNFα after intravenous injection of 370 MBq of ^{99m}Tc-infliximab. Whole body images and planar static images of chest were acquired at 6 h and 24 h after injection with a large field of view, two head, gamma camera (Sky Light, Philips, NL) equipped with low-energy high-resolution collimators and 20% energy windows centred at 140 KeV. Whole body images (matrix 512 × 1024) were acquired at a speed of 10 cm/min at 6 h and 5 cm/min at 24 h taking into account the decay of the radionuclide. Anterior and posterior thorax images (matrix 256 × 256) were acquired for 300 seconds at 6 h and 600 seconds at 24 h.

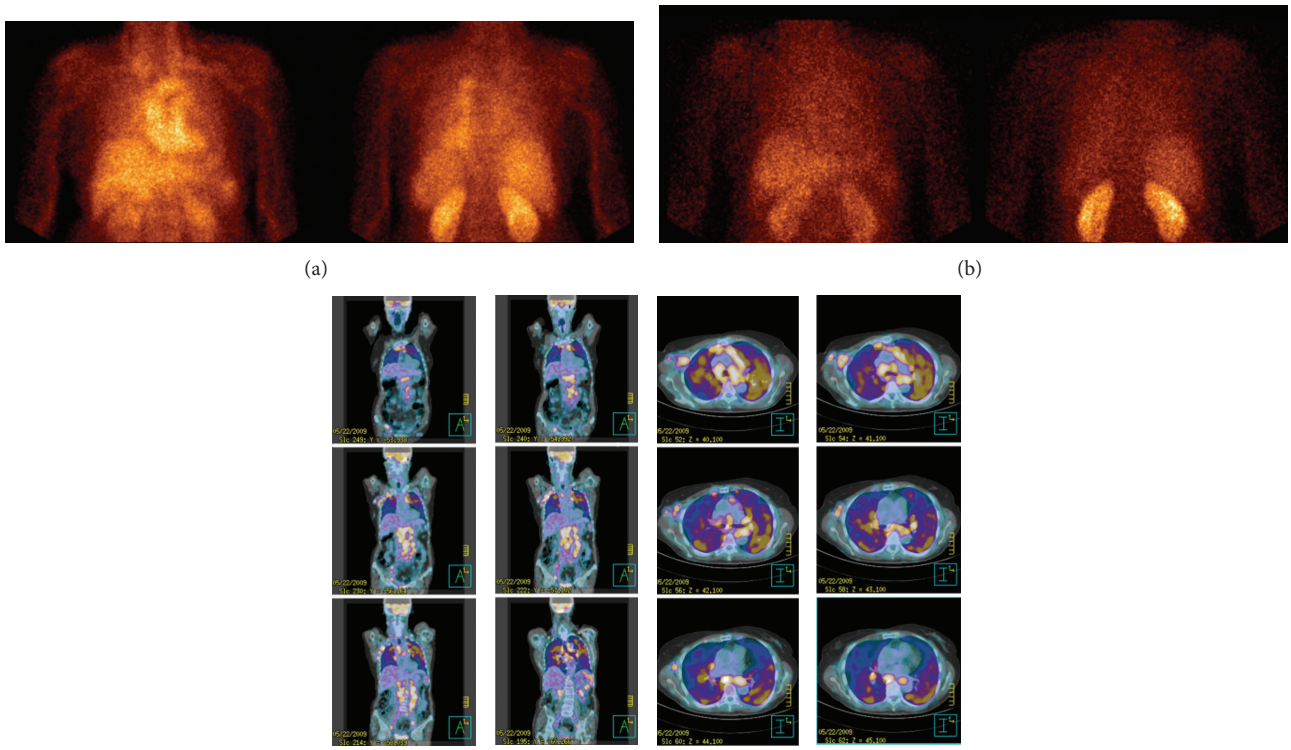

(a) (b)

(c)

Figure 1: ^{99m}Tc-Infliximab scintigraphy of a sarcoidosis patient (patient 3/F) acquired at 6 h (anterior and posterior views (a)) and at 24 h (anterior and posterior views (b)) showing a moderate and diffuse uptake in the lung parenchyma. [^{18}F]-FDG PET/CT images of the same patient showing a focal/hyleal uptake (coronal and transaxial sections (c)).

The results of scintigraphic studies were qualitatively analysed to identify any labelled mAb uptake and were visually compared with the pathological findings on PET images. A semiquantitative analysis was performed drawing ROIs over each lung parenchyma (ROI_{lung}) including hilum, but excluding heart and spine, and a ROI over the upper right arm (ROI_{arm}) as background, excluding joints. The counts were normalized by area and the target-to-background (*T/B*) ratio (ROI_{lung}/ROI_{arm}) was calculated at 6 h and 24 h for each lung in anterior and in posterior views. The average value of anterior and posterior values was considered for each patient. Results were compared with control subjects that underwent ^{99m}Tc-infliximab for RA and therefore considered "pulmonary negative."

2.4. Statistical Analysis. For each patient the average values of SUV_{max} and SUV_{mean}, obtained in lung parenchyma, were calculated in both sarcoidosis patients and controls, obtaining for each group the mean value ± SD. Similarly, the mean values ± SD of *T/B* ratios in sarcoidosis patients and control group were calculated at each time point (6 h and 24 h). In sarcoidosis population correlations were made between mean SUV values and mean *T/B* ratio, mean SUV values and lymphocytes immune-phenotyping on BAL, and mean *T/B* ratio and lymphocytes immune-phenotyping on BAL, in order to assess the diagnostic accuracy of each methodology to evaluate disease activity. Student's *t*-test was applied to assess the significance of relationship between the *T/B* ratio of sarcoidosis group and *T/B* ratio of control subjects.

3. Results

3.1. [^{18}F]-FDG PET/TC. The qualitative analysis performed on PET/CT studies in lungs showed complete agreement with the staging previously made by pulmonologists according to radiological and biochemical findings (Figure 1). Furthermore, in 3/10 patients PET showed other extrapulmonary sites of disease, with involvement of axillary and abdominal-pelvic lymph nodes, not previously known, demonstrating its high sensitivity. The mean values ± SD of SUV_{max} obtained in patients with sarcoidosis were 4.43 ± 3.20 whereas in control subjects mean values ± SD of SUV_{max} were 1.18 ± 0.20 ($P < 0.001$). These data are an expression of inflammation involvement of lung parenchyma in patients with sarcoidosis. The values of SUV_{max} and SUV_{mean} correlated perfectly; therefore for subsequent analysis only SUV_{max} will be reported even if also SUV_{mean} has always been considered. Despite the higher values of SUV_{max} in patients with sarcoidosis with respect to controls, it was not possible to find a cut-off value that could allow the correlation of the extent of uptake in the lung parenchyma with the degree of alveolitis. It was not also possible to obtain a significant correlation between lymphocyte immune-phenotyping results of BAL (with particular reference to $CD4^+/CD8^+$ ratio) and the

Table 1: Summary of SUV obtained by [^{18}F]-FDG PET/CT and *T/B* values (average of right and left lung calculated in anterior and posterior images) in patients with sarcoidosis.

Number/Sex	Stage	SUV_{max}	SUV_{mean}	*T/B* 6 h	*T/B* 24 h
1/F	I	1.91	0.54	4.16	2.84
2/F	II	3.47	0.99	4.34	2.75
3/F	II	4.38	2.19	3.52	3.49
4/F	II	2.64	0.79	4.82	3.97
5/M	I-II	3.05	1.02	3.61	3.14
6/F	II	5.28	1.25	4.77	3.24
7/M	I	2.23	0.73	4.14	2.72
8/F	II	12.87	4.55	4.73	3.41
9/F	II	3.01	0.88	3.43	2.49
10/F	II	5.48	0.90	4.73	3.42
Mean ± SD		4.43 ± 3.2	1.38 ± 1.2	4.22 ± 0.55	3.15 ± 0.45

SUV_{max} values of patients with sarcoidosis. No correlation was also observed between SUV_{max} or SUV_{mean} values and the $CD4^+/CD8^+$ ratio in blood.

3.2. ^{99m}Tc-Infliximab Scintigraphy. The qualitative analysis of scintigraphy with ^{99m}Tc-infliximab showed no pathological focal accumulation of the labeled antibody (Table 1). Both images at 6 h, characterized by high vascular activity, and images at 24 h did not show the same pathological uptakes highlighted in the preliminary PET study (Figures 1 and 2). The pulmonary distribution of the two radiopharmaceuticals was different, being predominantly diffused in the case of ^{99m}Tc-infliximab and rather focal with ileal involvement in the PET scans.

Comparing *T/B* ratios on ^{99m}Tc-infliximab scintigraphy at 6 h and 24 h, with SUV_{max} values of pulmonary uptake of FDG, no significant correlation was observed between these parameters. In only three patients a detectable diffuse bilateral lung uptake of anti-TNFα at 6 h and 24 h on scintigraphic images was present, which could indicate increased levels of TNFα in lung parenchyma of these patients. When we compared the mean values of lung uptake of labelled anti-TNFα mAb in sarcoidosis patients and control subjects, we found significant differences at 6 h (4.28 ± 0.57 versus 3.2 ± 0.74; patients versus controls; $P = 0.002$) but not at 24 h (3.15 ± 0.45 versus 2.7 ± 0.65; patients versus controls; $P = 0.057$). A moderate correlation was found between $CD4^+/CD8^+$ ratio peripheral blood lymphocytes and the value of *T/B* ratio at 6 h (Figure 3) but no correlation was found between average value of *T/B* ratio at 6 h or 24 h and, respectively, $CD4^+/CD8^+$ ratio and cellularity of BAL (Figure 4).

4. Discussion

In the last decade, systemic autoimmune disease therapy has been revolutionized by the availability of biological drugs or monoclonal antibodies, directed against a specific target implicated in the pathogenesis of disease. In patients with active sarcoidosis, the release of TNFα by activated alveolar macrophages has been widely documented in a lot of previous studies [17–21]. Infliximab (Remicade) is a chimeric monoclonal antibody of the type IgG1κ, with a variable region derived from murine antihuman TNFα and a constant sequence of human-derived IgG1. It was one of the first biological drugs to be used for the treatment of patients with sarcoidosis refractory to conventional therapy [5, 6, 22–24]. In particular, the multicenter phase II study of Baughman et al. [25] showed that in patients with sarcoidosis, symptomatic, refractory to corticosteroid therapy, treated with infliximab, there was a significant improvement of the forced vital capacity (FVC) without significant side effects related to the use of the drug. However, Panselinas et al. [26] showed, in a retrospective study, that in the majority of patients treated with infliximab, there was a recurrence of the disease about 3 months after discontinuation of the drug. Since biological therapies, such as infliximab, are extremely expensive, it would be desirable to be able to accurately select patients who really might benefit from this type of therapies. To date, however, there are no diagnostic markers for therapy decision making. In order to answer this question, we undertook a study to assess whether scintigraphy with ^{99m}Tc-infliximab, showing directly the presence of TNFα in the lesions, may represent a marker for predicting the efficacy of biological therapy with anti-TNFα and then select the patients suitable for this type of treatment [27, 28]. Infliximab was labelled with high labelling efficiency, high specific activity, and stability. Preliminary studies *in vitro* in animals and humans have shown its usefulness in the evaluation of patients with Crohn's disease and rheumatoid arthritis [29–31]. [^{18}F]-FDG PET has proven to be a very sensitive method in the evaluation of disease activity. Many studies have shown its higher sensitivity compared to ^{67}Gallium-citrate scintigraphy in the evaluation of disease and follow-up of therapy [14, 32–38]. However, [^{18}F]-FDG PET lacks specificity and cannot be used for the selection of patients to be treated with anti-TNFα. Its main role remains the diagnostic confirmation of disease, evaluation of the extension of the sites of disease, and the follow-up. It is therefore right to compare the role

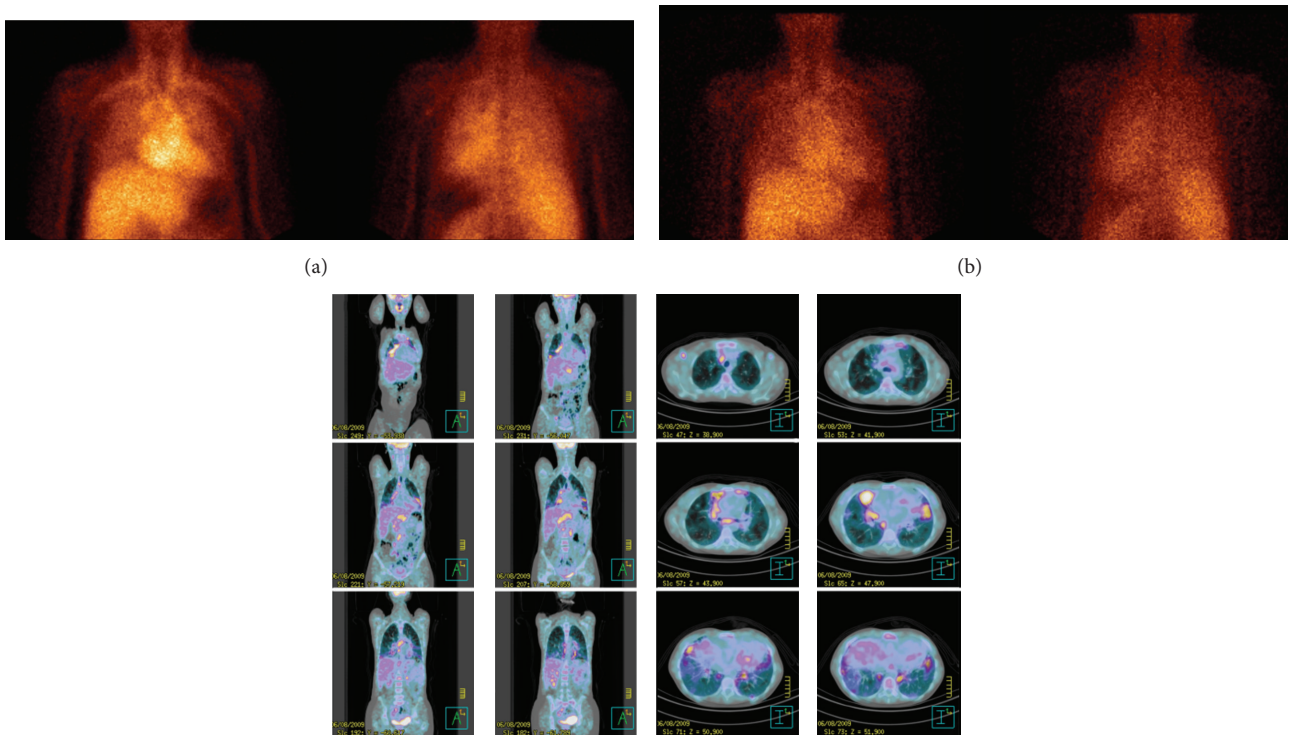

(a) (b) (c)

Figure 2: ^{99m}Tc-Infliximab scintigraphy of a sarcoidosis patient (patient 4/F) acquired at 6 h (anterior and posterior views (a)) and at 24 h (anterior and posterior views (b)) showing a moderate and diffuse uptake in the lung parenchima. [^{18}F]-FDG PET/CT images of the same patient showing a focal/hyleal uptake (coronal and transaxial sections (c)).

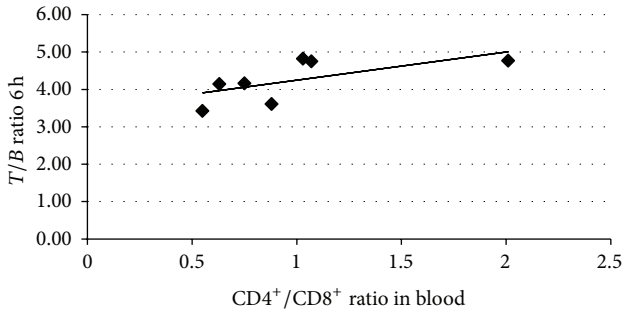

Figure 3: Correlation between lung uptake of ^{99m}Tc-infliximab at 6 h (*T/B* ratio) and CD4$^+$/CD8$^+$ ratio in peripheral blood lymphocytes. Correlation coefficient is $r = 0.2357$ and $P = 0.05$.

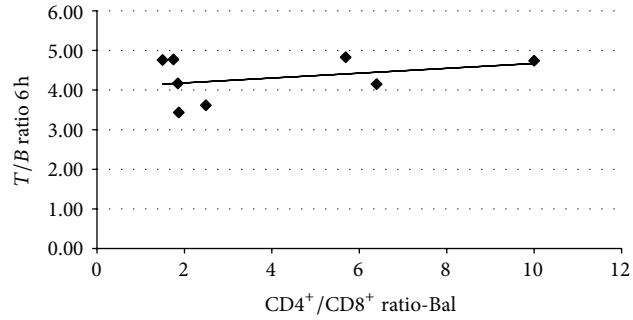

Figure 4: Correlation between lung uptake of ^{99m}Tc-infliximab at 6 h (*T/B* ratio) and CD4$^+$/CD8$^+$ ratio in lymphocytes from BAL. Correlation coefficient is $r = 0.6487$ and $P =$ n.s.

of scintigraphy with ^{99m}Tc-infliximab in the evaluation of disease with the findings obtained with [^{18}F]-FDG PET, but mainly for the selection of patients suitable for treatment with unlabelled anti-TNFα mAb. From our data, although on a limited series, it appears that with a qualitative examination, PET confirmed the staging performed by pulmonologists and allowed us to identify locations of extrathoracic disease, like axillaries and abdominopelvic lymph nodes. Inflammatory events in the lung parenchyma of sarcoidosis patients have been confirmed by higher SUV_{max} and SUV_{mean} with respect to normal subjects. The lack of correlation between the CD4$^+$/CD8$^+$ lymphocytes ratio in BAL and the values of both SUV_{max} and SUV_{mean} in the lung could be explained by the fact that the [^{18}F]-FDG is taken up by various cell types involved in the inflammatory sarcoid granuloma, confirming its poor specificity. Alternatively BAL is performed in a single lung segment whereas SUV was calculated over the whole lungs. Scintigraphy with labelled anti-TNFα mAb was qualitatively positive in 4 out of 10 patients, showing at 6 h and 24 h a widespread uptake of the radiopharmaceutical in both lungs. The values of *T/B* ratio calculated, on both the 6 h

and 24 h images, did not correlate with the values of SUV_{max} and SUV_{mean} calculated on ROI_{lung} of PET.

There are many possible explanations for this different pattern of ^{18}F-FDG and ^{99m}Tc-infliximab in sarcoidosis patients. One of them is that the two radiopharmaceuticals show different aspects of the same phenomenon: the intense [^{18}F]-FDG uptake by the cell populations responsible of alveolitis (macrophages, lymphocytes, etc.) and the presence of TNFα revealed by radiolabelled ^{99m}Tc-infliximab. Alternatively, there may be individual variability in the production of TNFα due to genetic reasons that depend on the stage of the disease. The lack of a clear focal uptake in some patients could also be caused by the long half-life of the anti-TNFα mAb that resulted in high background activity from the blood. This phenomenon is critical in highly perfused organs such as the lungs. In this case, the use of isotopes with longer half-life (^{89}Zr or ^{111}In) could help allowing to acquire images at later time points (e.g., 48 h or 72 h) thus improving *T/B* ratio due to clearance of radiopharmaceutical from the blood. Moreover, it should be kept in mind that, contrarily to what happens in lesions where the targets of a radiopharmaceutical are membrane bound receptors, TNFα is also a soluble molecule and a possible washout or low concentration in the lesions could prevent the visualization of distinctive foci. Indeed, on the basis of the review of literature, the most responsive patients to therapy with infliximab appear to be those with extrapulmonary disease, with involvement of skin, nervous system, bone, and ocular disease; it would be interesting to study these patients with ^{99m}Tc-infliximab scintigraphy in order to effectively assess the presence of TNFα in other extrapulmonary tissues affected by sarcoidosis.

Our choice was to investigate patients with newly diagnosed sarcoidosis that did not undergo prior therapies, based on the need to study "naive" patients in which no previous immunosuppressive therapy was administered. Despite what we expected the *T/B* ratio calculated at 6 h and 24 h did not correlate with the amount of lymphocytes in BAL, indicating that not all immune-mediated phenomena are characterized by high production of TNFα.

5. Conclusions

Labelled anti-TNFα mAb scintigraphy could be a good tool for the selection of patients to be treated with anti-TNFα drugs; however, in our study most of the examined patients showed a negative ^{99m}Tc-infliximab scintigraphy, underlining a low presence of TNFα even if [^{18}F]-FDG PET/CT was highly positive.

Conflict of Interests

The authors declare that there is no conflict of interests regarding the publication of this paper.

Authors' Contribution

Filippo Galli and Tiziana Lanzolla equally contributed to this paper.

References

[1] R. P. Baughman, E. E. Lower, and R. M. Du Bois, "Sarcoidosis," *The Lancet*, vol. 361, no. 9363, pp. 1111–1118, 2003.

[2] M. A. Judson, "Sarcoidosis: clinical presentation, diagnosis, and approach to treatment," *The American Journal of the Medical Sciences*, vol. 335, no. 1, pp. 26–33, 2008.

[3] A. P. Croft, D. Situnayake, O. Khair et al., "Refractory multisystem sarcoidosis responding to infliximab therapy," *Clinical Rheumatology*, vol. 31, no. 6, pp. 1013–1018, 2012.

[4] J. P. Utz, A. H. Limper, S. Kalra et al., "Etanercept for the treatment of stage II and III progressive pulmonary sarcoidosis," *Chest*, vol. 124, no. 1, pp. 177–185, 2003.

[5] J. D. Doty, J. E. Mazur, and M. A. Judson, "Treatment of sarcoidosis with infliximab," *Chest*, vol. 127, no. 3, pp. 1064–1071, 2005.

[6] S. Saleh, S. Ghodsian, V. Yakimova, J. Henderson, and O. P. Sharma, "Effectiveness of infliximab in treating selected patients with sarcoidosis," *Respiratory Medicine*, vol. 100, no. 11, pp. 2053–2059, 2006.

[7] D. Sánchez-Cano, J. L. Callejas-Rubio, R. Ruiz-Villaverde, R. Ríos-Fernández, and N. Ortego-Centeno, "Off-label uses of anti-TNF therapy in three frequent disorders: behçet's disease, sarcoidosis , and noninfectious uveitis," *Mediators of Inflammation*, vol. 2013, Article ID 286857, 10 pages, 2013.

[8] P. Korsten, M. Mirsaeidi, and N. J. Sweiss, "Nonsteroidal therapy of sarcoidosis," *Current Opinion in Pulmonary Medicine*, vol. 19, no. 5, pp. 516–523, 2013.

[9] J. Domagała-Kulawik, T. Skirecki, M. Maskey-Warzechowska, H. Grubek-Jaworska, and R. Chazan, "Bronchoalveolar lavage total cell count in interstitial lung diseases—does it matter?" *Inflammation*, vol. 35, no. 3, pp. 803–809, 2012.

[10] R. P. Baughman, Y. Ploysongsang, R. D. Roberts, and L. Srivastava, "Effects of sarcoid and steroids on angiotensin-converting enzyme," *American Review of Respiratory Disease*, vol. 128, no. 4, pp. 631–633, 1983.

[11] R. H. Winterbauer, J. Lammert, M. Selland, R. Wu, D. Corley, and S. C. Springmeyer, "Bronchoalveolar lavage cell populations in the diagnosis of sarcoidosis," *Chest*, vol. 104, no. 2, pp. 352–361, 1993.

[12] Y. Nishiyama, Y. Yamamoto, K. Fukunaga et al., "Comparative evaluation of 18F-FDG PET and 67Ga scintigraphy in patients with sarcoidosis," *Journal of Nuclear Medicine*, vol. 47, no. 10, pp. 1571–1576, 2006.

[13] J. J. Braun, R. Kessler, A. Constantinesco, and A. Imperiale, "^{18}F-FDG PET/CT in sarcoidosis management: review and report of 20 cases," *European Journal of Nuclear Medicine and Molecular Imaging*, vol. 35, no. 8, pp. 1537–1543, 2008.

[14] N. Milman, J. Mortensen, and C. Sloth, "Fluorodeoxyglucose PET scan in pulmonary sarcoidosis during treatment with inhaled and oral corticosteroids," *Respiration*, vol. 70, no. 4, pp. 408–413, 2003.

[15] R. G. Keijsers, F. J. Verzijlbergen, J. M. van den Bosch et al., "18F-FDG PET as a predictor of pulmonary function in sarcoidosis," *Sarcoidosis Vasculitis and Diffuse Lung Diseases*, vol. 28, no. 2, pp. 123–129, 2011.

[16] F. Conti, G. Malviya, F. Ceccarelli et al., "Role of scintigraphy with ^{99m}Tc-infliximab predicting the response of intraarticular in patients with refractory monoarthritis," *European Journal of Nuclear Medicine and Molecular Imaging*, vol. 39, no. 8, pp. 1339–1347, 2012.

[17] R. P. Baughman and M. Iannuzzi, "Tumour necrosis factor in sarcoidosis and its potential for targeted therapy," *BioDrugs*, vol. 17, no. 6, pp. 425–431, 2003.

[18] M. Steffen, J. Petersen, M. Oldigs et al., "Increased secretion of tumor necrosis factor-alpha, interleukin-1-beta, and interleukin-6 by alveolar macrophages from patients with sarcoidosis," *Journal of Allergy and Clinical Immunology*, vol. 91, no. 4, pp. 939–949, 1993.

[19] M. W. Ziegenhagen, U. K. Benner, G. Zissel, P. Zabel, M. Schlaak, and J. Müller-Quernheim, "Sarcoidosis: TNF-α release from alveolar macrophages and serum level of sIL-2R are prognostic markers," *The American Journal of Respiratory and Critical Care Medicine*, vol. 156, no. 5, pp. 1586–1592, 1997.

[20] M. W. Ziegenhagen, M. E. Rothe, G. Zissel, and J. Müller-Quernheim, "Exaggerated TNFα release of alveolar macrophages in corticosteroid resistant sarcoidosis," *Sarcoidosis Vasculitis and Diffuse Lung Diseases*, vol. 19, no. 3, pp. 185–190, 2002.

[21] R. P. Baughman, S. A. Strohofer, J. Buchsbaum, and E. E. Lower, "Release of tumor necrosis factor by alveolar macrophages of patients with sarcoidosis," *Journal of Laboratory and Clinical Medicine*, vol. 115, no. 1, pp. 36–42, 1990.

[22] R. P. Baughman and E. E. Lower, "Infliximab for refractory sarcoidosis," *Sarcoidosis Vasculitis and Diffuse Lung Diseases*, vol. 18, no. 1, pp. 70–74, 2001.

[23] L. Mallbris, A. Ljungberg, M. A. Hedblad, P. Larsson, and M. Ståhle-Bäckdahl, "Progressive cutaneous sarcoidosis responding to anti-tumor necrosis factor-α therapy," *Journal of the American Academy of Dermatology*, vol. 48, no. 2, pp. 290–293, 2003.

[24] S. D. Roberts, D. S. Wilkes, R. A. Burgett, and K. S. Knox, "Refractory sarcoidosis responding to infliximab," *Chest*, vol. 124, no. 5, pp. 2028–2031, 2003.

[25] R. P. Baughman, M. Drent, M. Kavuru et al., "Infliximab therapy in patients with chronic sarcoidosis and pulmonary involvement," *The American Journal of Respiratory and Critical Care Medicine*, vol. 174, no. 7, pp. 795–802, 2006.

[26] E. Panselinas, J. K. Rodgers, and M. A. Judson, "Clinical outcomes in sarcoidosis after cessation of infliximab treatment," *Respirology*, vol. 14, no. 4, pp. 522–528, 2009.

[27] G. Malviya, F. Galli, I. Sonni, M. Pacilio, and A. Signore, "Targeting T and B lymphocytes with radiolabeled antibodies for diagnostic and therapeutic applications," *Quarterly Journal of Nuclear Medicine and Molecular Imaging*, vol. 54, no. 6, pp. 654–676, 2010.

[28] A. Signore, C. Lauri, and F. Galli, "Radiolabelled probes targeting infection and inflammation for personalized medicine," *Current Pharmaceutical Design*, vol. 20, no. 14, pp. 2338–2345, 2014.

[29] F. Conti, R. Priori, M. S. Chimenti et al., "Successful treatment with intraarticular infliximab for resistant knee monarthritis in a patient with spondylarthropathy: a role for scintigraphy with 99mTc-infliximab," *Arthritis and Rheumatism*, vol. 52, no. 4, pp. 1224–1226, 2005.

[30] M. Chianelli, C. D'Alessandria, F. Conti et al., "New radiopharmaceuticals for imaging rheumatoid arthritis," *Quarterly Journal of Nuclear Medicine and Molecular Imaging*, vol. 50, no. 3, pp. 217–225, 2006.

[31] C. D'Alessandria, G. Malviya, A. Viscido et al., "Use of a 99mTc labeled anti-TNFα monoclonal antibody in Crohn's disease: in vitro and in vivo studies," *Quarterly Journal of Nuclear Medicine and Molecular Imaging*, vol. 51, no. 4, pp. 334–342, 2007.

[32] A. Alavi, C. A. Buchpiguel, and A. Loessner, "Is there a role for FDG PET imaging in the management of patients with sarcoidosis?" *Journal of Nuclear Medicine*, vol. 35, no. 10, pp. 1650–1652, 1994.

[33] H. Zhuang and A. Alavi, "18-Fluorodeoxyglucose positron emission tomographic imaging in the detection and monitoring of infection and inflammation," *Seminars in Nuclear Medicine*, vol. 32, no. 1, pp. 47–59, 2002.

[34] G. El-Haddad, H. Zhuang, N. Gupta, and A. Alavi, "Evolving role of positron emission tomography in the management of patients with inflammatory and other benign disorders," *Seminars in Nuclear Medicine*, vol. 34, no. 4, pp. 313–329, 2004.

[35] L. H. Brudin, S. O. Valind, C. G. Rhodes et al., "Fluorine-18 deoxyglucose uptake in sarcoidosis measured with positron emission tomography," *European Journal of Nuclear Medicine*, vol. 21, no. 4, pp. 297–305, 1994.

[36] Y. Nishiyama, Y. Yamamoto, K. Fukunaga et al., "Comparative evaluation of ^{18}F-FDG PET and ^{67}Ga scintigraphy in patients with sarcoidosis," *Journal of Nuclear Medicine*, vol. 47, no. 10, pp. 1571–1576, 2006.

[37] E. Prager, M. Wehrschuetz, B. Bisail et al., "Comparison of 18F-FDG and 67Ga-citrate in sarcoidosis imaging," *NuklearMedizin*, vol. 47, no. 1, pp. 18–23, 2008.

[38] A. S. Teirstein, J. Machac, O. Almeida, P. Lu, M. L. Padilla, and M. C. Iannuzzi, "Results of 188 whole-body fluorodeoxyglucose positron emission tomography scans in 137 patients with sarcoidosis," *Chest*, vol. 132, no. 6, pp. 1949–1953, 2007.

Hindawi Publishing Corporation
BioMed Research International
Volume 2015, Article ID 914692, 8 pages
http://dx.doi.org/10.1155/2015/914692

Research Article

Large-Vessel Vasculitis: Interobserver Agreement and Diagnostic Accuracy of ^{18}F-FDG-PET/CT

K. D. F. Lensen,[1] E. F. I. Comans,[2] A. E. Voskuyl,[3] C. J. van der Laken,[3] E. Brouwer,[4] A. T. Zwijnenburg,[5] L. M. Pereira Arias-Bouda,[6] A. W. J. M. Glaudemans,[7] R. H. J. A. Slart,[7] and Y. M. Smulders[1]

[1]*Department of Internal Medicine and Institute for Cardiovascular Research (ICaR-VU), VU University Medical Center, 1007 MB Amsterdam, Netherlands*
[2]*Department of Nuclear Medicine and Radiology, VU University Medical Center, 1007 MB Amsterdam, Netherlands*
[3]*Department of Rheumatology, VU University Medical Center, 1007 MB Amsterdam, Netherlands*
[4]*Department of Rheumatology, University Medical Center Groningen, 9700 RB Groningen, Netherlands*
[5]*Department of Nuclear Medicine, Spaarne Hospital, 2130 AT Hoofddorp, Netherlands*
[6]*Department of Nuclear Medicine, Rijnland Hospital, 2350 CC Leiderdorp, Netherlands*
[7]*Department of Nuclear Medicine and Molecular Imaging, University Medical Center Groningen, 9700 RB Groningen, Netherlands*

Correspondence should be addressed to Y. M. Smulders; y.smulders@vumc.nl

Received 2 June 2014; Revised 23 September 2014; Accepted 24 September 2014

Academic Editor: Francois Rouzet

Introduction. ^{18}F-FDG-PET visualises inflammation. Both atherosclerosis and giant cell arteritis cause vascular inflammation, but distinguishing the two may be difficult. The goal of this study was to assess interobserver agreement and diagnostic accuracy of ^{18}F-FDG-PET for the detection of large artery involvement in giant cell arteritis (GCA). *Methods*. 31 ^{18}F-FDG-PET/CT scans were selected from 2 databases. Four observers assessed vascular wall ^{18}F-FDG uptake, initially without and subsequently with predefined observer criteria (i.e., vascular wall ^{18}F-FDG uptake compared to liver or femoral artery ^{18}F-FDG uptake). External validation was performed by two additional observers. Sensitivity and specificity of ^{18}F-FDG-PET were determined by comparing scan results to a consensus diagnosis. *Results*. The highest interobserver agreement (kappa: 0.96 in initial study and 0.79 in external validation) was observed when vascular wall ^{18}F-FDG uptake higher than liver uptake was used as a diagnostic criterion, although agreement was also good without predefined criteria (kappa: 0.68 and 0.85). Sensitivity and specificity were comparable for these methods. The criterion of vascular wall ^{18}F-FDG uptake equal to liver ^{18}F-FDG uptake had low specificity. *Conclusion*. Standardization of image assessment for vascular wall ^{18}F-FDG uptake promotes observer agreement, enables comparative studies, and does not appear to result in loss of diagnostic accuracy compared to nonstandardized assessment.

1. Introduction

^{18}F-Fluorodeoxyglucose Positron Emission Tomography (FDG-PET), usually combined with low-dose CT (FDG-PET/CT), may be used to detect vascular wall inflammation [1]. The most common causes of vascular wall inflammation are, by far, atherosclerosis and vasculitis, particularly giant cell arteritis (GCA). An infectious etiology (e.g., syphilis) is far less common [2–4]. Therefore, the primary goal for a clinician is to differentiate between GCA and atherosclerotic plaque inflammation when vascular wall ^{18}F-FDG uptake is present [5]. GCA, a granulomatous vasculitis of unknown origin, may present clinically as temporal arteritis which is characterised by temporal headache, jaw claudication and visual symptoms. Large arteries are frequently involved [6]. However, temporal arteries are not always affected. This clinical phenotype, in which the clinical presentation is less specific, has been referred to as "silent," "occult" or large-vessel vasculitis (LVV) [7, 8].

Several criteria for the qualitative (visual) assessment of FDG-PET for the detection of large artery involvement in GCA have been introduced, ranging from "increased"

circumferential ^{18}F-FDG uptake (i.e., not further specified) in a segment of the arterial wall to equal or more intense vascular wall uptake than liver uptake [9–12].

It has been recommended that only those with specific expertise and experience should assess vascular wall ^{18}F-FDG uptake [9]. In clinical practice, and in our own experience, interobserver agreement among such experts is not always sufficient. However, this has been tested in only a few studies (Table 1) As low levels of agreement are problematic, since they preclude diagnostic accuracy [13], the primary objective of this study was to establish interobserver agreement for the visual assessment of vascular wall ^{18}F-FDG uptake using various scoring methods. As a secondary objective, different FDG-PET/CT scoring methods were compared with the final clinical diagnosis.

Table 1: Overview of articles reporting imaging findings in GCA/large-vessel vasculitis and assessment of observer agreement of visual assessment. (n.r.: not reported, ^{18}F-FDG-PET: ^{18}F-fluorodeoxyglucose positron emission tomography, MRI: magnetic resonance imaging, CT: computed tomography, and US: ultrasound).

Article (year of publication)	Imaging modality	Number of observers	Observer agreement
Blockmans et al., 2000 [21]	^{18}F-FDG-PET	4 (2 teams)	n.r.
Blockmans et al., 2006 [22]		2	n.r.
Walter et al., 2005 [12]		2	93% (28/30)
Henes et al., 2008 [9]	^{18}F-FDG-PET/CT	At least 2	n.r.
Lehmann et al., 2011 [10]		2	85% (Cohen's kappa 0.7)
Papathanasiou et al., 2012 [23]		2	n.r.
Fuchs et al., 2012 [3]		3	n.r.
Brodmann et al., 2004 [24]	^{18}F-FDG-PET and US	1	n.r.
Meller et al., 2003 [11]	^{18}F-FDG-PET and MRI	2	n.r.
Scheel et al., 2004 [25]		2	n.r.
Both et al., 2008 [26]		2	n.r.
Agard et al., 2008 [27]	CT	1	n.r.
Marie et al., 2009 [28]		1	n.r.
Prieto-González et al., 2012 [6]		2	98%
Schmidt et al., 2002 [29]	US	2	89%
Schmidt et al., 2008 [30]		?	n.r.
DE et al., 2009 [31]		29	0.847 (kappa)
Narvaez et al., 2005 [32]	MRI	n.r.	n.r.
Koenigkam-Santos et al., 2011 [33]		2	0.73 (kappa)

2. Methods

2.1. Patient Characteristics. 31 FDG-PET/CT scans were selected from the databases of the Department of Nuclear Medicine and PET Research of the VU University Medical Center (VUMC) and the Department of Nuclear Medicine and Molecular Imaging of the University Medical Center Groningen (UMCG). These FDG-PET/CT scans were performed in clinical practice in order to (1) determine the cause of inflammation of unknown origin ($n = 12$) (this was a subset of patients from a study addressing the value of FDG-PET in patients with systemic inflammation of unknown origin) [14], (2) investigate whether large-vessel vasculitis was present in patients with diagnosed temporal arteritis ($n = 6$) or polymyalgia rheumatic (PMR) ($n = 7$), or (3) do a follow-up procedure in patients with a history of cancer ($n = 6$) who were considered to be in clinical remission, from which a random selection was made.

The first two groups were selected as a high incidence of large-vessel vasculitis was expected. A diagnosis of temporal arteritis (according to the ACR criteria for GCA) [15] or PMR (in accordance with Healy criteria) was made by the treating physician. Two patients with a diagnosis of temporal arteritis and one patient with a diagnosis of PMR used prednisone prior to the FDG-PET/CT scan. The third (reference) group was selected because malignancy is the most common indication for an FDG-PET/CT scan making these scans easy to obtain. In addition, the incidence of large-vessel vasculitis was expected to be low. Table 2 shows patient characteristics of these groups.

A Philips Gemini TOF (VUMC) and a Siemens Biograph (UMCG) PET/CT scanner (Philips Medical Systems, Eindhoven, Netherland and Siemens Medical Systems, Knoxville, TN) were used. A standardised protocol according to European Association of Nuclear Medicine (EANM) guidelines was used for the acquisition of scans [16]. In short, after fasting for at least four hours, whole-body (from head to knees) or total-body (from head to toes) PET-scans were acquired 60 (±5) minutes after intravenous injection of 3 MBq/kg ^{18}F-FDG. A low-dose CT scan was acquired prior to the PET-emission scan for attenuation correction and anatomic localization. Each scan was given a specific study code before analysis assuring that observers were blinded for original scan report and clinical data. Finally, the observers were unaware of the number of patients with large-vessel vasculitis that were included. Blinding for medical center was impossible because PET/CT scans from two different vendors were used.

2.2. Image Analysis. Four observers used three distinct methods to visually (qualitatively) assess ^{18}F-FDG vascular wall uptake (vascular uptake). These methods were applied in a consecutive manner in all scans and were consistently used by the observers. The level of experience varied among the observers, that is, 12, 8, 5 (three nuclear medicine physicians),

Table 2: Patient characteristics, total and ordered by group.

	Total (n = 31)	Inflammation of unknown origin (n = 12)	Temporal arteritis (n = 6)	Polymyalgia rheumatica (n = 7)	Control group (n = 6)
Age (years)*	70 (12)	73 (13)	67 (10)	73 (7)	62 (13)
Sex (female)•	65%	58%	100%	57%	50%
ESR (mm/h)*	70 (32)	79 (27)	64 (42)	58 (30)	Unknown
BMI (kg/m^2)*	23,4 (7,3)	23,7 (8,6)	23,3 (4,6)	21,6 (9,9)	25 (1,7)

*Mean (standard deviation), •percentage.

and 2 years (one general physician working as a researcher in the field of PET/CT and large-vessel inflammation).

First, vascular uptake was assessed without using predefined criteria and was therefore based on first impression. This method was selected as it is often used in clinical practice, due to the absence of established observer criteria (qualitative and quantitative), such as comparing vascular uptake with uptake in other organs (e.g., the liver). Vascular wall uptake was scored as 1: normal, 2: atherosclerosis, or 3: large-vessel vasculitis (method (I)). The term large-vessel vasculitis was used as temporal artery involvement cannot be assessed using PET/CT due to a relatively low resolution of the scan and potential spill over from adjacent (physiological) brain ^{18}F-FDG uptake [5].

Subsequently, the intensity of vascular uptake was systematically compared with the intensity of ^{18}F-FDG liver uptake and scored as 0: absent, 1: less intense, 2: equally intense, or 3: more intense (method (II)).

The arterial segments that were studied in these first two methods included carotid, vertebral, subclavian, iliac, and femoral arteries, the aortic arch, and the ascending, descending, and abdominal aorta.

In the third method, femoral artery uptake was chosen as reference since the femoral artery is rarely involved in GCA and has a high incidence of atherosclerosis [17, 18]. The intensity of vascular uptake in the other arterial segments was compared with the intensity of femoral artery uptake and was scored as 0: less intense, 1: equally intense, or 2: more intense (method (III)).

The distribution pattern, either focal (in all segments <2 cm) or diffuse (at least one segment comprising more than 2 cm of contiguous vascular wall uptake), and presence of arterial calcification on low-dose CT were also scored.

After the first reading, a consensus meeting was held with the goal to clarify causes of disagreement.

Finally, interobserver agreement was calculated using definitions of large-vessel vasculitis for each of the applied methods. These definitions were

(I) first impression (no predefined criteria),

(IIa) diffuse vascular wall uptake, *equal to or higher than liver* uptake in more than one vascular segment,

(IIb) diffuse vascular wall uptake, *higher than liver* uptake in more than one vascular segment,

(III) diffuse uptake, *higher than femoral artery* uptake.

2.3. Clinical Diagnosis of Large Artery Involvement in GCA. To date, there is no clinical reference standard for a diagnosis of large artery involvement in GCA (either with or without temporal artery involvement). Furthermore, there is no consensus on which imaging modality or imaging criteria should be used. Therefore, in order to compare FDG-PET/CT results to a clinical diagnosis of large artery involvement in GCA, we defined the latter as

(1) temporal arteritis according to ACR criteria [15], accompanied by an FDG-PET/CT scan that was unanimously classified as large-vessel vasculitis by all observers for at least one of the methods applied,

(2) inflammation (i.e., elevated ESR) of unknown origin, not fulfilling ACR criteria for GCA, accompanied by FDG-PET/CT results that were unanimously classified as large-vessel vasculitis by all observers for at least two of the methods applied.

In both groups, a good clinical response to immunosuppressive therapy (prednisone), defined as rapid resolution of signs and symptoms, accompanied by normalisation of inflammatory parameters, was mandatory for the diagnosis. Additionally, no other diagnosis was allowed to have been established during a follow-up period of at least 3 months.

This clinical diagnosis was used to determine sensitivity and specificity for the 4 FDG-PET/CT scoring methods.

2.4. External Observers. Based on the results of the first four observers, the definitions of large-vessel vasculitis that showed high levels of agreement between observers and with the clinical diagnosis were used for external validation. The first four observers are employees at a university hospital and have specific interest and experience in large-vessel vasculitis and PET/CT reporting. Therefore, two community hospital nuclear medicine physicians were asked to score the same scans by these definitions. Again, interobserver agreement was determined.

2.5. Statistical Analysis. Levels of agreement were quantified using Fleiss' kappa (κ) for multiple raters and Cohen's kappa for two raters. κ-values are reported using the benchmarks of Landis and Koch (with 0.81–1 being almost perfect agreement; 0.61–0.8 being substantial agreement; 0.41–0.6 being moderate agreement; 0.21–0.4 being fair agreement; 0.01–0.2 being slight agreement; and ≤0 being poor agreement) [19]. The statistical program *R* was used to calculate Fleiss' kappa

Table 3: Average number of vasculitis PET/CT scores (individual observer scores), Fleiss' kappa, sensitivity, and specificity (95%-CI) according to the different methods applied.

Method	Average number of vasculitides (x_1, x_2, x_3, x_4)	Fleiss' kappa	Sensitivity*	Specificity*
(I) First impression	9 (6, 9, 10, 11)	0,68	92% (52–98%)	90% (70–97%)
(IIa) Diffuse uptake, ≥liver uptake	16 (14, 16, 17, 18)	0,78	100% (61–100%)	60% (39–78%)
(IIb) Diffuse uptake, >liver uptake	7 (7, 7, 7, 8)	0,96	100% (61–100%)	98% (82–100%)
(III) Diffuse uptake, >femoral artery uptake	7 (6, 6, 6, 10)	0,81	80% (41–94%)	96% (79–99%)

*The average sensitivity and specificity of the results of the 4 observers (x_1–x_4) were calculated.

[20]. SPSS was used to calculate Cohen's kappa (SPSS version 20; SPSS inc.).

3. Results

3.1. First Impression Potentially Influences Comparison to Liver. After all scans were analysed, a remarkably high disagreement (i.e., 1/3 of all cases) was noticed when vascular uptake was compared to liver uptake. In a subgroup of patients vascular uptake was scored as less intense than liver uptake by some of the observers, whereas it was scored equally intense by other observers. During the consensus meeting, the observers concluded that in some cases vascular wall uptake was considered to be less intense than liver uptake based on their first impression that large-vessel vasculitis was not present. Therefore, a reanalysis of these scans was performed. Furthermore, the observers agreed that vascular uptake was only consistent with vasculitis if it showed a diffuse uptake pattern. The presence of calcification was ignored as it was present in all patients on low-dose CT scans.

3.2. Interobserver Agreement. Table 3 shows the average number (and individual scores of all 4 observers) of scans that were scored as large-vessel vasculitis. A remarkably high number of large-vessel vasculitis diagnoses were made when definition (IIa) was used. Figure 1 shows examples of FDG-PET/CT images in which there was complete agreement on absence or presence of large-vessel vasculitis according to all methods (Figures 1(a) and 1(c)) and an image in which there was disagreement (Figure 1(b)) according to method (II).

All observers agreed in 21 of 30 cases (70%) when assessing scans according to method (I). The corresponding Fleiss' kappa was 0,68 (0,72 without the results of the least experienced observer).

There was agreement between all observers in 19 of 30 patients (63%) when scoring according to method (IIa), and kappa was 0,78 (0,81 without results of the least experienced observer) (Table 3). When method (IIb) was applied, there was agreement between all observers in 29 of 30 cases (97%), resulting in a kappa of 0,96 (1 without the results of the least experienced observer).

Finally, for method (III), all observers agreed in 27 of 30 cases (90%) with a resulting kappa of 0,81 (1 without the results of the least experienced observer).

3.3. PET/CT Results and Clinical Diagnosis. In 4 patients (13%), we were unable to obtain sufficient follow-up data to ascertain a clinical diagnosis. One patient (from the group of inflammation of unknown origin who was suspected of large-vessel vasculitis after PET/CT) died the week after the scan was performed; autopsy was not performed. Three patients were lost to follow-up. In the remaining 27 patients, a clinical diagnosis of large-vessel vasculitis was established in 6 (22%) according to the previously mentioned criteria. The average sensitivity and specificity for all definitions are shown in Table 3. All definitions provide high sensitivity and specificity, with the exception of a low specificity for definition (IIa).

Of 6 patients with temporal arteritis, 4 had large artery involvement on FDG-PET/CT according to all observers. Two of these four patients had a negative temporal artery biopsy, whereas one biopsy was inconclusive (not arterial tissue). The two patients with a negative FDG-PET/CT scan, both, had a positive temporal artery biopsy. One of the 7 patients with PMR had large-vessel vasculitis on FDG-PET/CT when using definition (IIa), whereas no large-vessel vasculitis was present using definitions (IIb) and (III).

3.4. External Observers. Table 4 shows the results of the external observers. Definition (IIa) was not used in the external validation because of low specificity in the first analysis. Agreement between the 2 observers was high using definitions (I) and (IIb) and moderate using definition (III). Sensitivity of definition (I) was highest, whereas definitions (IIb) and (III) had the highest specificities.

4. Discussion

Our study suggests a preference for standardized observer criteria for the assessment of large-vessel vasculitis on ^{18}F-FDG-PET/CT images. Among dedicated and experienced observers, assessment of diffuse vascular uptake that exceeds liver uptake provides the highest observer agreement. Additionally, sensitivity and specificity appear to be superior, although the results show considerable overlap in the confidence intervals, at least partly due to the limited number of patients in this study. Among less experienced observers, agreement was more or less similar for standardized criteria (i.e., comparing vascular uptake to liver uptake) versus "first impression." Altogether, standardization of imaging criteria

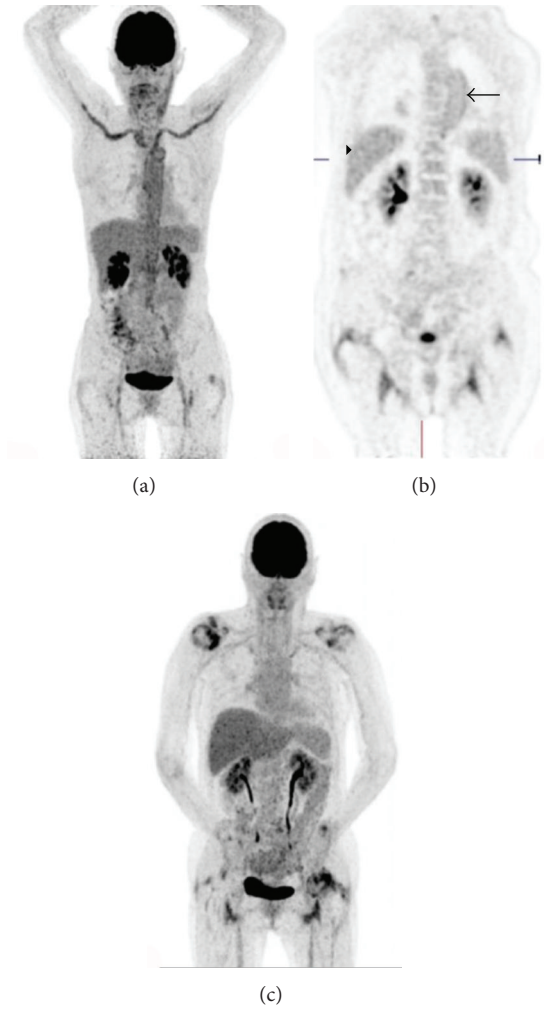

Figure 1: ^{18}F-FDG PET/CT scans showing: (a) Maximum intensity projection (MIP) image: scored as large-vessel vasculitis by all observers according to all methods, (b) coronal image: ^{18}F-FDG uptake in descending aorta (arrow) scored as equal to liver uptake (arrowhead) by 2 observers and lower than liver uptake by 2 other observers, none of the observers scored higher than liver or femoral artery uptake, (c) MIP image of a PMR patient that was scored negative for large-vessel vasculitis by all observers. (Cerebral and urinary tract 18-^{18}F-FDG uptake are physiological).

is equal to or superior to using first impression. In addition, standardization of imaging criteria will undoubtedly facilitate communication, both in clinical practice and in science, bearing in mind the increasing use of FDG-PET/CT in clinical practice and hence the assessment of vascular ^{18}F-FDG uptake by observers with varying degrees of experience.

High interobserver agreement was suggested in two previous studies which also compared vascular uptake with liver uptake [10, 12]. In these observer-blinded studies, only two experienced observers assessed all scans, potentially reducing generalizability of their findings. In addition, only one method was used to assess uptake in these studies. As in most studies, vascular uptake was considered to reflect large-vessel vasculitis when uptake was equal to or higher than liver uptake. Our findings challenge the specificity of this criterion and suggest overestimation of the prevalence of large-vessel vasculitis using this definition. However, misclassification of our control patients cannot be excluded, since our criteria for the clinical diagnosis of large-vessel vasculitis were relatively strict. In addition, it has been suggested that immunosuppressive therapy may attenuate vascular uptake and hence require different interpretation (i.e., loss of sensitivity of definition (IIb)) [23]. Two of our patients (with a clinical diagnosis of temporal arteritis) used prednisone. In both, vascular uptake was not higher than liver uptake (one equal to and one less intense than liver uptake), and they did not fulfil our clinical criteria for large-vessel vasculitis. Regrettably, absence of histological proof, as is virtually always the case, precludes a definitive diagnosis. Finally, most of the earlier studies were performed using a stand-alone ^{18}F-FDG-PET scanner. Modern (i.e., "hybrid") PET/CT scans may be more sensitive, due to attenuation correction, thereby potentially detecting vascular uptake (either resulting from physiological processes, atherosclerosis, or low-grade/subclinical inflammation/vasculitis) in large arteries in "healthy" controls [34].

Our study has some strengths and limitations. One of the strengths is that observer agreement was studied in a group of observers with a varying degree of experience, enhancing the generalizability of the results. Additionally, external validation by nonacademical nuclear medicine physicians confirmed the results, which is important as many studies addressing this topic are performed solely in an academic setting. In clinical practice, FDG-PET/CT scans will be assessed by nuclear medicine physicians or radiologists with a varying amount of clinical experience. The clinical reference standard that we constructed is also a strength of this study. Although we do realise that the definitions we used to establish a clinical diagnosis of large-vessel vasculitis are not universally accepted diagnostic criteria, we at least made a serious attempt to relate imaging tests to a clinical diagnosis. Our proposed criteria incorporate the most important characteristics of GCA (clinical signs and symptoms, inflammation and rapid response to steroids) and a consensus among multiple observers regarding imaging characteristics of vasculitis in large arteries. This approach enabled us to establish that changing the cut-off value for ^{18}F-FDG uptake (higher than liver uptake as opposed to equal to or higher) did not seem to affect sensitivity of the clinical diagnosis but increased specificity. Another strength is the application of different criteria in a single study to investigate whether one definition possesses both high interobserver agreement and diagnostic accuracy. In the current study, vascular wall uptake was also compared with femoral artery uptake, as we have experienced that, in the elderly (i.e., patients over 50 years of age), the femoral artery invariably displays ^{18}F-FDG uptake. It remains to be elucidated whether this results from atherosclerotic plaque inflammation, which is known to be common in the elderly [18], or from physiological activity. Large-vessel vasculitis infrequently involves femoral arteries [17]. Although using vascular wall uptake in the femoral artery as reference has a theoretical drawback of a lower

Table 4: Average number of vasculitis PET/CT scores (individual observer scores), Cohen's kappa, sensitivity, and specificity (95%-CI) according to the different methods applied.

Method	Average vasculitis score (x_1, x_2)	Cohen's kappa	Sensitivity*	Specificity*
(I) First impression	10 (9, 11)	0,85	100% (61–100%)	88% (67–96%)
(IIb) Diffuse uptake, >liver uptake	6 (5, 7)	0,79	83% (46–95%)	100% (84–100%)
(III) Diffuse uptake, >femoral artery uptake	7 (7, 7)	0,63	83% (44–97%)	93% (73–98%)

*The average sensitivity and specificity of the results of the 2 observers (x_1–x_2) were calculated.

sensitivity (when the femoral artery is involved in the disease process, as observed in our study), its specificity and degree of observer agreement render it a good alternative when liver uptake is unclear (e.g., in patients with liver diseases causing nondiffuse liver uptake).

A limitation is the absence of a true reference standard for the diagnosis of large-vessel vasculitis, which would need to be histopathological evidence. Obviously, our clinical diagnosis comprises the test under study which may introduce bias. However, as a "practical gold standard" to establish large-vessel vasculitis is currently not present, we believe that this approach may be a first step towards establishing such a gold standard. We are inclined to think that the criteria we used for a patient to be classified as a large-vessel vasculitis patient were appropriate.

The limited sample size may also be considered a limitation. Although we included patients with inflammation of unknown origin and apparently healthy patients (after follow-up for malignancy) as controls, which further enhances the external validity of our study, the limited size of all groups warrants corroboration in a larger group of similar patients. Finally, it has been suggested that not two but four characteristics might differentiate vasculitis from atherosclerotic plaque inflammation [5]. These include intensity of vascular wall uptake (vasculitis being more intense), distribution pattern (vasculitis being more diffuse and affecting primarily the thoracic arteries, subclavian, and vertebral arteries, whereas atherosclerotic plaque inflammation is supposed to be focal, mainly affecting the abdominal aorta and the iliofemoral arteries), calcification (atherosclerosis patients having more calcification), and quantification of FDG uptake. Our study mainly addressed the first two characteristics. Calcification was also assessed in all patients. However, as 28 of 30 patients displayed calcification on low-dose CT (results not shown) this characteristic was not expected to contribute to differentiation. Moreover, quantitative assessment in patients with atherosclerotic disease has suggested that vascular inflammation is lower in vascular segments showing calcification [35–37], although studies are not unequivocal [38]. Using a semiquantitative approach may help to incorporate calcification in the differentiation between patients with GCA and atherosclerosis [38]. Standardized uptake values (SUVs) may be calculated in regions of interest (ROIs) in the vascular wall (whether SUVmax or SUVmean should be used remains to be established) and in the liver to determine ratios.

5. Conclusion

In conclusion, predefined standardized criteria (comparing vascular uptake to liver uptake) have high interobserver agreement and probably have good diagnostic accuracy for large-vessel vasculitis. All patients with a clinical diagnosis of large-vessel vasculitis displayed diffuse vascular wall uptake higher than liver uptake. We recommend that observers consider scans with these characteristics to be consistent with large-vessel vasculitis when using modern PET/CT scanners. In case of irregular liver uptake, femoral artery uptake may be used as an alternative reference standard, bearing in mind that sensitivity might be slightly lower if the femoral artery is involved in the disease process. Finally, these results may not apply to patients that used steroids prior to the FDG-PET/CT scan. Future studies need to address the effect of steroids on vascular uptake (i.e., establishing time interval between start of steroids and resolution of characteristics on FDG-PET/CT) and the potential value of semiquantitative methods (SUVs).

Conflict of Interests

The authors declare that there is no conflict of interests regarding the publication of this paper.

References

[1] S. Basu, H. Zhuang, D. A. Torigian, J. Rosenbaum, W. Chen, and A. Alavi, "Functional imaging of inflammatory diseases using nuclear medicine techniques," *Seminars in Nuclear Medicine*, vol. 39, no. 2, pp. 124–145, 2009.

[2] J. H. F. Rudd, K. S. Myers, S. Bansilal et al., "Atherosclerosis inflammation imaging with ^{18}F-FDG PET: carotid, iliac, and femoral uptake reproducibility, quantification methods, and recommendations," *Journal of Nuclear Medicine*, vol. 49, no. 6, pp. 871–878, 2008.

[3] M. Fuchs, M. Briel, T. Daikeler et al., "The impact of 18F-FDG PET on the management of patients with suspected large vessel vasculitis," *European Journal of Nuclear Medicine and Molecular Imaging*, vol. 39, no. 2, pp. 344–353, 2012.

[4] K. Kösters, C. P. Bleeker-Rovers, R. van Crevel, W. J. G. Oyen, and A. J. A. M. van der Ven, "Aortitis diagnosed by F-18-fluorodeoxyglucose positron emission tomography in a patient with syphilis and HIV coinfection," *Infection*, vol. 33, no. 5-6, pp. 387–389, 2005.

[5] T. Belhocine, D. Blockmans, R. Hustinx, J. Vandevivere, and L. Mortelmans, "Imaging of large vessel vasculitis with 18FDG PET: illusion or reality? A critical review of the literature data," *European Journal of Nuclear Medicine and Molecular Imaging*, vol. 30, no. 9, pp. 1305–1313, 2003.

[6] S. Prieto-González, P. Arguis, A. García-Martínez et al., "Large vessel involvement in biopsy-proven giant cell arteritis: prospective study in 40 newly diagnosed patients using CT angiography," *Annals of the Rheumatic Diseases*, vol. 71, no. 7, pp. 1170–1176, 2012.

[7] A. Brack, V. Martinez-Taboada, A. Stanson, J. J. Goronzy, and C. M. Weyand, "Disease pattern in cranial and large-vessel giant cell arteritis," *Arthritis & Rheumatology*, vol. 42, no. 2, pp. 311–317, 1999.

[8] P. C. Grayson, K. Maksimowicz-McKinnon, T. M. Clark et al., "Distribution of arterial lesions in Takayasu's arteritis and giant cell arteritis," *Annals of the Rheumatic Diseases*, vol. 71, no. 8, pp. 1329–1334, 2012.

[9] J. C. Henes, M. Müller, J. Krieger et al., "[18F] FDG-PET/CT as a new and sensitive imaging method for the diagnosis of large-vessel vasculitis," *Clinical and Experimental Rheumatology*, vol. 26, no. 3, supplement 49, pp. S47–S52, 2008.

[10] P. Lehmann, S. Buchtala, N. Achajew et al., "18F-FDG PET as a diagnostic procedure in large vessel vasculitis-a controlled, blinded re-examination of routine PET scans," *Clinical Rheumatology*, vol. 30, no. 1, pp. 37–42, 2011.

[11] J. Meller, F. Strutz, U. Siefker et al., "Early diagnosis and follow-up of aortitis with [18F]FDG PET and MRI," *European Journal of Nuclear Medicine and Molecular Imaging*, vol. 30, no. 5, pp. 730–736, 2003.

[12] M. A. Walter, R. A. Melzer, C. Schindler, J. Müller-Brand, A. Tyndall, and E. U. Nitzsche, "The value of [^{18}F]FDG-PET in the diagnosis of large-vessel vasculitis and the assessment of activity and extent of disease," *European Journal of Nuclear Medicine and Molecular Imaging*, vol. 32, no. 6, pp. 674–681, 2005.

[13] D. Coggon, C. Martyn, K. T. Palmer, and B. Evanoff, "Assessing case definitions in the absence of a diagnostic gold standard," *International Journal of Epidemiology*, vol. 34, no. 4, pp. 949–952, 2005.

[14] K.-J. D. F. Lensen, A. E. Voskuyl, C. J. van der Laken et al., "18F-fluorodeoxyglucose positron emission tomography in elderly patients with an elevated erythrocyte sedimentation rate of unknown origin," *PLoS ONE*, vol. 8, no. 3, Article ID e58917, 2013.

[15] G. G. Hunder, D. A. Bloch, B. A. Michel et al., "The American College of Rheumatology 1990 criteria for the classification of giant cell arteritis," *Arthritis and Rheumatism*, vol. 33, no. 8, pp. 1122–1128, 1990.

[16] R. Boellaard, M. J. O'Doherty, W. A. Weber et al., "FDG PET and PET/CT: EANM procedure guidelines for tumour PET imaging: version 1.0," *European Journal of Nuclear Medicine and Molecular Imaging*, vol. 37, no. 1, pp. 181–200, 2010.

[17] T. A. Kermani, E. L. Matteson, G. G. Hunder, and K. J. Warrington, "Symptomatic lower extremity vasculitis in giant cell arteritis: a case series," *The Journal of Rheumatology*, vol. 36, no. 10, pp. 2277–2283, 2009.

[18] D. M. Nuenninghoff, G. G. Hunder, T. J. H. Christianson, R. L. McClelland, and E. L. Matteson, "Mortality of large-artery complication (aortic aneurysm, aortic dissection, and/or large-artery stenosis) in patients with giant cell arteritis: a population-based study over 50 years," *Arthritis & Rheumatism*, vol. 48, no. 12, pp. 3532–3537, 2003.

[19] J. R. Landis and G. G. Koch, "The measurement of observer agreement for categorical data," *Biometrics*, vol. 33, no. 1, pp. 159–174, 1977.

[20] R Foundation for Statistical Computing, *R: A Language and Environment for Statistical Computing*, R Foundation for Statistical Computing, Vienna, Austria, 2012.

[21] D. Blockmans, S. Stroobants, A. Maes, and L. Mortelmans, "Positron emission tomography in giant cell arteritis and polymyalgia rheumatica: evidence for inflammation of the aortic arch," *American Journal of Medicine*, vol. 108, no. 3, pp. 246–249, 2000.

[22] D. Blockmans, C. L. De, S. Vanderschueren, D. Knockaert, L. Mortelmans, and H. Bobbaers, "Repetitive ^{18}F-fluorodeoxyglucose positron emission tomography in giant cell arteritis: a prospective study of 35 patients," *Arthritis & Rheumatism*, vol. 55, no. 1, pp. 131–137, 2006.

[23] N. D. Papathanasiou, Y. Du, L. J. Menezes et al., " ^{18}F-Fludeoxyglucose PET/CT in the evaluation of large-vessel vasculitis: diagnostic performance and correlation with clinical and laboratory parameters," *The British Journal of Radiology*, vol. 85, no. 1014, pp. e188–e194, 2012.

[24] M. Brodmann, R. W. Lipp, A. Passath, G. Seinost, E. Pabst, and E. Pilger, "The role of 2-^{18}F-fluoro-2-deoxy-D-glucose positron emission tomography in the diagnosis of giant cell arteritis of the temporal arteries," *Rheumatology (Oxford)*, vol. 43, no. 2, pp. 241–242, 2004.

[25] A. K. Scheel, J. Meller, R. Vosshenrich et al., "Diagnosis and follow up of aortitis in the elderly," *Annals of the Rheumatic Diseases*, vol. 63, no. 11, pp. 1507–1510, 2004.

[26] M. Both, K. Hmadi-Simab, M. Reuter et al., "MRI and FDG-PET in the assessment of inflammatory aortic arch syndrome in complicated courses of giant cell arteritis," *Annals of the Rheumatic Diseases*, vol. 67, no. 7, pp. 1030–1033, 2008.

[27] C. Agard, J. H. Barrier, B. Dupas et al., "Aortic involvement in recent-onset giant cell (temporal) arteritis: a case-control prospective study using helical aortic computed tomodensitometric scan," *Arthritis & Rheumatism*, vol. 59, no. 5, pp. 670–676, 2008.

[28] I. Marie, A. Proux, P. Duhaut et al., "Long-term follow-up of aortic involvement in giant cell arteritis: a series of 48 patients," *Medicine (Baltimore)*, vol. 88, no. 3, pp. 182–192, 2009.

[29] W. A. Schmidt, A. Natusch, D. E. Moller, K. Vorpahl, and E. Gromnica-Ihle, "Involvement of peripheral arteries in giant cell arteritis: a color Doppler sonography study," *Clinical and Experimental Rheumatology*, vol. 20, no. 3, pp. 309–318, 2002.

[30] W. A. Schmidt, A. Seifert, E. Gromnica-Ihle, A. Krause, and A. Natusch, "Ultrasound of proximal upper extremity arteries to increase the diagnostic yield in large-vessel giant cell arteritis," *Rheumatology (Oxford)*, vol. 47, no. 1, pp. 96–101, 2008.

[31] M. E. De, C. Castillo, A. Rodriguez, and J. J. De Agustin, "Learning and reliability of colour Doppler ultrasound in giant cell arteritis," *Clinical and Experimental Rheumatology*, vol. 27, no. 1, supplement 52, pp. S53–S58, 2009.

[32] J. Narvaez, J. A. Narvaez, J. M. Nolla, E. Sirvent, D. Reina, and J. Valverde, "Giant cell arteritis and polymyalgia rheumatica: usefulness of vascular magnetic resonance imaging studies in the diagnosis of aortitis," *Rheumatology (Oxford)*, vol. 44, no. 4, pp. 479–483, 2005.

[33] M. Koenigkam-Santos, P. Sharma, B. Kalb et al., "Magnetic resonance angiography in extracranial giant cell arteritis," *Journal of Clinical Rheumatology*, vol. 17, no. 6, pp. 306–310, 2011.

[34] K. M. Mäki-Petäjä, M. Elkhawad, J. Cheriyan et al., "Anti-tumor necrosis factor-α therapy reduces aortic inflammation and stiffness in patients with rheumatoid arthritis," *Circulation*, vol. 126, no. 21, pp. 2473–2480, 2012.

[35] A. L. Figueroa, S. S. Subramanian, R. C. Cury et al., "Distribution of inflammation within carotid atherosclerotic plaques with high-risk morphological features a comparison between positron emission tomography activity, plaque morphology, and histopathology," *Circulation: Cardiovascular Imaging*, vol. 5, no. 1, pp. 69–77, 2012.

[36] J. H. F. Rudd, K. S. Myers, S. Bansilal et al., "Relationships among regional arterial inflammation, calcification, risk factors, and biomarkers: a prospective fluorodeoxyglucose positron-emission tomography/computed tomography imaging study," *Circulation: Cardiovascular Imaging*, vol. 2, no. 2, pp. 107–115, 2009.

[37] S. S. Silvera, H. E. Aidi, J. H. F. Rudd et al., "Multimodality imaging of atherosclerotic plaque activity and composition using FDG-PET/CT and MRI in carotid and femoral arteries," *Atherosclerosis*, vol. 207, no. 1, pp. 139–143, 2009.

[38] A. Rominger, T. Saam, S. Wolpers et al., "18F-FDG PET/CT identifies patients at risk for future vascular events in an otherwise asymptomatic cohort with neoplastic disease," *Journal of Nuclear Medicine*, vol. 50, no. 10, pp. 1611–1620, 2009.

Hindawi Publishing Corporation
BioMed Research International
Volume 2015, Article ID 509295, 11 pages
http://dx.doi.org/10.1155/2015/509295

Research Article

Sustained Macrophage Infiltration upon Multiple Intra-Articular Injections: An Improved Rat Model of Rheumatoid Arthritis for PET Guided Therapy Evaluation

Durga M. S. H. Chandrupatla,[1] Karin Weijers,[1] Yoony Y. J. Gent,[1] Inge de Greeuw,[2] Adriaan A. Lammertsma,[2] Gerrit Jansen,[1] Conny J. van der Laken,[1] and Carla F. M. Molthoff[2]

[1] *Department of Rheumatology, VU University Medical Center, De Boelelaan 1117, 1081 HV Amsterdam, The Netherlands*
[2] *Department of Radiology & Nuclear Medicine, VU University Medical Center, De Boelelaan 1117, P.O. Box 7057, 1007 MB, 1081 HV Amsterdam, The Netherlands*

Correspondence should be addressed to Carla F. M. Molthoff; cfm.molthoff@vumc.nl

Received 6 June 2014; Revised 27 August 2014; Accepted 7 September 2014

Academic Editor: Filippo Galli

To widen the therapeutic window for PET guided evaluation of novel anti-RA agents, modifications were made in a rat model of rheumatoid arthritis (RA). Arthritis was induced in the right knee of Wistar rats with repeated boosting to prolong articular inflammation. The contralateral knee served as control. After immunization with methylated bovine serum albumin (mBSA) in complete Freund's adjuvant and custom Bordetella pertussis antigen, one or more intra-articular (i.a.) mBSA injections were given over time in the right knee. Serum anti-mBSA antibodies, DTH response, knee thickness, motion, and synovial macrophages were analyzed and [18F]FDG(-general inflammation) and (*R*)-[11C]PK11195 (macrophages-)PET was performed followed by *ex vivo* tissue distribution. Significant anti-mBSA levels, DTH, swelling of arthritic knee, and sustained and prolonged macrophage infiltration in synovial tissue were found, especially using multiple i.a. injections. Increased [18F]FDG and (*R*)-[11C]PK11195 accumulation was demonstrated in arthritic knees as compared to contralateral knees, which was confirmed in *ex vivo* tissue distribution studies. Boosting proved advantageous for achieving a chronic model without remission. The model will offer excellent opportunities for repeated PET studies to monitor progression of disease and efficacy of novel therapeutic agents for RA in the same animal.

1. Introduction

Rheumatoid arthritis (RA) is an autoimmune disease that results in chronic and systemic inflammation of the joints, affecting approximately 0.5–1% of the adult population [1]. It is characterized by inflammation of the joints resulting in synovial hyperplasia by infiltration of immune cells further leading to cartilage and bone destruction [2]. Timely recognition of RA will allow for earlier start of therapy preventing more severe expansion of the disease. Moreover, several studies have shown that tight control as a treatment strategy in individual RA patients seems promising in achieving predefined level of low disease activity or preferably remission within a reasonable period of time [3, 4]. To this end, noninvasive imaging modalities may serve as sensitive and accurate tools for assessment and monitoring of disease activity during therapy to evaluate therapeutic efficacy.

Positron emission tomography (PET) is a promising noninvasive imaging modality that can be used to visualize active arthritis at a molecular level in RA [5] via targeting macrophages [6, 7]. Most human studies targeting macrophages by PET have been performed with the macrophage tracer (*R*)-[11C]PK11195 in various inflammatory diseases [8]. (*R*)-[11C]PK11195 targets the 18-kd translocator protein (formerly known as peripheral benzodiazepine

Table 1: Arthritis induction in rat: variations of the original model to the modified groups.

Code group	Original	Group A	Group B	Group C	Group D	Group E (control)	Group F (control)
Number of boost	No	No	No	3	5	No	No
Sacrificed (days post)	6	6	28	19	28	6	28
1st immunization (mBSA/CFA/CBP antigen)*							
No. of rats	11	3	4	3	6	4	4
Volume (μL)	200	200	200	200	200	200	200
Administration route	s.c.	s.c.	s.c.	s.c.	s.c.	s.c.	s.c.
Administration location	Tail base	Tail base	Tail base	Tail base	Tail base	Tail base	Tail base
2nd immunization (mBSA/CFA/CBP antigen)*							
Volume (μL)	200	100	100	100	100	100	100
Administration route	s.c.	s.c.	s.c.	s.c.	s.c.	s.c.	s.c.
Administration location	Tail base	Neck and upper flank	Neck and upper flank	Neck and upper flank	Neck and upper flank	Neck and upper flank	Neck and upper flank
Delayed time hypersensitivity (DTH) CBP antigen							
Volume (μL)**		25	25	25	25	25	25
Route	s.c.	s.c.	s.c.	s.c.	s.c.	s.c.	s.c.
Administration site	Right ear	Right ear	Right ear	Right ear	Right ear	Right ear	Right ear
	Local (i.a.) arthritis induction (mBSA)					Saline	
i.a. injection (mBSA*** or saline)	1	1	1	1	1	1	1
mBSA#, boost i.a. injections	0	0	0	3	5	0	0
Injected volume (μL)	20	60	60	60	60	60	60
Route	i.a.	i.a.	i.a.	i.a.	i.a.	i.a.	i.a.
Administration site	knee joint	knee joint	knee joint	knee joint	knee joint	knee joint	knee joint

*50 mg mBSA in 1 mL 0.9% NaCl emulsified with an equal volume of complete Freund's adjuvant antigen (CFA) and custom Bordetella pertussis (CBP) antigen (1×10^{11} cells/mL), **CBP antigen (2.7×10^{10} cells/mL 0.9% NaCl), ***10 mg mBSA in 1 mL 0.9% NaCl, and #1 mg mBSA in 1 mL 0.9% NaCl.

receptor) a mitochondrial membrane protein that is upregulated in activated macrophages [8]. Histological studies have shown that macrophages are an important biomarker for prediction and monitoring of therapeutic effects of a wide range of disease modifying antirheumatic drugs and biologics [9, 10]. Jahangier et al. demonstrated a clear positive clinical effect in RA patients after intra-articular treatment with Yttrium-90 and glucocorticoids correlating effect with a decrease in total numbers of macrophages [11].

Animal models can be applied for in vivo evaluation of efficacy of new therapeutic agents for RA [12]. As it takes some time for most antirheumatic drugs to read out their mode of action on arthritis activity with macrophage infiltration as a biomarker, a chronic RA animal model is required with sustained arthritis activity characterized by macrophage infiltration in synovial tissue. As currently no suitable rat model is available that would allow noninvasive macrophage PET guided evaluation of the therapeutic agents, we have optimized an antigen induced model with persistent arthritis in rats offering sufficiently sized inflamed joints to enable quantitative measurements of PET tracer uptake in inflamed joints as well as the opportunity for comparison to contralateral noninflamed control joints within the same animals.

2. Materials and Methods

2.1. Animals. Wistar rats (male, 150–200 grams, Charles River International Inc, Sulzfeld, Germany) were provided with standard food (16% protein rodent diet, Harlan Laboratories Inc., Madison, WI, USA) and water *ad libitum*. Rats were housed in groups of three or four in conventional cages and kept in a room with a 12-hour light/dark cycle and constant room temperature (21°C) and humidity level (50%). All animal experiments were carried out in accordance with the Dutch law on animal experimentation and were approved by the VU Medical Center Institutional Committee on Animal Experimentation.

2.2. Antigen Induced Rat Model. As reference in this paper, the methylated bovine serum albumin (mBSA) induced rat model as described by Van De Putte et al. [13] and Dijkstra et al. [14] was applied (Table 1), indicated hereafter as "original model." In short, according to the descriptions of the original model, rats were immunized subcutaneously (s.c.) twice at days 0 and 7 with an emulsion containing mBSA (Sigma-Aldrich Chemie BV, Zwijndrecht, The Netherlands) dissolved with complete Freund's adjuvant (CFA) (Sigma Aldrich, Steinheim, Germany) and custom *Bordetella pertussis* (CBP) antigen (Becton Dickinson, Breda, The Netherlands) [14]. Rats were immunized with two administrations of 200 uL solution containing 50 mg mBSA in 1 mL 0.9% NaCl emulsified with an equal volume of complete Freund's adjuvant antigen (CFA) and custom *Bordetella pertussis* (CBP) antigen (1×10^{11} cells/mL). Both the first and the second immunization were performed in the tail base. At day 21, local arthritis was induced by injecting 20 μL mBSA solution containing 10 mg mBSA [15] in 1 mL 0.9% NaCl intra-articular (i.a.) in the right knee (RA knee); the contralateral left knee served as an internal control (Con-RA). The i.a. injection was situated between femur and tibia and behind the patella tendon.

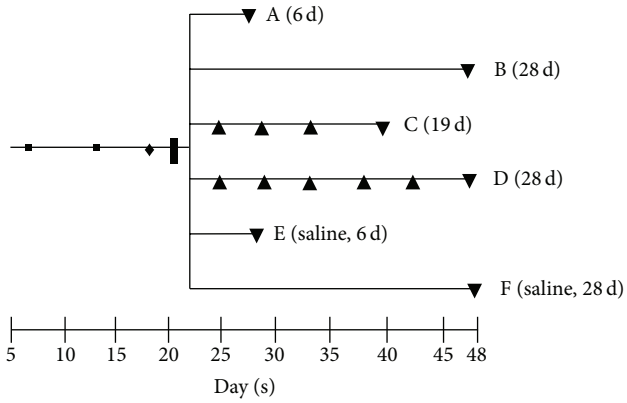

Figure 1: Time line of RA rat model. 1st (■) and 2nd (■) immunization, DTH (♦), i.a. injection (▮), boost i.a. injections (▲), PET and/or, ex vivo tissue distribution, and (immuno-) histopathology of groups A (6 d), B (28 d), C (19 d), D (28 d), E (saline, 6 d), and F (saline, 28 d) (▼).

2.3. Modifications of Original Rat Model. Three modifications were performed as compared to the original model (Table 1). At first, the second immunization (initially 200 uL in the original model) step was adapted. To minimize animal discomfort by multiple immunizations at a single location (as was performed in the original model), of second immunization was divided into two injections with one in the neck and one in the upper flank (away from the knees) with each injection consisting a volume of 100 uL. Secondly, the i.a. injection volume of mBSA was increased to 60 uL while in the original it was 20 uL. Both modifications were applied in groups A, B, C, and D.

The last modification comprised repeated i.a. injections (resp., 3x (group C) and 5x (group D)) while in group A and B no boosts were applied. The difference between groups A and B was the sacrificing day: 6 and 28 days after i.a. injection for groups A and B, respectively (Figure 1). Control rats received an i.a. injection in the right knee with sterile physiological saline instead of mBSA. Subgroups of control rats were sacrificed at 6 (group E) and 28 (group F) days, respectively.

2.4. Validation Experiments

(i) Examination of Immunization Status

Serum Levels of Anti-MBSA. Blood samples before and after the immunization procedure were obtained from the tail vein with a Microvette (cb300, Sarstedt BV, Etten-Leur, The Netherlands). After centrifugation at room temperature (5 min/2500 ×g), serum samples were stored at −80°C until use. Anti-mBSA levels were determined by ELISA [16]. Briefly, 96-well microplates (Greiner bio-one, Alphen a/d Rijn, The Netherlands) were precoated overnight with 100 μL/well of 5 μg mBSA/mL phosphate buffered saline (PBS) at 37°C. After washing with PBS (100 μL/well, 5 times) wells were blocked with 0.1% gelatin (Baker Chemical Co, Austin, Texas, USA) in PBS for 30 minutes at 37°C. Subsequently, 1 : 100, 1 : 200, and 1 : 400 diluted serum samples were added and incubated for 1 hour at room temperature. After washing with PBS, horseradish peroxidase (HRP) labeled to rabbit-anti-rat (RαR) IgG1 antibody 1 : 1000 (Invitrogen, NY, USA) was added to the wells and incubated for 2 hrs at room temperature. Enzyme reaction was visualized with 0.8 mg aminosalicylic acid (Sigma-Aldrich Chemie BV, Zwijndrecht, The Netherlands) and 0.5 μL of 30% hydrogen peroxide (H_2O_2) dissolved in 1 mL distilled water. Absorption at 450 nm was measured using an ELISA reader (Tecan, Spectra Fluor, MTX Labsystems, Inc, Vienna, USA).

Delayed Type Hypersensitivity Test (DTH). At day 19, immunization status was examined by DTH [17, 18] response. CBP antigen (25 μL, 2.7×10^{10} cells/mL 0.9% NaCl) was injected s.c. in the right ear of the rat. The left ear served as an internal control. A control group of rats was injected with sterile physiological saline in the left ear. Subsequently, ear thickness was measured at 0, 6, 24, and 48 hours after injection using a digital micrometer.

(ii) Macroscopic Evaluation of Arthritis Activity. Macroscopic evaluation of the severity of arthritis was assessed by knee measurements prior to (at the same day) every i.a. injection. In between, knees were measured 3 times a week until rats were sacrificed. Knees were measured by caliper measurement of knee thickness in mediolateral direction.

2.5. Histopathology and Immunohistochemistry. Both knees were dissected *in toto* and fixed for 7 days at 4°C in 10% freshly made paraformaldehyde in PBS with 2% sucrose (pH = 7.3) prior to decalcification in 123 mM sodium ethylenediaminetetraacetic acid (Na_2-EDTA·$2H_2O$) (Merck, Darmstadt, Germany) and 113 mM sodium hydroxide (NaOH) (Sigma-Aldrich Chemie BV, Zwijndrecht, The Netherlands) (pH = 7.2) for ~5.5 weeks at 4°C. Decalcified knees were rinsed for 24 hours in 2% sucrose (Sigma-Aldrich Chemie BV, Zwijndrecht, The Netherlands) in PBS (pH = 7.2) and 24 hours in 2% sucrose in PBS and 50 mM NH_4Cl (Sigma-Aldrich Chemie BV, Zwijndrecht, The Netherlands) (pH = 7.1). Thereafter, knees were embedded in paraffin. Sections of 5 μm were cut through the center of the joint in longitudinal direction and stained with haematoxylin and eosin to assess the degree of inflammation in synovial tissue.

Immunohistochemical localization of rat macrophages was determined by a mouse anti-rat monoclonal antibody ED1 (HM3029, Hycult, PA, USA) a lysosomal membrane related antigen on rat macrophages and by a mouse anti-rat monoclonal antibody ED2 (MCBI,VU University Medical Center, Amsterdam) cell surface glycoprotein related antigen on rat macrophages [19]. An IgG1 isotype antibody (HI1016, Hycult, PA, USA) was used as negative control antibody. Briefly, after antigen retrieval with a solution of 0.1% pepsin (Sigma-Aldrich Chemie BV, Zwijndrecht, The Netherlands) with 0.1% of HCl 37% in PBS per slide for 30 min at 37°C, sections were incubated for 1 h with 1 : 100 diluted ED1, ED2, or isotype control antibody in 0.1% BSA/PBS for a period of 1 h. The detection EnVision kit (K4063 dual-link-HRP

rabbit/mouse, DAKO, Glostrup, UK) was used according to instructions of the manufacturer for a period of 30 min. After washing with PBS, slides were stained for peroxidase activity with 3.3′-diaminobenzidine tetrahydrochloride (DAB) containing 0.01% H_2O_2. Subsequently, sections were counterstained with haematoxylin, dehydrated, and mounted. Negative controls were included by replacement of the primary antibody with an isotype specific control antibody. Images were captured using a Leica 4000B microscope and Leica digital camera DC500 (Microsystems B.V. Rijswijk, The Netherlands).

2.6. PET and Ex Vivo Tissue Distribution Studies. [18F]FDG with a radiochemical purity of >97% was purchased from BV Cyclotron VU (Amsterdam, The Netherlands). (*R*)-[11C]PK11195 was synthesized as described previously [20], with radiochemical purity of >98% and a mean specific activity of 95.7 ± 28.4 GBq/μmol. Rats were anesthetized using inhalation anesthetics (isoflurane 2–2.5% and oxygen 0.45 volume %). The jugular vein was cannulated with a polyurethane 3 French cannula. During all procedures vital body signs like, body temperature, heartbeat, respiratory rate, and blood oxygen saturation were monitored continuously using a rectal temperature probe and pulse oxygen meter with SpO_2 sensor. Anesthetized rats were positioned in a double-layer LSO high resolution research tomograph (HRRT) (Siemens/CTI, Knoxville, TN, USA), a small animal, and human brain 3D scanner with high spatial resolution (2.3–3.4 mm full width at half maximum) and high sensitivity [21]. First, a 6-minute transmission scan was acquired using a 740 MBq ^{137}Cs rotating point source. Next, [18F]FDG (21.1 ± 5.1 MBq) or (*R*)-[11C]PK11195 (10.5 ± 2.9 MBq) was administered i.v. through the cannula and a dynamic emission scan of 1 hour was acquired. PET data were normalized and corrected for scatter, random, attenuation, decay, and dead time. Data were acquired in 64-bit list mode and converted into 16 sinograms with frame durations increasing from 15 up to 300 seconds. Images were reconstructed using an iterative 3D ordinary Poisson ordered-subsets expectation-maximization (OSEM) algorithm with 8 iterations and 16 subsets and a matrix size of 256 × 256 × 207, resulting in a cubic voxel size of 1.21 × 1.21 × 1.21 mm^3. PET images were made of rats from the original model and of rats in group A. Sixty minutes after PET scanning, rats were sacrificed and knees, blood, and various tissues were excised and weighed and the amount of radioactivity was determined using an LKB 1282 Compugamma CS gamma counter (LKB, Wallac, Turku, Finland). Rats without PET scanning (groups B–E) were sacrificed 60 minutes after tracer injection followed by ex vivo tissue biodistribution. Results were expressed as percentage of the injected dose per gram tissue (%ID/g). PET images were analyzed using AMIDE software (Amide's Medical Image Data Examiner, version 0.9.2) [22]. Fixed size ellipsoidal shaped regions of interest (ROI) (dimensions: 6.0 × 17.7 × 7.4 mm^3) were manually drawn over the area of the left and right knees in the last frame of the image. ROIs were projected onto the dynamic image sequence, and time-activity curve (TAC) data were extracted. TACs were expressed as standardized uptake values (SUV): mean ROI radioactivity concentration normalized for injected dose and body weight [7].

2.7. Statistical Analysis. Statistical tests were performed using IBM SPSS version 20. A one-sample Kolmogorov-Smirnov test was to test for normal distribution taking (P value) criteria for t-test. A Wilcoxon signed rank (exact) test was used to determine differences between paired observations (e.g., tracer uptake in right versus Con-RA knee, thickness of the antigen-induced versus control ear, and mediolateral thickness of RA knee versus Con-RA knee). A Mann-Whitney (exact) test was used to determine differences in absorbance before and after immunization. A P value <0.05 was considered statistically significant. A Bonferroni correction was applied when necessary.

3. Results

During the entire study, no major change in body weight was observed and knee functionality was never dramatically impaired during the course of the induction of arthritis in the RA knee of the rats.

3.1. Immunization Status. All rats showed a significant increase ($P < 0.001$) in the level of mBSA antibody titers as comp ared with mBSA levels before immunization (Figure 2(a)).

In addition, a DTH test was executed and all rats showed a good DTH response with a significant ($P = 0.001$) increase in ear thickness of the right ear at 6, 24, and 48 hours after injection compared with the control left ear (Figure 2(b)) and compared to control rat ear's injected with saline (data not shown).

3.2. Arthritis Evaluation of No-Boost Model. As negative control, healthy rat knee sections, stained with the ED1 and ED2 rat macrophage specific antibodies, showed no signs of inflammation in the synovial tissue (Figure 3, left panels). Some macrophages were found in the single layered synovial lining. In contrast, the RA knees of the rats in the firstly adapted no-boost group (group A, 0x boost panels) showed a moderate influx of inflammatory cells in the synovium with a hyperplasia of synovial tissue consisting of 3-4 layers.

PET tracer [18F]FDG uptake in the RA knees of rats from group A was also low and showed no obvious difference as compared to the Con-RA knees, as shown in Figure 5(a).

3.3. Arthritis Evaluation of the Modifications in the Rat Model

3.3.1. Macroscopic Evaluation of Arthritis Activity. In the no-boost group A, a significant difference was observed in knee thickness between the RA knees compared to the Con-RA knees ($P = 0.01$), which persisted until day 6 after i.a. injection ($P = 0.01$) (Figure 2(c)). In the no-boost group followed for 28 days (group B, Figure 2(c)), differences between the RA versus Con-RA knee were significant ($P = 0.001$) at day 4 but gradually decreased ($P = 0.1$) in 28 days. Continued observation without boosting demonstrated that the RA knee thickness decreased significantly ($P < 0.0001$) between 6 and 28 days (group A versus group B). Although

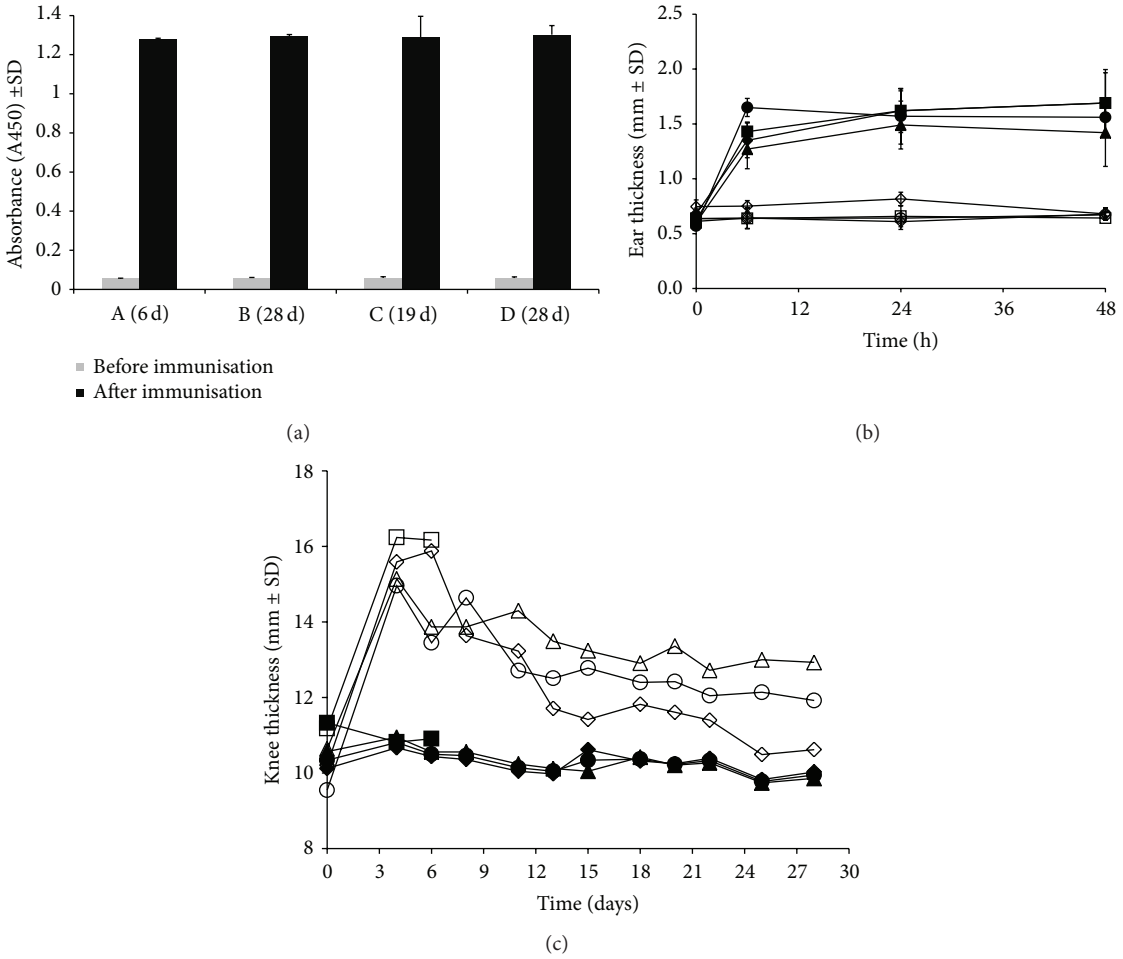

Figure 2: (a) Measurement of anti-mBSA in serum in rats before immunization (left) and after immunization (right) ($P < 0.001$). (b) Caliper measurement of right ear swelling of (■) A (6 d); (♦) B (28 d); (●) C (19 d); (▲) D (28 d), compared to the control ear of (□) A (6 d); (◊) B (28 d); (○) C (19 d); (△) D (28 d), as a response to s.c. injection of antigen ($P < 0.001$). (c). Knee thickness of arthritic knee of (□) A (6 d); (◊) B (28 d); (○) C (19 d); (△) D (28 d), compared to control Con-RA knee of (■) A (6 d); (♦) B (28 d); (●) C (19 d); (▲) D (28 d). All results depicted represent mean ± SD.

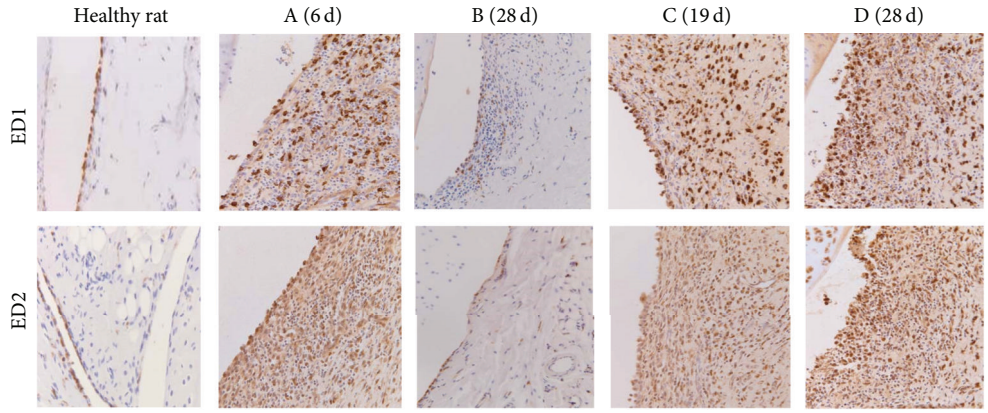

Figure 3: Immunohistochemistry. Images (200x) of ED1 (upper panel) and ED2 (lower panel) staining in knees of healthy rats (left panel; limited amounts of macrophages); knees from rats in the no boost groups (A (6 d) and B (28 d)); showing clear influx of positively stained ED1 and ED2 macrophages in the inflamed synovium; knees from rats in the boost groups C (19 d) and D (28 d); showing strong influx of positively stained ED1 and ED2 macrophages in the multilayered synovial linings.

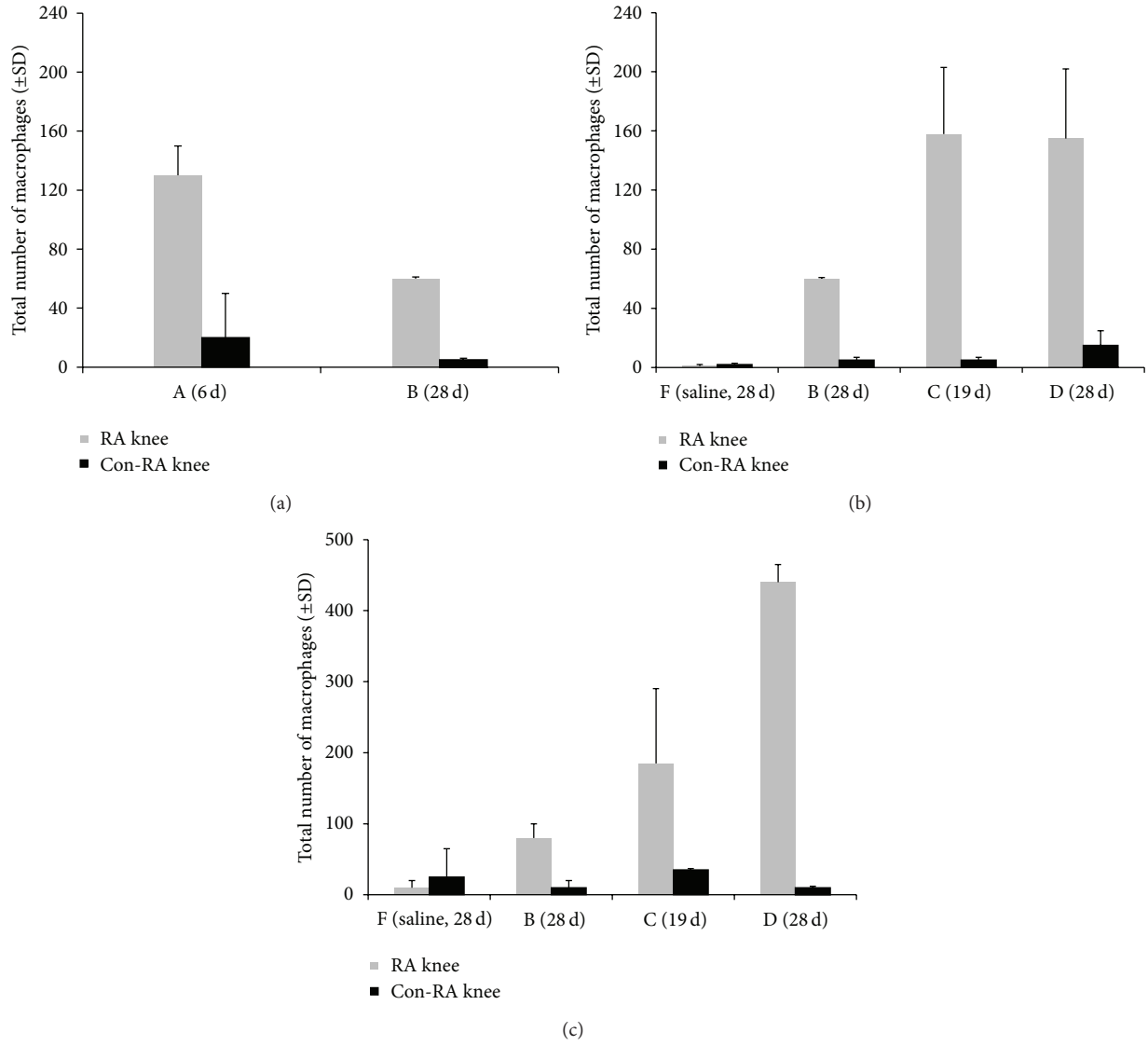

Figure 4: Macrophage counting in histological knee sections. (A) Total number (±SD) of ED1 positive macrophages in the lining and sublining of the knee synovial tissue from the no boost rats (A (6 d) and B (28 d)); RA knee, light grey bars, Con-RA knee, black bars. (B) Total number (±SD) of ED1 positive macrophages in the lining and sublining of the knee synovial tissue from the groups B (28 d), C (19 d), and D (28 d) are added next to saline control rats group F (28 d). (C (19 d)) Total number (±SD) of ED2 positive macrophages in the lining and sublining of the knee synovial tissue from the groups B (28 d), C (19 d), and D (28 d) are added next to saline control rats group F (28 d).

significantly decreased in size, the knee thickness did not normalize completely at 28 days when compared to the Con-RA knees of the same rats.

When the rats were dosed with 3 boost injections (group C) significant differences were found in knee thickness of the RA versus Con-RA knee ($P = 0.002$ and $P = 0.003$ at day 4 as well as at the sacrificing day, resp.). In the group of rats dosed with 5 boost injections (group D), also significant differences were observed between the RA and Con-RA knees ($P = 0.0001$ and $P < 0.0001$ at days 4 and 28, resp.).

Comparing the boost groups C and group D (3x and 5x boosts) on the day those rats were sacrificed, a significant difference in RA knee thickness was observed, with group C < group D ($P = 0.024$). Comparing group A (no boost) with both boost groups (C and D) with respect to RA knee measurements, significant differences were observed (group A versus group C and group A versus group D: $P = 0.003$ and $P < 0.0001$, resp.).

3.3.2. Immunohistochemistry. As shown in Figure 3, synovial tissue of healthy rat knees showed no signs of inflammation (Figure 3, left panel) and RA knees in group A (no boost) showed a moderate influx of inflammatory cells in the synovium with a hyperplasia of synovial tissue consisting of 3-4 layers. In contrast, the representative images of the knees from rats in group C and group D demonstrated a clear increase in ED1 and ED2 positively stained macrophages and multilayered synovial tissue (>5; see also next paragraph).

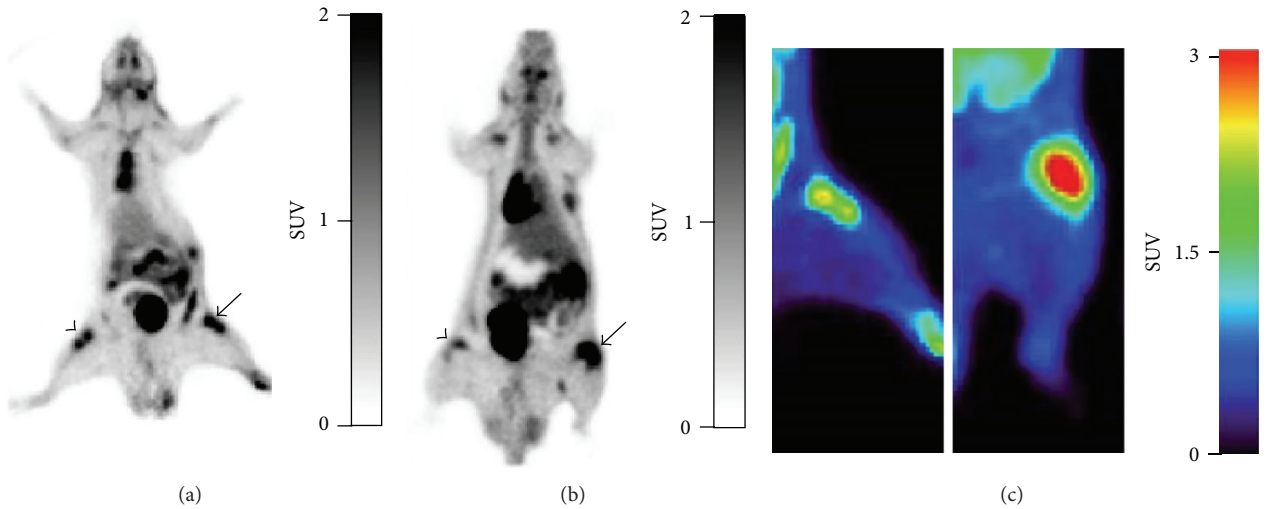

Figure 5: Representative coronal PET images of (a) [18F]FDG and (b) *(R)*-[11C]PK11195 in arthritic rats group A (6 d). Uptake of both tracers is clearly shown in the right arthritic knee (arrow) compared with the contralateral knee (arrowhead). (c) PET images of [18F]FDG uptake in arthritic rats, original model (left) and group A (6 d) (right).

The infiltration of macrophages was quantified in the different groups of rats (between 2 and 4 rats per group). In Figure 4(a), the results for ED1 positive macrophages in group A and group B are shown. In comparison to group A, group B showed significantly lower numbers of ED1+ macrophages ($P = 0.028$) (but still significantly higher than the control group F ($P < 0.0001$)). In Figure 4(b) (ED1) and Figure 4(c) (ED2), the ED1 and ED2 positive macrophages in knees of rats in all groups are represented, including rats injected with saline (showing very low numbers of macrophages). On comparing those numbers in group C and group B, RA knees from rats in group C clearly displayed more ED1 and ED2 positive macrophages. For those in group D an even higher amount of ED2+ macrophages was found as compared to the no-boost groups (Figure 4(c)). In Figure 3, representative images of ED1 and ED2 staining sections of different groups are shown.

PET and Ex Vivo Tissue Distribution Studies. The feasibility of PET evaluation of arthritis activity in the rats of group A (0x boost) as compared to the original model was assessed. Figures 5(a) and 5(b) show representative [18F]FDG and *(R)*-[11C]PK11195 images. The uptake of [18F]FDG in the RA knee of the group A was clearly higher than that in the original model (Figure 5(c), left; original model). Time-activity curves (SUV versus time after tracer injection) of the tracers up to 6 days are depicted in Figure 6. The SUV in the RA knee as compared to the Con-RA knee for [18F]FDG in group A rats was significantly increased (2.78 ± 0.366 versus 1.38 ± 0.189; $P = 0.001$; Figure 6(a)) and the ratio of uptake in the RA knee was 2 times higher than the Con-RA knee (Figure 6(c)). The SUV for *(R)*-[11C]PK11195 (Figure 6(b)) also increased in the RA knee (2.00 ± 0.55 versus 1.11 ± 0.45) and the ratio in the RA knee uptake is 1.8 times more than the Con-RA knee in group A (Figure 6(c)).

After PET, ex vivo tissue distribution of group A rats was performed and both [18F]FDG and *(R)*-[11C]PK11195 (Figure 7) showed increased accumulation in the RA knee (1.6 and 1.4 times higher, resp.) compared to uptake in Con-RA knee [18F]FDG and *(R)*-[11C]PK11195 (0.52 ± 0.06 and 0.79 ± 0.05 in RA knees; 0.33 ± 0.04 and 0.57 ± 0.05, resp.). Furthermore, both tracers showed increased uptake in macrophage rich tissues such as spleen, liver, and bone (marrow). Moreover, increased uptake of *(R)*-[11C] PK11195 in the heart could be related to TSPO expression on myocardial cells. Both tracers showed accumulation in the intestinal system and renal system (Figure 7) due to excretion of the tracers via hepatobiliary and renal route. Physiological uptake of [18F]FDG was noted in heart and brain tissue.

Results from the ex vivo tissue distribution one hour after injection of *(R)*-[11C] PK11195 in the no-boost groups (A and B) and the boost groups C and D are depicted in Figure 8. For all groups, extra-articular tracer uptake was again observed in macrophage rich tissue and physiological uptake in the intestines.

No-boost groups (A and B) (Figure 8(a)): a 1.45 times higher uptake of *(R)*-[11C] PK11195 was measured in group A between the RA and Con-RA knee. In group B, a 1.2 times higher uptake in the RA knee (0.46 ± 0.05) was found compared to Con-RA knee (0.39 ± 0.03) ($P = 0.05$). Comparing group A with B, it was observed that the tracer uptake in the RA knee from rats in group B was a little bit less (although not significantly different from that of group A).

Multiple boost group C versus group D (Figure 8(b)): the uptake of *(R)*-[11C]PK11195 in RA knees was higher in rats from group C and group D as compared to that in group B, although a level of significance was not reached between the no-boost B and group C. However, comparing no-boost (group B) with the boost group (group D) a significant difference in tracer uptake was found ($P = 0.01$).

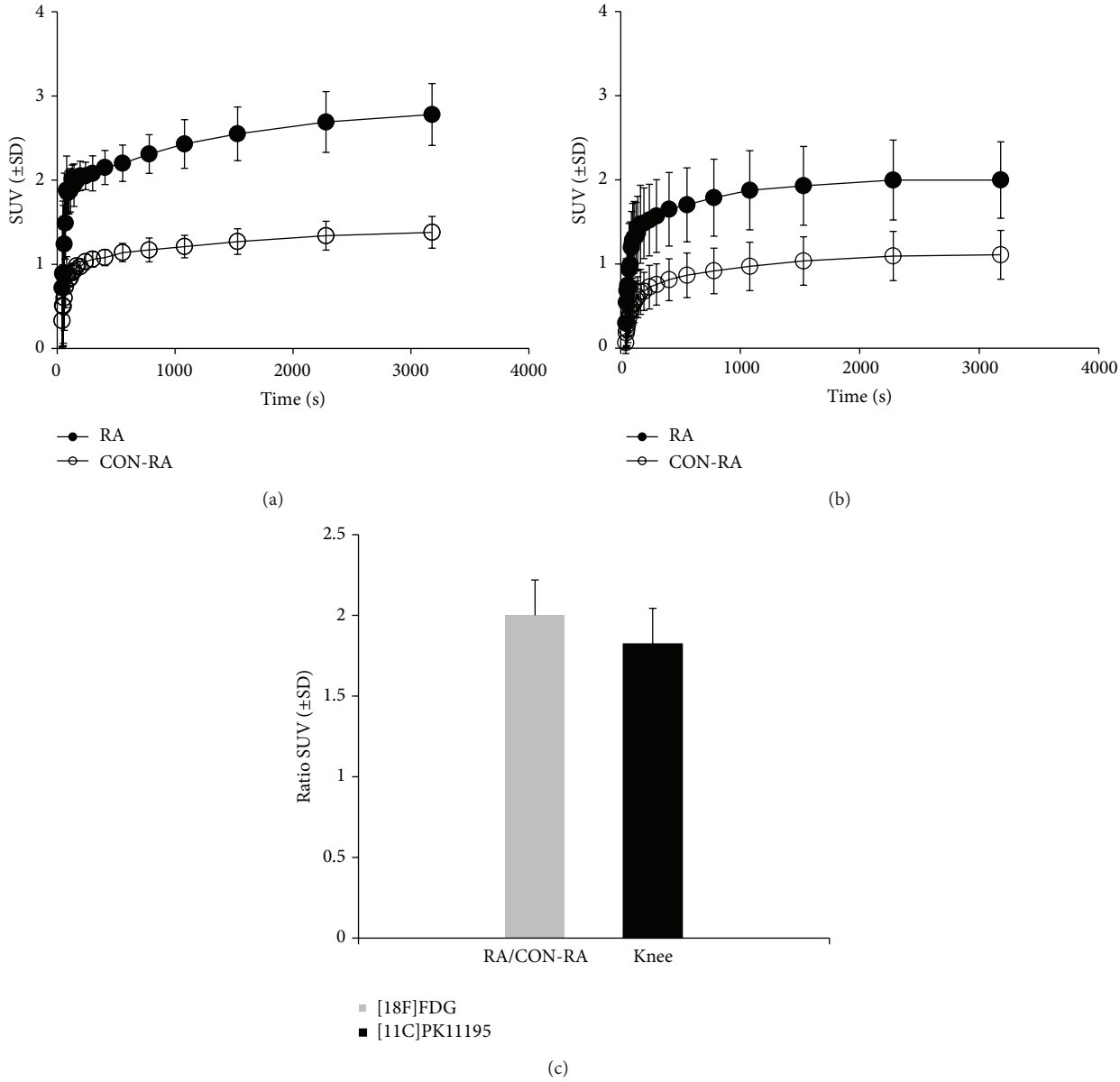

Figure 6: Time-activity-curves of tracer uptake expressed as SUV (± SD) in RA knee (•) and Con-RA knee (○) of (a) [18F]FDG and (b) *(R)*-[11C]PK11195 in rats of group A (6 d). (c) SUV ratios for RA/Con-RA are depicted.

Zooming in on the rats sacrificed at day 28 ((groups B, D, E, and F) and for group C at day 19) after the last i.a. injection a linear correlation was found between uptake and total number of ED1 positive macrophages. In contrast, no correlation could be demonstrated with respect to ED2 positive macrophages.

4. Discussion

In this study an mBSA-induced RA rat model was described with sustained and prolonged RA condition. Adaptations with respect to the original model described by Van De Putte et al. [13] and Dijkstra et al. [14] resulted in a model that allows evaluation of arthritis activity and therapeutic efficacy of novel antirheumatic drugs with PET. The modifications resulted in significantly higher influx of macrophages in synovial tissue, corresponding to improved visualization of arthritis with PET.

So far, no animal model was available for PET guided imaging and monitoring of therapeutic efficacy with a sustained and prolonged arthritic condition, long enough to test new drugs as well as showing some level of systemic disease. With our focus on detection of (sub)clinical arthritis versus noninflamed joints, animal models with predominant bone destruction and those with polyarticular distribution are not favored. Various rodent models of RA (acute and chronic) have been described where the very acute models are not very useful for monitoring therapeutic efficacy [23]. Chronic

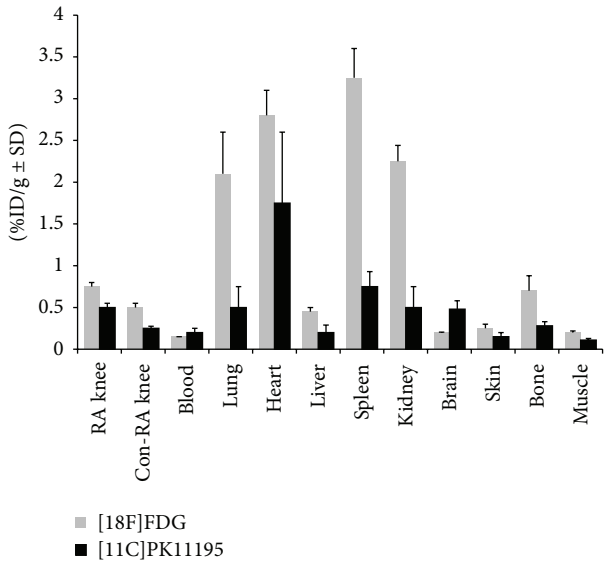

Figure 7: Ex vivo tissue distribution of [18F]FDG ($n = 6$), light grey bars, and (*R*)-[11C]PK11195 ($n = 5$, black bars) at 1 h after injection in rats of group A (6 d). Results are expressed as percentage of the injected dose per gram (%ID/g ± SD).

models such as collagen induced arthritis (CIA), bacterial (streptococcal) cell wall contents induced arthritis (SCW) and adjuvant induced arthritis (AIA) have their specific characteristics [24]. In AIA, rats develop polyarthritis with prominent bone destruction. In CIA [24] and SCW [25], swelling of paws and limbs appears with periods of remission dampening the readouts for therapeutic intervention, whereas SCW shows low significant systemic effect.

Several advantages of our present RA model are presented: it is monoarthritic; hence the contralateral knee could be used as an internal control, its robustness, and, after the immunization period, the relative rapid development of arthritis within a week characterized by clear macrophage infiltration in the synovium of one joint, resembling human RA, and with the other joints as internal control. Using the boosting procedure, the therapeutic window was largely enhanced. Macrophages play an important role in early RA and may therefore be exploited as potential targets for the development of new treatment and imaging agents [26, 27]. This model might also be particularly useful for PET purposes, since arthritis is induced in a relatively large knee joint, which is an advantage as detection of arthritis in smaller joints could be hampered by limited spatial resolution of PET scanners. Also, injection of larger volumes associated with low specific activity of some PET tracers is more problematic in mice than in rats. For monitoring response with PET imaging, quantification is essential. To this end, assessment of tracer levels in blood will be needed at any time after injection of the PET tracer which poses a problem with respect to frequent blood sampling in mice.

Limitations of the mBSA induced RA rat model are possibly the longer total time period (immunizations, i.a., and boost injections, frequent knee measurements). Also, skilled biotechnicians are needed to perform the precise intra-articular injection in the knee joint. Although the model consists of only one macroscopically inflamed knee joint, the contralateral knee also showed a low level of microscopic abnormalities related to the infiltration of macrophages in the synovium, being indicative for some systemic inflammatory effects, as also observed in a study by Meyer et al. [28]. Nevertheless, the clear difference of macrophage infiltration in the arthritic versus the noninflamed knee allowed internal comparison on PET.

PET studies showed increased uptake of both [18F]FDG and *(R)*-[11C]PK11195 in RA compared to that in Con-RA knees. Both tracers, however, have limitations for clinical imaging of arthritis activity. [18F]FDG has high sensitivity but low specificity for imaging of arthritis. In a previous clinical study, absolute uptake of RA joints and osteoarthritic joints was comparable [29]. Although *(R)*-[11C]PK11195 is a more specific tracer targeting mainly macrophages a limitation of this tracer is the background uptake in periarticular tissues [30]. The background binding of the PET tracer to both the noninflamed knee joint and periarticular bone (marrow) (in both knees and other physiological locations) could lead to underestimation of targeting properties of the applied PET tracer since PET imaging of a target relies on the contrast between the target and its background. Obtaining high, arthritic to background ratios is of particular clinical relevance to detect very early (sub)clinical synovitis as it is often only subtly present at this stage of the disease. Therefore, further research of new specific targets on activated macrophages in the early phase of RA remains warranted. An alternative candidate target in this respect is the folate receptor being selectively expressed on activated macrophages [31, 32]. Based on nanomolar binding affinities for folate and folate-conjugated ligands, this receptor might be an attractive target for both imaging and therapeutic applications, with folate linked therapeutic agents showing little or no collateral toxicity to normal tissue [33] and specifically target the activated macrophages rather than the nonactivated macrophages [34].

5. Conclusions

In conclusion, in this study, a rat arthritis model suitable for PET guided evaluation of antirheumatic drugs was optimized and validated. The boost regimen proved advantageous for achieving a chronic model with sustained arthritis activity. This model is excellent for in vivo testing of novel PET tracers for their suitability for imaging of arthritis (activity) as well as for PET monitoring of efficacy of novel therapeutic agents for RA.

Conflict of Interests

The authors declare that there is no conflict of interests regarding the publication of this paper.

Acknowledgments

The authors thank R. Bergstra and M. Verlaan for excellent assistance in surgical procedures, tissue biodistribution, and

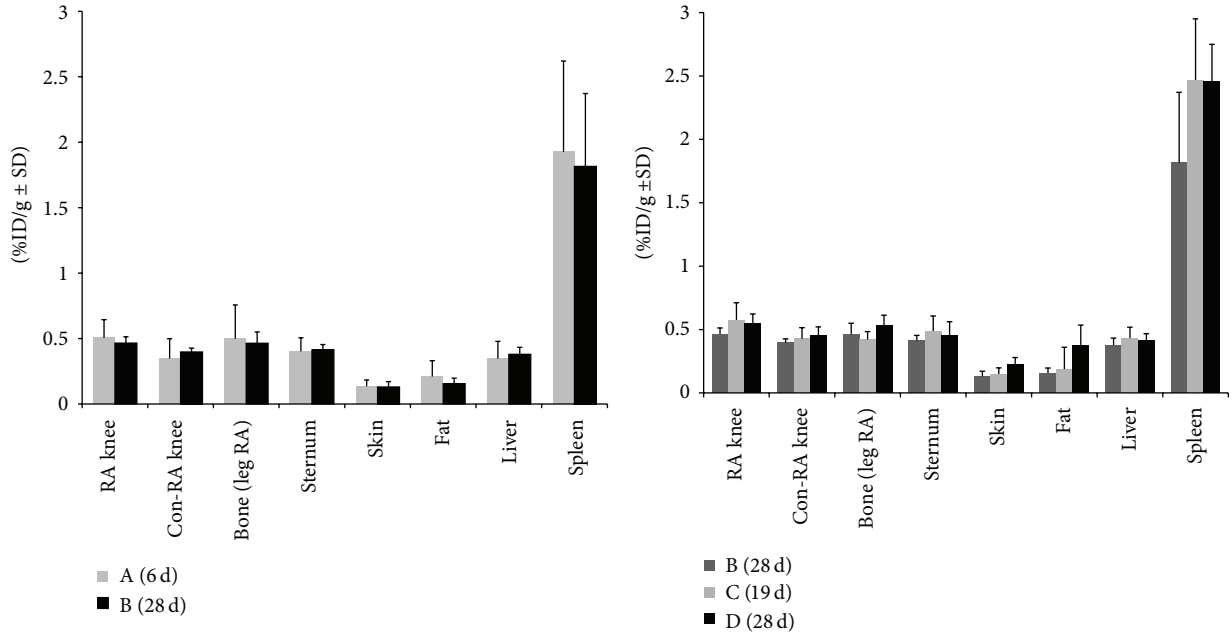

Figure 8: Ex vivo tissue distribution of *(R)*-[11C] PK11195 at 1 h after injection in rats of (a) no boost groups A (6 d) and B (28 d); (b) no boost group B (28 d), boost groups C (19 d), and D (28 d). Results are expressed as percentage of the injected dose per gram (%ID/g ± SD).

PET studies and analysis; M. Mooijer for tracer planning; M.C.M Al for help with DTH measurement and tissue distribution; Dr. G. Scheffer for help with ELISA; and Professor Dr. P. van der Valk and Professor Dr. C.J.F. van Noorden for histopathological advice and helpful discussions. Funding was received from the Dutch Arthritis Association (NRF-09-01-404).

References

[1] M. Feldmann, F. M. Brennan, and R. N. Maini, "Rheumatoid arthritis," *Cell*, vol. 85, no. 3, pp. 307–310, 1996.

[2] I. B. McInnes and G. Schett, "The pathogenesis of rheumatoid arthritis," *The New England Journal of Medicine*, vol. 365, no. 23, pp. 2205–2219, 2011.

[3] Y. P. M. Goekoop-Ruiterman, J. K. de Vries-Bouwstra, C. F. Allaart et al., "Clinical and radiographic outcomes of four different treatment strategies in patients with early rheumatoid arthritis (the best study): a randomized, controlled trial," *Arthritis and Rheumatism*, vol. 52, no. 11, pp. 3381–3390, 2005.

[4] M. F. Bakker, J. W. G. Jacobs, S. M. M. Verstappen, and J. W. J. Bijlsma, "Tight control in the treatment of rheumatoid arthritis: efficacy and feasibility," *Annals of the Rheumatic Diseases*, vol. 66, no. 3, pp. iii56–iii60, 2007.

[5] C. Beckers, C. Ribbens, B. André et al., "Assessment of disease activity in rheumatoid arthritis with ^{18}F-FDG PET," *Journal of Nuclear Medicine*, vol. 45, no. 6, pp. 956–964, 2004.

[6] K. Kubota, K. Ito, M. Morooka et al., "Whole-body FDG-PET/CT on rheumatoid arthritis of large joints," *Annals of Nuclear Medicine*, vol. 23, no. 9, pp. 783–791, 2009.

[7] Y. Y. J. Gent, K. Weijers, C. F. M. Molthoff et al., "Evaluation of the novel folate receptor ligand [18F]fluoro-PEG-folate for macrophage targeting in a rat model of arthritis," *Arthritis Research and Therapy*, vol. 15, no. 2, article R37, 2013.

[8] R. B. Banati, J. Newcombe, R. N. Gunn et al., "The peripheral benzodiazepine binding site in the brain in multiple sclerosis. Quantitative *in vivo* imaging of microglia as a measure of disease activity," *Brain*, vol. 123, no. 11, pp. 2321–2337, 2000.

[9] J. J. Haringman, D. M. Gerlag, A. H. Zwinderman et al., "Synovial tissue macrophages: a sensitive biomarker for response to treatment in patients with rheumatoid arthritis," *Annals of the Rheumatic Diseases*, vol. 64, no. 6, pp. 834–838, 2005.

[10] M. D. Smith, M. C. Kraan, J. Slavotinek et al., "Treatment-induced remission in rheumatoid arthritis patients is characterized by a reduction in macrophage content of synovial biopsies," *Rheumatology*, vol. 40, no. 4, pp. 367–374, 2001.

[11] Z. N. Jahangier, J. W. G. Jacobs, M. C. Kraan et al., "Pretreatment macrophage infiltration of the synovium predicts the clinical effect of both radiation synovectomy and intra-articular glucocorticoids," *Annals of the Rheumatic Diseases*, vol. 65, no. 10, pp. 1286–1292, 2006.

[12] B. Bolon, M. Stolina, C. King et al., "Rodent preclinical models for developing novel antiarthritic molecules: comparative biology and preferred methods for evaluating efficacy," *Journal of Biomedicine and Biotechnology*, vol. 2011, Article ID 569068, 21 pages, 2011.

[13] L. B. A. Van De Putte, J. W. Lens, W. B. Van Den Berg, and M. W. M. Kruijsen, "Exacerbation of antigen-induced arthritis after challenge with intravenous antigen," *Immunology*, vol. 49, no. 1, pp. 161–167, 1983.

[14] C. D. Dijkstra, E. A. Dopp, I. M. C. Vogels, and C. J. F. van Noorden, "Macrophages and dendritic cells in antigen-induced arthritis. An immunohistochemical study using cryostat sections of the whole knee joint of rat," *Scandinavian Journal of Immunology*, vol. 26, no. 5, pp. 513–523, 1987.

[15] R. J. Griffiths, "Characterisation and pharmacological sensitivity of antigen arthritis induced by methylated bovine serum albumin in the rat," *Agents and Actions*, vol. 35, no. 1-2, pp. 88–95, 1992.

[16] P. L. E. M. van Lent, W. B. van Den Berg, J. Schalkwijk, L. B. van de Putte, and L. van den Bersselaar, "Allergic arthritis induced by cationic antigens: relationship of chronicity with antigen retention and T-cell reactivity," *Immunology*, vol. 62, no. 2, pp. 265–272, 1987.

[17] S. M. Atkinson, P. A. Usher, P. H. Kvist, H. Markholst, C. Haase, and A. Nansen, "Establishment and characterization of a sustained delayed-type hypersensitivity model with arthritic manifestations in C57BL/6J mice," *Arthritis Research and Therapy*, vol. 14, no. 3, article R134, 2012.

[18] D. Tanaka, T. Kagari, H. Doi, and T. Shimozato, "Administration of anti-type II collagen antibody sustains footpad swelling of mice caused by a delayed-type hypersensitivity reaction and induces severe arthritis," *Clinical and Experimental Immunology*, vol. 148, no. 2, pp. 360–367, 2007.

[19] C. D. Dijkstra, E. A. Dopp, P. Joling, and G. Kraal, "The heterogeneity of mononuclear phagocytes in lymphoid organs: distinct macrophage subpopulations in the rat recognized by monoclonal antibodies ED1, ED2 and ED3," *Immunology*, vol. 54, no. 3, pp. 589–599, 1985.

[20] H. Folkersma, J. C. Foster Dingley, B. N. M. van Berckel et al., "Increased cerebral (*R*)-[^{11}C]PK11195 uptake and glutamate release in a rat model of traumatic brain injury: a longitudinal pilot study," *Journal of Neuroinflammation*, vol. 8, article 67, 2011.

[21] F. E. Froklage, S. Syvänen, N. H. Hendrikse et al., "[^{11}C]Flumazenil brain uptake is influenced by the blood-brain barrier efflux transporter P-glycoprotein," *EJNMMI Research*, vol. 2, article 12, 2012.

[22] A. M. Loening and S. S. Gambhir, "AMIDE: a free software tool for multimodality medical image analysis," *Molecular Imaging*, vol. 2, no. 3, pp. 131–137, 2003.

[23] D. L. Asquith, A. M. Miller, I. B. McInnes, and F. Y. Liew, "Animal models of rheumatoid arthritis," *European Journal of Immunology*, vol. 39, no. 8, pp. 2040–2044, 2009.

[24] L. Bevaart, M. J. Vervoordeldonk, and P. P. Tak, "Evaluation of therapeutic targets in animal models of arthritis: how does it relate to rheumatoid arthritis?" *Arthritis and Rheumatism*, vol. 62, no. 8, pp. 2192–2205, 2010.

[25] R. C. Schimmer, D. J. Schrier, C. M. Flory et al., "Streptococcal cell wall-induced arthritis: requirements for IL-4, IL- 10, IFN-γ, and monocyte chemoattractant protein-1," *Journal of Immunology*, vol. 160, no. 3, pp. 1466–1471, 1998.

[26] F. Chauveau, N. van Camp, F. Dollé et al., "Comparative evaluation of the translocator protein radioligands 11C-DPA-713, 18F-DPA-714, and 11C-PK11195 in a rat model of acute neuroinflammation," *Journal of Nuclear Medicine*, vol. 50, no. 3, pp. 468–476, 2009.

[27] C. R. Fischer, C. Müller, J. Reber et al., "[^{18}F]fluoro-deoxy-glucose folate: a novel PET radiotracer with improved in vivo properties for folate receptor targeting," *Bioconjugate Chemistry*, vol. 23, no. 4, pp. 805–813, 2012.

[28] P. Meyer, H. Burkhardt, E. Palombo-Kinne et al., "123I-antileukoproteinase scintigraphy reveals microscopic cartilage alterations in the contralateral knee joint of rats with "monarticular" antigen-induced arthritis," *Arthritis & Rheumatology*, vol. 43, pp. 298–310, 2000.

[29] E. H. Elzinga, C. J. van der Laken, E. F. I. Comans, A. A. Lammertsma, B. A. C. Dijkmans, and A. E. Voskuyl, "2-Deoxy-2-[F-18]fluoro-D-glucose joint uptake on positron emission tomography images: rheumatoid arthritis versus osteoarthritis," *Molecular Imaging and Biology*, vol. 9, no. 6, pp. 357–360, 2007.

[30] Y. Y. J. Gent, A. E. Voskuyl, R. W. Kloet et al., "Macrophage positron emission tomography imaging as a biomarker for preclinical rheumatoid arthritis: findings of a prospective pilot study," *Arthritis and Rheumatism*, vol. 64, no. 1, pp. 62–66, 2012.

[31] J. W. van der Heijden, R. Oerlemans, B. A. C. Dijkmans et al., "Folate receptor β as a potential delivery route for novel folate antagonists to macrophages in the synovial tissue of rheumatoid arthritis patients," *Arthritis and Rheumatism*, vol. 60, no. 1, pp. 12–21, 2009.

[32] E. L. Matteson, V. J. Lowe, F. G. Prendergast et al., "Assessment of disease activity in rheumatoid arthritis using a novel folate targeted radiopharmaceutical Folatescan TM," *Clinical and Experimental Rheumatology*, vol. 27, no. 2, pp. 253–259, 2009.

[33] C. M. Paulos, M. J. Turk, G. J. Breur, and P. S. Low, "Folate receptor-mediated targeting of therapeutic and imaging agents to activated macrophages in rheumatoid arthritis," *Advanced Drug Delivery Reviews*, vol. 56, no. 8, pp. 1205–1217, 2004.

[34] W. Xia, A. R. Hilgenbrink, E. L. Matteson, M. B. Lockwood, J.-X. Cheng, and P. S. Low, "A functional folate receptor is induced during macrophage activation and can be used to target drugs to activated macrophages," *Blood*, vol. 113, no. 2, pp. 438–446, 2009.

Hindawi Publishing Corporation
BioMed Research International
Volume 2015, Article ID 914516, 8 pages
http://dx.doi.org/10.1155/2015/914516

Review Article

Imaging Atherosclerosis with Hybrid Positron Emission Tomography/Magnetic Resonance Imaging

Rasmus Sejersten Ripa and Andreas Kjær

Department of Clinical Physiology, Nuclear Medicine & PET, Rigshospitalet & Cluster for Molecular Imaging, Faculty of Health and Medical Sciences, University of Copenhagen, KF-4012 Rigshospitalet, Blegdamsvej 9, 2100 Copenhagen, Denmark

Correspondence should be addressed to Andreas Kjær; akjaer@sund.ku.dk

Received 23 June 2014; Accepted 16 September 2014

Academic Editor: Francois Rouzet

Noninvasive imaging of atherosclerosis could potentially move patient management towards individualized triage, treatment, and followup. The newly introduced combined positron emission tomography (PET) and magnetic resonance imaging (MRI) system could emerge as a key player in this context. Both PET and MRI have previously been used for imaging plaque morphology and function: however, the combination of the two methods may offer new synergistic opportunities. Here, we will give a short summary of current relevant clinical applications of PET and MRI in the setting of atherosclerosis. Additionally, our initial experiences with simultaneous PET/MRI for atherosclerosis imaging are presented. Finally, future potential vascular applications exploiting the unique combination of PET and MRI will be discussed.

1. Introduction

Molecular imaging can be defined as noninvasive visualization and quantification of distinct molecular pathways. Important features of molecular imaging are the ability to target a molecular process in living organisms without perturbing them. Both positron emission tomography (PET) and magnetic resonance imaging (MRI) are classic methods used for molecular imaging.

Atherosclerosis is traditionally assessed using luminal stenosis by anatomical imaging such as angiography or ultrasound. However, atherosclerosis is now recognized as a systemic degenerative inflammatory vascular disease that develops over decades, with a long subclinical period. Postmortem analyses have shown that most fatal vascular events originate from nonstenotic atherosclerotic lesions [1], and about half of all patients who die from coronary heart disease have no prior diagnosis or symptoms of cardiac disease [2]. Despite this fact, screening asymptomatic adults for cardiovascular risk by imaging is considered inappropriate in most cases by current guidelines [3].

The concept of the vulnerable plaque is a hallmark in atherosclerosis. The vulnerable atherosclerotic plaques are those with a high short-term risk of rupture and thrombosis. The vulnerability of a plaque is characterized by a number of factors like a thin, collagen-poor fibrous cap, a large necrotic core, and abundant macrophages in the cap, whereas the luminal protrusion is not a marker of vulnerability [4].

The current goal in noninvasive imaging is to identify vulnerable atherosclerotic plaques that may subsequently lead to myocardial infarction or stroke. This identification could lead to more optimal and individualized risk stratification and thereby enabling personalized therapy.

The aim of this review is to give a summary of current relevant clinical applications of PET and MRI in the setting of atherosclerosis and to discuss potential future uses of the newly introduced combined PET/MRI system.

2. Why Hybrid Imaging with PET and MRI?

A state-of-the-art MRI scanner offers the ability to perform both anatomical and functional examinations. The atherosclerotic plaque components can be differentiated using dedicated imaging sequences (Figure 1). T1-, T2-, and proton density weighted imaging of carotid plaques allows for identification of the lipid-rich necrotic core, calcification, and

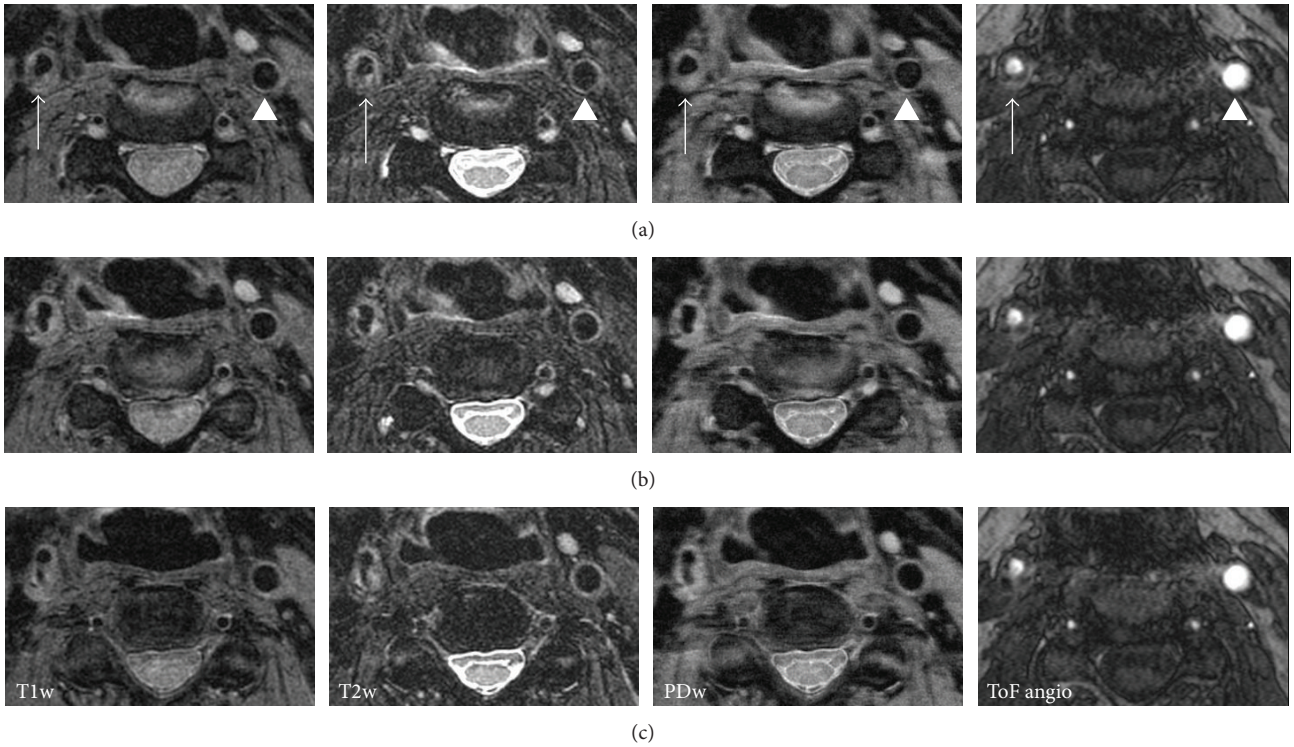

Figure 1: Example of multisequence MRI of a plaque in the right carotid artery (arrow). Each column shows three slices from the right common carotid artery (top row) to the internal carotid artery (bottom row). The nonstenotic left coronary artery is shown for comparison (arrowhead). Four different MR sequences are shown (T1 weighted, T2 weighted, proton density weighting, and time-of-flight angiography).

intraplaque hemorrhage. The high spatial resolution of MRI even allows for identification and assessment of the fibrous cap. One study published as early as 2002 included 60 patients scheduled for carotid endarterectomy. The carotid arteries were imaged in vivo with a 1.5-T scanner (time of flight and T1-, PD-, and T2-weighted). The plaque classification from this multisequence MRI showed good agreement with the American Heart Association classifications from the subsequent histological examination (Cohen's kappa of 0.74) [5]. Since then, the imaging technique has been improved by optimization of the image sequences used, the introduction of new imaging sequences, and increased magnetic field strength in the MRI system. The fibrous cap is a major contributor to the vulnerability of the plaque. The feasibility of fibrous cap visualization by MRI in the carotid artery is well established [6, 7], and fibrous cap rupture is associated with cerebrovascular symptoms in both prospective and cross-sectional studies [8, 9]. Neoangiogenesis in the atherosclerotic plaque is also considered a hallmark of the unstable plaque. Some studies indicate that dynamic contrast enhanced MRI utilizing gadolinium-based extracellular contrast agents can be used to assess microvessel density in the plaques [10].

MRI for plaque characterization in the coronary arteries is technically more challenging than carotid plaques due to cardiac and respiratory motion of the often small tortuous vessels. Several methods are under development to deal with these challenges. Some studies have in fact shown that positive remodeling and intracoronary thrombus detection is feasible in the coronary arteries [11, 12].

Molecular imaging with MRI is also possible using specific contrast agents that allow for visualization of processes in the atherosclerotic plaque at the molecular level. Target specific MRI contrast agents are typically based on paramagnetic gadolinium or iron oxide. Clinical studies have demonstrated uptake of small iron oxide (USPIO) particles in carotid plaques and the uptake was found to correspond to areas of macrophage infiltration [13]. One study has even used USPIO-enhanced carotid MRI to assess the therapeutic response of short term aggressive lipid lower therapy [14]. Fibrin is another molecular target of MRI utilizing a fibrin-specific gadolinium-based contrast agent. This agent has been used in a few clinical studies for thrombi detection [15]. A number of other target specific MRI contrast agents for imaging atherosclerosis are currently being tested in animal models (review in [16]).

It is relevant in this context to consider what PET can add to the "MRI-one-stop-shop." Clinical PET has a spatial resolution around 3 mm at best and can thus in no way compete with the spatial resolution of MRI. PET is based on photon emission from positron emitting radioactive tracers and does not contain anatomical information. Thus, PET cannot be used to image morphological components of the plaque. PET, however, is a sublime technique for molecular imaging. Molecular imaging with MRI has a limited sensitivity typically in the micromolar range, whereas a typical

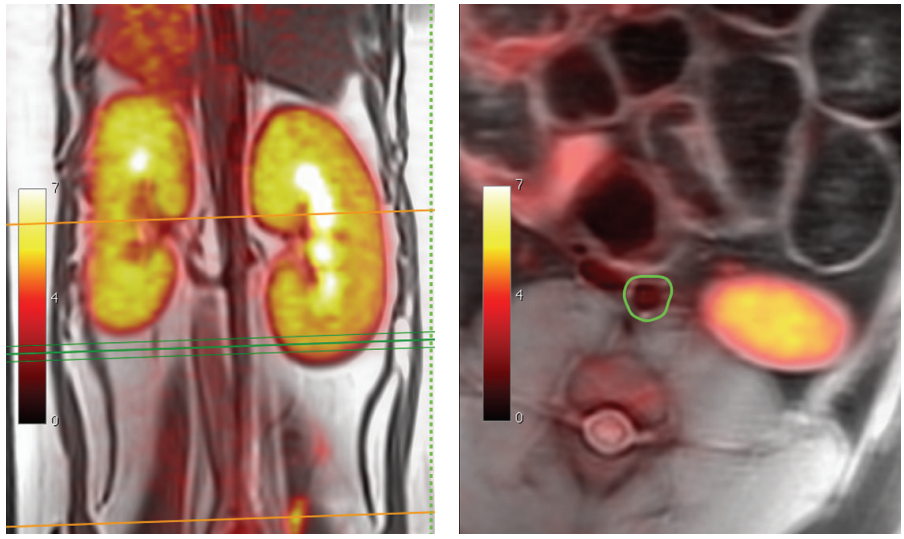

(a) (b)

Figure 2: Example of vascular simultaneous FDG-PET/MRI from porcine model. The abdominal aorta is outlined in green (reproduced from [18] with permission from the editor).

clinical PET scanner can detect concentrations in nano- to picomoles per liter. This sensitivity, however, is lower in plaque imaging since the plaque size is near the spatial resolution of the system and thus subject to signal loss by partial volume effects.

PET is based on the tracer principle for imaging. The radioactive tracer utilized in PET is a compound where an atom is replaced by a radioisotope or a radioisotope is added. Only traces of the substance are applied; therefore, it has no pharmacologic effect in vivo. Typically, the tracer is a biomolecule that reflects a particular body function or metabolism. PET tracers can be nonspecific following a biochemical pathway or allowing for measurement of tissue extraction or metabolism. These radiotracers include the glucose analogue fluorine-18-fluorodeoxyglucose (FDG) which is taken up by high-glucose-utilizing cells, where FDG is trapped intracellularly by phosphorylation to allow tissue glucose metabolism assessment. PET tracers can also be specific radioligands involved in an interaction with receptors. PET tracer distribution can be quantified in absolute terms and with dynamic measurement of PET tracer uptake and distribution kinetic analysis is possible.

In summary, we find that molecular imaging with PET in most cases will be far superior to molecular imaging with MRI. In our opinion, optimal utilization of the complementary information from hybrid PET/MR system will require a better understanding and foremost a better use of the pathophysiologic information that can be acquired by MRI. Simply using the anatomical information in conjunction with the metabolic information from the PET will be a suboptimal utilization of the potential of the system.

3. Initial Clinical Experience

3.1. Large Animal Model. As compared to preclinical animal scanners, human hybrid PET/MRI systems can physically contain larger animals. This opens the opportunity to study atherosclerosis in human-like atherosclerosis models such as rabbits and porcines. So far, few feasibility data on this topic has been published; Dregely et al. [17] presented feasibility data from 4 high-cholesterol fed rabbits as an abstract at the 2012 annual meeting of Society of Nuclear Medicine and Molecular Imaging. Likewise, our institution is working with a porcine model of atherosclerosis (Figure 2). At our hand, simultaneous PET/MRI of this large animal model is feasible but requires some optimization [18].

3.2. Vascular Imaging in Humans without Atherosclerosis. Our institution recently performed a study aiming at evaluating the feasibility of integrated PET/MR imaging of the carotid arteries in humans [19]. Six HIV patients with increased risk of atherosclerosis but without any symptoms of cardiovascular disease were included to a single-FDG-injection dual-imaging protocol of simultaneous PET/MR and subsequent integrated PET/CT on the same day. It is clear from Figure 3 that MR allowed for superior delineation of both the inner and outer walls of the carotid artery as compared to the CT in the study. The study found a high congruence between FDG-uptake quantification using the two systems despite the inherent methodological differences between the two systems such as method of attenuation correction, the use of time-of-flight in PET, and the potential interference of the MR signal from PET detectors inside the MR scanner.

3.3. PET/MRI of Human Atherosclerosis in the Carotid Arteries. PET imaging of atherosclerosis has so far focused primarily on FDG. The first report on FDG accumulation in the large arteries emerged in 2001 [20], and since then, a large body of evidence has materialized linking FDG uptake to the macrophage contents of high-risk plaques [21–23].

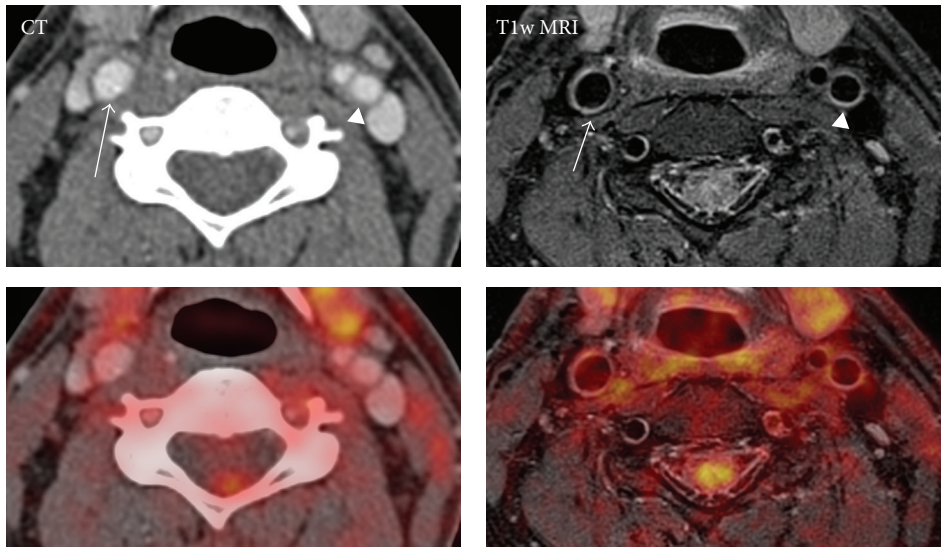

Figure 3: Comparison of contrast enhanced CT (a) with T1 weighted MRI (b) for vessel delineation in patients without significant carotid plaque. The right common carotid artery (arrow) and left internal carotid artery (arrowhead) are shown. The bottom row shows fusion with FDG-PET. This patient was part of a previous published trial [19].

The idea of combining FDG-PET with MRI is not new. In fact several studies have used sequential PET and MRI for imaging atherosclerotic plaques in animal models [24] as well as in carotid plaques in humans [25–29]. In our experience carotid plaque with simultaneous FDG-PET/MRI is feasible (Figure 4). Future studies will have to show if FDG-PET/MRI has superior prognostic information as compared to FDG-PET/CT.

One very interesting trial is the ongoing prospective observational PESA study [30]. A subgroup of 1,300 participants within this study which have evidence of atherosclerosis on ultrasound or increased coronary artery calcium score will undergo hybrid FDG PET/MRI study of both the carotid and iliofemoral arteries and the FDG PET/MRI study will be repeated at 6 years of followup.

4. Potential Vascular PET/MRI Applications

4.1. New PET Tracers. PET imaging of atherosclerosis has thus far focused primarily on FDG. A major drawback of imaging atherosclerosis with FDG PET, however, is the lack of specificity of the tracer. Another limitation is the high uptake of FDG in the myocardium, which produces a suboptimal signal-to-noise ratio when coronary arteries are imaged. As an alternative, some researchers have suggested 18F-deoxymannose as a more atherosclerosis specific tracer than FDG [31], but this needs to be confirmed in clinical trials.

A hunt for new and more specific tracers has started. The tracers should specifically target cell-mediated key molecular processes associated with the vulnerable atherosclerotic plaque. The most prominent of these targets include macrophage infiltration, apoptosis, hypoxia, and neoangiogenesis of the intima/media. Activated macrophages express the somatostatin receptor subtype 2, and this could be a target for PET imaging. ^{68}Ga-DOTATATE is utilized in diagnosis and staging of neuroendocrine tumors and has high affinity for somatostatin receptors and a few studies have suggested a future role in plaque imaging [32–34]. PET tracers for imaging apoptosis, hypoxia, and neoangiogenesis are available, but their use in imaging atherosclerosis is very limited thus far [35–37].

Another promising PET tracer for plaque imaging is ^{18}F-sodium fluoride (NaF). This tracer is deposited by chemisorptions onto hydroxyapatite and is used in oncology to identify bone metastasis. Recent evidence suggests that NaF uptake is not equivalent to calcification as identified by CT imaging [38] but that it can identify "spotty" metabolic active calcification in the plaques thought to promote plaque vulnerability. Using hybrid PET/CT and a retrospective approach, it was recently described how NaF accumulated in atheroma of the aorta, iliac, femoral, and carotid arteries [39]; however, coincidental NaF and FDG uptake (14 of 215 lesions) is rare [40]. Joshi et al. [41] recently published an interesting study indicating that NaF PET can identify culprit and ruptured plaques in patients with recent myocardial infarction.

In summary, we find that the combination of morphologic and functional information from the MRI with molecular imaging from PET may lead to optimal characterization of the plaque and thus improved individualized counseling and therapy.

4.2. Spectroscopy and Hyperpolarization. Image-guided proton magnetic resonance spectroscopy (^{1}H-MRS) of atherosclerotic plaques in carotid arteries using clinical 3-T MR systems is feasible [42]. The proton spectrum is collected from image-localized plaques, so that the specific proton

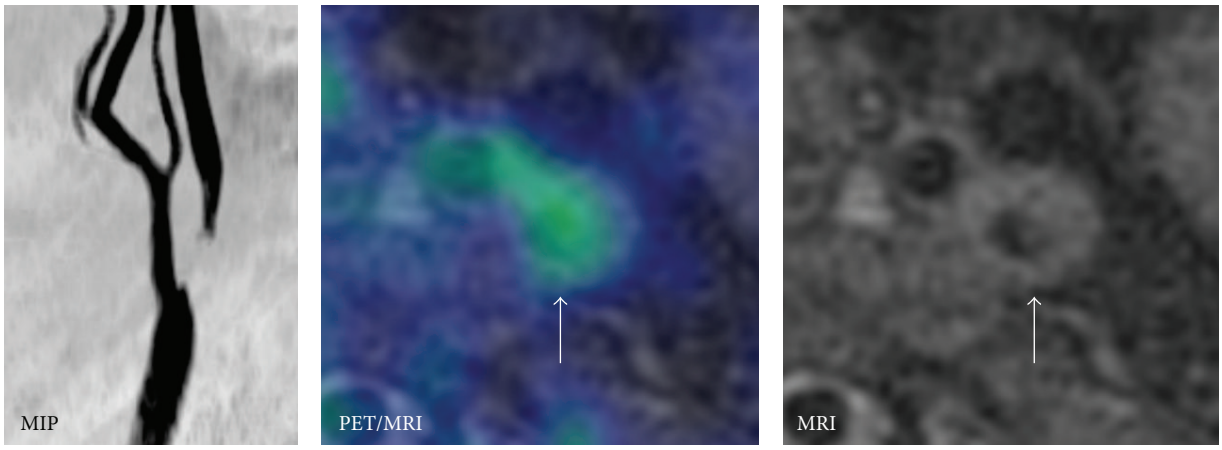

Figure 4: Example of simultaneous acquisition FDG-PET and MRI using biograph mMR. (a) MR angiography with severe proximal stenosis of left internal carotid artery. (b) Fusion of FDG-PET (color) and MRI with increased FDG-uptake in the internal carotid artery. (c) Transverse MR showing stenosis of internal carotid artery.

resonances can be identified. Duivenvoorden et al. [42] have recently used this method to identify liquid phase cholesteryl ester in carotid plaques. The trial was not without challenges though. The proton spectra were collected from a voxel of $5 \times 5 \times 5$ mm with 13 minutes acquisition time. Only 49% of the obtained spectra were of adequate quality for analysis. No studies combining proton spectroscopy with PET have so far been published in the field of atherosclerosis.

Our institution has recently installed a hyperpolarizer with our PET/MRI system allowing us to do simultaneous hyperpolarized MR and PET (HyperPET). Hyperpolarization of nuclear spins like ^{13}C can increase the MR signal with a factor of more than 10^5. Chemical compounds (tracers) like pyruvate can be enriched with ^{13}C and injected into humans or animals following ex vivo hyperpolarization. The increased signal from the ^{13}C allows both imaging and spectroscopy of the tracer within a limited time window. Hyperpolarized MRI for atherosclerosis has only been reported in few preclinical reports [43]. The HyperPET offers several new applications for in vivo molecular imaging of atherosclerosis. Due to its physical nature, PET can only image one radioactive tracer at the time. In comparison, HyperPET can measure several biological processes simultaneously; for example, plaque glycolysis can be assessed with hyperpolarized ^{13}C-pyruvate and plaque hypoxia can be assessed with a specific radiolabelled PET tracer like ^{64}Cu-ATSM simultaneously. In this way, HyperPET can combine two molecular imaging techniques with a possible synergistic effect in atherosclerosis. HyperPET, however, is a very demanding and expensive solution that will most likely be restricted to experimental use in few selected cases. Nevertheless, the distinct and small volume of interest, the plaque, makes HyperPET more realistic to be applied than in diseases where whole body evaluation is needed.

4.3. Research Platform. The acquisition of a PET/MRI system is a huge task that requires widespread knowhow by technicians, physicists, and physicians in addition to extensive funding both initially and for running costs. It is our expectation that this will limit the technique to mainly experimental use in a limited number of major university centers for some time. At our institution, we have set up an atherosclerosis research workflow in collaboration with the vascular surgeons (Figure 5). This workflow allows our staff technicians to become familiar with the multimodality setup, but at the same time gives us flexibility to introduce new imaging sequences, reconstructions, or ex vivo molecular techniques.

One apparent area for simultaneous PET/MRI is cross validation of new imaging modalities when similar molecular imaging probes exist in PET and MRI. The simultaneous acquisition allows for experiments to be performed under one and the same physiologic condition. One very elegant example is the use of a reporter gene approach. Higuchi et al. [44] transduced endothelial progenitor cells with the sodium iodide symporter gene for reporter gene imaging by PET and also labeled the cells with iron oxides for visualization by MRI. After intramyocardial injection, cells were followed with both PET and MRI. The PET tracer uptake decreased and was undetectable on day 7, whereas the MRI signal remained unchanged throughout the follow-up period. Histological analysis confirmed the presence of labeled transplanted cells at the site on day 1 but not on day 7, when only iron-loaded macrophages were seen [44]. This example clearly states the difference between anatomical imaging with MRI and molecular imaging with PET.

4.4. Interventional Studies of Atherosclerosis. Both PET and MRI have been used for followup after clinical intervention. The dal-PLAQUE study randomly assigned 130 patients with, or with high risk of, coronary heart disease to placebo or dalcetrapib [45]. Coprimary endpoints were MRI-assessed structural changes in the arterial wall after 24 months and assessment of arterial inflammation with FDG PET/CT. Also,

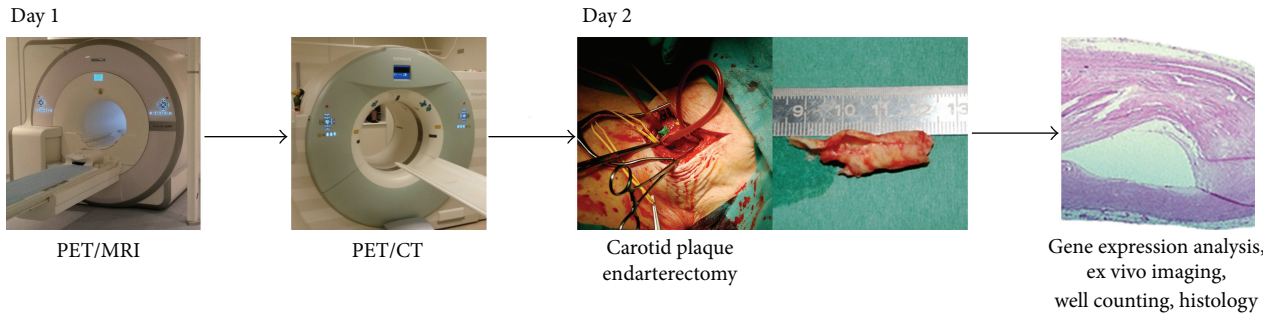

Figure 5: Example of multimodality imaging workflow from our institution.

some animal studies have utilized sequential PET/CT and MRI as endpoint in interventional trials [46, 47]. There are, however, clear advantages of using simultaneous PET/MRI as compared to PET/CT and stand-alone MRI in this setting. The simultaneous acquisition diminishes the problem with correct alignment between sequential examinations; this could be of particular importance in a follow-up trial where the expected plaque changes might be small. The use of repetitive CT examinations inflicts a nonnegligible radiation dose to the patients that is avoided when using MRI.

To date, no interventional studies of human atherosclerosis using hybrid PET/MRI have been published.

5. Conclusion

We have presented our initial experiences with simultaneous PET/MRI in the field of atherosclerosis. It is our belief that the synergy between PET and MRI will justify its use in atherosclerotic imaging despite its higher cost and more complex management. At the same time though, we do not see a translation from experimental applications to clinical routine in the very near future.

We expect a continuous development of the integration of molecular, functional, and anatomical imaging as well as the clinical indications within atherosclerosis. This novel imaging methods may lead to early detection of high-risk vulnerable plaques, enabling clinicians to improve risk stratification and thus paving the way for individualized therapy.

Conflict of Interests

The authors declare that there is no conflict of interests regarding the publication of this paper.

Acknowledgments

The authors have received generous unrestricted support from the John & Birthe Meyer Foundation, the National Advanced Technology Foundation, Danish Medical Research Council, Rigshospitalets Research Foundation, Svend Andersen Foundation, AP Møller Foundation, Novo Nordisk Foundation, and Lundbeck Foundation. All of the staff in the PET center are thanked for their skillful assistance. The sublime cooperation with Professor Sillesen and Dr. Sandholt from the Department of Vascular Surgery is gratefully acknowledged.

References

[1] A. P. Burke, A. Farb, G. T. Malcom, Y.-H. Liang, J. Smialek, and R. Virmani, "Coronary risk factors and plaque morphology in men with coronary disease who died suddenly," *The New England Journal of Medicine*, vol. 336, no. 18, pp. 1276–1282, 1997.

[2] H. Ni, S. Coady, W. Rosamond et al., "Trends from 1987 to 2004 in sudden death due to coronary heart disease: the Atherosclerosis Risk in Communities (ARIC) study," *American Heart Journal*, vol. 157, no. 1, pp. 46–52, 2009.

[3] P. Greenland, J. S. Alpert, G. A. Beller et al., "2010 ACCF/AHA guideline for assessment of cardiovascular risk in asymptomatic adults: A report of the american college of cardiology foundation/american heart association task force on practice guidelines," *Circulation*, vol. 122, no. 25, pp. e584–e636, 2010.

[4] J. F. Bentzon, F. Otsuka, R. Virmani, and E. Falk, "Mechanisms of plaque formation and rupture," *Circulation Research*, vol. 114, no. 12, pp. 1852–1866, 2014.

[5] J.-M. Cai, T. S. Hatsukami, M. S. Ferguson, R. Small, N. L. Polissar, and C. Yuan, "Classification of human carotid atherosclerotic lesions with in vivo multicontrast magnetic resonance imaging," *Circulation*, vol. 106, no. 11, pp. 1368–1373, 2002.

[6] C. Yuan, S.-X. Zhang, N. L. Polissar et al., "Identification of fibrous cap rupture with magnetic resonance imaging is highly associated with recent transient ischemic attack or stroke," *Circulation*, vol. 105, no. 2, pp. 181–185, 2002.

[7] T. S. Hatsukami, R. Ross, N. L. Polissar, and C. Yuan, "Visualization of fibrous cap thickness and rupture in human atherosclerotic carotid plaque in vivo with high-resolution magnetic resonance imaging," *Circulation*, vol. 102, no. 9, pp. 959–964, 2000.

[8] A. Millon, J.-L. Mathevet, L. Boussel et al., "High-resolution magnetic resonance imaging of carotid atherosclerosis identifies vulnerable carotid plaques," *Journal of Vascular Surgery*, vol. 57, no. 4, pp. 1046–1051, 2013.

[9] N. Takaya, C. Yuan, B. Chu et al., "Association between carotid plaque characteristics and subsequent ischemic cerebrovascular events: a prospective assessment with MRI—initial results," *Stroke*, vol. 37, no. 3, pp. 818–823, 2006.

[10] W. S. Kerwin, M. Oikawa, C. Yuan, G. P. Jarvik, and T. S. Hatsukami, "MR imaging of adventitial vasa vasorum in carotid atherosclerosis," *Magnetic Resonance in Medicine*, vol. 59, no. 3, pp. 507–514, 2008.

[11] W. Y. Kim, M. Stuber, P. Börnert, K. V. Kissinger, W. J. Manning, and R. M. Botnar, "Three-dimensional black-blood cardiac magnetic resonance coronary vessel wall imaging detects positive arterial remodeling in patients with nonsignificant coronary artery disease," *Circulation*, vol. 106, no. 3, pp. 296–299, 2002.

[12] S. Ehara, T. Hasegawa, S. Nakata et al., "Hyperintense plaque identified by magnetic resonance imaging relates to intracoronary thrombus as detected by optical coherence tomography in patients with angina pectoris," *European Heart Journal Cardiovascular Imaging*, vol. 13, no. 5, pp. 394–399, 2012.

[13] R. A. Trivedi, C. Mallawarachi, J.-M. U-King-Im et al., "Identifying inflamed carotid plaques using in vivo USPIO-enhanced MR imaging to label plaque macrophages," *Arteriosclerosis, Thrombosis, and Vascular Biology*, vol. 26, no. 7, pp. 1601–1606, 2006.

[14] T. Y. Tang, S. P. S. Howarth, S. R. Miller et al., "The ATHEROMA (atorvastatin therapy: effects on reduction of macrophage activity) study: evaluation using ultrasmall superparamagnetic iron oxide-enhanced magnetic resonance imaging in carotid disease," *Journal of the American College of Cardiology*, vol. 53, no. 22, pp. 2039–2050, 2009.

[15] J. Vymazal, E. Spuentrup, G. Cardenas-Molina et al., "Thrombus imaging with fibrin-specific gadolinium-based MR contrast agent EP-2104R: results of a phase II clinical study of feasibility," *Investigative Radiology*, vol. 44, no. 11, pp. 697–704, 2009.

[16] M. R. Makowski and R. M. Botnar, "MR imaging of the arterial vessel wall: Molecular imaging from bench to bedside," *Radiology*, vol. 269, no. 1, pp. 34–51, 2013.

[17] I. Dregely, I. Laitinen, C. Baumgartner et al., "Characterization of atherosclerotic plaques with simultaneous PET/MR: preliminary results in a rabbit model," *Journal of Nuclear Medicine*, vol. 53, no. 1, abstracts no. 1759, 2012.

[18] S. F. Pedersen, T. P. Ludvigsen, H. H. Johannesen et al., "Feasibility of simultaneous PET/MR in diet-induced atherosclerotic minipig: a pilot study for translational imaging," *American Journal of Nuclear Medicine and Molecular Imaging*, vol. 4, no. 5, pp. 448–458, 2014.

[19] R. S. Ripa, A. Knudsen, A. M. Hag et al., "Feasibility of simultaneous PET/MR of the carotid artery: first clinical experience and comparison to PET/CT," *American Journal of Nuclear Medicine and Molecular Imaging*, vol. 3, no. 4, pp. 361–371, 2013.

[20] M. Yun, D. Yeh, L. I. Araujo, S. Jang, A. Newberg, and A. Alavi, "F-18 FDG uptake in the large arteries: a new observation," *Clinical Nuclear Medicine*, vol. 26, no. 4, pp. 314–319, 2001.

[21] M. Græbe, S. F. Pedersen, L. Borgwardt, L. Højgaard, H. Sillesen, and A. Kjær, "Molecular pathology in vulnerable carotid plaques: correlation with [18]-fluorodeoxyglucose positron emission tomography (FDG-PET)," *European Journal of Vascular and Endovascular Surgery*, vol. 37, no. 6, pp. 714–721, 2009.

[22] S. F. Pedersen, M. Graebe, A. M. Fisker Hag, L. Højgaard, H. Sillesen, and A. Kjaer, "Gene expression and 18FDG uptake in atherosclerotic carotid plaques," *Nuclear Medicine Communications*, vol. 31, no. 5, pp. 423–429, 2010.

[23] J. H. F. Rudd, E. A. Warburton, T. D. Fryer et al., "Imaging atherosclerotic plaque inflammation with [^{18}F]-fluorodeoxyglucose positron emission tomography," *Circulation*, vol. 105, no. 23, pp. 2708–2711, 2002.

[24] A. Millon, S. D. Dickson, A. Klink et al., "Monitoring plaque inflammation in atherosclerotic rabbits with an iron oxide (P904) and 18F-FDG using a combined PET/MR scanner," *Atherosclerosis*, vol. 228, no. 2, pp. 339–345, 2013.

[25] J. Wang, H. Liu, J. Sun et al., "Varying correlation between 18F-fluorodeoxyglucose positron emission tomography and dynamic contrast-enhanced MRI in carotid atherosclerosis: implications for plaque inflammation," *Stroke*, vol. 45, no. 6, pp. 1842–1845, 2014.

[26] M. T. B. Truijman, R. M. Kwee, R. H. M. van Hoof et al., "Combined 18F-FDG PET-CT and DCE-MRI to assess inflammation and microvascularization in atherosclerotic plaques," *Stroke*, vol. 44, no. 12, pp. 3568–3570, 2013.

[27] H. Saito, S. Kuroda, K. Hirata et al., "Validity of dual MRI and F-FDG PET imaging in predicting vulnerable and inflamed carotid plaque," *Cerebrovascular Diseases*, vol. 35, no. 4, pp. 370–377, 2013.

[28] C. Calcagno, S. Ramachandran, D. Izquierdo-Garcia et al., "The complementary roles of dynamic contrast-enhanced MRI and 18F-fluorodeoxyglucose PET/CT for imaging of carotid atherosclerosis," *European Journal of Nuclear Medicine and Molecular Imaging*, vol. 40, no. 12, pp. 1884–1893, 2013.

[29] S. S. Silvera, H. E. Aidi, J. H. F. Rudd et al., "Multimodality imaging of atherosclerotic plaque activity and composition using FDG-PET/CT and MRI in carotid and femoral arteries," *Atherosclerosis*, vol. 207, no. 1, pp. 139–143, 2009.

[30] A. Fernández-Ortiz, L. J. Jiménez-Borreguero, J. L. Peñalvo et al., "The progression and early detection of subclinical atherosclerosis (PESA) study: rationale and design," *American Heart Journal*, vol. 166, no. 6, pp. 990–998, 2013.

[31] N. Tahara, J. Mukherjee, H. J. De Haas et al., "2-deoxy-2-[^{18}F]fluoro-d-mannose positron emission tomography imaging in atherosclerosis," *Nature Medicine*, vol. 20, no. 2, pp. 215–219, 2014.

[32] X. Li, S. Samnick, C. Lapa et al., "68Ga-DOTATATE PET/CT for the detection of inflammation of large arteries: correlation with 18F-FDG, calcium burden and risk factors," *EJNMMI Research*, vol. 2, article 52, 2012.

[33] X. Li, W. Bauer, M. C. Kreissl et al., "Specific somatostatin receptor II expression in arterial plaque: 68Ga-DOTATATE autoradiographic, immunohistochemical and flow cytometric studies in apoE-deficient mice," *Atherosclerosis*, vol. 230, no. 1, pp. 33–39, 2013.

[34] A. Rominger, T. Saam, E. Vogl et al., "In vivo imaging of macrophage activity in the coronary arteries using 68Ga-DOTATATE PET/CT: correlation with coronary calcium burden and risk factors," *Journal of Nuclear Medicine*, vol. 51, no. 2, pp. 193–197, 2010.

[35] A. J. Beer, J. Pelisek, P. Heider et al., "PET/CT imaging of integrin $\alpha v\beta 3$ expression in human carotid atherosclerosis," *JACC: Cardiovascular Imaging*, vol. 7, no. 2, pp. 178–187, 2014.

[36] E. M. Laufer, M. H. M. Winkens, M. F. Corsten, C. P. M. Reutelingsperger, J. Narula, and L. Hofstra, "PET and SPECT imaging of apoptosis in vulnerable atherosclerotic plaques with radiolabeled Annexin A5," *Quarterly Journal of Nuclear Medicine and Molecular Imaging*, vol. 53, no. 1, pp. 26–34, 2009.

[37] J. M. U. Silvola, A. Saraste, S. Forsback et al., "Detection of hypoxia by [^{18}F]EF5 in atherosclerotic plaques in mice," *Arteriosclerosis, Thrombosis, and Vascular Biology*, vol. 31, no. 5, pp. 1011–1015, 2011.

[38] M. R. Dweck, M. W. L. Chow, N. V. Joshi et al., "Coronary arterial 18F-sodium fluoride uptake: a novel marker of plaque biology," *Journal of the American College of Cardiology*, vol. 59, no. 17, pp. 1539–1548, 2012.

[39] T. Derlin, U. Richter, P. Bannas et al., "Feasibility of 18F-sodium fluoride PET/CT for imaging of atherosclerotic plaque," *Journal of Nuclear Medicine*, vol. 51, no. 6, pp. 862–865, 2010.

[40] T. Derlin, Z. Tóth, L. Papp et al., "Correlation of inflammation assessed by ^{18}F-FDG PET, active mineral deposition assessed by ^{18}F-fluoride PET, and vascular calcification in atherosclerotic plaque: a dual-tracer PET/CT study," *Journal of Nuclear Medicine*, vol. 52, no. 7, pp. 1020–1027, 2011.

[41] N. V. Joshi, A. T. Vesey, M. C. Williams et al., "18F-fluoride positron emission tomography for identification of ruptured and high-risk coronary atherosclerotic plaques: a prospective clinical trial," *The Lancet*, vol. 383, no. 9918, pp. 705–713, 2014.

[42] R. Duivenvoorden, D. Van Wijk, M. Klimas, J. J. P. Kastelein, E. S. G. Stroes, and A. J. Nederveen, "Detection of liquid phase cholesteryl ester in carotid atherosclerosis by 1H-MR spectroscopy in humans," *JACC: Cardiovascular Imaging*, vol. 6, no. 12, pp. 1277–1284, 2013.

[43] P. Bhattacharya, E. Y. Chekmenev, W. F. Reynolds et al., "Parahydrogen-induced polarization (PHIP) hyperpolarized MR receptor imaging *in vivo*: a pilot study of ^{13}C imaging of atheroma in mice," *NMR in Biomedicine*, vol. 24, no. 8, pp. 1023–1028, 2011.

[44] T. Higuchi, M. Anton, K. Dumler et al., "Combined reporter gene PET and iron oxide MRI for monitoring survival and localization of transplanted cells in the rat heart," *Journal of Nuclear Medicine*, vol. 50, no. 7, pp. 1088–1094, 2009.

[45] Z. A. Fayad, V. Mani, M. Woodward et al., "Safety and efficacy of dalcetrapib on atherosclerotic disease using novel non-invasive multimodality imaging (dal-PLAQUE): a randomised clinical trial," *The Lancet*, vol. 378, no. 9802, pp. 1547–1559, 2011.

[46] E. Vucic, S. D. Dickson, C. Calcagno et al., "Pioglitazone modulates vascular inflammation in atherosclerotic rabbits: noninvasive assessment with FDG-PET-CT and dynamic contrast-enhanced MR imaging," *JACC: Cardiovascular Imaging*, vol. 4, no. 10, pp. 1100–1109, 2011.

[47] E. Vucic, C. Calcagno, S. D. Dickson et al., "Regression of inflammation in atherosclerosis by the LXR agonist R211945: a noninvasive assessment and comparison with atorvastatin," *JACC: Cardiovascular Imaging*, vol. 5, no. 8, pp. 819–828, 2012.

Hindawi Publishing Corporation
BioMed Research International
Volume 2015, Article ID 284354, 12 pages
http://dx.doi.org/10.1155/2015/284354

Research Article

Synthesis, ^{68}Ga-Radiolabeling, and Preliminary *In Vivo* Assessment of a Depsipeptide-Derived Compound as a Potential PET/CT Infection Imaging Agent

Botshelo B. Mokaleng,[1] Thomas Ebenhan,[1,2] Suhas Ramesh,[3] Thavendran Govender,[3] Hendrik G. Kruger,[3] Raveen Parboosing,[4] Puja P. Hazari,[5] Anil K. Mishra,[5] Biljana Marjanovic-Painter,[6] Jan R. Zeevaart,[7] and Mike M. Sathekge[1]

[1] *Department of Nuclear Medicine, University of Pretoria & Steve Biko Academic Hospital, Corner Malherbe and Steve Biko Road, Pretoria 0001, South Africa*
[2] *School of Chemistry and Physics, Westville Campus, University Road, Westville, Durban 3630, South Africa*
[3] *School of Health Sciences, Catalysis and Peptide Research Unit, E-Block 6th Floor, Westville Campus, University Road, Westville, Durban 3630, South Africa*
[4] *Department of Virology, University of KwaZulu-Natal, National Health Laboratory Service, P.O. Box 1900, Westville, Durban 3630, South Africa*
[5] *Division of PET Imaging & Radiochemistry, Molecular Imaging Research Centre, INMAS, Brig S. K. Mazumdar Marg, Timarpur, Delhi 110054, India*
[6] *Radiochemistry Section Necsa, Building P1600, Pelindaba, Brits, North West Province, South Africa*
[7] *Department of Science and Technology, Preclinical Drug Development Platform, North West University, 11 Hoffman Street, Potchefstroom 2520, South Africa*

Correspondence should be addressed to Mike M. Sathekge; mike.sathekge@up.ac.za

Received 7 June 2014; Revised 28 July 2014; Accepted 5 August 2014

Academic Editor: Alberto Signore

Noninvasive imaging is a powerful tool for early diagnosis and monitoring of various disease processes, such as infections. An alarming shortage of infection-selective radiopharmaceuticals exists for overcoming the diagnostic limitations with unspecific tracers such as $^{67/68}$Ga-citrate or ^{18}F-FDG. We report here TBIA101, an antimicrobial peptide derivative that was conjugated to DOTA and radiolabeled with ^{68}Ga for a subsequent *in vitro* assessment and *in vivo* infection imaging using *Escherichia coli*-bearing mice by targeting bacterial lipopolysaccharides with PET/CT. Following DOTA-conjugation, the compound was verified for its cytotoxic and bacterial binding behaviour and compound stability, followed by ^{68}Gallium-radiolabeling. μPET/CT using ^{68}Ga-DOTA-TBIA101 was employed to detect muscular *E. coli*-infection in BALB/c mice, as warranted by the *in vitro* results. ^{68}Ga-DOTA-TBIA101-PET detected *E. coli*-infected muscle tissue (SUV = 1.3–2.4) > noninfected thighs ($P = 0.322$) > forearm muscles ($P = 0.092$) > background ($P = 0.021$) in the same animal. Normalization of the infected thigh muscle to reference tissue showed a ratio of 3.0 ± 0.8 and a ratio of 2.3 ± 0.6 compared to the identical healthy tissue. The majority of the activity was cleared by renal excretion. The latter findings warrant further preclinical imaging studies of greater depth, as the DOTA-conjugation did not compromise the TBIA101's capacity as targeting vector.

1. Introduction

Radiopharmaceuticals are a powerful tool in managing patients with infectious diseases. However, discerning infection from sterile inflammation is still one of the most common problems in nuclear medicine. For this reason several radiopharmaceuticals have been studied to find the solution to this difficult situation. Commercially available

radiopharmaceuticals, such as labeled leucocytes, Gallium-67- (^{67}Ga-) citrate, Indium-111- (^{111}In-) IgG, Technetium-99m- (^{99m}Tc-) labeled ciprofloxacin, and Flouride-18- (^{18}F-) FDG may result in false-positive diagnostics and, in some cases, a definite differential diagnosis between infection and aseptic inflammation cannot be achieved [1, 2]. Because some antimicrobial peptides (AMP) selectively target structures of the bacterial cell wall envelope, they have recently been investigated; preliminary data has suggested that these AMP have the potential to distinguish infection from aseptic inflammation [2, 3]. ^{99m}Tc-UBI29-41 has been shown to have the ability to detect bacterial infection using SPECT in clinical trials [4] but an increase in the availability and accessibility of PET/CT facilities has sparked renewed interest in generator-based PET radiopharmaceuticals. Gallium-68 (^{68}Ga), in particular, has received attention as an alternative positron emitter since it is not limited by the need for a nearby cyclotron and may be especially valuable in the imaging of infection/inflammation. ^{68}Ga-labeled peptides have also become relevant for diagnostic imaging because of their favourable pharmacokinetics [5]. The approach using ^{68}Ga-NOTA-UBI29-41 motivated for the strategy, that specific short peptides make perfect vector molecules to detect bacteria if joined by a suitable ^{68}Ga-carrier molecule such as DOTA (1,4,7,10-tetraazacyclododecane-1,4,7,10-tetraacetic acid) without compromising the compounds targeting capacity.

Depsipeptides, a class of natural antimicrobial cyclic peptides, which include one or more ester (depside) bonds as part of their amide backbone, have been characterized in many natural environments and show a wide spectrum of biological activity. Owing to this unique and stabilizing motif, depsipeptides became relevant for drug discovery [6]. One depsipeptide is depsidomycin ($C_{38}H_{65}N_9O_9$, molecular weight of 978 g/mol). Depsidomycin is a heptadepsi-peptide isolated from the cultured broth of *Streptomyces lavendofoliae* and exhibits significant antimicrobial and immunosuppressive activity. Recently, depsidomycin analogues have been shown to be active against both normal and multidrug-resistant strains of *Mycobacterium tuberculosis* as well [7].

At present, no approaches to radiolabeling depsidomycin-derived compounds have been found with medicinal isotopes for subsequent validation for noninvasive diagnostic imaging. In this proof of concept study, we synthesized and evaluated methods to radiolabel the depsidomycin derivative DOTA-TBIA101 with ^{68}Ga. We also report in this paper the preliminary findings of the antimicrobial *in vitro* behaviour of ^{68}Ga-DOTA-TBIA101 and its potential for targeting infection with noninvasive imaging in an *E. coli*-bearing mice model.

2. Materials and Methods

2.1. Chemicals, Bacteria, and Material. Chemicals for peptide synthesis (GL Biochem, Shanghai, China; Sigma-Aldrich, Kempton Park, South Africa) and DOTA-tris(*t*Bu)ester (CheMatech, Dijon, France) were purchased commercially. All other solvents and reagents were procured in the highest grade quality (Merck, Modderfontein, South Africa) and used unprocessed. The bacterial strains, *Staphylococcus aureus* (ATCC 25923) (*S. aur*) and *E. coli* (ATCC 25922) were kindly provided by the Microbiology Department, University of KwaZulu-Natal. Instant thin layer chromatography silica gel paper (ITLC-SG) (Pall Life Science, Midrand, South Africa) was utilized for analysis. A ^{68}Ge-^{68}Ga generator was purchased for daily ^{68}Ga-elution (iThemba LABS, Somerset West, South Africa). A Bruker Autoflex III MALDI-TOF-MS (matrix-assisted laser desorption ionization-time of flight mass spectrometry) was provided by the Catalysis and Peptide Research Unit, University of KwaZulu-Natal.

2.2. Peptide Synthesis and DOTA Conjugation. The derivative TBIA101 consists of nine amino acids (PLPVLTI-GG) with a molecular weight of 1250 g/mol. All reactions were performed under an inert atmosphere (nitrogen). The peptide synthesis (0.1 mmol) was carried out using rink amide-AM resin (0.6 mmol/g loading) on a Liberty Blue semiautomated solid-phase peptide synthesizer (CEM Corporation, Matthews, NC, USA) [7] using concentrations of amino acids, *N*,*N*-diisopropylethylamine (DIPEA), and 2-(1*H*-benzotrialzol-1-yl)-1,1,3,3-tetramethyluronium-hexa-fluorophosphate (HBTU) of 0.1, 0.4, and 0.2 mM, respectively. The on-resin conjugation of TBIA101 and DOTA-tris(*t*Bu-ester) (3 equiv) was carried out using *N*,*N*-diisopropylcarbodiimide (DIC) (3 equiv.)/Oxyma pure (3 equiv.) in *N*,*N*-dimethylformamide (DMF) (2 mL) as solvent for 2 h. The global deprotection of DOTA-TBIA101 (Figure 1) from the resin and tris(*t*Bu-ester) was accomplished within 1.5 h using a mixture of 3 mL solution of Trifluoroacetic acid/Triisopropylsilane/Water (95/2.5/2.5 v/v), cold ether was added to precipitate the peptide, centrifuged, washed twice with ether and dissolved the precipitate in double distilled water [8]. The crude DOTA-TBIA101 was used for purification.

2.2.1. Purification and Analysis of DOTA-TBIA101. A reverse-phase high performance liquid chromatography (RP-HPLC), a Shimadzu 6AD instrument (Shimadzu Scientific Instruments, Kyoto, Japan), was engaged for the compound purification with an UV/VIS detector (set at 215 nm) running an ACE C18 column (150 mm × 21.2 mm × 5 μ) (Advanced Chromatography Technologies, Aberdeen, Scotland) at a flow rate of 15 mL/min. Buffer A consisted of 0.1% TFA/H_2O (v/v) and buffer B consisted of 0.1% TFA/H_2O (v/v), with a linear gradient from 0–50% B in 30 min. The peak was collected at 17 min and the molecular weight of DOTA-TBIA101 (1250 g/mol) was confirmed by a Shimadzu LCMS 2020 mass spectrometric analysis (Shimadzu Scientific Instruments, Kyoto, Japan) in the positive mode with a X-bridge C18 column (150 mm × 4.6 mm × 5 μ) (Waters Corporation, Eschborn, Germany).

2.3. MALDI-TOF-MS Analysis. MALDI-TOF-MS analysis was performed on an Autoflex III MALDI-TOF mass spectrometer (Bruker, Coventry, United Kingdom) with a 337 nm nitrogen laser operating in a linear mode at an accelerated voltage of 20 kV. The α-cyano-4-hydroxycinnamic acid

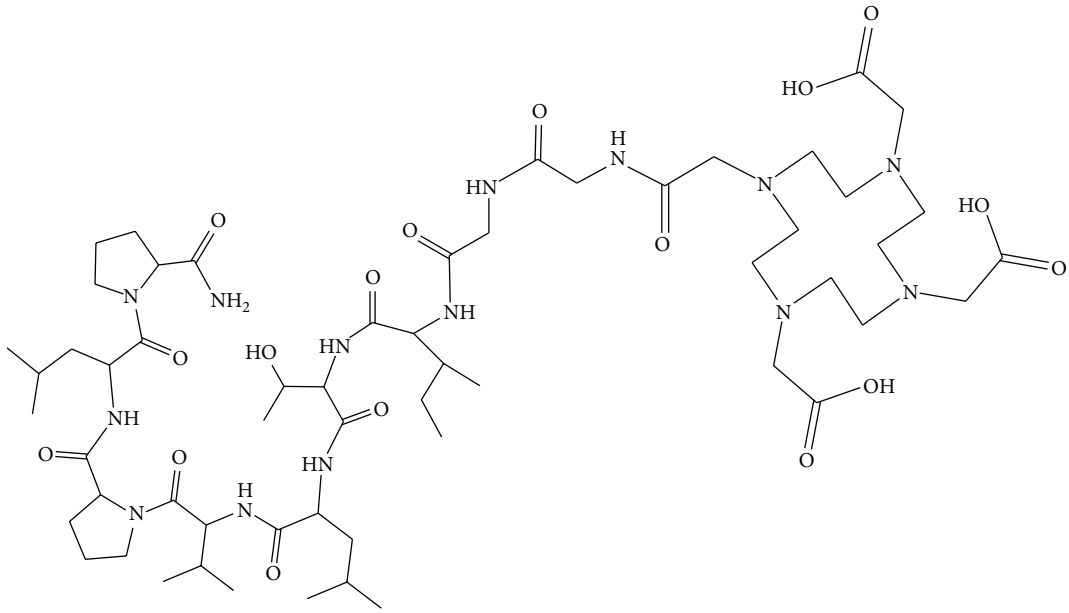

Figure 1: Structure of DOTA-TBIA101.

matrix was applied: the matrix solution was prepared by making a saturated solution of the matrix powder into TA30 solution (30% ACN and 70% water containing 0.1% TFA). A MALDI plate-sandwich method was used by spotting the compounds between spots of matrix solution. Analyses were done in triplicates; spectra were collected manually and the mass peak intensities were recorded.

2.4. ^{nat}Gallium-Complexation. The nonradioactive "cold" labeling was performed according to a described method [9]. Briefly, 100 μg of gallium trichloride (pH 3.5-4) was mixed with 25 μg DOTA-TBIA101 stock solution and vortexed for 30 sec. The reaction mixture was incubated for 10 min at 100°C. The crude ^{nat}Ga-DOTA-TBIA101 was purified using a C_{18} Sep-pak cartridge. The cartridge was preconditioned with 2 mL of ethanol and 1 mL of water, sequentially. After passing the crude sample through the C_{18} Sep-pak, 4 mL of water was used to rinse out uncomplexed gallium. A mixture of 1% trifluoroacetic acid (TFA) in acetonitrile (ACN) (5 mL) was used to desorb ^{nat}Ga-DOTA-TBIA101; its molecular weight (1319 g/mol) was confirmed using MALDI-TOF-MS.

2.5. Bacterial Association Assay. *S. aur* and *E. coli* strains were cultured at 37°C overnight and tested with the peptide (TBIA101), the peptide-conjugate (DOTA-TBIA101), and the gallium(III)-complexed derivative (^{nat}Ga-DOTA-TBIA101). The bacterial concentration was kept at 1.5×10^8 colony forming units (CFU). Five different concentrations (20, 40, 60, 80, and 100 μM) of the above-mentioned compounds were used for all experiments, following the described method [10]. The final reaction volume was 600 μL. Bacteria and compound mixtures were incubated at 37°C in an orbital shaker at 100 rpm for 3 h. After incubation, the cells were centrifuged at 3000 ×g for 20 min and the supernatant was removed. The bacterial pellet was washed twice with 200 μL of phosphate buffered saline (pH 7.4) and 200 μL of 80% ACN containing 0.1% TFA was added to dissolve the pellet followed by vigorous mixing followed by centrifugation at 3000 ×g for 20 min. The supernatant (*sample 1*) was collected, representing the membrane-associated compound fraction. The residual pellet was treated with 200 μL of 80% ACN (*sample 2*), representing the cell-internalized compound fraction. Bacterial persistence in samples 1 and 2 was qualified with MALDI-TOF-MS.

2.6. Cytotoxicity Test. The reduction of 2,3-bis-(2-methoxy-4-nitro-5-sulfophenyl)-2-H-tetrazolium-5-carboxanilide (XTT) was used to determine the cellular cytotoxicity of TBIA101, DOTA-TBIA101, and ^{nat}Ga-DOTA-TBIA101, as described by Scudiero et al. [11]. MT-4 cells were obtained through the NIH AIDS Reagent Program, Division of AIDS, NIAID, NIH: MT-4 from Dr. Douglas Richman and were cultured and all incubations were done in RPMI medium containing 10% fetal calf serum at 37°C and 5% CO_2-atmosphere. A 6×10^5 cells/mL concentration was used to seed cells into 96-well culture plates (total cell number of 2×10^4 per well) followed by exposure to eight 5-fold dilutions of the stock compound solutions (1 mg/mL). The plates were incubated for 5 days before XTT was added to react for 4 h. Formazan production was quantified, measuring absorbance at 450 nm (reference wavelength 620 nm), and related to the absorbance of untreated control cells (RPMI background).

Cytotoxicity was determined by extrapolating the inhibitory concentration at 50% (IC_{50}).

2.7. ^{68}Ge-^{68}Ga Generator Elution. Gallium-68 was routinely obtained from a SnO_2-based ^{68}Ge-^{68}Ga generator but for animal studies a TiO_2-based ^{68}Ge-^{68}Ga generator (Eckert & Ziegler Isotope Products, Valencia, CA, USA) was employed. ^{68}Ga-radioactivity was eluted manually using eluate volume fractionation methods as described [12, 13] and measured in a dose calibrator (CRC15, Capintec Inc, Pittsburgh, PA, USA). All ^{68}Ga-activity data is expressed as decay corrected (half-life of ^{68}Ga is 68 min, 88% decay by emitting positron of 1.92 MeV and 11% by electron capture).

2.8. ^{68}Ga-DOTA-TBIA101 Radiolabeling: Optimization of Radiolabeling Conditions. Radiolabeling attempts were based on a labeling procedure described for DOTA-TATE [13]. In order to achieve efficient, high-yield ^{68}Ga-labelling, the following conditions were investigated regarding an optimal ^{68}Ga-DOTA-TBIA101 yield: (a) temperature influence (room temperature, 60°C and 100°C) with different incubation duration of 5–45 min, (b) influence of decreasing eluate acidity (i.e., pH values up to pH 7), and (c) influence of decreasing DOTA-TBIA101 molarity of 40–0.00128 μM. The percentage labeling efficiency (%LE) and radiochemical purity (RCP) of the crude samples was determined utilizing ITLC-SG, and HPLC.

2.8.1. Quality Control. The 10 × 1 cm ITLC stationary phase was spiked with a radioactive sample and exposed to the following mobile phases: (a) 0.1 M sodium citrate pH 4–4.5 (R*f* (^{68}Ga) = 0.8–1.0, R*f* (^{68}Ga-peptide) = 0.0–0.3) and (b) 1 M ammonium acetate/methanol (1 : 1 v/v) (R*f* (colloidal ^{68}Ga) = 0.0–0.2, R*f* (^{68}Ga-peptide) = 0.8–1.0). Peaks were identified and compared by region-of-interest (ROI) analysis. HPLC analysis was conducted as described [14]. Radiochemical purity was determined using a Symmetry C 18 column (4.6 mm × 250 mm × 5 μ) (Waters Corporation, Milford, MA, USA) coupled to 6100 quadruple MS detector (Agilent Technologies, Santa Clara, CA, USA) diode array detector and Gina Star radioactive detector (Raytest Isotopenmessgeräte, Straubenhardt, Germany) using 0.1% TFA in water (solvent A) and 0.1% TFA in ACN (solvent B) as a mobile phase. Gradient elution was carried out at 40°C with a 1.0 mL/min flow rate using 0–2 min (5% B), 2–32 min (65% B), and 32–35 min (5% B).

2.8.2. Routine Labeling Method for ^{68}Ga-DOTA-TBIA101. For routine radiolabeling, 1.5 mL eluted activity was directly added to the reaction mixture (pH 3–3.5 buffered using 2.5 M sodium acetate, DOTA-TBIA101: 40 μM) and incubated for 15 min at >95°C. The reaction mixture was purified using a Sep-pak C_{18} cartridge to allow for uncomplexed radioactive gallium and traces of ^{68}Ge to rinse off with saline solution. Desorption of the labeled product was performed with a 50% ethanolic saline solution and was aseptically filtered (low protein binding filter) before tracer administration.

2.8.3. Radiochemical Integrity and Blood Stability. The radiochemical integrity determination of the final product was performed at 0, 30, 60, 120, and 180 min. The ^{68}Ga percentage of unbound and bound ^{68}Ga-DOTA-TBIA101 was analyzed by ITLC as described earlier. ^{68}Ga-DOTA-TBIA101 stability was determined on whole blood, plasma, and serum. The blood sample (50 mL) was collected with ACD anticoagulant, 10 mL was kept for blood assessment and the remainder was allowed to separate for 20–30 min followed by plasma collection after centrifugation at 1500 rpm for 10 min. Serum was collected similar to plasma from a blood sample collected without anticoagulant. All samples were used immediately and tests were conducted in triplicate; 1 mL of ^{68}Ga-DOTA-TBIA101 (38–50 MBq) was incubated with 1 mL of whole blood, plasma, or serum and analyzed by ITLC.

2.9. Small Animal μPET/CT Imaging. Animal studies were conducted according to the guidelines of the Institute of Nuclear Medicine & Allied Sciences (INMAS) Animal Ethics Committee (CPCSEA Registration no.8/GO/a/99). Immune competent BALB/c mice (male, 26–30 g, 6–8 weeks old) were used for the study and allowed water and food *ad libitum* for the duration of the study. A 0.2 mL aliquot of viable *E. coli* (5×10^8 CFU/mL) was inoculated into the right hind thigh muscle and allowed to form the infection site for 4-5 days.

2.9.1. Image Acquisition, Reconstruction, and Quantification. Mice were injected with ^{68}Ga-DOTA-TBIA101 intravenously into the tail vein in a single bolus of 0.1-0.2 mL tracer solution. All animals were anesthetized by injection of a mixture of 10 mg/kg xylazine (Xylavet, Kempton Park, South Africa) and 80 mg/kg ketamine (Anaket V, Centaur Laboratories, Isando, South Africa) before they were placed on the scanner bed in the prone position (head first). CT scans and PET images were acquired at 25 min after injection (whole body images or single field-of-view) of ^{68}Ga-DOTA-TBIA101 in list mode. All acquired images were scatter- and transmission-corrected (CT-based) and reconstructed by the ordered-subsets expectation maximization (OSEM) algorithm, yielding 3D iterative PET/CT overlay images in axial, sagittal, and coronal orientation. The tracer distribution was determined with three-dimensional volume of interest (VOI) areas surrounding (a) whole body; (b) background, and (c) all tracer target organs such as heart, liver, kidneys, urinary bladder, lung, and noninfected and infected muscles. ^{68}Ga-DOTA-TBIA101 organ distribution, represented by percentage of injected dose (%ID) calculation, and ^{68}Ga-DOTA-TBIA101 concentration, represented by the calculation of standardized uptake values (SUV), were performed from the same VOI of areas.

2.10. Statistical Analysis. Unless stated otherwise, data was expressed as mean and standard error of mean (SEM) using Microsoft Excel Software. The significance of a statistical difference between two mean values was calculated by a *Student's t-test*. The level of significance was set at $P \leq 0.05$.

3. Results

3.1. Synthesis of the DOTA-TBIA101. The linear DOTA-TBIA101 was synthesized by a solid phase method on a rink amide resin. DOTA was protected with a tris(*t*Bu)-moiety at three of its four carboxyl groups. The fourth unprotected carboxyl group was used to form a stable amide bond between the DOTA and the peptide's N-terminus. The DOTA-TBIA101 (Figure 1) was purified by reversed-phase-HPLC and resulted in >99% purity and the correct molecular weight of 1250 g/mol was confirmed by LC-MS and MALDI-TOF-MS for DOTA-TBIA101.

3.2. ^{nat}Ga-DOTA-TBIA101 Complexes. The labeling experiments were initially done using gallium trichloride to determine radiolabeling conditions that would avert unnecessary exposure to radiation. The molecular weight (1319 g/mol) of ^{nat}Ga-DOTA-peptide was established with MALDI-TOF-MS, confirming the complexation of gallium to DOTA-TBIA101. Post-C_{18} Sep-pak cartridge ^{nat}Ga-DOTA-TBIA101 showed >99% purity.

3.3. Bacterial Association Assay. The qualitative justification of the bacterial binding and internalization of all relevant compounds resulted in affinity binding constants (K) for TBIA101, DOTA-TBIA101, and ^{nat}Ga-DOTA-TBIA101 which were 0.022 ± 0.006 nM, 0.028 ± 0.006 nM, and 2.58 ± 1.04 nM for *E. coli* and 0.023 ± 0.007 nM, 0.029 ± 0.006 nM, and 2.97 ± 0.86 nM for *S. aur*. TBIA101 showed binding and internalization for both bacterial strains. DOTA-TBIA101 showed binding and no detectable internalization for both bacterial cells. A significantly higher *K* value for *S. aur* or *E. coli* was found for ^{nat}Ga-DOTA-TBIA101 compared to both TBIA101 and DOTA-TBIA101.

3.4. Cytotoxicity Test. The normalized IC_{50} values of TBIA101, DOTA-TBIA101, and ^{nat}Ga-DOTA-TBIA101 were calculated as 63.2, 42.1, and 33.7 μM, respectively. These values indicated no obvious toxic effect at the concentrations tested.

3.5. ^{68}Ge-^{68}Ga Generator Elution. The SnO_2-based generator provided 94 ± 3% and 85 ± 0.4% of the total calculated activity at day 10 and day 250, respectively. For this study, the total activities eluted from the TiO_2-based ^{68}Ge-^{68}Ga generator were 125 ± 57 MBq (n = 3) and 1437 ± 489 MBq (n = 23) for SnO_2-based ^{68}Ge-^{68}Ga generator (Table 1). Ninety percent to ninety-five percent of the eluted activity was obtained with fractionated elution for subsequent labeling.

3.6. Assessment of Radiolabeling Conditions and Routine Labeling. Labeling efficiency of the crude ^{68}Ga-DOTA-TBIA101 labeled at room temperature, 60°C and 100°C at different time points, is presented in Figure 2. High radiolabeling was obtained after 5 min at 100°C already (range: 86–96%). A significantly lower %LE was calculated for samples incubated at 60°C compared to 100°C (P = 0.004, range 75–83%). The radiolabeling at room temperature (negative control) compared to 100°C and 60°C (both $P \leq 0.001$) amounted to %LE of 28 ± 14, 19 ± 7, 40 ± 4, 30 ± 3, 27 ± 12, and 28 ± 1% for 5, 10, 15, 20, 30, and 45 min, respectively. A pH-optimum was found at 3 to 3.5, yielding a ^{68}Ga-complexation of 98 ± 3% to DOTA-TBIA101. Significantly lower %LE was determined for all other pH-values [1.5 ± 0.5% (pH 1-2), 24 ± 20% (pH 4), 9 ± 3% (pH 5), 2.1 ± 1.9% (pH 6), and 1.4 ± 1.4% (pH 7)]. A DOTA-TBIA101 concentration of 40 μM led to optimal ^{68}Ga-complexation (92 ± 0.7%); 5- and 20-fold lower-peptide concentration yielded 44 ± 20% and 22 ± 3%; nanomolar (nM) concentration led to 15–18% %LE. Quantitative HPLC analysis of crude and pure ^{68}Ga-DOTA-TBIA101 samples (40 μM) showed crude radiochemical purities of bound activity to be ≥92.1% and 100% radiochemical purity (Figures 3(a) and 3(b)). In comparison the 20 μM crude ^{68}Ga-DOTA-TBIA101 samples showed ≤14.4%LE and ≥98.0% radiochemical purity. The labeling method caused moderate activity losses to instruments, surface material, and colloid forming (18 ± 8%).

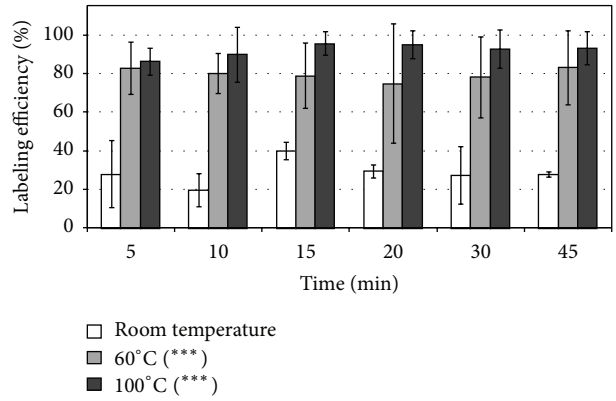

Figure 2: (a) Percentage labeling efficiency of ^{68}Ga-DOTA-TBIA101 at different incubation temperatures, comparing room temperature (open bars), 60°C (light grey bars), and 100°C (dark grey bars) using incubation durations of 5–45 minutes. Mean and standard error of mean are presented from n = 6 experiments. Student's t-test returned a P value < 0.001 (***) when compared to values concerning incubation at room temperature for all time durations.

3.6.1. Routine Radiolabeling. Twenty-three radiosyntheses were routinely performed as described in a 1.34 mL reaction volume (Table 1) within 34–41 min. The desorption of ^{68}Ga-DOTA-TBIA101 from the C_{18} Sep-pak cartridge using ethanol/saline mixture (1 : 1) recovered 77 ± 21% (n = 6). The average %LE was 64 ± 19 (n = 23) with good reproducibility [%LE < 25 (n = 1), %LE ≤ 25 ≤ 60 (n = 6), and %LE > 70 (n = 12)]. The final ^{68}Ga-DOTA-TBIA101 formulation in sterile saline solution showed a pH of 5.5–6 and contained ≤ 4% ethanol. In comparison, experiments using the TiO_2-based generator yielded a %LE of 61 and 94 ^{68}Ga-DOTA-TBIA101 in 30 min.

3.6.2. Quality Control. The %RCP using mobile phase 1 was detected at 99.0 ± 0.9% (n = 23). The Rf values for unbound ^{68}Ga and ^{68}Ga-DOTA-TBIA101 were calculated

Table 1: ^{68}Ga-DOTA-TBIA101 radiolabeling using a SnO_2-based ^{68}Ge-^{68}Ga generator.

Peptide conjugate	^{68}Ga-DOTA-TBIA101
Number of radiosyntheses (n)[$]	23
Generator elution	
Total ^{68}Ga-activity eluted (MBq)	1437 ± 489
Waste fraction (%)	7.1 ± 2.2
Generator use (days), (range [n])	198 ± 113, (11–279, [13])
^{68}Ga-activity added (MBq)	1201 ± 475
Buffer solution/peptide concentration (μM)	2.5 M Sodium acetate/40
Optimal pH value	3.5 ± 0.4
Temperature (°C)/duration (min)	95/10
SPE C18-unit type	
Small sample volume <0.5 mL	C18 Sep-pak light 100 mg
Large sample volume >0.5 mL	C18 Sep-pak 500 mg
SPE C18-unit elution mixture	
Standard mix (v/v)	EtOH/Saline (1 : 1)
Alternative mix (v/v)	CH_3CN/PBS (1 : 4)
Unit desorption ratio (%)	77 ± 21 (n = 6)
Specific activity (GBq/μmol)	12.4 ± 6
Time EOL to purified product (min)	39 ± 6 (n = 8)
Recovery of radioactivity (%)	102 ± 2 (n = 8)
Radiochemical purity	
Crude/final product HPLC (%)	>92/99 (n = 2)
Crude/final product ITLC (%)	>90/99 (n = 4)
Loss to apparatus and colloids (%)	18 ± 8 (n = 8)
Reproducibility	
Average %LE ITLC (range min–max)	64 ± 18.5 (16–85)
LE <25%: n (%)	1, (4.3)
LE 25–60%: n, (%)	6, (26.0)
LE >70%: n, (%)	12, (52.0)
End product activity half scale (MBq)[*]	668 ± 385

[$]Unless stated otherwise results are presented as mean ± SD of 23 of radiosyntheses. %LE = percentage labeling efficiency. [*]Details are given in Section 2.

0.85–1.0 and 0.05-0.15, respectively. Using mobile phase 2, the %RCP was 99.9 ± 0.5% (n = 3), with Rf values of 0.05–0.10 for colloidal ^{68}Ga and 0.9-1.0 for ^{68}Ga-DOTA-TBIA101. The yielded product activity was 476–856 MBq (7.7–19.5 GBq/μmol).

3.7. Compound Integrity and Blood Stability. The RCP of ^{68}Ga-DOTA-TBIA101 was found to be 95–100% over 180 min after radiolabeling (n = 3) and no significant unbound ^{68}Ga was observed. *In vitro* stability tests showed that ^{68}Ga-DOTA-TBIA101 was intact in whole blood, plasma, and serum (n = 3). The stability was determined by ITLC. The RCP was ≥97.2% for all time points up to 180 min at which no unbound ^{68}Ga was present.

3.8. Small Animal PET/CT Study. ^{68}Ga-DOTA-TBIA101 (19± 11 MBq) was injected in single bolus with short-term adverse reaction observed upon injection. Image acquisition at 25 min post-injection was analysed to demonstrate tracer biodistribution (%ID) and activity concentration (mean SUV) for three infected animals and compared to one healthy animal (Table 2). In this study, no significant differences in the tracer distribution (%ID per organ or tissue) were observed: healthy animal (range: 0.45–36.5%) and infected animal (range: 0.45–36.4%) when comparing heart, lung, liver, kidneys, brain, intestines, and urinary tract including bladder as well as healthy forearm and thigh muscles. Approximately 48% of the injected radioactivity was considered excreted (represented in kidneys, urinary tract, and bladder); heart and liver showed enhanced uptake (due to perfusion) and very low activity was distributed in lung, brain, intestine, forearm muscle, and hind muscle. The SUV values reflected a similar pattern regarding the organ activity concentration compared to %ID calculation, but it was noted that most SUV values of the healthy animals were less than of the infected animals (particularly relevant for heart and liver). A higher tracer concentration (SUV = 1.3–2.4) was calculated for 3/3 *E. coli*-infected muscles compared to the contralateral thigh (SUV = 1.2–2.2; P = 0.322; 1.21-fold), to the forearm muscles (SUV = 0.7–1.5; P = 0.092; 1.62-fold), or to the background (SUV = 0.66–0.78; P = 0.021; 2.3-fold) of the

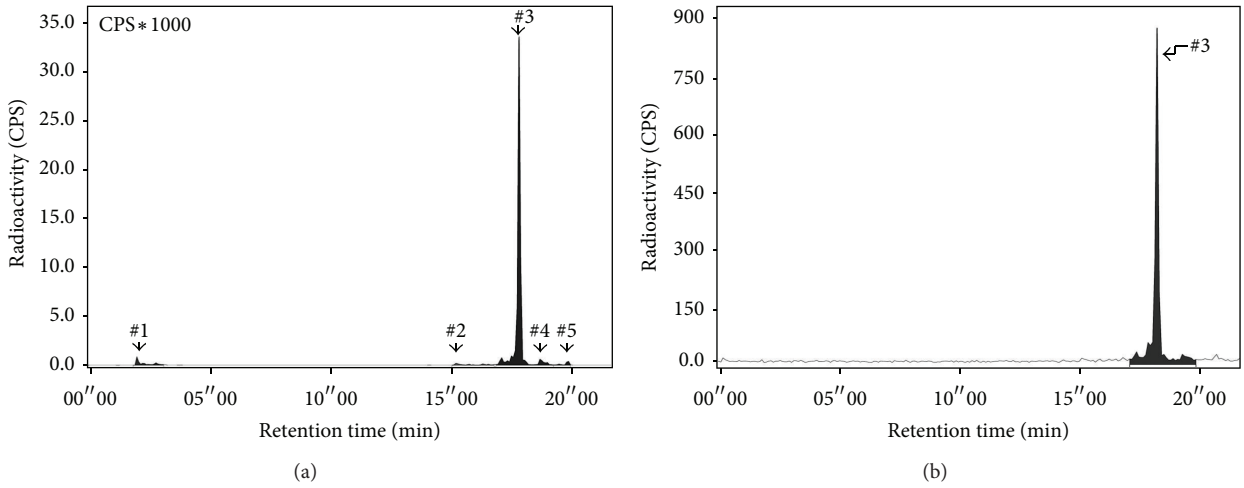

Figure 3: Radioanalytical HPLC chromatogram of ^{68}Ga-DOTA-TBIA101 (a) before and (b) after successful C_{18} Sep-pak cartridge purification. Reg. number 3 confirmed the elution of ^{68}Ga-DOTA-TBIA101 including traces of unbound ^{68}Ga (Reg. number 1) and by-products (Reg. number 2, number 4, and number 5) which were successfully removed (b).

Table 2: Organ/tissue concentration and biodistribution of ^{68}Ga-DOTA-TBIA101 in *Escherichia coli* infected mice.

Organ/tissue	Activity concentration (SUV)		Compound distribution (%ID)	
	Infected	Healthy control*	Infected	Healthy control
Heart	**16 ± 2.2**	0.43	9.5	8.9
Lung	**0.73 ± 0.03**	0.48	0.50	0.50
Liver	**25 ± 3.9**	14	14	14
Kidneys	**59 ± 6.3**	35	36	36
Brain	**0.90 ± 0.1**	0.55	0.55	0.57
Intestine	**0.90 ± 0.1**	0.54	0.58	0.57
Urinary tract/bladder	**34 ± 2.9**	20	21	21
Forearm muscle	**1.1 ± 0.2**	0.58	0.63	0.60
Hind muscle (CL)	**1.5 ± 0.3**	0.73	0.77	0.76
Hind muscle (*E.coli*)	**1.7 ± 0.3**	0.73	0.94	0.76
Hind muscle (CL) to forearm muscle	**1.4 ± 0.1**	NA	NA	NA
Hind muscle (*E.coli*) to background ratio	**2.3 ± 0.5**	NA	NA	NA
Hind muscle (*E.coli*) to forearm muscle	**1.6 ± 0.1**	NA	NA	NA
Hind muscle (*E.coli*) hind muscle (CL)	**1.2 ± 0.1**	NA	NA	NA

Values expressed as mean ± SEM. *E.coli* = *Escherichia coli* 22952 ($n = 3$), healthy control ($n = 1$), and CL = contralateral. *The SUV values were calculated from the same region of interest area using one healthy animal.

same animal. Normalization of the infected thigh muscle to reference tissue (forearm muscle in a healthy animal) showed a ratio of 3.0 ± 0.8 and a ratio of 2.3 ± 0.6 compared to the identical tissue (right hind thigh in the healthy animal).

The reconstructed PET/CT images showed positive tracer uptake with a moderate signal-to-noise ratio and visualization of the infected target area (Figure 4(a)-B), that is, right hind muscle tissue. In 3/3 animals the infection site was clearly localized by ^{68}Ga-DOTA-TBIA101, as represented in the three-dimensional slides (Figure 4(b)). No notable uptake was observed in the contralateral muscle tissue. Bacterial persistence in murine muscular tissue was not assessed with bacterial culturing postmortem. Unspecific uptake was detected in heart (blood pool) and liver and the excreted ^{68}Ga-DOTA-TBIA101-related radioactivity was represented by the avid kidney and bladder signal (Figure 4(a)-A).

4. Discussion

Noninvasive whole body imaging technologies like PET/CT can assist in identifying infections of unknown origin or those following surgery or transplantation. However, current radiotracers that image infectious foci (e.g., radiolabeled blood elements) are host dependent, require complex procedures,

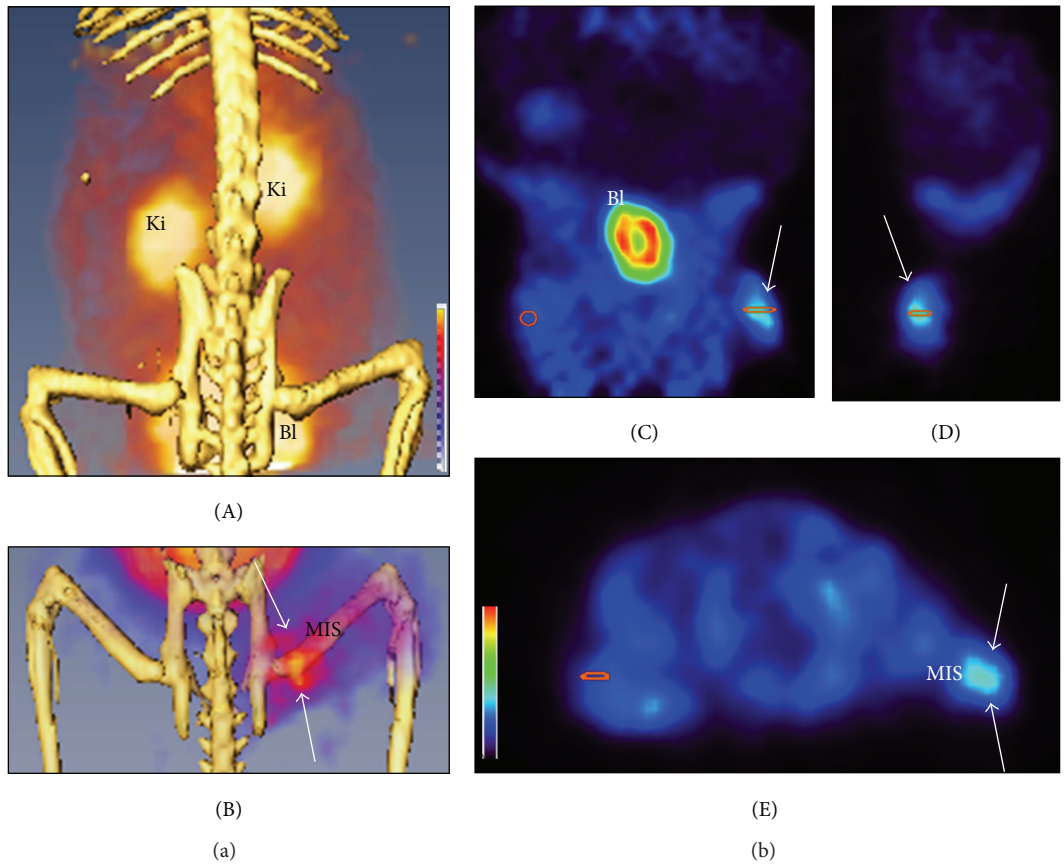

Figure 4: Images of BALB/c mice acquired using a Triumph μPET/CT preclinical imaging system (GE Healthcare, Buckinghamshire, United Kingdom). (a) Representative μPET/CT images acquired at 25 min after ^{68}Ga-DOTA-TBIA101 administration, (A) maximum intensity projection (MIP) image of a healthy animal demonstrating renal excretion, (B) pelvis projection including the muscular infection site (MIS) located in the right hind muscle tissue. The arrows indicate ^{68}Ga-DOTA-TBIA101 activity uptake at the site of infection. No activity uptake was noted in the contralateral muscle tissue. (b) Three-dimensional μPET images show activity uptake at the infection site (indicated by the white arrows) in (C) coronal, (D) sagittal, and (E) axial orientation. Ki is Kidney and Bl is Bladder.

or lack specificity. Although ^{18}F-FDG is commonly used as imaging agent in PET and ^{67}Ga-citrate in SPECT for infection/inflammation imaging, their specificity is even lower when compared with radiolabeled leukocytes. TBIA101 (PLPVLTI-GG) is a derivative of depsidomycin (PLPVLTI), an uncharged cyclic depsiheptapeptide that was extended by two glycine molecules, causing enhanced antibacterial properties. When the peptide structure is given, it is possible to design new analogues containing one or two additional glycine or alanine molecules, in order to improve efficiency against bacteria without increasing harmful side effects [15]. Three possible folding patterns can be expected: nonhydrogen, β-turn, and α-helical turn for depsipeptides. Alanine has a higher α-helical-forming tendency than glycine. The major conformational feature is β-turn, involving glycine and proline [16].

Although the mode of action for depsipeptides is not entirely understood, it is postulated that there is a possible interaction with lipopolysaccharide (LPS) structures of the bacterial cell envelope. Studies involving the related β-sheet peptides report effective disruption of the lipid organization and may induce lipid flip-flop or undergoing membrane translocation without causing significant calcein release from the membrane system; however no long-living pores are being formed [17]. To date, no attempts have been made to conjugate TBIA101 with DOTA to allow for complexation of the PET-radioisotope ^{68}Ga. This will consequently facilitate studies of the *in vivo* distribution including targeting infectious tissue in preclinical animal models. Thus, we aimed to synthesise and radiolabel DOTA-TBIA101 with generator-eluted ^{68}Ga to detect *E. coli*-based infection by μPET/CT imaging of a BALB/c mice model.

As a prerequisite, the TBIA101 synthesis was successfully achieved and conjugated using DOTA-tris(*t*Bu) ester in an N-terminal peptide position based on a resin method [18]. This conjugation is limited to the N-terminal position and exhibits moderately long deprotection times for the complete cleavage of the tris(*t*Bu) ester [7]. Furthermore, DOTA-TBIA101 was nonradioactively labeled with gallium (III) trichloride to form ^{nat}Ga-DOTA-TBIA101 for subsequent evaluation of its bacterial binding properties and to

perform *in vitro* cytotoxicity studies whilst preventing unnecessary radiation exposure. Owing to their involvement in the innate human immune response, antimicrobial peptides are not considered cytotoxic [19], although amending the structure or conjugation and complexation with radiogallium may cause unexpected cytotoxic behavior. The IC_{50}-values reported in this paper were significantly lower than DOTAVAP-P1, which is also considered for preclinical studies of inflammation and infection [20]. For the μPET study, the mice were injected with approximately 500-fold less ^{68}Ga-DOTA-TBIA101 (8 nM), which was well tolerable for PET/CT imaging. The administered dose of ^{68}Ga-DOTA-TBIA101 is considered nontoxic for mammalian cells but also not bactericidal. Interestingly, based on MALDI-TOF-MS analysis, DOTA-TBIA101 showed a differentiated bacterial binding and a lack of internalization in both tested *S. aur* and *E. coli* strains, compared to TBIA101, despite their near-equal *K*-values. We have reason to believe that the DOTA-conjugation does not compromise the initial interaction to LPS but may affect the peptide property of initiating a membrane flip-flop mechanism, which might be due to lack of membrane occupancy with the compound, as most often a distinct threshold must be reached to alter membrane potential. It was reported that the entry into the cell by the peptides requires a minimum number, or threshold concentration, of antimicrobial peptides to accumulate on the surface of the lipid membrane. This event can be affected by factors other than concentration—such as the ability of the peptides to multimerize and also the features of the phospholipid membrane itself (e.g., its lipid composition, head group size, and fluidity) [21]. The transmembrane potential of the bilayer may also influence the way in which the peptide enters the membrane, since a highly negative transmembrane potential will facilitate membrane pore formation [22]. The ^{nat}Ga-DOTA-TBIA101 also exhibited a 200-fold lower binding affinity than DOTA-TBIA101, which was unexpected but might indicate a slower pharmacodynamic once gallium is complexed. A pragmatic explanation might be the use of solvents within the preparation. All three compounds showed interaction with both bacterial cells tested and the unexpected internalization of ^{nat}Ga-DOTA-TBIA101 might be due to tight integration into the cell wall. We cannot fully explain the reason for the internalization of cold labeled ^{nat}Ga-DOTA-TBIA101 for both bacterial cells as compared to unlabeled TBIA101 and DOTA-TBIA101. MALDI-TOF MS has offered a highly sensitive method for mass recovery in cellular samples but more in-depth experiments with an array of known peptides would support further justification of ^{nat}Ga-DOTA-TBIA(101).

As one main achievement we report the successful radiolabeling with a "high-yield"/"high-purity" approach for ^{68}Ga-DOTA-TBIA101 using state-of-the-art ^{68}Ge-^{68}Ga-generator technology, which makes radiopharmaceutical production easy, cost efficient, and available to hospitals without access to a cyclotron infrastructure [23]. A small volume containing the majority of the eluted ^{68}Ga can be used for research; however, the breakthrough of Germanium-68 (^{68}Ge) and other metals or chemical impurities may hinder the complexation if the generator matrix is eluted over a prolonged duration. Consequently, we observed this direct radiolabeling method routinely and confirmed good robustness as well as high specific activities and found no relation between the %LE of ^{68}Ga-DOTA-TBIA101 and the life span of the generator, which was also complemented by the low contents of competing ions, as reported previously [13, 24]. However, daily elution is required to keep the concentration of the metal ions and ^{68}Ge breakthrough as low as possible and the use of a C_{18} Sep-pak cartridge is mandatory for this method before the final product is dispensed. Prepurification methods of the crude ^{68}Ga eluate are available that exhibit minimal losses of activity but employ an additional cartridge purification step [25]. Our findings, as summarised in Table 1, are comparable with the previous findings reported in study that employed a SnO_2-based generator [23, 24] and also supported the efficient separation of ^{68}Ga-DOTA-TBIA101 from uncomplexed or colloidal ^{68}Ga by altering polarity on the C_{18} Sep-pak cartridge unit. It has been indicated that the amount of ^{68}Ge is reduced by at least 100- to 1000-fold in the final product after the C_{18} Sep-Pak cartridge has been used, but the ^{68}Ge content in the final ^{68}Ga preparation cannot be measured prior to tracer administration. We were able to desorb between 56% and 99% radiochemical-pure ^{68}Ga-DOTA-TBIA101 as qualified and quantified by using a two-strip ITLC system or HPLC with reasonable activity losses due to the labeling protocol. ^{68}Ga-DOTA-TBIA101 was found stable in human blood, serum, and plasma against transchelation over 180 min (≥97.2%) as compared to 39% plasma binding of ^{68}Ga-DOTAVAP-P1 [20]. The stability of ^{68}Ga-DOTA-TBIA101 was determined by ITLC as successfully carried out by other workgroup studies that examined various tracer blood stabilities [26–29] but it might lack accuracy in determining potential metabolites. Conversely, HPLC was used by Ujula et al. to assess DOTAVAP-P1 stability in human- and rat-plasma; the amount of intact product after 4 h of incubation was 88% and 87%, respectively.

The findings from a small-scale proof-of-concept experiment that set out to prove the capability of ^{68}Ga-DOTA-TBIA101-PET to localize *E. coli*-infected muscle tissue after 4-5-day incubation led to contradictory results. Despite the fact that ^{68}Ga-DOTA-TBIA101-PET was able to localize the infectious tissue, the authors cannot conclude that the tracer represented infection by directly targeting the bacteria. Additional results from a parallel project using the same animals returned positive visualization of the infection site with ^{18}F-FDG-PET; however, ^{68}Ga-NOTA-UBI29-41 was not localized congruently [30] at a late stage of infection (5-7-d). These results may raise a question on the infection-specific uptake observed with ^{68}Ga-DOTA-TBIA101 or ^{18}F-FDG. Except from a significant signal-to-noise ratio (P = 0.021), ^{68}Ga-DOTA-TBIA101-PET amounted in a low T/NT SUV ratio (1.2 ± 0.1) if one compares infected muscle to the uninfected contralateral muscle tissue of the same animal. The latter T/NT ratio contradicts the study performed by Akhtar et al. using dual-time point SPECT with ^{99m}Tc-UBI29-41 in *E. coli*-infected rabbits (T/NT =1.5 ± 0.4 at 30 min and 1.7 ± 0.4 at 60 min p.i.) [31]. Dual time point

imaging protocol including a rescan at ≥60 min p.i. would have indicated whether the early-onset tracer uptake can be verified as target-specific accumulation. Initial uptake could be also caused by inflammatory processes or enhanced perfusion. Some compromising limitations have revealed themselves after this preliminary infection-imaging study was conducted. Experiments of greater depth and including positive controls are required to clarify outstanding matters regarding the *in vivo* performance of ^{68}Ga-DOTA-TBIA101. Imaging evaluation of sterile inflammatory processes would help to cast doubt on tracer specificity particularly. The use of a well-understood infection model, including the type of bacteria and incubation duration up to PET/CT imaging, could be helpful in accommodating a certain imaging setup. Supporting imaging results with postmortem histopathology and bacterial recovery from infectious tissue may aid interpretation of noninvasive findings in future studies. For example, ^{68}Ga-DOTAVAP-V1 studies were carried out two days after bacilli injection with 2-fold more injected bacteria [20]. The infected muscle to background ratio of ^{68}Ga-DOTA-TBIA101 (2.3 ± 0.3) was in the same range as reported by Ujula et al. (2.3 ± 0.7) and lower compared to ^{18}F-FDG (3.1 ± 0.6) for infection imaging but important control measures were carried out by the authors. In this paper %ID and SUV calculation reported on showed most of the activities recovered in the kidneys and urinary tract, suggesting rapid renal excretion and early-onset after injection. A similar study that used ^{68}Ga-DOTAVAP-PEG-P2 showed rapid renal excretion from 5–120 min [32]. Besides liver uptake observed in this study, there was no significant uptake in other organs such as lung or heart. Higher liver accumulation was detected in a previous study that used ^{68}Ga-DOTA-nitroimidazole where the authors reasoned that the tracer accumulation in the liver might be due to the compound's high lipophilicity [33].

Despite the high specific activity and acceptable binding affinity of ^{68}Ga-DOTA-TBIA101, imaging of *E. coli* was considered suboptimal. For this reason further matters should be addressed that might be involved in causing lower uptake in an active infection site. Whilst the advanced state of the infection duration could have likely led to a strong eradication of the bacilli in immunocompetent animals, it cannot be ascertained that this was the case with the particular amount of *E. coli* injected originally in the reported experiment. In some cases the bacterial burden following an intramuscular or subcutaneous inoculum of laboratory bacterial is almost negligible; the recovery rate from the infection site returned very low. In this way a reduced bacterial multiplication could occur and include a prolonged lag (bacteriopause) phase. More virulent strains, however, can cause massive wounds even after a short incubation period. As some depsipeptides form the active part of streptogramins, an antibiotic class of compound targeting the bacterial ribosomal activity, it could be concluded that a quiescent (homoeostatic) bacterial state is unlikely to be targeted by depsipeptide-based tracers [34]. Therefore, particularly in unestablished animal infection models, a 24-hour-old microbiological tissue culture including CFU counting is encouraged. Furthermore, bacteria are naturally equipped with surface-bound and/or secretory proteases, a considerable defence mechanism that can inactivate antimicrobial compounds like DOTA-TBIA101 and that may result in a reduced tracer accumulation, even though viable bacteria are present. For example, the outer-membrane (OmpT) protease (of an enterohemorrhagic *E. coli* strain) disunites and inactivates an α-helical AMP (LL-37) but cannot cleave a disulfide-bond-stabilized AMP (HNP-1) [35, 36]. In addition there are further protective shielding strategies that bacteria employ to resist antimicrobial action; two of these strategies are modulation of the host innate immune response [37] and bacterial DNA mediated downregulation of bactericidal peptides in enteric infections [38]. Furthermore, bacteria can make use of cationic capsule polysaccharides or membrane phosphate charge masking mechanism or activation of ATP-binding cassette (ABC) transporters [39].

The results warrant further preclinical imaging studies as the DOTA-conjugation to TBIA101 did not appear to compromise the TBIA101 capacity as the targeting vector. These studies should include sterile inflammation-control experiments as well as ensure viable bacteria in the target site over a shorter time span after inoculation with aerobic bacterial strains; thus, the lack of an experiment of greater depth might be the reason for the lower-than-expected target-to-nontarget ratio.

5. Conclusion

We reported on the depsipeptides-deriving compound ^{68}Ga-DOTA-TBIA101 and its "proof-of-concept" approach to target infected muscle tissue (although in low-target-to-nontarget ratios), providing noninvasive imaging of infection using PET/CT at a late stage. As prerequisites, ^{68}Ga-DOTA-TBIA101 radiolabeling, bacterial binding, cytotoxicity, integrity, and stability met the criteria to warrant the envisaged imaging studies to approve its target-to-nontarget ratio before further animal studies could commence.

Conflict of Interests

The authors declare that there is no conflict of interests regarding the publication of this paper.

Authors' Contribution

Botshelo B. Mokaleng, Thomas Ebenhan, and Jan R. Zeevaart have contributed equally to this publication.

Acknowledgments

The project was kindly funded by the Department of Nuclear Medicine at the University of Pretoria and supported by the Catalysis & Peptide Research Unit and the Department of Virology at the University of KwaZulu-Natal. The authors thank Dr. S. Pawar, Dr. D. Tiwari, and Ms. L. Motisa for their excellent assistance. The authors acknowledge the Nuclear Technologies in Medicine and the Biosciences Initiative

(NTeMBI), a national technology platform developed and managed by the South African Nuclear Energy Corporation (Necsa) and funded by the Department of Science and Technology (DST). Barbara English of the research office of the University of Pretoria's Faculty of Health Sciences is thanked for her language editing.

References

[1] G. Malviya and A. Sinore, "Infection and inflammation imaging," *Nuclear Medicine and Biology*, vol. 41, no. 6, p. 488, 2014.

[2] A. Signore, C. Lauri, and F. Galli, "Radiolabelled probes targeting infection and inflammation for personalized medicine," *Current Pharmaceutical Design*, vol. 20, no. 14, pp. 2338–2345, 2014.

[3] M. M. Welling, S. Mongera, A. Lupetti et al., "Radiochemical and biological characteristics of 99mTc-UBI 29-41 for imaging of bacterial infections," *Nuclear Medicine and Biology*, vol. 29, no. 4, pp. 413–422, 2002.

[4] G. Ferro-Flores, F. D. M. Ramírez, L. Meléndez-Alafort, C. A. D. Murphy, and M. Pedraza-López, "Molecular recognition and stability of 99mTc-UBI 29-41 based on experimental and semiempirical results," *Applied Radiation and Isotopes*, vol. 61, no. 6, pp. 1261–1268, 2004.

[5] T. Ebenhan, J. R. Zeevaart, J. D. Venter et al., "Preclinical evaluation of 68Ga-labeled 1, 4, 7-triazacyclononane-1, 4, 7-triacetic acid-ubiquicidin as a radioligand for PET infection imaging," *Journal of Nuclear Medicine*, vol. 55, no. 2, pp. 308–314, 2014.

[6] J. S. Davies, "The cyclization of peptides and depsipeptides," *Journal of Peptide Science*, vol. 9, no. 8, pp. 471–501, 2003.

[7] V. K. Narayanaswamy, F. Albericio, Y. M. Coovadia et al., "Total synthesis of a depsidomycin analogue by convergent solid-phase peptide synthesis and macrolactonization strategy for antitubercular activity," *Journal of Peptide Science*, vol. 17, no. 10, pp. 683–689, 2011.

[8] H. Li, B. Li, H. Song, L. Breydo, I. V. Baskakov, and L.-X. Wang, "Chemoenzymatic synthesis of HIV-1 V3 glycopeptides carrying two N-glycans and effects of glycosylation on the peptide domain," *The Journal of Organic Chemistry*, vol. 70, no. 24, pp. 9990–9996, 2005.

[9] B. Behnam Azad, V. A. Rota, D. Breadner, S. Dhanvantari, and L. G. Luyt, "Design, synthesis and in vitro characterization of Glucagon-Like Peptide-1 derivatives for pancreatic beta cell imaging by SPECT," *Bioorganic and Medicinal Chemistry*, vol. 18, no. 3, pp. 1265–1272, 2010.

[10] S. M. Mandal, L. Migliolo, and O. L. Franco, "The use of MALDI-TOF-MS and in Silico studies for determination of antimicrobial peptides' affinity to bacterial cells," *Journal of the American Society for Mass Spectrometry*, vol. 23, no. 11, pp. 1939–1948, 2012.

[11] D. A. Scudiero, R. H. Shoemaker, K. D. Paull et al., "Evaluation of a soluble tetrazolium/formazan assay for cell growth and drug sensitivity in culture using human and other tumor cell lines," *Cancer Research*, vol. 48, no. 17, pp. 4827–4833, 1988.

[12] W. A. P. Breeman, M. de Jong, E. de Blois, B. F. Bernard, M. Konijnenberg, and E. P. Krenning, "Radiolabelling DOTA-peptides with 68Ga," *European Journal of Nuclear Medicine and Molecular Imaging*, vol. 32, no. 4, pp. 478–485, 2005.

[13] D. D. Rossouw and W. A. P. Breeman, "Scaled-up radiolabelling of DOTATATE with68Ga eluted from a SnO2-based68Ge/68Ga generator," *Applied Radiation and Isotopes*, vol. 70, no. 1, pp. 171–175, 2012.

[14] M. Ocak, M. Antretter, R. Knopp et al., "Full automation of 68Ga labelling of DOTA-peptides including cation exchange prepurification," *Applied Radiation and Isotopes*, vol. 68, no. 2, pp. 297–302, 2010.

[15] D. Billot-Klein, D. Shlaes, D. Bryant et al., "Presence of UDP-N-Acetylmuramyl-Hexapeptides and -Heptapeptides in enterococci and staphylococci after treatment with ramoplanin, tunicamycin, or vancomycin," *Journal of Bacteriology*, vol. 179, no. 15, pp. 4684–4688, 1997.

[16] I. L. Karle, D. Ranganathan, M. G. Kumar, and R. Nagaraj, "Design, synthesis, conformational and membrane ion transport studies of proline-adamantane hybrid cyclic depsipeptides," *Biopolymers*, vol. 89, no. 5, pp. 471–478, 2008.

[17] L. Zhang, A. Rozek, and R. E. W. Hancock, "Interaction of cationic antimicrobial peptides with model membrane," *The Journal of Biological Chemistry*, vol. 276, no. 21, pp. 35714–35722, 2001.

[18] L. M. de León-Rodriguez, Z. Kovacs, G. R. Dieckmann, and A. D. Sherry, "Solid-phase synthesis of DOTA-peptides," *Chemistry*, vol. 10, no. 5, pp. 1149–1155, 2004.

[19] M. S. Akhtar, M. B. Imran, M. A. Nadeem, and A. Shahid, "Antimicrobial peptides as infection imaging agents: better than radiolabeled antibiotics," *International Journal of Peptides*, vol. 2012, Article ID 965238, 19 pages, 2012.

[20] T. Ujula, S. Salomäki, P. Virsu et al., "Synthesis, 68Ga labeling and preliminary evaluation of DOTA peptide binding vascular adhesion protein-1: a potential PET imaging agent for diagnosing osteomyelitis," *Nuclear Medicine and Biology*, vol. 36, no. 6, pp. 631–641, 2009.

[21] L. Yang, T. M. Weiss, R. I. Lehrer, and H. W. Huang, "Crystallization of antimicrobial pores in membranes: magainin and protegrin," *Biophysical Journal*, vol. 79, no. 4, pp. 2002–2009, 2000.

[22] H. W. Huang, "Action of antimicrobial peptides: two-state model," *Biochemistry*, vol. 39, no. 29, pp. 8347–8352, 2000.

[23] E. de Blois, H. S. Chan, C. Naidoo, D. Prince, E. P. Krenning, and W. A. P. Breeman, "Characteristics of SnO_2-based $^{68}Ge/^{68}Ga$ generator and aspects of radiolabelling DOTA-peptides," *Applied Radiation and Isotopes*, vol. 69, no. 2, pp. 308–315, 2011.

[24] T. Ebenhan, N. Chadwick, M. M. Sathekge et al., "Peptide synthesis, characterization and ^{68}Ga-radiolabeling of NOTA-conjugated ubiquicidin fragments for prospective infection imaging with PET/CT," *Nuclear Medicine and Biology*, vol. 41, no. 5, pp. 390–400, 2014.

[25] D. Mueller, I. Klette, R. P. Baum, M. Gottschaldt, M. K. Schultz, and W. A. P. Breeman, "Simplified NaCl based 68Ga concentration and labeling procedure for rapid synthesis of 68Ga radiopharmaceuticals in high radiochemical purity," *Bioconjugate Chemistry*, vol. 23, no. 8, pp. 1712–1717, 2012.

[26] R. Lesche, G. Kettschau, A. V. Gromov et al., "Preclinical evaluation of BAY 1075553, a novel 18F-labelled inhibitor of prostate-specific membrane antigen for PET imaging of prostate cancer," *European Journal of Nuclear Medicine and Molecular Imaging*, vol. 41, no. 1, pp. 89–101, 2014.

[27] A. R. Jalilian, H. Yousefnia, K. Shafaii, A. Novinrouz, and A. A. Rajamand, "Preparation and biodistribution studies of a radiogallium-acetylacetonate bis (thiosemicarbazone) complex in tumor-bearing rodents," *Iranian Journal of Pharmaceutical Research*, vol. 11, no. 2, pp. 523–531, 2012.

[28] B. Y. Yang, J. M. Jeong, Y. J. Kim et al., "Formulation of 68Ga BAPEN kit for myocardial positron emission tomography imaging and biodistribution study," *Nuclear Medicine and Biology*, vol. 37, no. 2, pp. 149–155, 2010.

[29] A. Fontes, M. I. M. Prata, C. F. Geraldes, and J. P. André, "Ga(III) chelates of amphiphilic DOTA-based ligands: synthetic route and in vitro and in vivo studies," *Nuclear Medicine and Biology*, vol. 38, no. 3, pp. 363–370, 2011.

[30] T. Ebenhan, O. Gheysens, G. E. M. Maguire et al., "[68Ga]NOTA-UBI-PET: a host-independent targeted method to non-invasively imaging of bacterial infection-preclinical evaluation in small animal models," (WFNMB accepted abstract publication), 2014.

[31] M. S. Akhtar, J. Iqbal, M. A. Khan et al., "99mTc-labeled antimicrobial peptide ubiquicidin (29–41) accumulates less in Escherichia coli infection than in Staphlococcus aureus infection," *Journal of Nuclear Medicine*, vol. 45, no. 5, pp. 849–856, 2004.

[32] J. Silvola, A. Autio, P. Luoto, S. Jalkanen, and A. Roivainen, "Preliminary evaluation of novel 68Ga-DOTAVAP-PEG-P2 peptide targeting vascular adhesion protein-1," *Clinical Physiology and Functional Imaging*, vol. 30, no. 1, pp. 75–78, 2010.

[33] L. Hoigebazar, J. M. Jeong, M. K. Hong et al., "Synthesis of 68Ga-labeled DOTA-nitroimidazole derivatives and their feasibilities as hypoxia imaging PET tracers," *Bioorganic & Medicinal Chemistry*, vol. 19, no. 7, pp. 2176–2181, 2011.

[34] C. Cocito, M. Di Giambattista, E. Nyssen, and P. Vannuffel, "Inhibition of protein synthesis by streptogramins and related antibiotics," *The Journal of Antimicrobial Chemotherapy*, vol. 39, supplement 1, pp. 7–13, 1997.

[35] J.-L. Thomassin, J. R. Brannon, J. Kaiser, S. Gruenheid, and H. le Moual, "Enterohemorrhagic and enteropathogenic *Escherichia coli* evolved different strategies to resist antimicrobial peptides," *Gut Microbes*, vol. 3, no. 6, pp. 556–561, 2012.

[36] J.-L. Thomassin, J. R. Brannon, B. F. Gibbs, S. Gruenheid, and H. Le Moual, "OmpT outer membrane proteases of enterohemorrhagic and enteropathogenic Escherichia coli contribute differently to the degradation of human LL-37," *Infection and Immunity*, vol. 80, no. 2, pp. 483–492, 2012.

[37] B. Sperandio, B. Regnault, J. Guo et al., "Virulent *Shigella flexneri* subverts the host innate immune response through manipulation of antimicrobial peptide gene expression," *The Journal of Experimental Medicine*, vol. 205, no. 5, pp. 1121–1132, 2008.

[38] D. Islam, L. Bandholtz, J. Nilsson et al., "Downregulation of bactericidal peptides in enteric infections: a novel immune escape mechanism with bacterial DNA as a potential regulator," *Nature Medicine*, vol. 7, no. 2, pp. 180–185, 2001.

[39] H. Le Moual, J.-L. Thomassin, and J. R. Brannon, "Antimicrobial peptidesas an alternative approach to treat bacterial infections," *Journal of Clinical & Cellular Immunology*, vol. S13, article 004, 2013.

Hindawi Publishing Corporation
BioMed Research International
Volume 2015, Article ID 127325, 7 pages
http://dx.doi.org/10.1155/2015/127325

Review Article

Nuclear Medicine in Diagnosis of Prosthetic Valve Endocarditis: An Update

Maria Musso and Nicola Petrosillo

National Institute for Infectious Diseases "L. Spallanzani", IRCCS, Via Portuense 292, 00149 Rome, Italy

Correspondence should be addressed to Maria Musso; musso_maria@yahoo.it

Received 6 June 2014; Accepted 14 October 2014

Academic Editor: Alberto Signore

Over the past decades cardiovascular disease management has been substantially improved by the increasing introduction of medical devices as prosthetic valves. The yearly rate of infective endocarditis (IE) in patient with a prosthetic valve is approximately 3 cases per 1,000 patients. The fatality rate of prosthetic valve endocarditis (PVE) remains stable over the years, in part due to the aging of the population. The diagnostic value of echocardiography in diagnosis is operator-dependent and its sensitivity can decrease in presence of intracardiac devices and valvular prosthesis. The modified Duke criteria are considered the gold standard for diagnosing IE; their sensibility is 80%, but in clinical practice their diagnostic accuracy in PVE is lower, resulting inconclusively in nearly 30% of cases. In the last years, these new imaging modalities have gained an increasing attention because they make it possible to diagnose an IE earlier than the structural alterations occurring. Several studies have been conducted in order to assess the diagnostic accuracy of various nuclear medicine techniques in diagnosis of PVE. We performed a review of the literature to assess the available evidence on the role of nuclear medicine techniques in the diagnosis of PVE.

1. Introduction

Endovascular infections, including infective endocarditis (IE) and prosthetic vascular infections, are uncommon pathologies associated with a poor prognosis. Over the past decades cardiovascular disease management has been substantially improved by the increasing introduction of medical devices as mechanical or biologic heart valves, pacemakers, defibrillators, coronary artery stents, and artificial arteries.

The patients' age has increased over the last years, leading to an increase in the number of cardiovascular surgical interventions and also in the infective risk of patients. Between 1990 and 1999 incidence of prosthetic valve endocarditis (PVE) has increased 50% [1, 2]; patients with heart valve prosthesis are exposed to a yearly rate of approximately 3 cases of IE per 1,000 patients [3].

These changes in the epidemiology also explain why, despite important improvements in IE management, the fatality rate of PVE has not decreased in the last forty years, with in-hospital fatality rate of about 20% [4].

PVE are mostly healthcare associated and are distinct in early onset (EO) and late onset (LO), according to the time spent from the intervention to the onset of symptoms; usually a cutoff of one year is adopted [2]. Rates of infection in PVE range from 1–6% to 15%, with higher rates in revision surgery [5].

PVE diagnosis may still be problematic. Imaging investigations traditionally used for diagnosis of PVE are transthoracic echocardiography (TTE) and transesophageal echocardiography (TEE), with a sensitivity of 70% and 90%, respectively [3]; however, the diagnostic value of echocardiography in IE diagnosis is operator-dependent and its sensitivity can decrease in presence of intracardiac devices, valvular prosthesis, severe preexisting lesions, and very small or no vegetation [4].

Over the past years nuclear medicine procedures gave an important contribution to the diagnostic assessment of endovascular infections, through the evaluation of the metabolic activity of the prosthetic material presenting

morphological alterations or before development of structural changes.

We performed a review of the literature to summarize the available evidence on the role of nuclear medicine techniques in the diagnosis of PVE.

2. Methods

Published papers from January 1980 to June 2014, represented by clinical studies, reviews, and case reports reporting data about use of nuclear medicine techniques to investigate prosthetic valve infections, were found through computerized literature searches using MEDLINE (National Library of Medicine, Bethesda, MD) and by reviewing the references of retrieved articles. Index search terms included the Medical Subjects Heading "nuclear medicine," "prosthetic," "valve," and "endocarditis." Only articles written in English, German, Spanish, and Italian were included.

Infective endocarditis in patients with an implanted cardiac device and vascular graft was out of the scope of this paper.

3. Results and Discussion

3.1. Prosthetic Valve Endocarditis Diagnosis

3.1.1. Current Practice in the Management of Endocarditis. The epidemiological characteristics of patients with IE differ between developed and developing countries; in the latter case the patient is younger and is affected by predisposing diseases, such as congenital heart disease or rheumatic fever. In developed countries medical progress has caused an increase in the age of patients with endocarditis and in the incidence of health care associated endocarditis, including PVE [4].

Infection of the cardiac prosthetic valve can occur by contamination at the time of its placement or as a result of hematogenous dissemination or by contiguous infection [2]. *Staphylococcus aureus* is the most common cause of PVE, followed by coagulase-negative staphylococci; *Streptococcus viridans* group, *Enterococcus* spp., and yeasts are more common in LO than in EO PVE. Culture-negative endocarditis represents approximately 13% of PVE, with reported rates of 31% [4] and they are more frequent in LO than in EO PVE. Chronic haemodialysis, diabetes, and intravascular devices, including cardiac prosthetic valve, are all predisposing factors to *S. aureus* endocarditis [24].

From a clinical point of view, the presentation of PVE does not substantially differ from the other forms of IE. Indeed, its nonspecific clinical presentation makes IE a cause of fever of unknown origin, with a high clinical suspicion needed to make diagnosis.

The modified Duke criteria are considered the gold standard for diagnosing IE [6] (Tables 1, 2, and 3). In epidemiological studies the sensitivity of Duke criteria is 80%, but in clinical practice their diagnostic accuracy is lower, especially in PVE; prosthetic material in fact compromises the sensitivity of echocardiography that results inconclusively in nearly 30% of cases [4].

PVE represents up to 30% of IE in developed countries, and the in-hospital mortality in patients with PVE can reach 47%, especially in *S. aureus* bacteremia; these data confirm that it is important to increase the ability to early diagnose this clinical condition [8].

3.1.2. The Contribution of Nuclear Medicine in the Diagnosis of PVE. Several nuclear medicine techniques, characterized by different kind of tracers and technologies, have been implemented in order to offer precious information about the metabolic activity of infected tissue. In the last years, these new imaging modalities have gained an increasing attention because they make it possible to diagnose an IE earlier than the structural alterations occurring.

Since the eighties to nowadays several papers have reported the experiences of nuclear medicine (NM) specialists in utilization of NM imaging modalities for PVE diagnosis. Our research provided 29 articles; seven were excluded because they were inadequate to our purpose.

Table 4 summarizes all techniques mentioned in papers reviewed [7–23]; we did not include 6 commentary articles to the prospective study of Saby et al. that we have already included in Table 4 [25–30].

Ten articles reported experiences regarding labeled leukocytes scintigraphy in PVE diagnosis [13–23]; in some of them this technique was associated with single photon emission computed tomography (SPECT) acquisition of images [16–19], because SPECT can provide accurate morphologic details.

Six papers regard ^{18}F-fluorodeoxyglucose positron emission tomography in association with computed tomography (^{18}F-FDG PET/CT) or with computed tomography angiography (CTA) in the diagnostic assessment of PVE or perivalvular infective complications in patient affected by PVE [12–21].

(1) ^{18}F-FDG PET/CT. ^{18}F-FDG PET/CT combines the assessment of metabolic activity of tissues (namely, the glycolytic activity) with the spatial resolution of CT.

A review published in 2013 has extensively collected the available data, mainly from case reports and case series, on the efficacy and usefulness of this technique and has stressed that there is currently no evidence from case-control studies comparing PET/CT with other diagnostic tools currently available [8].

To date there has been only one published prospective study that aims to investigate the diagnostic power of this technique [7]. Seventy-two patients with suspected PVE, initially assessed by using the modified Duke criteria, underwent PET/CT. Although the diagnosis of endocarditis was not always confirmed by histological examination of the prosthetic valve, the authors point out that all those cases of endocarditis undergoing surgery and confirmed by pathologists were identified by ^{18}F-FDG PET/CT [7].

Sensitivity and specificity reported in this study (73% and 80%, resp.) did not differ greatly from the values found in a recent study on the use of ^{18}F-FDG PET/CT for the diagnosis of endocarditis on pacemakers and implantable defibrillators where sensitivity and specificity were 63% and 86, respectively [31].

Table 1: Modified Duke criteria for the diagnosis of prosthetic valve endocarditis (PVE) [6].

Definite PVE
Clinical criteria
(1) 2 major criteria
Or
(2) 1 major criterion and 3 minor criteria
Or
(3) 5 minor criteria
Pathological criteria
(1) Microorganisms demonstrated by culture or histological examination of a vegetation, a vegetation that has embolized
Or
(2) An intracardiac abscess specimen or pathological lesions; vegetation or intracardiac abscess confirmed by histological examination showing active endocarditis
Possible PVE
(1) 1 major criterion and 1 minor criterion
Or
(2) 3 minor criteria
Rejected PVE
(1) Firm alternate diagnosis explaining evidence of infective endocarditis
Or
(2) Resolution of infective endocarditis syndrome with antibiotic therapy for ≤4 days
Or
(3) No pathological evidence of infective endocarditis at surgery or autopsy, with antibiotic therapy for ≤4 days
Or
(4) Does not meet criteria for possible infective endocarditis, as above

Table 2: Major criteria according to Li et al. [6] and new major criteria according to Saby et al. [7] for the diagnosis of prosthetic valve endocarditis (PVE).

Li et al. [6]	Saby et al. [7]
Blood culture positive for infective endocarditis (i) Typical microorganisms consistent with infective endocarditis from 2 separate blood cultures. *Viridans streptococci, Streptococcus bovis, HACEK group, Staphylococcus aureus,or community-acquired enterococci, in the absence of a primary focus* (ii) Microorganisms consistent with infective endocarditis from persistently positive blood cultures, defined as follows. *≥2 positive cultures of blood samples drawn* >12 h *apart or all of 3 or a majority of ≥4 separate cultures of blood (with first and last sample drawn at least* 1 h *apart)* (iii) Single positive blood culture for *Coxiella burnetii* or antiphase I IgG antibody titer >1 : 800 Evidence of endocardial involvement (i) Echocardiogram (TTE and/or TEE) positive for infective endocarditis defined as follows. *Oscillating intracardiac mass on valve or supporting structures, in the path of regurgitant jets, or on implanted material in the absence of an alternative anatomic explanation or* *abscess or* *new partial dehiscence of prosthetic valve* (ii) New valvular regurgitation (worsening or changing of preexisting murmur not sufficient).	Duke major criteria and positive ^{18}F-FDG PET/CT: abnormal FDG uptake at the site of prosthetic valve

18F-FDG: 18F-fluorodeoxyglucose; HACEK: *Haemophilus* species, *Actinobacillus actinomycetemcomitans*, *Cardiobacterium hominis*, *Eikenella corrodens*, and *Kingella* species; IgG: immunoglobulin G; PET/CT: positron emission tomography/computed tomography; TEE: transesophageal echocardiography; TTE: transthoracic echocardiography.

Table 3: Minor criteria for the diagnosis of prosthetic valve endocarditis (PVE) [6].

(i) Predisposition, predisposing heart condition, or injection drug use
(ii) Fever, temperature ≥38°C
(iii) Vascular phenomena: major arterial emboli, septic pulmonary infarcts, mycotic aneurysm, intracranial hemorrhage, and conjunctival hemorrhages
(iv) Janeway lesions
(v) Immunological phenomena: glomerulonephritis, Osler nodes, Roth spots, and rheumatoid factor
(vi) Microbiological evidence: positive blood culture but does not meet a major criterion as noted above or serological evidence of active infection with organism consistent with infective endocarditis

Table 4: Nuclear medicine (NM) in the diagnosis of prosthetic valve endocarditis (PVE): review of the literature.

NM imaging modalities	Number of articles/number of patients	Type of paper/reference/year
^{18}F-FDG-PET/TC	1/not valuable	Review/[8]/2013
	1/72	Prospective study/[7]/2013
	2/2	Case report/[9, 10]/2013, 2009
	1/6	Case series/[11]/2014
CT angiography and ^{18}F-FDG-PET	1/7	Case series/[12]/2013
^{111}Indium labeled leukocytes scintigraphy	2/2	Case report/[13, 14]/1990, 1988
	1/2	Case series/[15]/1989
^{67}Gallium citrate-SPECT and SPECT/TC	4/4	Case report/[16–19]/2005, 2009, 2002, 1991
^{99m}Technetium-HMPAO-WBC-SPECT/TC	1/131	Prospective study/[20]/2012
	1/42	Prospective study/[21]/2013
^{99m}Technetium anti-G mAb-SPECT	1/1	Case report/[22]/1991
	1/38	Prospective study/[23]/1995

FDG: fluorodeoxyglucose; PET/TC: positron emission tomography/computed tomography; CT: computed tomography; SPECT/TC: single photon emission computed tomography/computed tomography; HMPAO: hexamethylpropylene amine oxime; WBC: white blood cells; anti-G mAb: anti-human granulocytes antibodies.

However, this study provides interesting data on the possible inclusion of ^{18}F-FDG PET/CT among the major criteria of Duke, as already proposed by Millar et al. [7, 8] (Table 2). In fact, the sensitivity of these "new" modified Duke criteria rises up to 97%, which would increase the rate of the so-called "defined" endocarditis [7].

New diagnostic algorithms have been proposed in order to ensure an early diagnosis of endocarditis in those cases in which the Duke criteria are inconclusive; this happens in case of culture-negative endocarditis or in those cases in which transthoracic echocardiography (TTE) and transesophageal echocardiography (TEE) do not visualize lesions of the valve [7, 8].

In this regard, in a case report, Gouriet et al. describe the representative contribution of PET/CT to the diagnosis of PVE in case of "possible endocarditis," according to the Duke criteria. In this study, PET/CT was performed in course of antibiotic therapy for a knee prostheses infection, after 3 TEEs repeated 7 days apart from each other because of a strong suspicion of IE. The new findings of mitral regurgitation and prolapse of one of the mitral cusps at the third TEE have led to the diagnosis of possible endocarditis; the PET TC subsequently performed made it possible to diagnose a definitive PVE [9].

New imaging modalities, as computed tomography angiography (CTA), have been proposed as a supplement to PET, as Tanis et al. reported in their case series [12]. The authors describe 7 cases of PVE, where the integration of the two techniques allowed diagnosing PVE unidentified by TEE, and periannular complication, that is, mycotic aneurism of coronary arteries and myocardial abscesses [12].

There are still some controversies about various issues related to the PET/CT methodology.

First, the resolving power of this technique permits the detection of lesions of 5 mm and over. However, according to some authors, this is not a limit to the diagnostic power as even smaller lesions, if there is a sufficient uptake, can be displayed. In this regard, Bertagna and colleagues observed that the standard protocol that is used in most nuclear medicine centers is the oncological one that consists of imaging acquisition performed 1 hour after glucose injection [26]. Therefore, they suggest acquiring images even at 2-3 hours after the injection of glucose in order to detect uptake by monocytes and macrophages at the level of the lesion and to increase the sensitivity of the PET/CT methodology [26].

Moreover, there is concern about the specificity of the method in the early period after prosthesis placement. A functional glucose uptake persists in fact from 1 month up to 1 year after surgery. This variability between individuals is influenced by various factors, such as age, clinical status, and overall cardiac condition of the patient. Some authors have also expressed concern about the lack of controls in the prospective study published by Saby et al. [7], because, in order to correctly interpret the values of uptake and the validity of the exam, it is necessary to compare with a normal pattern of glucose uptake, in the absence of infection [30].

(2) Labeled Leukocytes Scintigraphy. ^{111}Indium is one of the first radiopharmaceuticals used in detecting cardiovascular infections (Table 4) [12–14]. Articles collected [12–14] describe scintigraphy with ^{111}Indium employed in diagnosing prosthetic aortic perivalvular abscesses that is a severe endocarditis complication undetectable with traditional radiological tools. This complication is common; it complicates PVE in approximately 50% of cases and needs an urgent surgical approach [20].

^{111}Indium seems more efficacious to detect perivalvular complications than valvular surface infections, but its time-consuming images' acquisition limits its utilization.

^{67}Gallium citrate has been used more often than ^{111}Indium as tracer for scintigraphy in cardiovascular infection field, and it has always been associated with SPECT views [16–19]. One of the articles regarding ^{67}Gallium citrate reports its capability to detect endocarditis in absence of any morphological alteration at echocardiography [18].

A retrospective study assessed the value of 99mTc-HMPAO- (hexamethylpropylene amine oxime-) WBC (white blood cells) scintigraphy including SPECT/CT acquisitions in a series of 131 consecutive patients with suspected IE, 68% of whom with prosthetic valves [20].

99mTc-HMPAO-WBC scintigraphy results were correlated with transthoracic or transesophageal echocardiography, blood cultures, and the Duke criteria. ^{99m}Technetium-HMPAO-SPECT/CT was positive in all cases of IE in which at least one major Duke criterion was present; moreover, it was positive in IE cases, ascertained by microbiological or clinical diagnosis, with a negative echocardiography [20].

^{99m}Technetium labelled monoclonal anti-human granulocytes antibodies (Anti-G mAb) may be employed to label leukocytes in vivo to detect inflammation and infection, but literature regarding its contribution to PVE diagnosis is scarce. Our literature search provided two papers reporting, respectively, a case report and a small prospective case-control study [22, 23]. In this latter article sensitivity and specificity of scintigraphy, in combination with echocardiography, were 100% and 80%, respectively, but the clinical sample was limited, that is, 18 cases and 20 controls [23]. Currently there are no sufficient evidences to suggest this technique as a reliable tool in PVE diagnosis.

3.1.3. The Contribution of Nuclear Medicine to the Diagnosis of Complications in IE, Including PVE. Complications of PVE are rare but worrying because they often require an urgent surgical intervention. They include septic embolism, perivalvular infection, myocardial abscesses, and prosthetic valve dehiscence.

In this regard a retrospective study provided interesting data about the usefulness of ^{99m}Technetium-HMPAO-SPECT/CT in assessment of cardiac surgery indications in patients with a suspect PVE [21].

With this technique the authors diagnosed extensive perivalvular infections and abscesses in patients with confirmed endocarditis and no perivalvular extension of the infection detected by TEE; surgery confirmed the presence of an abscess in those patients with positive scintigraphy who underwent surgical intervention, with a positive predictive value for the presence of an abscess of 100% [21].

It is well known that nuclear medicine contributes to the diagnosis of septic metastatic foci in cases of systemic infections, as reported by Vos et al. in a prospective study regarding 115 patients affected by bacteremia [32].

Embolization and/or metastatic infection occurs in more than half of patients with IE and most commonly involves the spleen, the kidney, the liver, and the iliac or mesenteric arteries [33].

Embolic events have been reported in 22–43% of patients with IE, mainly in the first 2 weeks after initiation of antibiotic therapy. A misdiagnosed septic embolism can cause a subsequent seeding of the infection at the metastatic site, a persistent bacteremia, and colonization of newly placed prosthetic valve [34].

Metastatic infection can occur with different form, for example, septic arthritis, spondylodiscitis, pericarditis, and abscess [33, 35]. Their presence influences the appropriate choice of antibiotic therapy and surgical management, the duration of followup, and the outcome of IE [34]. The contribution of ^{18}F-FDG PET/CT to the early diagnosis of embolism and metastatic infection in patients with IE has been reported in recent prospective studies [34, 36]; peripheral embolism and/or metastatic infection were detected in 44% of IE episodes, 40% of which were PVE [34].

Moreover, PET/CT detected unexpected extracardiac sites of infection, that is, asymptomatic cases, in 24%–28% of IE [34, 36].

Finally, a retrospective study by Erba et al. on the ^{99m}Technetium-HMPAO-SPECT/CT contribution to the assessment of suspected IE reported the usefulness of this technique for the identification of septic emboli, detected in 41% of patients, even in the absence of the typical echocardiographic predictors of systemic embolism [20].

4. Conclusions

The early diagnosis of PVE represents a challenge for clinicians involved in its management, including infectious diseases specialist, cardiologist, cardiosurgeons, and imaging physicians, because a delay in antibiotic therapy and cardiac surgery has negative effects on clinical outcomes.

Promising NM techniques, as ^{18}F-FDG PET/CT and ^{99m}Technetium-HMPAO-SPECT/CT, have been demonstrated to be effective imaging options in the management of PVE. PET has been proposed as a method to increase the sensitivity of the Duke criteria for PVE, and ^{99m}Technetium-HMPAO-SPECT/CT is a promising technique that requires further studies. Finally, NM techniques can identify important complications in the course of PVE, including perivalvular abscesses and metastatic embolization, even in asymptomatic patients.

Conflict of Interests

Nicola Petrosillo received honoraria fees as speaker for Novartis, Astellas, MSD, Pfizer, Johnson & Johnson, CareFusion, and Gilead.

Acknowledgment

This work is supported by Ricerca Corrente, IRCCS.

References

[1] C. H. Cabell, P. A. Heidenreich, V. H. Chu et al., "Increasing rates of cardiac device infections among Medicare beneficiaries: 1990–1999," *American Heart Journal*, vol. 147, no. 4, pp. 582–586, 2004.

[2] L. M. Baddour and W. R. Wilson, "Infections of prosthetic valves and other cardiovascular devices," in *Mandell, Douglas and Benett's Principles and Practice of Infectious Diseases*, E. C. Livingstone, Ed., vol. 1, pp. 1022–1144, Churchill Livingstone, Philadelphia, Pa, USA, 7th edition, 2005.

[3] B. Iung, P. A. Erba, N. Petrosillo, and E. Lazzeri, "Common diagnostic flowcharts in infective endocarditis," *The Quarterly Journal of Nuclear Medicine and Molecular Imaging*, vol. 58, no. 1, pp. 55–65, 2014.

[4] F. Thuny, D. Grisoli, F. Collart, G. Habib, and D. Raoult, "Management of infective endocarditis: challenges and perspectives," *The Lancet*, vol. 379, no. 9819, pp. 965–975, 2012.

[5] N. Petrosillo, "Epidemiology of infections in the new century," in *Diagnostic Imaging of Infections and Inflammatory Diseases: A Multidisciplinary Approach*, A. Signore and A. M. Quintero, Eds., pp. 3–14, Wiley Blackwell, New Jersey, NJ, USA, 2014.

[6] J. S. Li, D. J. Sexton, N. Mick et al., "Proposed modifications to the Duke criteria for the diagnosis of infective endocarditis," *Clinical Infectious Diseases*, vol. 30, no. 4, pp. 633–638, 2000.

[7] L. Saby, O. Laas, G. Habib et al., "Positron emission tomography/computed tomography for diagnosis of prosthetic valve endocarditis: increased valvular ^{18}F-fluorodeoxyglucose uptake as a novel major criterion," *Journal of the American College of Cardiology*, vol. 61, no. 23, pp. 2374–2382, 2013.

[8] B. C. Millar, B. D. Prendergast, A. Alavi, and J. E. Moore, "^{18}FDG-positron emission tomography (PET) has a role to play in the diagnosis and therapy of infective endocarditis and cardiac device infection," *International Journal of Cardiology*, vol. 167, no. 5, pp. 1724–1736, 2013.

[9] F. Gouriet, S. Bayle, Y. le Dolley et al., "Infectious endocarditis detected by PET/CT in a patient with a prosthetic knee infection: Case report and review of the literature," *Scandinavian Journal of Infectious Diseases*, vol. 45, no. 7, pp. 570–574, 2013.

[10] S. Moghadam-Kia, A. Nawaz, B. C. Millar et al., "Imaging with ^{18}F-FDG-PET in infective endocarditis: promising role in difficult diagnosis and treatment monitoring," *Hellenic Journal of Nuclear Medicine*, vol. 12, no. 2, pp. 165–198, 2009.

[11] M. Bartoletti, F. Tumietto, G. Fasulo et al., "Combined computed tomography and fluorodeoxyglucose positron emission tomography in the diagnosis of prosthetic valve endocarditis: a case series," *BMC Research Notes*, vol. 7, no. 1, article 32, 2014.

[12] W. Tanis, A. Scholtens, J. Habets et al., "CT angiography and ^{18}F-FDG-PET fusion imaging for prosthetic heart valve endocarditis," *JACC: Cardiovascular Imaging*, vol. 6, no. 9, pp. 1008–1013, 2013.

[13] G. L. Purnell, C. W. Walker, J. W. Allison, and G. V. Dalrymple, "Indium-111 leukocyte localization in infected prosthetic graft," *Clinical Nuclear Medicine*, vol. 15, no. 8, pp. 585–586, 1990.

[14] E. Oates and R. C. Sarno, "Detection of a prosthetic aortic valvular abscess with indium-111-labeled leukocytes," *Chest*, vol. 94, no. 4, pp. 872–874, 1988.

[15] M. D. Cerqueira and A. F. Jacobson, "Indium-111 leukocyte scintigraphic detection of myocardial abscess formation in patients with endocarditis," *Journal of Nuclear Medicine*, vol. 30, no. 5, pp. 703–706, 1989.

[16] L. E. J. Thomson, M. P. Goodman, T. Z. Naqvi et al., "Aortic root infection in a prosthetic valve demonstrated by gallium-67 citrate SPECT," *Clinical Nuclear Medicine*, vol. 30, no. 4, pp. 265–268, 2005.

[17] A. Yavari, T. Ayoub, L. Livieratos, V. Raman, and E. T. McWilliams, "Diagnosis of prosthetic aortic valve endocarditis with gallium-67 citrate single-photon emission computed tomography/computed tomography hybrid imaging using software registration," *Circulation: Cardiovascular Imaging*, vol. 2, no. 6, pp. e41–e43, 2009.

[18] F. J. Pena, I. Banzo, R. Quirce et al., "Ga-67 SPECT to detect endocarditis after replacement of an aortic valve," *Clinical Nuclear Medicine*, vol. 27, no. 6, pp. 401–404, 2002.

[19] K. O'Brien, D. Barnes, R. H. Martin, and J. R. Rae, "Gallium-SPECT in the detection of prosthetic valve endocarditis and aortic ring abscess," *Journal of Nuclear Medicine*, vol. 32, no. 9, pp. 1791–1793, 1991.

[20] P. A. Erba, U. Conti, E. Lazzeri et al., "Added value of ^{99m}Tc-HMPAO-labeled leukocyte SPECT/CT in the characterization and management of patients with infectious endocarditis," *The Journal of Nuclear Medicine*, vol. 53, no. 8, pp. 1235–1243, 2012.

[21] F. Hyafil, F. Rouzet, L. Lepage et al., "Role of radiolabelled leucocyte scintigraphy in patients with a suspicion of prosthetic valve endocarditis and inconclusive echocardiography," *European Heart Journal: Cardiovascular Imaging*, vol. 14, no. 6, pp. 586–594, 2013.

[22] H. J. Bair, W. Becker, H. J. Volkholz, and F. Wolf, "99mTc-labelled anti NCA-95 antibodies in prosthetic heart valve endocarditis," *NuklearMedizin*, vol. 30, no. 4, pp. 149–150, 1991.

[23] A. J. Morguet, D. L. Munz, V. Ivancevic, G. S. Werner, and H. Kreuzer, "Clinical value of radioimaging using the murine monoclonal antigranulocyte antibody BW 250/183 in the diagnosis of prosthetic valve endocarditis," *Deutsche Medizinische Wochenschrift*, vol. 120, no. 24, pp. 861–866, 1995.

[24] C. Liu, A. Bayer, S. E. Cosgrove et al., "Clinical practice guidelines by the Infectious Diseases Society of America for the treatment of methicillin-resistant *Staphylococcus aureus* infections in adults and children: executive summary," *Clinical Infectious Diseases*, vol. 52, no. 3, pp. 285–292, 2011.

[25] V. Dilsizian, S. Achenbach, and J. Narula, "Adding or selecting imaging modalities for incremental diagnosis: a case study of ^{18}FDG PET/CT in prosthetic valve endocarditis," *JACC Cardiovascular Imaging*, vol. 6, no. 9, pp. 1020–1021, 2013.

[26] F. Bertagna, R. Giubbini, and G. Treglia, "Positron emission tomography/computed tomography for diagnosis of prosthetic valve endocarditis: suggestions to increase diagnostic accuracy," *Journal of the American College of Cardiology*, vol. 63, no. 4, pp. 378–379, 2014.

[27] A. Sharma, "Positron emission tomography/computed tomography for diagnosis of prosthetic valve endocarditis," *Journal of the American College of Cardiology*, vol. 62, no. 9, p. 861, 2013.

[28] F. Thuny, L. Saby, L. Tessonier, S. Cammilleri, D. Raoult, and G. Habib, "Reply: positron emission tomography/computed tomography for diagnosis of prosthetic valve endocarditis," *Journal of the American College of Cardiology*, vol. 62, no. 9, pp. 861–862, 2013.

[29] F. Thuny, O. Lass, L. Saby et al., "Reply: positron emission tomography/computed tomography for diagnosis of prosthetic

valve endocarditis," *Journal of the American College of Cardiology*, vol. 63, no. 2, pp. 187–189, 2014.

[30] W. Tanis, A. Scholtens, J. Habets et al., "Positron emission tomography/computed tomography for diagnosis of prosthetic valve endocarditis: increased valvular ^{18}F-fluorodeoxyglucose uptake as a novel major criterion," *Journal of the American College of Cardiology*, vol. 63, no. 2, pp. 186–187, 2014.

[31] M. Graziosi, C. Nanni, M. Lorenzini et al., "Role of ^{18}F-FDG PET/CT in the diagnosis of infective endocarditis in patients with an implanted cardiac device: a prospective study," *European Journal of Nuclear Medicine and Molecular Imaging*, vol. 41, no. 8, pp. 1617–1623, 2014.

[32] F. J. Vos, C. P. Bleeker-Rovers, P. D. Sturm et al., " ^{18}F-FDG PET/CT for detection of metastatic infection in gram-positive bacteremia," *The Journal of Nuclear Medicine*, vol. 51, no. 8, pp. 1234–1240, 2010.

[33] E. Mylonakis and S. B. Calderwood, "Infective endocarditis in adults," *The New England Journal of Medicine*, vol. 345, no. 18, pp. 1318–1330, 2001.

[34] J. van Riet, E. E. Hill, O. Gheysens et al., " ^{18}F-FDG PET/CT for early detection of embolism and metastatic infection in patients with infective endocarditis," *European Journal of Nuclear Medicine and Molecular Imaging*, vol. 37, no. 6, pp. 1189–1197, 2010.

[35] L. A. Cone, J. Hirschberg, C. Lopez et al., "Infective endocarditis associated with spondylodiscitis and frequent secondary epidural abscess," *Surgical Neurology*, vol. 69, no. 2, pp. 121–125, 2008.

[36] R. Bonfiglioli, C. Nanni, J. J. Morigi et al., "^{18}F-FDG PET/CT diagnosis of unexpected extracardiac septic embolisms in patients with suspected cardiac endocarditis," *European Journal of Nuclear Medicine and Molecular Imaging*, vol. 40, no. 8, pp. 1190–1196, 2013.

Hindawi Publishing Corporation
BioMed Research International
Volume 2014, Article ID 424652, 10 pages
http://dx.doi.org/10.1155/2014/424652

Research Article

The Longitudinal Assessment of Osteomyelitis Development by Molecular Imaging in a Rabbit Model

Jim C. E. Odekerken,[1] Geert H. I. M. Walenkamp,[1] Boudewijn T. Brans,[2] Tim J. M. Welting,[1] and Jacobus J. C. Arts[1]

[1] *Laboratory for Experimental Orthopaedics, Department of Orthopaedic Surgery, CAPHRI School for Public Health and Primary Care, Maastricht University Medical Centre, P.O. Box 5800, 6202 AZ Maastricht, The Netherlands*
[2] *Department of Nuclear Medicine, Maastricht University Medical Centre, P.O. Box 5800, 6202 AZ Maastricht, The Netherlands*

Correspondence should be addressed to Jacobus J. C. Arts; j.arts@mumc.nl

Received 4 June 2014; Accepted 22 August 2014; Published 11 September 2014

Academic Editor: Andor Glaudemans

Introduction. Osteomyelitis is a severe orthopaedic complication which is difficult to diagnose and treat. Previous experimental studies mainly focussed on evaluating osteomyelitis in the presence of an implant or used a sclerosing agent to promote infection onset. In contrast, we focused on the longitudinal assessment of a nonimplant related osteomyelitis. *Methods*. An intramedullary tibial infection with *S. aureus* was established in NZW rabbits. Clinical and haematological infection status was evaluated weekly, combined with X-ray radiographs, biweekly injections of calcium binding fluorophores, and postmortem micro-CT. The development of the infection was assessed by micro-PET at consecutive time points using ^{18}F-FDG as an infection tracer. *Results*. The intramedullary contamination of the rabbit tibia resulted in an osteomyelitis. Haematological parameters confirmed infection in mainly the first postoperative weeks (CRP at the first 5 postoperative weeks, leucocyte differentiation at the second and sixth postoperative weeks, and ESR on the second postoperative week only), while micro-PET was able to detect the infection from the first post-operative week onward until the end of the study. *Conclusions*. This study shows that osteomyelitis in the rabbit can be induced without use of an implant or sclerosing agent. The sequential follow-up indicates that the diagnostic value of each infection parameter is time point dependant. Furthermore, from all parameters used, the diagnostic value of ^{18}F-FDG micro-PET is the most versatile to assess the presence of an orthopaedic infection in this model.

1. Introduction

Currently, posttraumatic and postoperative osteomyelitis remains to be one of the most severe complications after bone trauma or surgery. During the last decades, much research has been conducted into prevention, diagnostics, and treatment modalities for orthopaedic infections. Most research studies focus on treatment or prevention and not on the diagnosis of bone infection. However, novel imaging modalities are made available in the clinical evaluation of osteomyelitic lesions, that is, combined ^{18}F-FDG PET and MRI [1].

The preclinical evaluation of any diagnostic tool requires a stable and consistent experimental preclinical model with a broad collection of relevant read-out parameters to yield reliable data with a precise follow-up. In this way, preclinical osteomyelitis models can be highly informative on the development of the disease and the accompanying diagnosis by novel tools like ^{18}F-FDG PET [2, 3].

To investigate the development of a nonimplant related osteomyelitis over time and to define a stable preclinical model, we aimed to establish an osteomyelitic lesion in the tibiae of rabbits, without the use of a sclerosing agent, since this destructs the local vascularisation of the bone and reduces the local immune capacity [4, 5].

To investigate the potential of novel diagnostic approaches, we evaluated the sequential use of ^{18}F-FDG as an infection specific micro-PET tracer on multiple time points during follow-up.

By combining the results of this study with our previously reported studies [6, 7], we also aimed to identify the most relevant parameters to diagnose naïve osteomyelitis by experimental conditions and describe how these infection parameters may differ in case of the presence or absence of an orthopaedic implant.

2. Materials and Methods

2.1. Animal Choice, Welfare, and Ethics. Eleven specified pathogen free (SPF) female New Zealand White (NZW) rabbits (Charles River, France), with a weight of 3.5–4 kg (approximately 6 months of age) were used in this study. Animals were allowed to acclimatize for 2 weeks before surgery was performed.

During the study, each animal served as its own control since preoperative measurements had been performed; these functioned as a baseline measurement. The nonoperated contralateral leg was also used as a control for the uncontaminated condition (radiology, micro-PET, and histology). Furthermore, preoperative micro-PET scans were supplemented with a historic control group [7] to reduce the exposure of the animals to ionising radiation in accordance with the ALARA-guideline [8]. Animal housing, feeding, pain treatment, humane endpoints, and sacrifice were performed according to our previously described study [6, 7].

The experimental follow-up scheme is displayed in Table 1.

This study was approved by the Maastricht University Animal Ethics Committee (DEC-UM, protocol 2010-089, Maastricht, the Netherlands).

2.2. Animal Surgery and Follow-Up. Animals were anaesthetized according to our previously published study [6]. Subsequently, a hand reamed 4 mm wide defect was drilled into the tibial plateau to open the tibial medullary canal. After reaming, the tibial medullary cavity was flushed with sterile saline to remove bone fragments and haematoma. All animals received intramedullary contamination of 3.8×10^5 CFU *S. aureus* (UAMS-1, ATCC 49230) in 100 μL saline.

The inoculation dose was freshly prepared before surgery from an overnight culture and diluted with sterile saline to an average concentration of 3.8×10^5 CFU per contamination, based on OD600 measurements (Amersham Biosciences, GE Healthcare, USA). The inoculation dose and preparation were based on previous studies [6, 7]. To confirm the inoculum size, the bacterial count of every inoculum was verified by quantitative culture on tellurite glycine agar (Difco, Becton Dickinson, France) before and after surgery.

After contamination, the defect was sealed with bone wax (Syneture, Covidien, USA) and the surrounding tissue was flushed with sterile saline. The patella tendon was apprimated with 4 resorbable sutures and the skin by 6 single intracutaneous inverted sutures (Syneture, Covidien, USA); aluminum-spray (Eurovet Animal Health, the Netherlands) was applied to protect the wound.

The animals were monitored during the 6-week follow-up for the use of their hind legs, the appearance of the wound, and on general signs of infection (redness, swelling, and fever). Body weight and temperature were measured and blood was collected by venipuncture from the jugular vein at the day of surgery and every week thereafter until the end of the experiment. Blood samples were collected weekly and analysed for changes in erythrocyte sedimentation rate (ESR) (Kabe Labortechnik, Germany), leucocyte differentiation (Euregio Laboratory, the Netherlands), and C-reactive protein levels (CRP) (E-15CRP, Immunology Consultants Laboratory, USA).

2.3. Radiographic Imaging. Standard X-ray radiographs were collected according to our previously described study [6]. All radiographs were independently scored, by 3 blinded observers, for osteomyelitis mediated bone morphological changes according to our modified scoring system [6].

Ex vivo micro-CT imaging of the affected tibiae was performed after 6-week follow-up, directly postmortem. The micro-CT-images were acquired on an X-rad 225 (Precision X-ray, USA) as described previously [6, 7].

2.4. ^{18}F-FDG Micro-PET. ^{18}F-FDG micro-PET was conducted to assess the local metabolic glucose uptake in the contaminated tissue, since infection is associated with an increased metabolic glucose turnover. Imaging data was collected by a preoperative scan and three postoperative scans (resp., at one, three, and six weeks after surgery) of each animal.

The entire micro-PET procedure of approximately 2 hours was performed under tiletamine-zolazepam sedation, initiated by a 15 mg/kg intramuscular dose and 3 additional intramuscular injections of 7.5 mg/kg. The time between the first and the subsequent second dose was 20 minutes, all injections following thereafter were given with 45-minute intervals.

The rabbits were fixed in a custom made PVC restrainer, which allowed the rabbit to breath freely without allowing movements of the hind legs [7]. Fifty MBq ^{18}F-FDG (GE Healthcare Medical Diagnostics, Eindhoven, the Netherlands) were diluted with sterile saline to a volume of 1 mL and were subsequently injected in the ear vein of the rabbit. Residual activity in the syringe was measured on a CRC-25R dose calibrator (Capintec, USA) to calculate the initially injected ^{18}F-FDG dose. A 1-hour incubation period was taken into account to allow uptake of the ^{18}F-FDG in the area of interest.

Data were analysed with the ASIPRO VM software package (version 6.7.1.2, Concorde Microsystems, Siemens, Germany). The imaging data were reconstructed by the OSEM2D protocol with an isotropic voxel size of 0.87 mm to align the tibial intramedullary cavity with the coronal, sagittal, and transversal planes to keep the volumes of interest (VOI) of all scans equal. A cylindrical VOI of 10.4 mm in diameter and 25.1 mm long (12 voxels in diameter and 29 voxels long) was used as a contour around the affected bony tissue. An equally sized VOI was placed in the contralateral leg on the equivalent location, to serve as an internal control. Each leg also contained an equally sized VOI in the *vastus lateralis* to

Table 1: Experimental parameters and follow-up.

	Quantification inoculum	Weight	Temperature	ESR	CRP	Leucocyte differentiation	X-ray	Micro-CT	^{18}F-FDG micro-PET	Calcium binding fluorophores	Bone tissue culture	Histology
Preoperative		X	X						X			
Day of surgery	X	X	X	X	X	X	X					
Week 1		X	X	X	X	X	X		X			
Week 2		X	X	X	X	X	X			X		
Week 3		X	X	X	X	X	X		X			
Week 4		X	X	X	X	X	X			X		
Week 5		X	X	X	X	X	X					
Week 6		X	X	X	X	X	X		X	X		
Postmortem								X			X	X

serve as a measurement for the soft tissue ^{18}F-FDG-uptake. The standardized uptake value (SUV) was calculated from the total activity in the selected VOI, corrected for the weight of the animal and the activity of ^{18}F-FDG in the animal at the time of emission scanning. Activity at the time of the scan was corrected for the injected activity and the calibration factor of the micro-PET and dose calibrator.

2.5. Bacteriology. After sacrifice, the tibiae were dissected aseptically. Swabs were taken from the knee joint cavity. To assess soft tissue infection, these swabs were evaluated for the presence of *S. aureus* on tellurite glycine agar plates. *S. aureus* growth was identified by the presence of black colonies, due to the coagulase positive character of the species. Other, coagulase negative bacterial species (e.g., *S. epidermidis*) would appear as white colonies. A 5 mm piece of the distal part of the *tuberositas tibiae* was excised from the tibia with a surgical drill (SM 12, Nouvag, Switzerland). After weight measurement, it was homogenized in 10 mL sterile saline (Ultra-Turrax T25, Ika, Germany) at 6000 rpm. The homogenates were cultured on tellurite glycine agar plates. After 24 hours, culture dishes were quantified for the specific bacterial growth.

2.6. Histology. During the experimental follow-up, three different calcium binding fluorophores were administered, by subcutaneous injection, to follow bone apposition and mineralization over time, which are to be detected in histological sections. Injection of Calcein Green (25 mg/kg, Fluka, Sigma Aldrich, Germany) was performed at 2 weeks and Xylenol Orange (30 mg/kg, Fluka, Sigma Aldrich, Germany) at 4 weeks, and Calcein Blue (25 mg/kg, Fluka, Sigma Aldrich, Germany) was injected on the day before sacrifice.

After sacrifice and sampling for bone culture, tibiae were fixated in 4% formaldehyde/PBS for 4 weeks and embedded in polymethylmethacrylate (PMMA) (Technovit 9100, Hereaus-Kulzer, Germany). After polymerization, sections were stained according to Masson-Goldner (Carl Roth, Germany) and Gram (without a safranin counterstain) and subsequently 50 μm sections were obtained using a saw microtome (SP 1600, Leica, Germany). Sections were analysed and digitized by light microscopy (Axioscope A1, AxioVision LE release 4.8.2, Carl Zeiss, Germany). The localization of calcium binding fluorophores in the bony tissue was visualized by fluorescence microscopy (Leica DMRB, Leica IM50 version 1.2 release 19, Leica, Germany) on unstained PMMA sections. Acquired images were merged using Photoshop CS3 (Adobe Systems, USA) to generate overview images.

2.7. Statistical Analysis. SPSS 21 (IBM, USA) was used for the statistical analyses. Each animal served as its own preoperative healthy control. Data were checked for normality using the Shapiro-Wilk test. Differences between time points were determined by a Wilcoxon Signed Ranks Test for nonparametric significance. In case of the micro-PET imaging, we randomly selected 3 animals to serve as a healthy preoperative control. The data of these 3 animals were supplemented by a historic control group of 10 animals [7], to reduce overall reduction of animal inconvenience (one-, two-hour episode of anaesthesia in combination with the injection of a 50 MBq ^{18}F-FDG). Therefore, the statistical analysis of the micro-PET-data was performed with a combination of the Wilcoxon Signed Ranks Test and the Mann-Whitney U Test. The significance level was determined at $P \leq 0.05$. Graphical representation of the data was performed in GraphPad Prism 5 (GraphPad, USA), and error bars represent standard error of mean.

3. Results

3.1. Animal Surgery and Follow-Up. Eleven rabbits were intramedullary (right proximal tibia) contaminated with 3.8×10^5 CFU *S. aureus* via a transpatellar tibial plateau administration route. Nine animals completed the 6-week follow-up, which all developed an osteomyelitis in the right proximal tibia after peroperative contamination. One animal did not recuperate from the surgical procedure and another animal was sacrificed 3 weeks after surgery due to complications (humane endpoints were defined as extensive weight loss of >20% and severe soft tissue infection).

3.2. In Vivo and Ex Vivo Data Analysis. After recovery from the surgical procedure, all animals showed limited function of the operated leg with partial weight bearing. Body temperature and weight (clinical indicators for infection) were monitored on a weekly basis. In comparison to the preoperative measurements, a significant increase in body temperature was noted in all but the second postoperative week (Figure 1(a); $P \leq 0.049$). All animals reduced weight significantly compared to preoperative values and did not regain their preoperative bodyweight values during follow-up (Figure 1(b); $P \leq 0.011$).

During the six-week follow-up period, the ESR increased during the first weeks after surgery compared to the preoperative rate, with a significant increase only at two weeks after surgery (Figure 1(c); $P = 0.042$).

CRP levels however showed a significant increase in the first 5 weeks after surgery (Figure 1(d); $P \leq 0.038$).

The weekly assessment of the leucocyte differentiation (Figure 1(e)) indicated that the lymphocytes fraction in the leucocyte differentiation was significantly decreased as compared to the preoperative values on all postoperative time points ($P \leq 0.017$). The neutrophilic granulocyte fraction was only significantly different on the second and sixth postoperative week ($P \leq 0.050$). The monocyte fraction was significantly increased in all but the second postoperative week ($P \leq 0.033$). The basophilic granulocyte fraction was significantly increased from the third postoperative week onward ($P \leq 0.038$). The eosinophilic granulocyte fraction was only significantly different at the fifth postoperative week ($P = 0.042$).

The bone morphological changes initiated by the peroperative contamination of the tibia were detectable on X-ray radiographs from the 3rd postoperative week onwards (Figure 2(a)), when scored according to our previously described osteomyelitis scoring system [6], focusing on bone

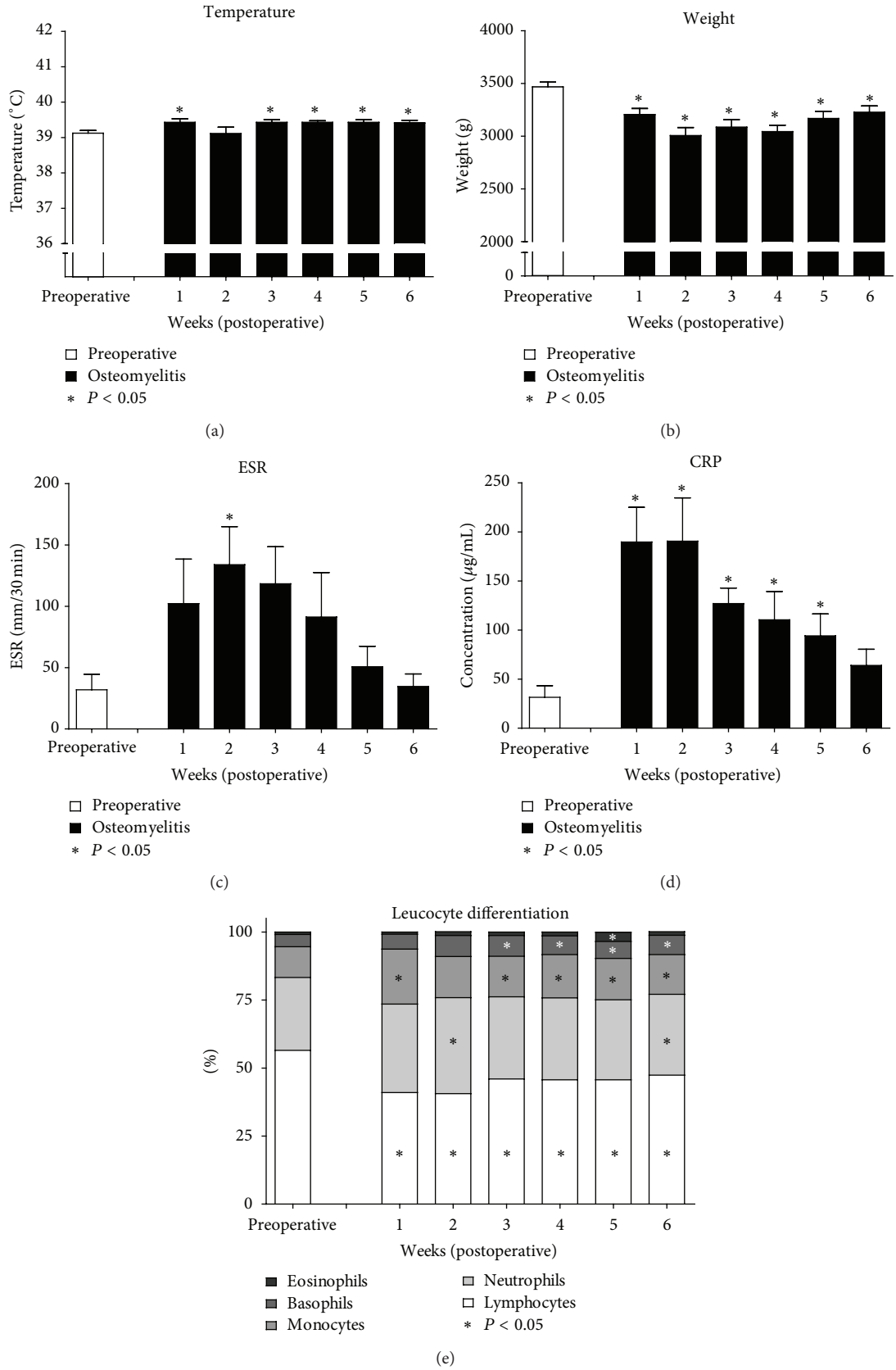

FIGURE 1: Physiological and haematological parameters. (a) Body temperature during follow-up. (b) Body weight during follow-up. (c) Erythrocyte sedimentation rate. (d) C-reactive protein levels. (e) Leucocyte differentiation. All postoperative values are compared with the preoperative values, in case of significant differences, asterisk indicates $P \leq 0.05$, and the error bars represent standard error of mean.

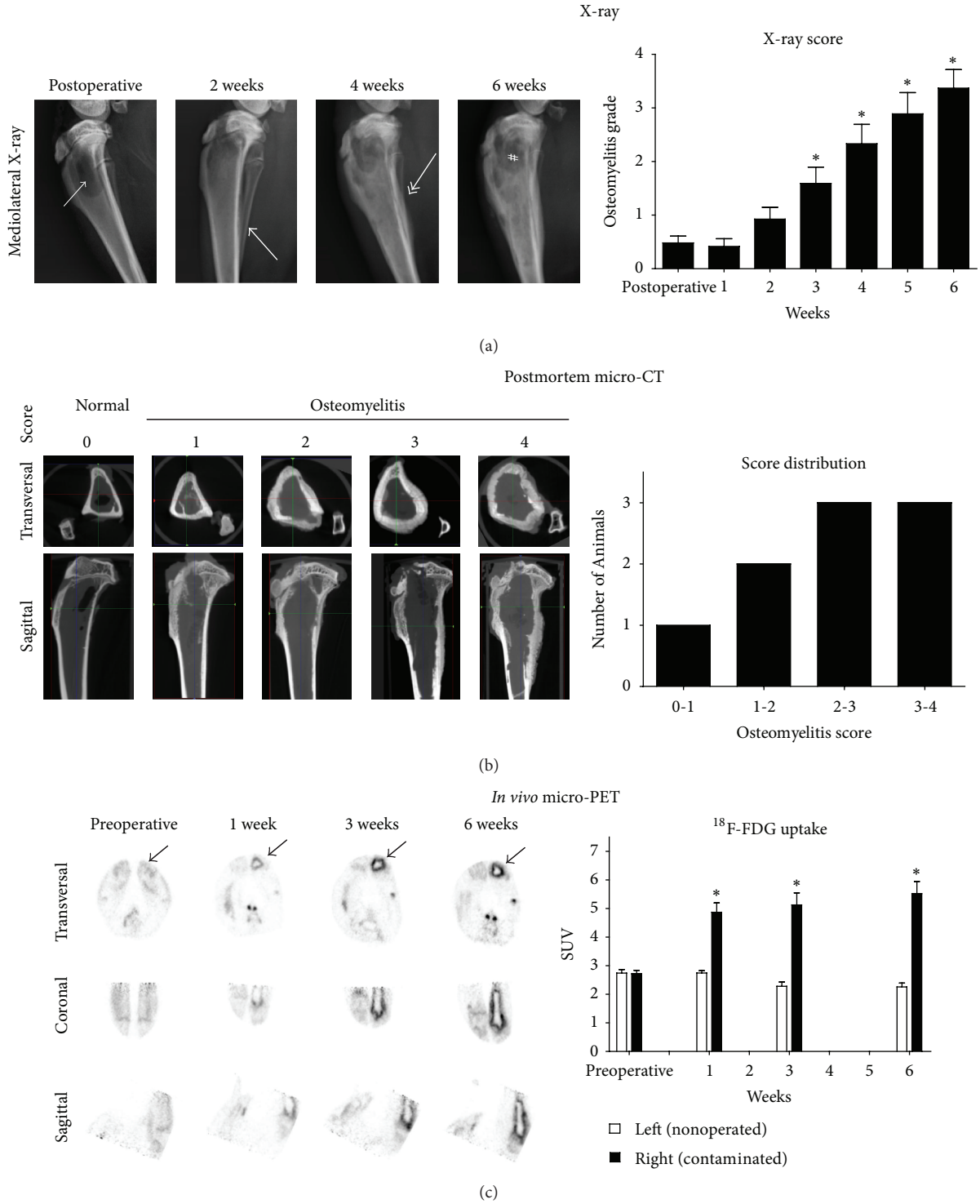

Figure 2: Imaging data. (a) Sequential X-ray radiographs during follow-up. The surgical procedure can result in radiologic symptoms for osteolysis (small arrow head). Two weeks after surgery, periosteal elevation can be detected (solid arrow head). After four weeks, cortical thickening (double headed arrow) and osteolysis can be detected (asterisk). At six weeks, the osteolysis is affecting the entire proximal part of the tibia (hash sign). Graph depicts the increase in radiological score during the developmental stage of an osteomyelitis. Radiological scores during follow-up were compared to the preoperative radiological score, asterisk indicates $P \leq 0.05$, and error bars indicate standard error of mean. (b) Representative postmortem micro-CT images taken after the six-week follow-up. (c) Reconstructed ^{18}F-FDG micro-PET data shows an increased tracer uptake in the operated area during the experimental follow-up (arrow). Asterisk indicates $P \leq 0.05$ and error bars indicate standard error of mean.

morphological changes like osteolysis, periosteal elevation, and cortical thickening. The micro-CT data (Figure 2(b)) allowed post-mortem assessment of the bone morphological changes as a result of the established osteomyelitis, confirming the X-ray data. The normal condition shows a clearly defined cortex without apparent signs of osteolysis, and the osteomyelitis conditions shows cortical thickening, loss of cortex integrity, and signs of moderate to severe osteolysis. The graph depicts the distribution of the radiological score in the experimental group.

Quantification of the micro-PET tracer uptake indicated that there was no statistical difference in tracer uptake in the proximal part of the tibia between the experimental preoperative group and the historic control group [7] (left leg $P = 0.371$; right leg $P = 0.112$).

There was no statistical difference in tracer uptake between the left and right leg of the combined preoperative control group (including the historic control group) ($P = 0.753$).

The ^{18}F-FDG uptake in the operated right leg was significantly increased at all postoperative time points compared to the uptake in the right tibia of the combined preoperative control group (Figure 2(c), preoperative black bar compared to postoperative black bars; $P \leq 0.001$).

All postoperative time points showed an increased ^{18}F-FDG uptake, indicated by the standardized uptake value (SUV) in the operated and contaminated right leg when compared to the uncontaminated left leg (Figure 2(c), white bars compared to black bars; $P \leq 0.012$).

Indicative for an active osteomyelitis, bacterial cultures of swabs taken from the knee joint cavities tested positive for *S. aureus* in 4 out of 9 cases, while bone tissue homogenate cultures tested positive for *S. aureus* in all cases (Figure 3(a)).

Histological staining of PMMA sections of the tibiae indicated the presence of Gram-positive cocci in the intramedullary cavity of the contaminated tibiae only (Figure 3(b)). Masson-Goldner staining indicated a clearly defined well-structured cortex, without signs of periosteal elevation or cortical thickening in uncontaminated left tibiae, while the contaminated right tibiae showed cortical thickening and loss of cortical integrity, indicating osteomyelitis (Figure 3(c)).

The state of bone remodelling was assessed by calcium binding fluorophores. In normal aseptic bone remodelling closely matched fluorescent signals (calcium deposition) are to be expected, whereas diseased bone remodelling would show calcium deposition in an outward direction in clearly defined layers (green: 2 weeks after operation, red: 4 weeks after operation; blue: the day before sacrifice). This allowed a clear discrimination between the normal left (unoperated and uncontaminated) and the right (operated and infected) tibia of all animals. The calcium binding fluorophores indicated undisputable signs of periosteal elevation and cortical thickening, in the infected tibiae (Figure 3(c)); these hallmarks for infection are confirmed by our previously published studies concerning orthopaedic implant infections.

4. Discussion

Osteomyelitis remains to be a major complication after an orthopaedic intervention or after bone trauma [9, 10]. The herein described study was conducted to provide insight into osteomyelitic development including the accompanying bone remodelling and the use of novel diagnostic approaches in the absence of an orthopaedic implant and a sclerosing agent to support infection development. Combining the results of this study with our previously published studies on orthopaedic implant infection [6] and the use of ^{18}F-FDG to detect implant infection by PET-imaging [7], we can provide an improved perspective on how the used infection parameters differ from each other in case of either implant or non-implant related orthopaedic infections.

Animal models for experimental (implant-related) osteomyelitis, like ours, are being used to evaluate the application resorbable biomaterials and antimicrobial coatings and their antimicrobial properties [11–14]. For this reason, no sclerosing agent like sodium morrhuate was used, since it poses a threat to resorbable biomaterials, due to the denaturing capacity of sodium morrhuate [15–18]. Furthermore, sodium morrhuate creates an abnormal bone anatomy by destructing the local vascularization [5, 19].

Common haematological parameters like ESR, CRP, and leucocyte differentiation are potent parameters for infection detection. However—there are some practical difficulties—the ESR is difficult to determine due to the used capillary detection system in our experimental setup, resulting in large deviations at the moment of readout. This issue makes this method of determination less accurate. The determination of the CRP concentration on the other hand is performed by ELISA, which is a very sensitive method, resulting in a more accurate readout. However, both ESR and CRP show the same trend, which is increased levels in the first weeks after surgery, after which the levels slowly decrease.

The leucocyte differentiation however shows a specific increase or decrease of a specific fraction of the leucocyte pool. For example, acute infection is generally related to a decrease in the lymphocyte fraction and a related increase in favour of the neutrophil and monocyte fraction. When we combine these haematological findings with the fact that the infection remains active (even when the ESR and CRP are decreasing but the shift in leucocyte differentiation remains present) our data suggests that the infection is stabilizing. This finding was confirmed by our previously performed study on orthopaedic implant infections.

X-ray radiographs allow detection of bone infection due to morphological changes like infection-initiated mineralization and osteolysis. Radiography is often used on single time points. The use of multiple imaging moments during follow-up allows monitoring of the bone morphological changes in the affected region. By detecting periosteal elevation, focal loss of cortex integrity, and osteolysis, an osteomyelitic lesion can be detected in time during radiological follow-up and thus allows monitoring of infection progression, whereas the presence of an implant may disturb radiologic detection of infection hallmarks due to implant related scatter of the X-rays; nonetheless, the influence (on radiologic imaging) of the

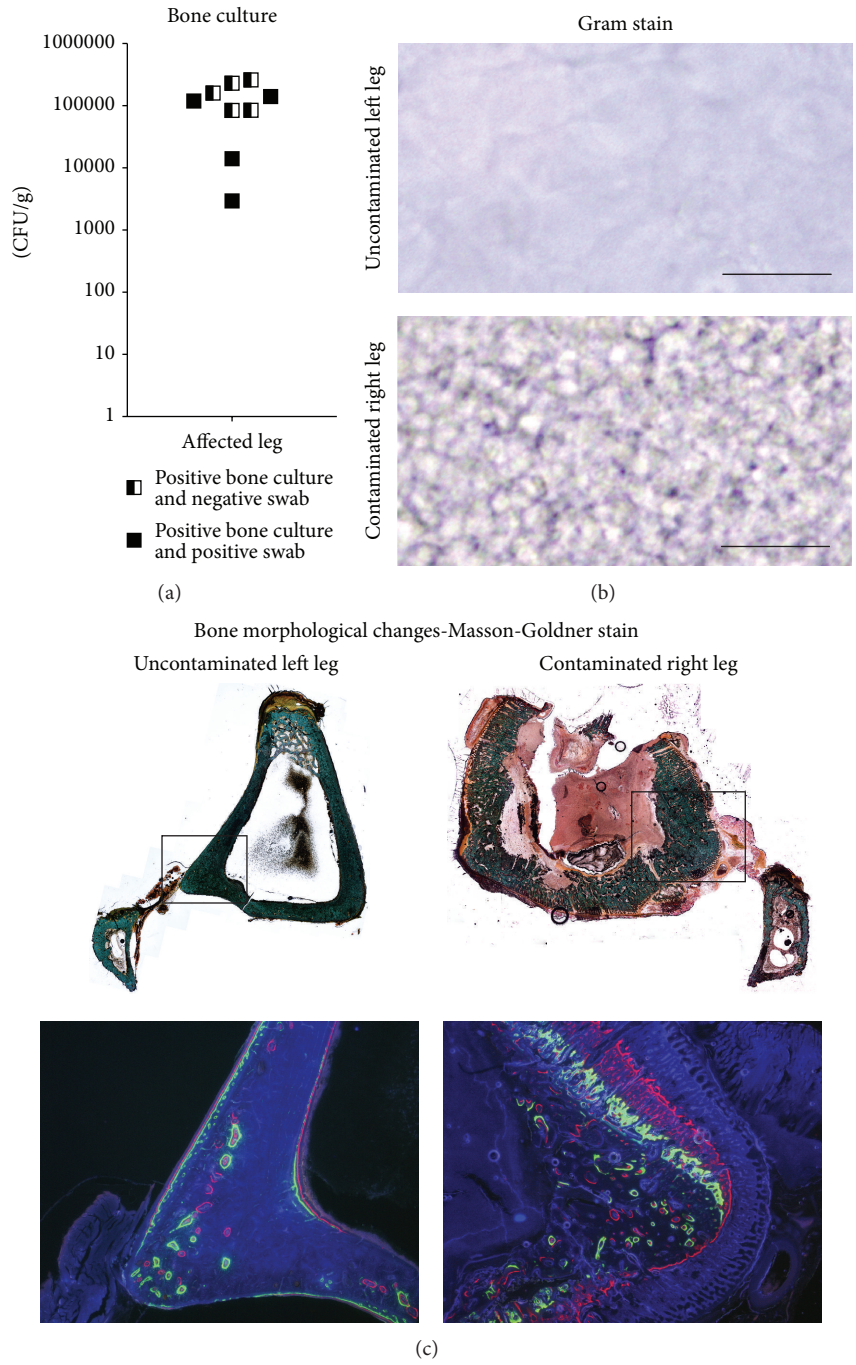

Figure 3: Bacterial culture and histology. (a) Postmortem bacterial culture of the excised part of the tibial tuberosity of the osteomyelitic tibia, indicating bacterial presence in all tibiae. (b) Histological confirmation of bacterial presence, by Gram stain, in the contaminated right leg only. (c) Bone morphological changes between left and right tibia. Tibial tuberosity is missing in the section of the right leg since this was used for bacterial culture. Fluorescence microscopy (insert) indicated normal bone remodelling in the left tibia, while it indicates cortex remodelling during the experimental follow-up in the right tibia (green at two weeks, red at four weeks, and blue at six weeks after surgery).

implant will remain equal during follow-up which will not hamper the sequential evaluation of bone mineralization and morphology over time.

^{18}F-FDG has been described as a clinical PET tracer for metabolic active processes (e.g., tumour growth, brain activity) [20, 21]. Together with previously published data of others, our data indicates the diagnostic potential of ^{18}F-FDG as a micro-PET tracer for the detection of osteomyelitis in relation to other relevant infection parameters, especially since ^{18}F-FDG micro-PET indicates abnormal metabolically active areas in the body [2, 7, 22]. Furthermore, our data indicates that ^{18}F-FDG micro-PET allows differentiation between

contaminated and uncontaminated bony tissue within one week after surgery. Due to the ability of ^{18}F-FDG micro-PET to distinguish between infected and uninfected tissue, this could be a powerful tool to assess novel infection interventions (coatings, antibiotic treatments). However, previously published studies have shown that the presence of an implant or an osteotomy/fracture can hamper early detection by PET due to implant-related scatter of the excited photons on the metallic implant surface or by tracer uptake due to a local sterile inflammation (fracture) [7, 22]. This indicates that the use of ^{18}F-FDG is a very sensitive method to detect increased metabolic activity in the bony tissue; however, the specificity is dedicated not only towards infection but also towards sterile inflammation due to tissue damage (by a surgical intervention or fracture) [7, 22].

Bacterial culture is considered the golden standard for the detection of active bone infections [23–25]. The additional histological analysis for bacterial presence, by Gram-staining, of the PMMA sections of the tibiae indicates the presence of bacteria in the affected tissue, while standard histological stainings indicate the bone morphological changes initiated by the bacterial infection.

Calcium binding fluorophores have been used in the past to follow bone remodelling and the mineralization of teeth [26–30]. In contrast to these previous studies, our data shows that these calcium binding fluorophores can also be of considerable value to monitor and quantify osteomyelitis related bone remodelling, specifically the mineralization of the periosteal elevation [6]. Furthermore, when these data are combined with the haematological data, they show that the infection-mediated bone mineralization remains progressing even after the ESR and CRP levels are decreasing, strengthening the indication for an acute stabilizing (potentially chronic) infection. Furthermore, when combined with our previously published data [6, 7], these data indicate that these changes in bone remodelling are infection dependent and not associated with the presence nor absence of an implant.

Our collected data provides novel insight into osteomyelitis development and suggestions of parameter usage in both preclinical and clinical perspectives. In the preclinical setting, the body weight and temperature provide general information about the condition of the animal and should be regarded as such. The use of weekly assessment of the CRP levels and leucocyte differentiation, in combination with weekly X-ray radiographs, histology, and bacterial culture, is recommended. Although ^{18}F-FDG microPET, post-mortem microCT and calcium bindingfluorophores provide optional information on the infection and its related bone mineralization, they are not absolutely necessary to determine if an antimicrobial coating or biomaterial is effective to prevent an osteomyelitis. While a combined follow-up with X-ray radiographs, histology, bacterial culture and haematological analysis will provide sufficient information to determine antimicrobial efficacy. However, when interested in prophylactic approaches, the determination of delayed onset of the actual infection, or infection mediated bone remodelling and osteolysis, ^{18}F-FDG micro-PET, and postmortem micro-CT, and the use of calcium binding fluorophores provide more in depth information about timing, metabolic activity, and bone mineralization.

When translated to the clinical situation, however, the situation is different, and CRP and leucocyte differentiation will still be useful and so will X-ray radiographs, but calcium binding fluorophores are not an option. Based on our data, ^{18}F-FDG PET (combined with CT/MRI in one clinical system) could considerably contribute to the early detection of an orthopaedic infection allowing early infection intervention and treatment in the clinical situation.

5. Conclusion

Our study describes the detection of different bone infection parameters and their correlations in an experimental osteomyelitis animal model (independent of the presence of an implant) and provides information on which parameters would be the most optimal infection parameters to be of use in the preclinical and potentially the clinical setting. Furthermore, our study showed that ^{18}F-FDG PET is a potent diagnostic tool for the early detection of orthopaedic infections, which can be of great value when applied in the clinical situation.

Conflict of Interests

The authors declare no conflict of interests.

Acknowledgments

This research forms part of the Project P4.01 NANTICO of the research program of the BioMedical Materials institute, cofunded by the Dutch Ministry of Economic Affairs. Furthermore, the authors would like to thank the employees of the animal facility of the Maastricht University Medical Centre for their assistance during this study. They would also like to thank I. Pooters, M. Visser, and C. Urbach from the Nuclear Medicine Department of the Maastricht University Medical Centre for their support during this study. And they would like to thank S. Bout and P. Dijkstra for their overall support during this study. The herein described animal study was approved by the Animal Ethics Committee of the Maastricht University Medical Centre, Protocol number 2010-089.

References

[1] A. Demirev, R. Weijers, J. Geurts, F. Mottaghy, G. Walenkamp, and B. Brans, "Comparison of [18 F]FDG PET/CT and MRI in the diagnosis of active osteomyelitis," *Skeletal Radiology*, vol. 43, no. 5, pp. 665–672, 2014.

[2] P. Lankinen, K. Lehtimäki, A. J. Hakanen, A. Roivainen, and H. T. Aro, "A comparative ^{18}F-FDG PET/CT imaging of experimental *Staphylococcus aureus* osteomyelitis and *Staphylococcus epidermidis* foreign-body-associated infection in the rabbit tibia," *EJNMMI Research*, vol. 2, no. 1, article 41, 2012.

[3] T. J. Mäkinen, P. Lankinen, T. Pöyhönen, J. Jalava, H. T. Aro, and A. Roivainen, "Comparison of 18F-FDG and 68Ga PET imaging in the assessment of experimental osteomyelitis due to

Staphylococcus aureus," *European Journal of Nuclear Medicine and Molecular Imaging*, vol. 32, no. 11, pp. 1259–1268, 2005.

[4] C. W. Norden, "Experimental osteomyelitis. I. A description of the model," *The Journal of Infectious Diseases*, vol. 122, no. 5, pp. 410–418, 1970.

[5] V. T. Andriole, D. A. Nagel, and W. O. Southwick, "A paradigm for human chronic osteomyelitis," *Journal of Bone and Joint Surgery—Series A*, vol. 55, no. 7, pp. 1511–1515, 1973.

[6] J. C. Odekerken, J. J. Arts, D. A. Surtel, and G. H. Walenkamp, "A rabbit osteomyelitis model for the longitudinal assessment of early post-operative implant infections," *Journal of Orthopaedic Surgery and Research*, vol. 8, no. 1, article 38, 2013.

[7] J. C. Odekerken, B. T. Brans, T. J. Welting, and G. H. Walenkamp, " ^{18}F-FDG microPET imaging differentiates between septic and aseptic wound healing after orthopedic implant placement A longitudinal study of an implant osteomyelitis in the rabbit tibia," *Acta Orthopaedica*, vol. 85, no. 3, pp. 305–313, 2014.

[8] N. T. Winkler, "ALARA concept—now a requirement," *Radiologic Technology*, vol. 51, no. 4, p. 525, 1980.

[9] Y. P. Acklin, A. F. Widmer, R. M. Renner, R. Frei, and T. Gross, "Unexpectedly increased rate of surgical site infections following implant surgery for hip fractures: problem solution with the bundle approach," *Injury*, vol. 42, no. 2, pp. 209–216, 2011.

[10] L. Montanaro, P. Speziale, D. Campoccia et al., "Scenery of Staphylococcus implant infections in orthopedics," *Future Microbiology*, vol. 6, no. 11, pp. 1329–1349, 2011.

[11] V. Alt, K. S. Lips, C. Henkenbehrens et al., "A new animal model for implant-related infected non-unions after intramedullary fixation of the tibia in rats with fluorescent in situ hybridization of bacteria in bone infection," *Bone*, vol. 48, no. 5, pp. 1146–1153, 2011.

[12] T. Kälicke, J. Schierholz, U. Schlegel et al., "Effect on infection resistance of a local antiseptic and antibiotic coating on osteosynthesis implants: an in vitro and in vivo study," *Journal of Orthopaedic Research*, vol. 24, no. 8, pp. 1622–1640, 2006.

[13] D. J. F. Moojen, H. C. Vogely, A. Fleer et al., "Prophylaxis of infection and effects on osseointegration using a tobramycin-periapatite coating on titanium implants: an experimental study in the rabbit," *Journal of Orthopaedic Research*, vol. 27, no. 6, pp. 710–716, 2009.

[14] M. W. Nijhof, H. P. Stallmann, H. C. Vogely et al., "Prevention of infection with tobramycin-containing bone cement or systemic cefazolin in an animal model," *Journal of Biomedical Materials Research*, vol. 52, no. 4, pp. 709–715, 2000.

[15] L. Rogers, "A note on sodium morrhuate in tuberculosis," *British Medical Journal*, vol. 1, no. 3032, pp. 147–148, 1919.

[16] I. S. Tunick and R. Nach, "Sodium morrhuate as a sclerosing agent in the treatment of varicose veins," *Annals of Surgery*, vol. 95, no. 5, pp. 734–737, 1932.

[17] J. Schaumburger, S. Trum, S. Anders et al., "Chemical synovectomy with sodium morrhuate in the treatment of symptomatic recurrent knee joint effusion," *Rheumatology International*, vol. 32, no. 10, pp. 3113–3117, 2012.

[18] D. F. Stroncek, S. W. Hutton, S. E. Silvis, G. M. Vercellotti, H. S. Jacob, and D. E. Hammerschmidt, "Sodium morrhuate stimulates granulocytes and damages erythrocytes and endothelial cells: probable mechanism of an adverse reaction during sclerotherapy," *The Journal of Laboratory and Clinical Medicine*, vol. 106, no. 5, pp. 498–504, 1985.

[19] A. C. Cremieux and C. Carbon, "Experimental models of bone and prosthetic joint infections," *Clinical Infectious Diseases*, vol. 25, pp. 1295–1302, 1997.

[20] H. Toyama, M. Ichise, J.-S. Liow et al., "Absolute quantification of regional cerebral glucose utilization in mice by 18F-FDG small animal PET scanning and 2-14C-DG autoradiography," *Journal of Nuclear Medicine*, vol. 45, no. 8, pp. 1398–1405, 2004.

[21] H. Toyama, M. Ichise, J.-S. Liow et al., "Evaluation of anesthesia effects on [18F]FDG uptake in mouse brain and heart using small animal PET," *Nuclear Medicine and Biology*, vol. 31, no. 2, pp. 251–256, 2004.

[22] L. Jones-Jackson, R. Walker, G. Purnell et al., "Early detection of bone infection and differentiation from post-surgical inflammation using 2-deoxy-2-[18F]-fluoro-D-glucose positron emission tomography (FDG-PET) in an animal model," *Journal of Orthopaedic Research*, vol. 23, no. 6, pp. 1484–1489, 2005.

[23] A. Trampuz and W. Zimmerli, "Antimicrobial agents in orthopaedic surgery: prophylaxis and treatment," *Drugs*, vol. 66, no. 8, pp. 1089–1105, 2006.

[24] G. L. Woods and D. H. Walker, "Detection of infection or infectious agents by use of cytologic and histologic stains," *Clinical Microbiology Reviews*, vol. 9, no. 3, pp. 382–404, 1996.

[25] F. A. Waldvogel, G. Medoff, and M. N. Swartz, "Osteomyelitis: a review of clinical features, therapeutic considerations and unusual aspects," *The New England Journal of Medicine*, vol. 282, no. 4, pp. 198–206, 1970.

[26] C. Pautke, T. Tischer, S. Vogt et al., "New advances in fluorochrome sequential labelling of teeth using seven different fluorochromes and spectral image analysis," *Journal of Anatomy*, vol. 210, no. 1, pp. 117–121, 2007.

[27] C. Pautke, S. Vogt, T. Tischer et al., "Polychrome labeling of bone with seven different fluorochromes: enhancing fluorochrome discrimination by spectral image analysis," *Bone*, vol. 37, no. 4, pp. 441–445, 2005.

[28] S. M. van Gaalen, M. C. Kruyt, R. E. Geuze, J. D. de Bruijn, J. Alblas, and W. J. A. Dhert, "Use of fluorochrome labels in in vivo bone tissue engineering research," *Tissue Engineering B: Reviews*, vol. 16, no. 2, pp. 209–217, 2010.

[29] W. W. Rittmann and S. M. Perren, *Corticale Knochenheilung nach Osteosynthese und Infektion. Biomechanik und Biologie*, Springer, Berlin, Germany, 1974.

[30] R. Feith, *Side-effects of acrylic cement implanted into bone [Ph.D. thesis]*, 1975.

Hindawi Publishing Corporation
BioMed Research International
Volume 2014, Article ID 574248, 11 pages
http://dx.doi.org/10.1155/2014/574248

Review Article

Giant Cell Arteritis: A Systematic Review of the Qualitative and Semiquantitative Methods to Assess Vasculitis with 18F-Fluorodeoxyglucose Positron Emission Tomography

Cristina Puppo,[1] Michela Massollo,[2] Francesco Paparo,[1] Dario Camellino,[3] Arnoldo Piccardo,[2] Mehrdad Shoushtari Zadeh Naseri,[2] Giampiero Villavecchia,[2] Gian Andrea Rollandi,[1] and Marco Amedeo Cimmino[3]

[1] *Department of Radiology, Department of Diagnostic Imaging, E.O. Ospedali Galliera, Mura della Cappuccine 14, 16128 Genoa, Italy*
[2] *Nuclear Medicine Unit, Department of Diagnostic Imaging, E.O. Ospedali Galliera, Mura della Cappuccine 14, 16128 Genoa, Italy*
[3] *Research Laboratory and Academic Unit of Clinical Rheumatology, Department of Internal Medicine, University of Genoa, V.le Benedetto XV 6, 16132 Genoa, Italy*

Correspondence should be addressed to Michela Massollo; michela.massollo@galliera.it

Received 5 June 2014; Accepted 28 July 2014; Published 1 September 2014

Academic Editor: Alberto Signore

Giant cell arteritis (GCA) is the most common vasculitis affecting medium and large vessels. It shows a close clinical association with polymyalgia rheumatica (PMR), a musculoskeletal inflammatory disorder, which is clinically characterized by girdles pain and stiffness. 18F-Fluorodeoxyglucose (18F-FDG) positron emission tomography (PET) is an effective tool for the diagnosis, grading, and follow-up of patients affected by GCA involving the aorta and its proximal branches, but the lack of a standardized method for the assessment of vascular inflammation remains a critical issue, potentially leading to misclassification. In our systematic review, including 19 original articles for a total of 442 GCA patients (with or without PMR symptoms) and 535 healthy controls, we described the different qualitative, semiquantitative and combined methods that have been proposed throughout the literature for assessing the presence and grading the severity of GCA-related vascular inflammation on 18F-FDG PET scans, focusing on the diagnostic performance and examining their respective advantages and limitations. The majority of the included studies adopted qualitative methods of PET image analysis, which are less sensitive but more specific than semiquantitative ones. Among the semiquantitative approaches, the aortic-to-blood pool uptake ratio of the aortic arch seems to be the most accurate method.

1. Introduction

Giant cell arteritis (GCA) is the most common vasculitis affecting medium and large vessels, with an incidence of 7–18 cases per 100,000 individuals and with women affected twice as often as men [1, 2]. GCA was initially described as temporal arteritis (Horton disease), but about 15–27% of patients have extracranial involvement, since the entire aorta and all its branches can be affected, including the carotid, subclavian, and iliac arteries [3–5]. Polymyalgia rheumatica (PMR) is an inflammatory disorder, two to three times more common than GCA and clinically characterized by girdles pain and stiffness. PMR can occur before and simultaneously with or develop after clinical manifestations of GCA [6–10].

Population-based studies have shown that PMR occurs in about 50% of patients with GCA, and approximately 15%–30% of PMR patients develop GCA [1, 11]. The presence of different clinical features common to both PMR and GCA (e.g., older age at onset with progressively increasing incidence rates after 50 years, similar sex ratio, substantial increase of acute-phase reactants, and rapid responsiveness to glucocorticoids) has suggested that they might be different manifestations of the same underlying process [1].

Although etiology, development mechanisms, and targets of inflammatory damage of both GCA and PMR have not been yet defined, there is increasing evidence that a combination of genetic, immunogenetic [12–17], and environmental factors may play a pivotal role [12, 18, 19].

Early detection of the involvement of thoracic aorta and its branches plays a fundamental role in patient management and treatment. Thoracic aortic aneurysms are more frequent in patients with GCA than in nonaffected people and tend to arise several years after the diagnosis, when other symptoms are less evident [5, 20].

Over the past recent years, 18F-FDG PET, computed tomography (CT) angiography, and magnetic resonance imaging (MRI) have revealed that extracranial involvement in GCA is more frequent than previously anticipated, occurring in 30–74% of patients [21–24].

18F-FDG PET is a functional imaging technique that has become an established tool in oncology [5] but it has demonstrated also a promising role in the field of inflammatory diseases [4, 5]. The main limitation of 18F-FDG PET/CT to become a reliable diagnostic tool is the lack of a standardized definition of vascular inflammation based on the intensity of the glucose analogue uptake. Several authors have proposed various 18F-FDG PET diagnostic criteria.

This systematic review is focused on the different qualitative and semiquantitative methods for diagnosis and grading of vascular inflammation in GCA patients (with or without associated PMR) by means of 18F-FDG PET. We also assessed the diagnostic performance and the clinical value of each method of evaluation.

Takayasu arteritis (TA) was not included in our analysis because, though sharing apparent similar FDG distributions with GCA, its target population, pathophysiology, evolution, and prognosis are not comparable with those of GCA.

2. Materials and Methods

2.1. Database Search. A systematic literature research was performed up to April 2014, with no time limits. PubMed and the Cochrane Library were searched for articles written in English that addressed the issue of 18F-FDG PET as a diagnostic tool in GCA with or without associated PMR. We used the MeSH query "giant cells arteritis" or "polymyalgia rheumatica" and "positron emission tomography."

A first selection was based on the exclusion of review articles, meta-analyses, abstracts, editorials or letters, case reports, and studies investigating 3 or fewer patients because they failed to provide sufficient evidence-based data. In this first stage, two researchers independently reviewed titles and abstracts of all retrieved articles. Studies addressing 18F-FDG-PET as diagnostic tool in GCA/PMR were included, while articles related to other vasculitides were excluded.

At the second stage, the same two researchers independently assessed the full-text version of all articles that were found to be potentially eligible for inclusion, using the same inclusion and exclusion criteria as mentioned above (Figure 1). At both stages, disagreements between the two researchers were discussed and resolved by consensus.

3. Results

A total of 199 citations were found using the database search. Nineteen full-text articles, written from 1999 to 2014, were included. Of them, 13 were prospective and 6 retrospective studies. In order to assess vascular inflammation in GCA, with or without associated PMR, 10 studies used exclusively qualitative 18F-FDG uptake criteria, 6 used only semiquantitative criteria, and 3 adopted both qualitative and semiquantitative criteria (Table 1).

3.1. Qualitative Methods for the Assessment of 18F-FDG PET. Ten studies [25–28, 30–32, 36, 38, 39] used exclusively qualitative methods of analysis to assess 18F-FDG uptake/accumulation within the walls of affected vessels in GCA/PMR patients (Figure 2).

Three of these articles [25, 26, 36] proposed a visual grading scale exclusively based on vascular 18F-FDG uptake and 5 studies [27, 31, 32, 38, 39] used a visual grading score based on the vessel-to-liver ratio. The remaining 2 studies [28, 30] defined each examination as positive or negative (i.e., abnormal versus normal), without specifying a positive threshold (Table 2).

In his first prospective study, Blockmans et al. [25] proposed a visual 4-point scale with scores ranging from 0 to 3, which was described as follows: a 0 score indicated no visualization of blood vessels; a score of 1 meant minimal 18F-FDG uptake, a score of 2 an increased 18F-FDG uptake, and a score of 3 18F-FDG a pronounced uptake. Blood vessels of the lower and upper limbs and the thoracic arteries were individually defined as positive for inflammatory involvement if the score was ≥2.

Brodmann et al. [30] examined 22 consecutive patients with clinical diagnosis of GCA confirmed by DUS: 18F-FDG PET scans were rated as negative or positive, without a definition of the criterion used (Figure 3). Meller et al. [27] proposed a visual grading scale, used by four other studies [31, 32, 38, 39], where large vessel 18F-FDG uptake was compared with that of the liver. According to this method, zero was defined as no uptake, 1 as uptake present but lower than liver uptake, 2 as uptake similar to liver uptake, and 3 as uptake higher than liver uptake (Figure 4). Three [27, 32, 39] out of these 5 studies concluded that a grade ≥2 for the thoracic aorta and a grade ≥1 in the other vascular regions were positive criteria for vasculitis. A smooth linear or long segmental pattern of 18F-FDG uptake in the aorta and its main branches, with an intensity higher than the liver uptake, was regarded as findings highly suggestive for GCA.

3.2. Semiquantitative Methods of Assessment of 18F-FDG PET. Six studies [21, 24, 33, 35, 40, 41] used a semiquantitative scoring method to evaluate vascular uptake (Table 3). Blockmans, in two prospective studies [21, 33], proposed a semiquantitative system that evaluates 18F-FDG uptake in 7 different vascular regions (thoracic aorta, abdominal aorta, subclavian arteries, axillary arteries, carotid arteries, iliac arteries, and femoral arteries) with the following grading: 0: no uptake; 1: minimal but not negligible uptake; 2: clearly increased uptake; and 3: very marked uptake. Based on this first evaluation, a total vascular score (TVS) was calculated, ranging from 0 (no vascular FDG uptake in any of the 7 vascular regions) to 21 (maximum vascular FDG uptake in

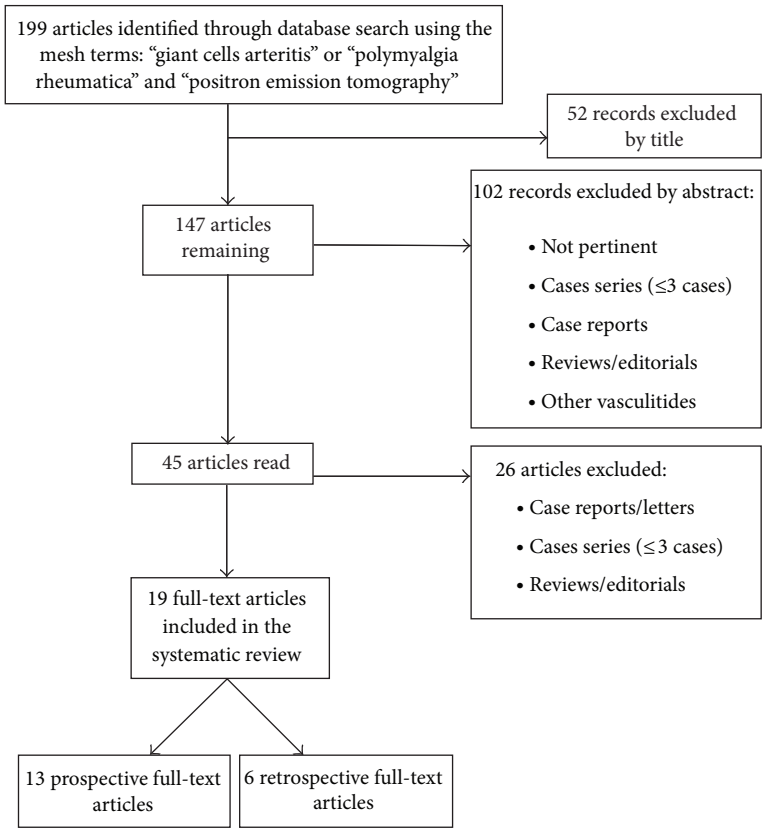

Figure 1: Flowchart of the review process.

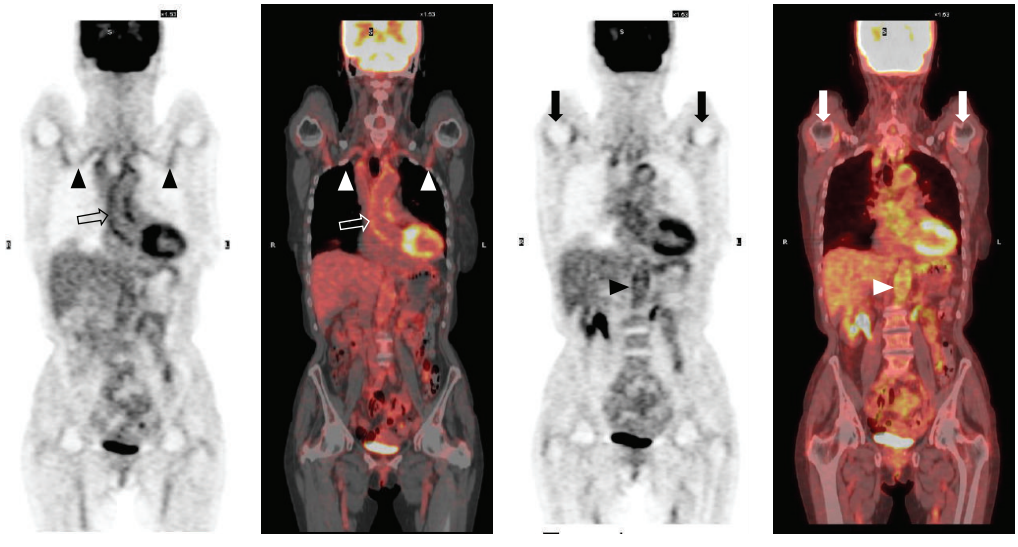

Figure 2: 65-year-old female patient with 18F FDG PET-CT findings indicating the clinical association of polymyalgia rheumatica and giant cell arteritis. Coronal PET (a) and PET-CT (b) images demonstrate a significant tracer uptake of the walls of the ascending aorta, aortic arch (void arrows in (a) and (b)), and subclavian arteries (arrowheads in (a) and (b)). The second pair of coronal PET (c) and PET-CT (d) images demonstrate the inflammatory involvement of the abdominal aorta (arrowheads in (c) and (d)). A bilateral uptake of the tracer of the glenohumeral joints is also seen (solid arrows).

Table 1: Current state of scoring methods of 18F-FDG PET in giant cell arteritis.

Author (year)	Study design	Patients	Controls	Technique	Method of analysis	Description	Standard of reference	Diagnostic performance
Blockmans et al. (1999) [25]	Prospective	11	23	PET	Qualitative	Visual grading scale	ACR criteria + TAB	Not specified
Blockmans et al. (2000) [26]	Prospective	25	44	PET	Qualitative	Visual grading scale	Clinical symptoms + TAB	Thoracic vessels Sensitivity: 56% Specificity: 98% PPV: 93% NPV: 80% Legs Sensitivity: 64% Specificity: 77%
Meller et al. (2003) [27]	Prospective	15	Group 1: 38 Group 2: 40	PET and PET/CT	Qualitative	Visual grading scale	ACR criteria	Sensitivity: 73% Specificity: 100%
Bleeker-Rovers et al. (2003) [28]	Retrospective	22	—	PET	Qualitative	Positive/negative	ACR criteria	Sensitivity: 77% Specificity: 100% PPV: 100% NPV: 82%
Moosig et al. (2004) [29]	Prospective	13	6	PET	Qualitative and semiquantitative	Positive/negative and SUV vascular/lung ratio	PMR: exclusion of other causes of inflammation + Chuang and Healy criteria	Sensitivity: 100% Specificity: 100%
Brodmann et al. (2004) [30]	Prospective	22	—	PET	Qualitative	Positive/negative	ACR criteria + positive hypoechogenic halo on DUS	Not specified
Scheel et al. (2004) [31]	Prospective	8	—	PET and PET/CT	Qualitative	Positive/negative	Clinical symptoms	Not specified
Walter et al. (2005) [32]	Prospective	20	26	PET	Qualitative	Visual grading scale	ACR criteria	Sensitivity: 60% Specificity: 99.8% PPV: 99.7% NPV: 67.9% Accuracy: 78.6%
Blockmans et al. (2006) [21]	Prospective	35	—	PET	Semiquantitative	Visual grading scale	TAB	Not specified
Blockmans et al. (2007) [33]	Prospective	35	—	PET	Semiquantitative	Visual grading scale	PMR: clinical + negative TAB	Not specified
Henes et al. (2008) [34]	Prospective	13	—	PET/CT	Qualitative and semiquantitative	Positive/negative and highest SUVmax vascular	Clinical and diagnostic work-up (including DUS, MRI, CT, and TAB)	Sensitivity: 90% Specificity: 100%
Hautzel et al. (2008) [35]	Prospective	18	Group 1: 36 Group 2: 18	PET	Semiquantitative	Highest SUVmax aorta/liver ratio	ACR criteria or diagnostic work-up (including DUS, TAB, CT, and MRI)	Cut-off: 1.0 Sensitivity: 88.9% Specificity: 94.4%–95.1% Accuracy: 91.7%–93.2% PPV: 78.8%–88.9% NPV: 95.1%–97.7%
Both et al. (2008) [36]	Prospective	25	—	PET	Qualitative	Visual grading scale	Birmingham vasculitis activity score (BVAS.2)	Not specified

Table 1: Continued.

Author (year)	Study design	Patients	Controls	Technique	Method of analysis	Description	Standard of reference	Diagnostic performance
Lehmann et al. (2011) [37]	Retrospective	20	20	PET	Qualitative and semiquantitative	Positive/negative and highest SUVmax	Clinical (ACR) diagnosis confirmed by histology or MRI angiography	Visual grading Sensitivity: 65% Specificity: 80% SUVmax (cut-off 1.78) Sensitivity: 90% Specificity: 45%
Henes et al. (2011) [38]	Retrospective	10	—	PET/CT	Qualitative	Visual grading scale	Clinical symptoms	Not specified
Hooisma et al. (2012) [39]	Retrospective	62	242	PET/CT	Qualitative	Positive/negative	Clinical symptoms	Not specified
Yamashita et al. (2012) [40]	Retrospective	27	17	PET/CT	Semiquantitative	Visual grading scale	PMR: Chuang et al. and Healy's criteria; no clinical evidence of temporal arteritis	Not specified
Besson et al. (2013) [41]	Retrospective	33	11	PET/CT	Semiquantitative	*A*: highest SUVmax arterial/liver ratio *A*′: average SUVmax arterial/liver ratio *B*: highest SUVmax arterial/lung ratio *B*′: average SUVmax arterial/lung ratio *C*: highest arterial SUVmax/highest venous SUVmax *C*′: average arterial SUVmax/venous blood pool activity	ACR criteria + TAB	Method C at aortic arch: cut-off value of 1.53 Sensitivity: 81.8% Specificity: 91%
Prieto-González et al. (2014) [24]	Prospective	32	20	PET/CT	Semiquantitative	Highest SUVmax vascular/liver ratio	TAB	Any vascular territory (cut-off of 1.89) Sensitivity: 80% Specificity: 79% Epiaortic vessels (cut-off of 1.70) Sensitivity: 81% Specificity: 79% Aorta (cut-off 2.25) Sensitivity: 90% Specificity: 42% Aorta (cut-off 2.65) Sensitivity: 58% Specificity: 90%

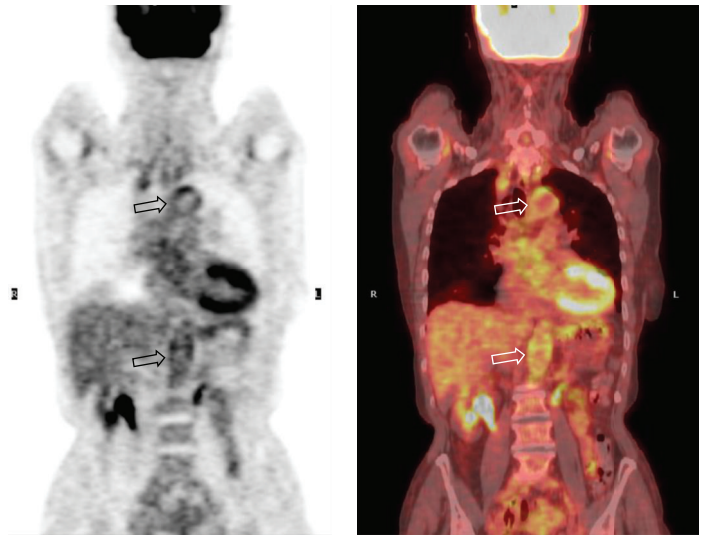

(a) (b)

Figure 3: 77-year-old female patient with clinical and PET-CT findings of giant cell arteritis. Coronal PET (a) and PET-CT (b) scans demonstrate the inflammatory involvement of aortic arch and abdominal aorta (void arrows), which is clearly appreciable by means of an immediate qualitative assessment of the images.

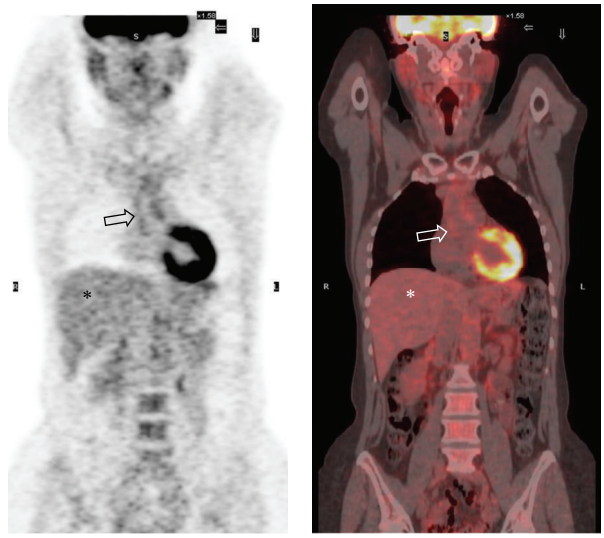

(a) (b)

Figure 4: 80-year-old male patient with clinical and PET-CT findings of giant cell arteritis. In this patient, coronal PET (a) and PET-CT (b) images demonstrate 18F FDG uptake of the walls of the ascending thoracic aorta (void arrows). The tracer uptake is similar to that of the liver parenchyma (asterisk), corresponding to grade 2 (significant vascular inflammation) according to the visual grading score proposed by Meller et al.

Table 2: 18F-FDG PET and PET/CT qualitative diagnostic criteria.

Number of studies	Description
2	Positive/negative or normal/abnormal
3	Visual grading scale 0: none; 1: slight; 2: marked; 3: intense
5	Visual grading scale 0: no uptake; 1: lower than liver; 2: similar to liver; 3: more than liver

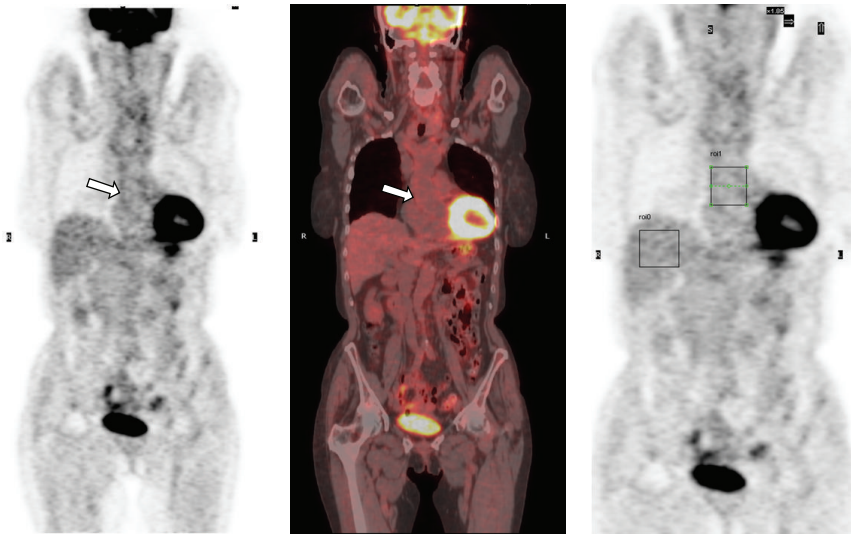

(a) (b) (c)

Figure 5: 65-year-old female patient with polymyalgia rheumatica and suspected giant cell arteritis. An immediate qualitative visual assessment of the coronal PET-CT scan ((a) and (b)) led to the diagnosis of inflammatory involvement of the ascending thoracic aorta (white arrows). In this patient, the semiquantitative method of analysis proposed by Hautzel et al. was further applied (aorta-to-liver SUVmax ratio). Placing a ROI on the ascending thoracic aorta in the coronal PET image (c), a SUVmax of 1.6 was obtained. The SUVmax obtained by drawing the same ROI comprehensive on the liver (c) was 2.2, and the resulting aorta-to-liver SUVmax ratio was 0.7, below the cut-off value of 1 for diagnosing significant vascular inflammation. This is an example of discrepancy between qualitative and semiquantitative methods of image analysis.

Table 3: 18F-FDG PET and PET/CT semiquantitative diagnostic criteria.

Number of studies	Description
3	Visual grading scale (0–3) and TVS
3	Highest SUVmax vascular/liver ratio
1	Average SUVmax vascular/liver ratio
1	Highest SUVmax vascular/lung ratio
1	Average SUVmax vascular/lung ratio
1	Highest SUVmax arterial/venous ratio
1	Average SUVmax arterial/venous ratio

all 7 locations). They found a mean TVS of 6 ± 0.2 at the time of diagnosis in 29 of 35 patients with GCA, with or without PMR. They also found a significantly lower mean TVS of 0.8 ± 1.7 in 31% of isolated PMR cases.

Hautzel et al. [35] introduced a semiquantitative aorta-to-liver SUVmax ratio. In their prospective study they found an optimal relationship of sensitivity to specificity at an aorta-to-liver ratio of 1.0, even in patients with altered hepatic metabolism (Figure 5).

In their retrospective controlled study [41], Besson et al. compared three different semiquantitative approaches. The first method was derived from that described by Hautzel et al. [35], including two variants for normalizing the arterial activity to the liver uptake (i.e., highest SUVmax vascular/liver ratio and average SUVmax vascular/liver ratio) [35, 41]. The second approach was adapted from that described by Moosig et al. [29] and included two variants, where the arterial activity was normalized to the lung uptake (i.e., highest SUVmax vascular/lung ratio and average SUVmax vascular/lung ratio). The third approach had not been previously applied in GCA/PMR, but it was originally tested in atherosclerosis patients to evaluate arterial wall inflammation [42]. It was based on the arterial-to-blood pool uptake ratio and included two variants: in the first, the highest arterial SUVmax was normalized to the highest venous SUVmax; in the second, the average arterial SUVmax was normalized to the venous blood pool activity. The latter one was calculated by averaging the values obtained from eight ROIs drawn on axial 18F-FDG images in the right internal jugular vein.

3.3. Combined Qualitative and Semiquantitative Methods. Three studies [29, 34, 37] used a first qualitative analysis to diagnose or rule out the presence of vasculitis, performing a further semiquantitative assessment on vascular 18F-FDG uptake.

In the study of Moosig et al. [29], the visual examination of PET scans showed an increased tracer uptake in the aorta or in its major branches in 12 out of 13 included patients. For the semiquantitative assessment, 9 vascular areas were identified and sampled by placing different regions of interest. A peripheral region of the lung served to represent the background uptake, and vessel-to-lung SUVmax ratio was calculated. According to this method, Moosig et al. found that patients with active disease had significantly greater 18F-FDG uptake than control patients (mean ROI index of 1.58 versus 0.93).

Henes et al. [34] focused their analysis on the vessel showing the highest accumulation of the tracer at a first qualitative visual assessment. Further, they measured the maximum SUV on 6 locations of the selected vascular region. They found a mean SUVmax of 3.4 for all patients. The SUVmax was 3.9 in untreated patients versus 3.0 in patients under medical treatment.

Lehmann et al. [37] used two different diagnostic approaches for image assessment: a first visual analysis of vessel wall uptake compared to the background activity of liver, followed by a semiquantitative reevaluation, consisting of calculating the SUVmax in predefined regions of interest. They found that the SUVmax cut-off value of 1.78 is characterized by a high sensitivity (90% versus 65% of the qualitative visual assessment) and a low specificity (45% versus 80% of the qualitative visual assessment).

4. Discussion

The aim of our systematic review, which included a total of 442 cases of GCA patients, with or without PMR symptoms, and 535 controls, was to analyze the different qualitative and semiquantitative methods for assessing the presence and grading the severity of GCA-related vascular inflammation on 18F-FDG PET scans that have been proposed in the literature. We found the need for a standardized 18F-FDG PET interpretation in order to optimize the diagnostic performance of this imaging technique. Indeed, the lack of a standardized reading approach to defining vascular inflammation remains a critical issue and may lead to misclassification. Currently, the diagnosis of GCA is mainly based on clinical evaluation, laboratory findings, and temporal artery biopsy (TAB). The American College of Rheumatology diagnostic criteria for GCA do not include any imaging modality [43].

In patients with a distinctive clinical presentation, the diagnosis of GCA is not difficult and TAB is able to confirm the clinical suspicion. By contrast, a correct diagnosis may become challenging when symptoms are nonspecific, given the wide range of clinical manifestations of GCA [3, 5, 44]. Currently, TAB is still the diagnostic standard of reference [1, 2], but its routine clinical application is hampered by low sensitivity with a high false-negative rate (15%–40%) [45–49] and the concrete risk of underdetection [1, 9–12, 50]. Furthermore, the involvement of the thoracic aorta or its main branches, which is present in more than 45% of newly diagnosed patients with GCA, is associated with a negative TAB in 50% of reported cases [20, 51–54]. 18F-FDG PET is a noninvasive, whole-body technique that is able to detect vascular involvement in GCA patients, with or without PMR symptoms [25, 26]. Other imaging techniques (i.e., DUS, Doppler ultrasonography, CT, and MRI) have been proposed for the assessment of vascular inflammation in GCA patients. However, while they are able to demonstrate anatomical changes in the affected vessels (mural thickening, dilatation and aneurysms, and enhancement of perivascular connective tissue) if the inflammatory process is well established, they are not sensitive enough to diagnose early inflammatory changes which are potentially reversible [28]. Furthermore, patient follow-up and the assessment of response to medical treatment are not easy to perform on the basis of morphological information alone [27, 28].

DUS of temporal arteries has emerged as a useful alternative tool when temporal biopsy cannot be performed [52], but this technique is not able to demonstrate the involvement of thoracic vessels. 18F-FDG may be particularly helpful in patients with inconclusive TAB and/or DUS results [55, 56].

From the results of our review, we found that qualitative analysis of 18F-FDG uptake is the most widely adopted method for assessing the presence and grading the activity of GCA-related vascular inflammation on 18F-FDG PET scans (13 out of 19 original papers). Qualitative analysis has been used both to perform dichotomous assessment (i.e., confirm or rule out the presence of vascular inflammation) [28–31, 34, 35, 37, 39] and to grade the severity of vascular involvement according to ordinal scales, with the 18F-FDG uptake of the vessel wall being visually analyzed or compared with that of a reference structure [25–27, 32, 34, 36]. Among visual grading systems, the vessel-to-liver ratio is the most frequently used. With regard to diagnostic performance, a previous systematic meta-analysis compared different qualitative and semiquantitative methods for assessing vasculitis on 18F-FDG PET, reporting a pooled sensitivity and a specificity of 80% and 89%, respectively [51].

The strength of qualitative methods, in addition to being more immediate and less time-consuming than semiquantitative ones, lies in their high specificity and small number of false positives, while sensitivity ranges from 56% to 77%. Moreover, qualitative methods display high interobserver agreement and intraobserver reproducibility (90% and 93.3%, resp.) [32]. By contrast, most authors [24, 26, 28, 41, 42, 57–60] have reported that when qualitative methods are applied, the diagnostic discrimination between vasculitis and atherosclerosis may be a critical issue.

However, there is a general consensus that 18F-FDG vascular uptake in vasculitis should be higher than in atherosclerosis. For these reasons, mild vascular 18F-FDG uptake, lower than or equal to that of the liver (i.e., grades 1 and 2 according to scoring systems that use the liver as a reference structure), is not indicative of GCA inflammatory involvement. The site of tracer accumulation and its changes in response to medical treatment have also been considered to distinguish large vessel vasculitis from atherosclerosis [60].

A complementary contrast-enhanced CT acquired immediately after 18F-FDG PET/CT may provide additional information on the morphology of the affected vessels and the presence of calcifications within the arterial wall [34]. The metabolic information obtained from 18F-FDG PET, combined with the demonstration of wall enhancement and thickness assessed by contrast-enhanced CT, could constitute an effective approach to the evaluation of extracranial GCA, thereby enabling a better differentiation between GCA- and atherosclerosis-related 18F-FDG vascular uptake.

With regard to the semiquantitative methods, some authors have proposed the evaluation of arterial SUVmax [24, 34, 37], while others have normalized arterial SUVmax

to the background activity, represented by the mean uptake value of a selected reference structure [29, 35, 41].

On comparing a SUVmax-based approach without normalization with visual qualitative analysis, Lehmann et al. [37] found high sensitivity (90% versus 65%) and low specificity (45% versus 80%) when a cut-off value of 1.78 was used. By contrast, Besson et al. [41] and Prieto-González et al. [24] found that SUVmax cut-off values obtained without normalization were population-specific and could not be applied to the general population.

From the results of our analysis, we observed that semiquantitative methods normalized to the background activity seem to outperform qualitative approaches and semiquantitative methods without normalization. We also noticed that the power of discrimination between GCA and control groups also depends on the anatomical structure chosen to represent the background uptake.

Besson et al. showed some limitations in the use of the liver as the background for normalization in GCA [41]. In particular, they found that the liver SUVmax differed significantly between patients and controls and that the liver SUVmax values in the GCA group were significantly higher than in the control group. Indeed, systemic inflammation affects liver metabolism and can influence the calculation of liver uptake values.

According to the results of our study, an interesting semiquantitative approach is the arterial-to-background ratio proposed by Moosig et al. [29]. These authors adopted a two-step procedure for assessing their patients. Initially, they applied a dichotomous qualitative method in order to identify positive cases; they then adopted a semiquantitative method, normalizing vascular 18F-FDG uptake to the lung. Indeed, the background activity of the lung displays low inter- and intrapatient variability owing to the low physiological uptake of 18F-FDG. Using this two-step procedure, Moosig et al. obtained maximal diagnostic performance values (i.e., both sensitivity and specificity of 100%) higher than those yielded by both qualitative and semiquantitative methods. Besson et al. [41] normalized vascular 18F-FDG uptake to the lung by means of a semiquantitative method similar to that of Moosig et al. and confirmed that the lung SUVmax values did not differ significantly between patients and controls. On the other hand, without performing the two-step combined procedure of Moosig et al. [29], Besson et al. [41] found lower values of sensitivity and specificity (81.8 and 72.7%, resp.).

Among all the semiquantitative methods for the assessment of 18F-FDG PET in GCA, the aortic-to-blood pool uptake ratio seems to outperform the other methods when liver and lung are used as reference structures for determining the background uptake.

This approach, tested by Rudd et al. in atherosclerosis to evaluate arterial wall inflammation, has proved to be robust and highly reproducible [57]. Rudd et al. normalized the arterial SUVmax values to blood pool activity, represented by the mean of 8 ROIs drawn in venous vessels (i.e., the inferior vena cava or the internal jugular vein). Besson et al. adapted this method in order to assess PET examinations of 11 GCA patients and 11 controls matched for age and sex and found high diagnostic sensitivity (81.8%) and specificity (91%).

5. Conclusion

In conclusion, 18F-FDG PET has been shown to have an important role in the diagnosis of extracranial vascular involvement in patients with GCA/PMR.

Qualitative methods are more specific than semiquantitative ones, but they have lower sensitivity. The aortic-to-blood pool uptake ratio is a promising semiquantitative method of analysis for the detection and grading of arterial inflammation. The normalization of the arterial wall uptake to the background activity of venous blood pool provides a good reference to assess vascular inflammation. Further prospective studies involving larger cohorts of GCA/PMR patients are required to better define the role of aortic-to-blood pool ratio as a reference method for the assessment of vasculitis in GCA patients.

Conflict of Interests

The authors declare that there is no conflict of interests regarding the publication of this paper.

References

[1] C. Salvarani, F. Cantini, L. Boiardi, and G. G. Hunder, "Polymyalgia rheumatica and giant-cell arteritis," *New England Journal of Medicine*, vol. 347, no. 4, pp. 261–271, 2002.

[2] M. A. Gonzalez-Gay, C. Garcia-Porrua, J. A. Miranda-Filloy, and J. Martin, "Giant cell arteritis and polymyalgia rheumatica: pathophysiology and management," *Drugs and Aging*, vol. 23, no. 8, pp. 627–649, 2006.

[3] D. M. Nuenninghoff, G. G. Hunder, T. J. H. Christianson, R. L. McClelland, and E. L. Matteson, "Incidence and predictors of large-artery complication (aortic aneurysm, aortic dissection, and/or large-artery stenosis) in patients with giant cell arteritis: a population-based study over 50 years," *Arthritis and Rheumatism*, vol. 48, no. 12, pp. 3522–3531, 2003.

[4] J. M. Evans, W. M. O'Fallon, and G. G. Hunder, "Increased incidence of aortic aneurysm and dissection in giant cell (temporal) arteritis: a population-based study," *Annals of Internal Medicine*, vol. 122, no. 7, pp. 502–507, 1995.

[5] T. Bongartz and E. L. Matteson, "Large-vessel involvement in giant cell arteritis," *Current Opinion in Rheumatology*, vol. 18, no. 1, pp. 10–17, 2006.

[6] S. Barber, "Myalgic syndrome with constitutional effects," *Annals of the Rheumatic Diseases*, vol. 16, pp. 230–237, 1957.

[7] J. M. Evans and G. G. Hunder, "Giant cell arteritis, temporal arteritis, and polymyalgia rheumatica in a Danish county. A prospective investigation, 1982–1985," *Arthritis and Rheumatism*, vol. 30, no. 3, pp. 294–299, 1987.

[8] C. Schaufelberger, B.-A. Bengtsson, and R. Andersson, "Epidemiology and mortality in 220 patients with polymyalgia rheumatica," *British Journal of Rheumatology*, vol. 34, no. 3, pp. 261–264, 1995.

[9] P. Elling, A. T. Olsson, and H. Elling, "Synchronous variations of the incidence of temporal arteritis and polymyalgia rheumatica in different regions of Denmark; association with epidemics of Mycoplasma pneumoniae infection," *Journal of Rheumatology*, vol. 23, no. 1, pp. 112–119, 1996.

[10] F. Cantini, L. Niccoli, L. Storri et al., "Are polymyalgia rheumatic and giant cell arteritis the same disease?" *Seminars in Arthritis and Rheumatism*, vol. 33, no. 5, pp. 294–301, 2004.

[11] C. Salvarani, C. S. Crowson, W. M. O'Fallon, G. G. Hunder, and S. E. Gabriel, "Reappraisal of the epidemiology of giant cell arteritis in Olmsted County, Minnesota, over a fifty-year period," *Arthritis Care and Research*, vol. 51, no. 2, pp. 264–268, 2004.

[12] E. Nordborg and C. Nordborg, "Giant cell arteritis: epidemiological clues to its pathogenesis and an update on its treatment," *Rheumatology*, vol. 42, no. 3, pp. 413–421, 2003.

[13] J. T. Gran and G. Myklebust, "The incidence of polymyalgia rheumatica and temporal arteritis in the county of Aust Agder, South Norway: a prospective study 1987–94," *The Journal of Rheumatology*, vol. 24, no. 9, pp. 1739–1743, 1997.

[14] P. Franzen, S. Sutinen, and J. von Knorring, "Giant cell arteritis and polymyalgia rheumatica in a region of Finland: an epidemiologic, clinical and pathologic study, 1984–1988," *Journal of Rheumatology*, vol. 19, no. 2, pp. 273–280, 1992.

[15] C. Salvarani, L. Boiardi, V. Mantovani et al., "HLA-DRB1 alleles associated with polymyalgia rheumatica in northern Italy: correlation with disease severity," *Annals of the Rheumatic Diseases*, vol. 58, no. 5, pp. 303–308, 1999.

[16] M. A. González-Gay, M. M. Amoli, C. Garcia-Porrua, and W. E. R. Ollier, "Genetic markers of disease susceptibility and severity in giant cell arteritis and polymyalgia rheumatica," *Seminars in Arthritis and Rheumatism*, vol. 33, no. 1, pp. 38–48, 2003.

[17] M. Bas-Lando, G. S. Breuer, Y. Berkun, M. Mates, M. Sonnenblick, and G. Nesher, "The incidence of giant cell arteritis in Jerusalem over a 25-year period: annual and seasonal fluctuations," *Clinical and Experimental Rheumatology*, vol. 25, supplement 44, no. 1, pp. S15–S17, 2007.

[18] P. Duhaut, S. Bosshard, and J.-P. Ducroix, "Is giant cell arteritis an infectious disease? Biological and epidemiological evidence," *Presse Medicale*, vol. 33, no. 19, pp. 1403–1408, 2004.

[19] C. Salvarani, F. Cantini, and G. G. Hunder, "Polymyalgia rheumatica and giant-cell arteritis," *The Lancet*, vol. 372, no. 9634, pp. 234–245, 2008.

[20] M. A. Gonzalez-Gay, C. Garcia-Porrua, A. Piñeiro, R. Pego-Reigosa, J. Llorca, and G. G. Hunder, "Aortic aneurysm and dissection in patients with biopsy-proven giant cell arteritis from Northwestern Spain: a population-based study," *Medicine*, vol. 83, no. 6, pp. 335–341, 2004.

[21] D. Blockmans, L. de Ceuninck, S. Vanderschueren, D. Knockaert, L. Mortelmans, and H. Bobbaers, "Repetitive 18F-fluorodeoxyglucose positron emission tomography in giant cell arteritis: a prospective study of 35 patients," *Arthritis Care and Research*, vol. 55, no. 1, pp. 131–137, 2006.

[22] S. Prieto-González, P. Arguis, A. García-Martínez et al., "Large vessel involvement in biopsy-proven giant cell arteritis: prospective study in 40 newly diagnosed patients using CT angiography," *Annals of the Rheumatic Diseases*, vol. 71, no. 7, pp. 1170–1176, 2012.

[23] M. Aschwanden, F. Kesten, M. Stern et al., "Vascular involvement in patients with giant cell arteritis determined by duplex sonography of 2x11 arterial regions," *Annals of the Rheumatic Diseases*, vol. 69, no. 7, pp. 1356–1359, 2010.

[24] S. Prieto-González, M. Depetris, A. García-Martínez et al., "Positron emission tomography assessment of large vessel inflammation in patients with newly diagnosed, biopsy-proven giant cell arteritis: a prospective, case-control study," *Annals of the Rheumatic Diseases*, vol. 73, no. 7, pp. 1388–1392, 2014.

[25] D. Blockmans, A. Maes, S. Stroobants et al., "New arguments for a vasculitic nature of polymyalgia rheumatica using positron emission tomography," *Rheumatology*, vol. 38, no. 5, pp. 444–447, 1999.

[26] D. Blockmans, S. Stroobants, A. Maes, and L. Mortelmans, "Positron emission tomography in giant cell arteritis and polymyalgia rheumatica: evidence for inflammation of the aortic arch," *The American Journal of Medicine*, vol. 108, no. 3, pp. 246–249, 2000.

[27] J. Meller, F. Strutz, U. Siefker et al., "Early diagnosis and follow-up of aortitis with [^{18}F]FDG PET and MRI," *European Journal of Nuclear Medicine and Molecular Imaging*, vol. 30, no. 5, pp. 730–736, 2003.

[28] C. P. Bleeker-Rovers, S. J. H. Bredie, J. W. M. van der Meer, F. H. M. Corstens, and W. J. G. Oyen, "F-I8-fluorodeoxyglucose positron emmission tomography in diagnosis and follow-up of patients with different types of vasculitis," *Netherlands Journal of Medicine*, vol. 61, no. 10, pp. 323–329, 2003.

[29] F. Moosig, N. Czech, C. Mehl et al., "Correlation between 18-fluorodeoxyglucose accumulation in large vessels and serological markers of inflammation in polymyalgia rheumatica: a quantitative PET study," *Annals of the Rheumatic Diseases*, vol. 63, no. 7, pp. 870–873, 2004.

[30] M. Brodmann, R. W. Lipp, A. Passath, G. Seinost, E. Pabst, and E. Pilger, "The role of 2-18F-fluoro-2-deoxy-D-glucose positron emission tomography in the diagnosis of giant cell arteritis of the temporal arteries," *Rheumatology*, vol. 43, no. 2, pp. 241–242, 2004.

[31] A. K. Scheel, J. Meller, R. Vosshenrich et al., "Diagnosis and follow up of aortitis in the elderly," *Annals of the Rheumatic Diseases*, vol. 63, no. 11, pp. 1507–1510, 2004.

[32] M. A. Walter, R. A. Melzer, C. Schindler, J. Müller-Brand, A. Tyndall, and E. U. Nitzsche, "The value of [18F]FDG-PET in the diagnosis of large-vessel vasculitis and the assessment of activity and extent of disease," *European Journal of Nuclear Medicine and Molecular Imaging*, vol. 32, no. 6, pp. 674–681, 2005.

[33] D. Blockmans, L. de Ceuninck, S. Vanderschueren, D. Knockaert, L. Mortelmans, and H. Bobbaers, "Repetitive 18-fluorodeoxyglucose positron emission tomography in isolated polymyalgia rheumatica: a prospective study in 35 patients," *Rheumatology*, vol. 46, no. 4, pp. 672–677, 2007.

[34] J. C. Henes, M. Müller, J. Krieger et al., "[18F] FDG-PET/CT as a new and sensitive imaging method for the diagnosis of large-vessel vasculitis," *Clinical and Experimental Rheumatology*, vol. 26, supplement 49, no. 3, pp. S47–S52, 2008.

[35] H. Hautzel, O. Sander, A. Heinzel, M. Schneider, and H. Müller, "Assessment of large-vessel involvement in giant cell arteritis with 18F-FDG PET: introducing an ROC-analysis-based cutoff ratio," *Journal of Nuclear Medicine*, vol. 49, no. 7, pp. 1107–1113, 2008.

[36] M. Both, K. Ahmadi-Simab, M. Reuter et al., "MRI and FDG-PET in the assessment of inflammatory aortic arch syndrome in complicated courses of giant cell arteritis," *Annals of the Rheumatic Diseases*, vol. 67, no. 7, pp. 1030–1033, 2008.

[37] P. Lehmann, S. Buchtala, N. Achajew et al., "18F-FDG PET as a diagnostic procedure in large vessel vasculitis-a controlled, blinded re-examination of routine PET scans," *Clinical Rheumatology*, vol. 30, no. 1, pp. 37–42, 2011.

[38] J. C. Henes, M. Mueller, C. Pfannenberg, L. Kanz, and I. Koetter, "Cyclophosphamide for large vessel vasculitis: assessment of response by PET/CT," *Clinical and Experimental Rheumatology*, vol. 29, no. 1, supplement 64, pp. S43–S48, 2011.

[39] G. A. Hooisma, H. Balink, P. M. Houtman, R. H. J. A. Slart, and K. D. F. Lensen, "Parameters related to a positive test result for FDG PET(/CT) for large vessel vasculitis: a multicenter retrospective study," *Clinical Rheumatology*, vol. 31, no. 5, pp. 861–871, 2012.

[40] H. Yamashita, K. Kubota, Y. Takahashi et al., "Whole-body fluorodeoxyglucose positron emission tomography/ computed tomography in patients with active polymyalgia rheumatica: evidence for distinctive bursitis and large-vessel vasculitis," *Modern Rheumatology*, vol. 22, no. 5, pp. 705–711, 2012.

[41] F. L. Besson, H. de Boysson, J. Parienti, G. Bouvard, B. Bienvenu, and D. Agostini, "Towards an optimal semiquantitative approach in giant cell arteritis: an ^{18}F-FDG PET/CT case-control study," *European Journal of Nuclear Medicine and Molecular Imaging*, vol. 41, no. 1, pp. 155–166, 2013.

[42] M. Tatsumi, C. Cohade, Y. Nakamoto, and R. L. Wahl, "Fluorodeoxyglucose uptake in the aortic wall at PET/CT: possible finding for active atherosclerosis," *Radiology*, vol. 229, no. 3, pp. 831–837, 2003.

[43] G. G. Hunder, D. A. Bloch, B. A. Michel et al., "The American College of Rheumatology 1990 criteria for the classification of giant cell arteritis," *Arthritis and Rheumatism*, vol. 33, no. 8, pp. 1122–1128, 1990.

[44] D. M. Nuenninghoff, G. G. Hunder, T. J. H. Christianson, R. L. McClelland, and E. L. Matteson, "Incidence and predictors of aortic aneurysm, aortic dissection and large artery stenosis in patients with giant cell arteritis in Olmsted county, MN, over a 50- year period," *Arthritis & Rheumatology*, vol. 46, supplement 9, p. S183, 2002.

[45] E. W. T. Chong and A. J. Robertson, "Is temporal artery biopsy a worthwhile procedure?" *ANZ Journal of Surgery*, vol. 75, no. 6, pp. 388–391, 2005.

[46] R. Taylor-Gjevre, M. Vo, D. Shukla, and L. Resch, "Temporal artery biopsy for giant cell arteritis," *Journal of Rheumatology*, vol. 32, no. 7, pp. 1279–1282, 2005.

[47] A. M. Roth, L. Milsow, and J. L. Keltner, "The ultimate diagnoses of patients undergoing temporal artery biopsies," *Archives of Ophthalmology*, vol. 102, no. 6, pp. 901–903, 1984.

[48] M. A. Gonzalez-Gay, C. Garcia-Porrua, J. Llorca, C. Gonzalez-Louzao, and P. Rodriguez-Ledo, "Biopsy-negative giant cell arteritis: clinical spectrum and predictive factors for positive temporal artery biopsy," *Seminars in Arthritis and Rheumatism*, vol. 30, no. 4, pp. 249–256, 2001.

[49] S. Hall, S. Persellin, J. T. Lie, P. C. O'Brien, L. T. Kurland, and G. G. Hunder, "The therapeutic impact of temporal artery biopsy," *The Lancet*, vol. 2, no. 8361, pp. 1217–1220, 1983.

[50] R. C. Brooks and S. R. McGee, "Diagnostic dilemmas in polymyalgia rheumatica," *Archives of Internal Medicine*, vol. 157, no. 2, pp. 162–168, 1997.

[51] F. L. Besson, J. Parienti, B. Bienvenu et al., "Diagnostic performance of 18F-fluorodeoxyglucose positron emission tomography in giant cell arteritis: a systematic review and meta-analysis," *European Journal of Nuclear Medicine and Molecular Imaging*, vol. 38, no. 9, pp. 1764–1772, 2011.

[52] W. A. Schmidt, A. Seifert, E. Gromnica-ihle, A. Krause, and A. Natusch, "Ultrasound of proximal upper extremity arteries to increase the diagnostic yield in large-vessel giant cell arteritis," *Rheumatology*, vol. 47, no. 1, pp. 96–101, 2008.

[53] C. Agard, J. Barrier, B. Dupas et al., "Aortic involvement in recent-onset giant cell (temporal) arteritis: a case-control prospective study using helical aortic computed tomodensitometric scan," *Arthritis Care and Research*, vol. 59, no. 5, pp. 670–676, 2008.

[54] A. Brack, V. Martinez-Taboada, A. Stanson, J. J. Goronzy, and C. M. Weyand, "Disease pattern in cranial and large-vessel giant cell arteritis," *Arthritis & Rheumatology*, vol. 42, pp. 311–317, 1999.

[55] M. A. Cimmino, D. Camellino, F. Paparo et al., "High frequency of capsular knee involvement in polymyalgia rheumatica /giant cell arteritis patients studied by positron emission tomography," *Rheumatology*, vol. 52, no. 10, pp. 1865–1872, 2013.

[56] F. Jamar, J. Buscombe, A. Chiti et al., "EANM/SNMMI guideline for ^{18}F-FDG use in inflammation and infection," *Journal of Nuclear Medicine*, vol. 54, no. 4, pp. 647–658, 2013.

[57] J. H. F. Rudd, K. S. Myers, S. Bansilal et al., "Atherosclerosis inflammation imaging with ^{18}F-FDG PET: carotid, iliac, and femoral uptake reproducibility, quantification methods, and recommendations," *Journal of Nuclear Medicine*, vol. 49, no. 6, pp. 871–878, 2008.

[58] M. P. S. Dunphy, A. Freiman, S. M. Larson, and H. W. Strauss, "Association of vascular 18F-FDG uptake with vascular calcification," *Journal of Nuclear Medicine*, vol. 46, no. 8, pp. 1278–1284, 2005.

[59] M. Yun, S. Jang, A. Cucchiara, A. B. Newberg, and A. Alavi, "18F FDG uptake in the large arteries: a correlation study with the atherogenic risk factors," *Seminars in Nuclear Medicine*, vol. 32, no. 1, pp. 70–76, 2002.

[60] T. Belhocine, D. Blockmans, R. Hustinx, J. Vandevivere, and L. Mortelmans, "Imaging of large vessel vasculitis with 18FDG PET: illusion or reality? A critical review of the literature data," *European Journal of Nuclear Medicine and Molecular Imaging*, vol. 30, no. 9, pp. 1305–1313, 2003.

Hindawi Publishing Corporation
BioMed Research International
Volume 2014, Article ID 897956, 15 pages
http://dx.doi.org/10.1155/2014/897956

Review Article

Assessment of Cardiac Sarcoidosis with Advanced Imaging Modalities

Makoto Orii, Toshio Imanishi, and Takashi Akasaka

Department of Cardiovascular Medicine, Wakayama Medical University, 811-1 Kimiidera, Wakayama 641-8510, Japan

Correspondence should be addressed to Toshio Imanishi; t-imani@wakayama-med.ac.jp

Received 5 June 2014; Revised 6 August 2014; Accepted 11 August 2014; Published 28 August 2014

Academic Editor: Andor Glaudemans

Sarcoidosis is a chronic systemic disease of unknown etiology that is characterized by the presence of noncaseating epithelioid granulomas, usually in multiple organs. Several studies have shown that sarcoidosis might be the result of an exaggerated granulomatous reaction after exposure to unidentified antigens in genetically susceptible individuals. Cardiac involvement may occur and lead to an adverse outcome: the heart mechanics will be affected and that causes ventricular failure, and the cardiac electrical system will be disrupted and lead to third degree atrioventricular block, malignant ventricular tachycardia, and sudden cardiac death. Thus, early diagnosis and treatment of this potentially devastating disease is critically important. However, sensitive and accurate imaging modalities have not been established. Recent studies have demonstrated the promising potential of cardiac magnetic resonance imaging (MRI) and ^{18}F-fluoro-2-deoxyglucose positron emission tomography (^{18}F-FDG PET) in the diagnosis and assessment of cardiac sarcoidosis (CS). In this review, we discuss the epidemiology, etiology, histological findings, and clinical features of sarcoidosis. We also introduce advanced imaging including ^{18}F-FDG PET and cardiac MRI as more reliable diagnostic modalities for CS.

1. Introduction

Sarcoidosis was first reported more than 120 years ago. It is a granulomatous inflammatory disease with an unclear etiology that affects multiple organs including the lungs, heart, skin, central nervous system, and eyes [1]. Although it is not commonly fatal, cardiac involvement may be responsible for more than two-thirds of deaths [2]. The clinical diagnosis of cardiac sarcoidosis (CS) is therefore critically important to the timely planning of therapeutic strategies.

Despite extensive research, the etiology of sarcoidosis has not been elucidated, although most evidence points to an aberrant immune response as the pathogenetic mechanism, which is driven by an unidentified antigen in genetically susceptible individuals. Although multiple candidate etiologic agents including microbial organisms and environmental agents have been identified, the results are inconclusive thus far.

Once the diagnosis of sarcoidosis is made, management may range from observation to long-term administration of steroids (often at high doses) or other immunosuppressive therapies, depending on disease severity and organ involvement [3]. Although immunosuppressive therapy may be required for CS, reliable biomarkers and effective imaging modalities have not been established for it. The diagnosis of CS is further hindered by the lack of any reliable and specific diagnostic test, as there are no imaging findings that allow for a definitive diagnosis of CS.

2. Epidemiology

Sarcoidosis is a systemic disease with a prevalence of about 4.7–64 in 100 000 and an incidence of 1.0–35.5 in 100 000 per year. The highest rates are reported in northern European and African-American individuals, particularly in women, and the lower rate is reported in Japan [4, 5]. Differences in prevalence and incidence are linked to age, sex, ethnic origin, and geographical location. The disease can occur in both sexes, with a female to male ratio of 1 : 1.46. Seventy percent of patients are aged 25–45 years, although a second incidence peak occurs in women older than 50 years in Europe and

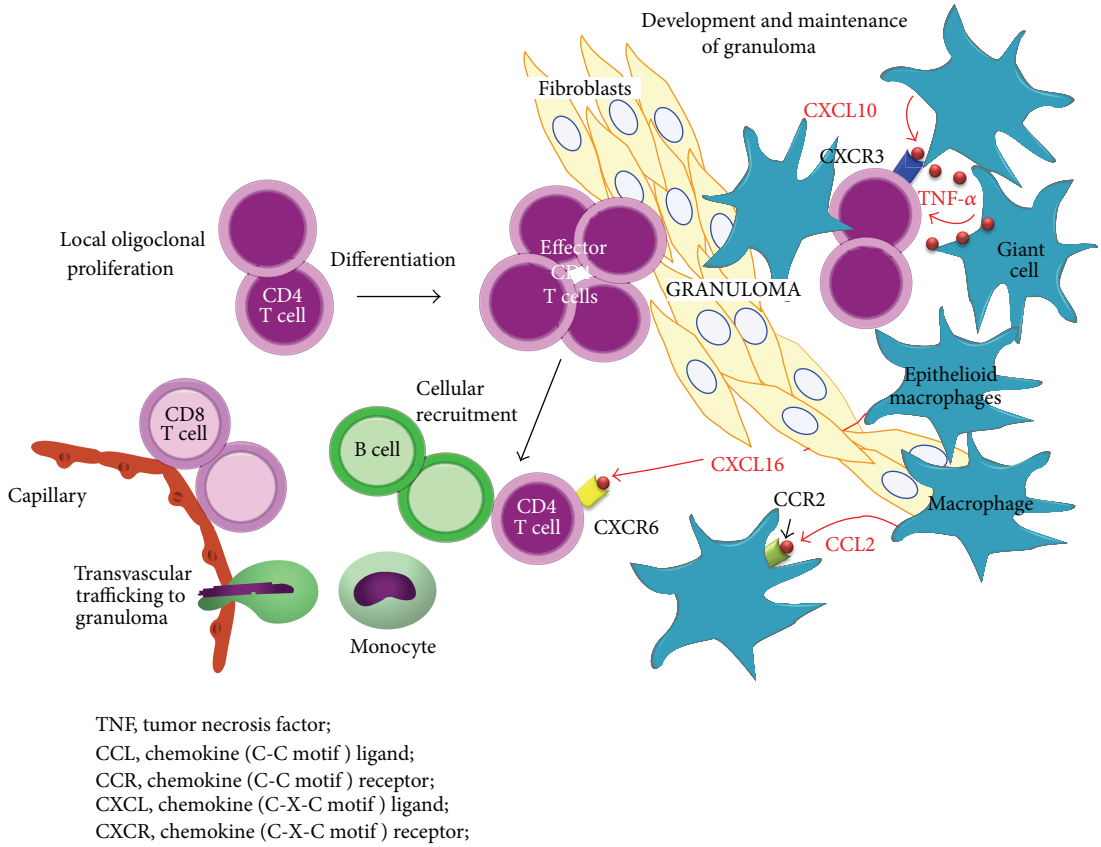

Figure 1: Recruitment of inflammatory cells and granuloma formation. Release of type 1 helper T (Th1) cytokines or chemokines promotes cellular accumulation and nidus formation, resulting in granuloma. Activated macrophages increase the expression of co-stimulatory molecules; released chemokines such as CXCL10 attract additional T cells with a CD4/Th1 phenotype.

Japan [4, 5]. The clinical expression of sarcoidosis is affected by epidemiological and socioeconomic factors. Elderly-onset sarcoidosis is much more common in women and shows higher rates of change in general health and extrapulmonary manifestations [6]. Sarcoidosis is usually sporadic, but is familial in 3.6–9.6% of cases [7]. Siblings have a higher risk of sarcoidosis than do parents, suggesting a recessive made of inheritance with incomplete penetrance [7]. An 80-fold increase in risk in monozygotic twins lends support to the notion that genetic factors might account for two-thirds of disease susceptibility [8].

3. Etiology

The exact etiology of sarcoidosis remains unknown. Many studies suggest that genetic susceptibility and environmental factors contribute to disease development [9–11]. Immunologically, sarcoidosis is an exaggerated immune response to as yet unknown antigens. Data on the clinical heterogeneity of sarcoidosis strongly suggest that the pathogen-associated molecular patterns of microbial antigens can trigger or amplify inflammation. There is no evidence that sarcoidosis is an infectious disease; rather, it is likely to be an exaggerated immune response to the pathogen-associated molecular patterns of killed and partly degraded mycobacteria and propionibacteria. Other organic and inorganic substances might also trigger sarcoidosis [12]. Mycobacteria and propionibacteria persist in macrophage phagosomes because the high lipid contents in their membranes make them acid-fast, and many of their glycolipoproteins are not very soluble and resist degradation.

4. Histologic Findings in Sarcoidosis (Granuloma Formation)

The histologic hallmark of sarcoidosis, irrespective of organ involvement, is noncaseating epithelioid granulomas. Granulomas typically consist of a compact central area of macrophages that differentiate into epithelioid cells and then fuse to form multinucleated giant cells surrounded by lymphocytes (Figure 1) [3]. These cells become the primary sources for angiotensin-converting enzyme (ACE). Lymphocytes scattered within granulomas tend to be CD4+ T helper cells, while those around the periphery are CD8+ T cells and to a lesser extent B cells (Figure 1).

There is generally minimal necrosis within sarcoid granulomas, unlike those associated with *Mycobacterium tuberculosis* infection [13]. Granulomas in sarcoidosis are thought to form around and isolate poorly degraded antigens as a means of preventing antigen dissemination and further tissue

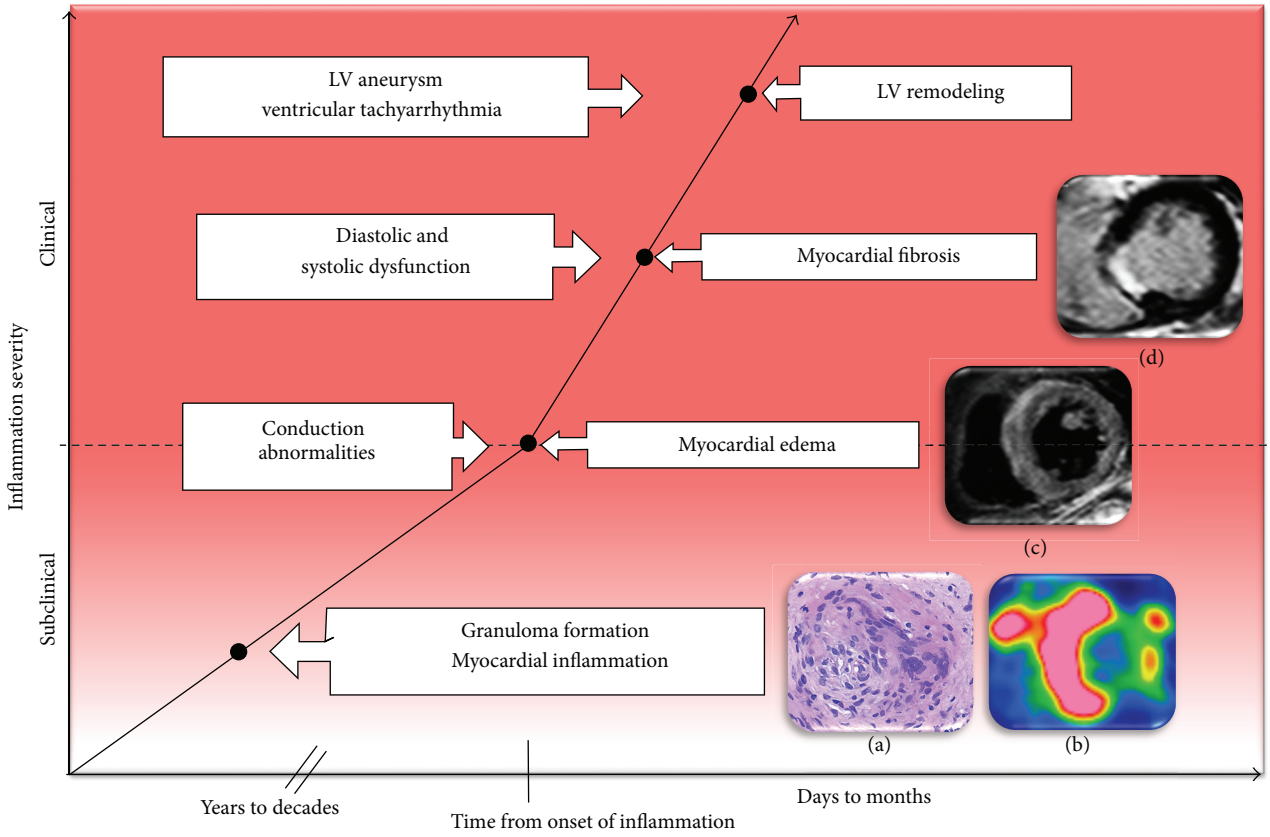

FIGURE 2: Imaging and inflammation cascade. In this schematic representation of disease progression, the infection point is represented by inflammation, edema, and fibrosis. Granuloma formation (a), ^{18}F-FDG PET of myocardial inflammation (b), cardiac magnetic resonance imaging of myocardial edema (c), and cardiac magnetic resonance imaging of myocardial fibrosis (d) are shown. ^{18}F-FDG PET: ^{18}F-fluorodeoxyglucose positron emission tomography.

damage. Why sarcoidosis spontaneously resolves in some patients and progresses in others is still poorly understood. With respect to progressive disease, it has been postulated that the antigen persists, thereby inducing a chronic immune response [14, 15]. Importantly, the detection of granulomas alone is not specific enough to diagnose sarcoidosis, especially noncaseating granulomas that are rarely found by subendomyocardial biopsy in CS [16]. Sarcoidosis is conventionally diagnosed by the appropriate combination of clinical, physiologic, and multimodality imaging. Histological findings of granuloma mainly serve to support, not definitively confirm, the diagnosis of sarcoidosis and exclude other potential etiologies from the differential diagnosis.

5. Manifestations

The incidence of CS varies by ethnic group and depends on the type of study performed. Studies based on clinical findings in known sarcoid patients are likely given a prevalence of cardiac involvement in 5% to 10% of affected patients [17]. An excellent American autopsy series published in 1978 showed that 27% of 84 autopsied patients with a diagnosis of sarcoidosis had CS, two-thirds of whom had clinically significant cardiac disease [18]. Although myocardial fibrosis is nonspecific, it can sometimes be the only manifestation of CS. This series did not consider myocardial fibrosis as evidence of cardiac involvement, so it likely underestimated the true prevalence of CS. A recent American study investigated 62 outpatients with documented sarcoidosis and no documented CS. They asked about cardiac symptoms and performed noninvasive tests (simple electrocardiography [ECG], Holter monitoring, and transthoracic echocardiography). Any patient who reported symptoms or had an abnormal study was sent for advanced imaging including cardiac magnetic resonance imaging (MRI) or ^{18}F-fluoro-2-deoxyglucose positron emission tomography (^{18}F-FDG PET). The results showed that almost 40% of outpatients with documented sarcoid had CS. Of these, slightly more than half were asymptomatic [19]. CS is most common among older, female Japanese sarcoid patients, with a reported rate of cardiac involvement of almost 80% [20].

CS can affect any part of the heart and its conduction system. The most frequently involved area is the ventricular septum (31.5%), followed by the inferior wall, anterior left ventricle, right ventricle, and lateral left ventricle [21]. Sarcoid granulomas and subsequent fibrosis may induce complete atrioventricular (AV) block, systolic and diastolic dysfunction, and ventricular tachycardia (VT) (Figure 2) [22–27].

Patients may present with syncope, heart failure, or sudden death. Because CS often occurs in the absence of apparent disease elsewhere, sarcoidosis should be considered in any nonischemic form of cardiomyopathy, particularly when rhythm disturbances are prominent.

A precise and early diagnosis would be needed to introduce effective anti-inflammatory therapy that could prevent an adverse outcome [19, 28]. However, the lack of gold standard in the diagnosis of CS remains a major problem.

6. Japanese Guidelines for the Diagnosis of CS

Clinical guidelines for the diagnosis of CS were first published by the Japanese Ministry of Health and Welfare (JMHW) in 1993 and they have been used most commonly in the diagnosis of CS and as the reference for comparison of various imaging techniques [29]. Electrophysiological studies should be used to evaluate patients with syncope or significant ECG abnormalities, but their sensitivity and ability to stratify patients by risk are poorly defined. A normal electrophysiological study at any one point does not predict future granulomatous infiltration and fibrosis in critical regions. This means that advanced imaging modalities such as cardiac MRI and ^{18}F-FDG PET are needed to assess disease activity and management. In 2006, the Joint Committee of the Japan Society of Sarcoidosis and Other Granulomatous Disorders and the Japanese College of Cardiology published a revised version of the guidelines, in which delayed enhancement (DE) in cardiac MRI was added as a minor criterion for the clinical diagnosis as shown in the following list [30, 31].

Japanese Ministry of Health and Welfare Criteria for Cardiac Sarcoidosis

Major Criteria

(a) Advanced atrioventricular block.

(b) Basal thinning of the interventricular septum.

(c) Positive 67 gallium uptake in the heart.

(d) Depressed ejection fraction of the left ventricle (50%).

Minor Criteria

(a) Abnormal ECG findings: ventricular arrhythmias (ventricular tachycardia, multifocal or frequent PVCs), CRBBB, axis deviation or abnormal Q-wave.

(b) Abnormal echocardiography: regional abnormal wall motion or morphological abnormality (ventricular aneurysm, wall thickening).

(c) Nuclear medicine: perfusion defect detected by 201 thallium or 99 m technetium myocardial scintigraphy.

(d) Gadolinium-enhanced CMR imaging: delayed enhancement of myocardium.

(e) Endomyocardial biopsy: interstitial fibrosis or monocyte infiltration over moderate grade.

CMR: cardiac magnetic resonance, CRBBB: complete right bundle branch block, ECG: electrocardiogram, and PVC: premature ventricular contraction.

(1) Two or more of the four major criteria are satisfied.

(2) One in two of the major criteria and two or more of the five minor criteria are satisfied.

Abnormal cardiac accumulation on ^{18}F-FDG PET was not added to the diagnostic criteria but was included in the additional statements. Several imaging studies have been published on utilizing ^{18}F-FDG PET and cardiac MRI for the diagnosis of CS to date, but almost all of them were validated using JMHW's original guidelines [32–40]. Two recent studies did, however, examine the diagnostic accuracy of ^{18}F-FDG PET based on the revised guidelines (Table 1) [37, 40].

7. Cardiac MRI

Cardiac MRI has emerged as the gold standard for the diagnosis of cardiac involvement in sarcoidosis. Early enhancement of sarcoid granulomas in T2-weighted images suggests the presence of inflammation and edema, whereas DE indicates fibrotic changes and scarring [41, 42]. Commonly, the two phases overlap. Smedema et al. evaluated the diagnostic role of cardiac MRI in 58 patients with suspected CS and reported that DE showed favorable sensitivity and specificity of 100% and 78%, respectively [42]. Kim et al. compared the prognostic value of DE in cardiac MRI with JMHW's criteria in an asymptomatic cohort of 81 patients with biopsy-proven extra-cardiac sarcoidosis [43]. CS was detected in 26% of patients by DE on cardiac MRI, but only 12% fulfilled JMHW's criteria. DE was associated with adverse events and cardiac death. These results were confirmed by a more recent study, in which 155 patients with extra-cardiac sarcoidosis underwent cardiac MRI and had a follow-up of approximately 2.6 years [41]. In addition to reliably, detecting the disease, DE may also be useful for assessing the response to steroid therapy [44, 45]. Unfortunately, however, the test is not effective for patients with non-MRI compatible pacemakers and defibrillators, or those with renal dysfunction.

8. ^{18}F-FDG PET

^{18}F-FDG PET is a noninvasive molecular imaging technique that is highly sensitive to metabolically active processes. ^{18}F-FDG is taken up by living cells via cell membrane glucose transporters (GLUT) and is phosphorylated intracellularly by a hexokinase into ^{18}F-FDG-6-phosphate (^{18}F-FDG-6-P). ^{18}F-FDG-6-P cannot be metabolized further along the glycolytic pathway and therefore accumulates within cells in direct proportion to their metabolic activity, a phenomenon known as metabolic trapping. In oncology, the uptake of ^{18}F-FDG by tumor cells makes PET the gold-standard technique for investigating metastases [46, 47]. The use of this technique for imaging inflammation has also been proposed, partly because ^{18}F-FDG has been noted at sites of inflammation during routine ^{18}F-FDG PET imaging of cancer patients [48]. The identification of sites of inflammation is related to the glycolytic activity of cells involved in the inflammatory response. In inflammatory cells, especially neutrophils

Table 1: Sensitivity and specificity of ^{18}F-FDG PET in the diagnosis of CS.

Authors	Year	Subjects studied	JMHW guidelines	No. of patients (n)	Fasting time (h)	Sensitivity (%)	Specificity (%)	Comments
Yamagishi et al. [38]	2003	With CS	1993	17	>5	82	NA	First systemic research
Okumura et al. [34]	2004	With sarcoidosis	1993	22	>12	100	91	PET is more sensitive than ^{67}Ga scintigraphy
Ishimaru et al. [35]	2005	With sarcoidosis	1993	32	>6	100	82	Pre-administered heparin
Ohira et al. [32]	2008	With suspected CS	1993	21	>12	88	39	Comparing ^{18}F-FDG PET and MRI
Langah et al. [36]	2009	With suspected CS	1993	76	>18	85	90	PET CT with prolonged fasting >18 h
Tahara et al. [37]	2010	With suspected CS	2006	24	>12	100	46 → 97	Analysis using the COV improved specificity
Manabe et al. [39]	2013	With suspected CS	1993	67	>6	96	62	^{18}F-FDG uptake was related to ECG abnormalities
McArdle et al. [40]	2013	With suspected CS	2006	134	>12	100	83	With a high-fat, low-carbohydrate diet on the day before PET
Blankstein et al. [33]	2013	With suspected CS	1993	118	>3	71	45	With a high-fat, high protein, low-carbohydrate diet

CS: cardiac sarcoidosis, ^{18}F-FDG PET: ^{18}F-fluorodeoxyglucose positron emission tomography, JMHW: Japanese Ministry of Health and Welfare, COV: coefficient of variation.

and monocytes/macrophages, cellular activation increases GLUT1 and GLUT3 in the cell membrane and hexokinase over the levels in resting cells [49, 50].

Under aerobic conditions, most myocardial energy consumption is derived from oxidation of free fatty acids (FFAs), followed by glucose and, to a smaller extent, amino acids. In the myocardium with a low concentration of glucose-6-phosphatase, ^{18}F-FDG-6-P does not enter into further enzymatic pathway and accumulates intracellularly, proportional to the glycolytic rate of the cell.

9. ^{18}F-FDG PET in the Diagnosis of CS

Recent studies have demonstrated the promising potential of ^{18}F-FDG PET in the diagnosis and assessment of CS [32–40, 51–53]. Accumulation of ^{18}F-FDG is associated with an active inflammatory process in patients with CS [54, 55]. Gallium 67 (Ga-67) scintigraphy has long been used for the diagnosis of CS, but it is now being replaced by ^{18}F-FDG PET, mainly because of its low diagnostic sensitivity, which does not exceed 36% owing to low image resolution [34, 35, 38]; ^{18}F-FDG PET has a markedly higher sensitivity (71–100%) for diagnosing CS in comparison (Table 1). Advances continue to be made in PET/CT technology, and ^{18}F-FDG PET offers less exposure to radiation, quantitative analysis capability, and greater sensitivity for diagnosing CS than other radioisotope imaging modalities such as thallium-201 or technetium-99 m perfusion single photon emission CT [34, 35, 38]. Langah et al. also reported favorable sensitivity (85%) and specificity (90%) of ^{18}F-FDG/CT in patients with suspected CS [36] (Table 1), while a series of case reports have hinted at the promise value of ^{18}F-FDG in detecting cardiac sarcoid lesions [56, 57]. For example, Smedema et al. reported that increased ^{18}F-FDG uptake indicated active myocardial inflammation in the heart in a patient with biopsy-proven CS [56]. Similarly, Koiwa et al. demonstrated that ^{18}F-FDG uptake in the heart corresponded well with the pathologically confirmed sarcoid lesions in an autopsy case [57]. Two studies of the diagnostic accuracy of ^{18}F-FDG PET have been published and were based on the JMHW revised guidelines in 2006. Tahara et al. reported that they utilized visual and quantitative analysis using ^{18}F-FDG PET images [37]. Mc Ardle et al. reported the sensitivity and specificity for diagnosing CS as 100% and 83%, respectively, and that CS patients with VT displayed higher cardiac uptake of ^{18}F-FDG when compared with those with advanced AV block [51]. The specificity of ^{18}F-FDG in the detection of CS varies and is relatively low (39–97%) compared with its sensitivity (Table 1). Possible explanations for this include nonspecific myocardial uptake of ^{18}F-FDG in the normal heart [58, 59] and early-stage sarcoid lesions in the heart of patients who do not meet the diagnostic criteria for CS [60].

Cardiac assessment can be combined with whole-body imaging to determine the presence and activity of extracardiac sarcoidosis lesions (Figure 3).

10. Minimizing Physiological ^{18}F-FDG Uptake in the Normal Myocardium

The identification of sites of inflammation is related to the glycolytic activity of the cells involved in the inflammatory response. It is important to determine whether ^{18}F-FDG uptake in inflammatory lesions can be distinguished from physiological ^{18}F-FDG uptake in the myocardium. Although a focal uptake pattern is most suggestive of CS (Figure 3), several studies have reported that fasting ^{18}F-FDG uptake is inhomogeneous throughout the left ventricle in healthy subjects [61] and in oncologic patients [62], with regional maximal uptake in the infero-lateral and basal myocardium, probably because of local differences in substrate use [62]. This physiological ^{18}F-FDG uptake by the normal myocardium is problematic because it could lead to blurring of the sarcoid lesions in the heart and/or false-positive results. Although there is currently no consensus on the best protocol for suppressing cardiac ^{18}F-FDG uptake, a recently proposed protocol that combines prolonged fasting [63], dietary modifications [64, 65], and unfractionated heparin load before imaging [35] appears to be an attractive solution. In the fasting condition, normal myocardial cells use FFAs for up to 90% of their oxygen consumption [66, 67]. In contrast, when plasma glucose or insulin levels are increased after eating, glucose use may become dominant over FFA use. For clear visualization of CS lesions with a high signal-to-noise ratio, fasting imaging is preferable to postprandial imaging because background ^{18}F-FDG uptake is more suppressed [68]. Williams and Kolodny have shown that a very high-fat, low-carbohydrate, protein-permitted diet suppresses myocardial ^{18}F-FDG uptake more effectively than overnight or 4 h fasting in an oncologic cohort [65]. Comparing the effectiveness of myocardial ^{18}F-FDG suppression with a low-carbohydrate, high-fat, and protein-permitted diet with prolonged fasting over 12 h in an oncologic cohort, Harisankar et al. found that dietary restriction better suppressed cardiac uptake than did prolonged fasting [64]. Unfractionated heparin increases plasma FFAs levels via activation of lipoprotein and hepatic lipases [69], which may cause a reduction of glucose consumption in the normal myocardium. In a Japanese CS study cohort after a fasting period of at least 6 h, 50 units of unfractionated heparin per kilogram of body weight were injected 15 min before application of ^{18}F-FDG [35]. This resulted in robust suppression of cardiac ^{18}F-FDG uptake. However, a more recent study comparing heparin with prolonged fasting of more than 17.5 h reported that cardiac uptake was inhibited to a greater degree by extended fasting [70].

If there is a more diffuse uptake, the suppression of myocardial physiologic uptake may have been insufficient and other pitfalls should be considered. These include insufficient myocardial uptake suppression leading to heterogeneous ^{18}F-FDG uptake (maximum in the basal and lateral walls); other nonischemic cardiomyopathy or other inflammatory diseases of the heart leading to a substrate shift toward glucose, resulting in (heterogeneous) myocardial ^{18}F-FDG uptake; and myocardial ischemia resulting in

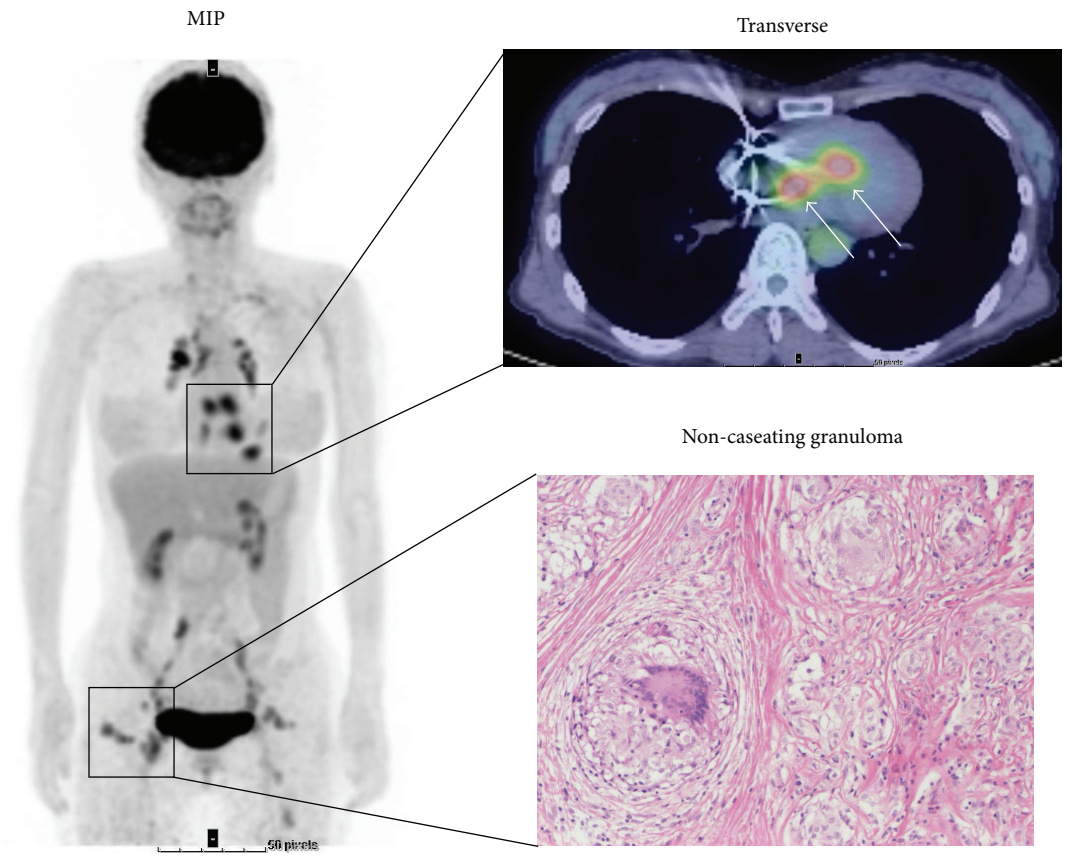

Figure 3: ^{18}F-FDG PET study in a subject with cardiac and extra-cardiac sarcoidosis. ^{18}F-FDG uptake is focally increased in the basal septal wall, consistent with active CS, and is suppressed in other left ventricular walls (white arrows). Whole-body study shows multiple extra-cardiac foci of ^{18}F-FDG uptake in chest, lymph nodes, and subcutaneous tissue consistent with active extensive systemic sarcoidosis. ^{18}F-FDG PET: ^{18}F-fluorodeoxyglucose positron emission tomography, MIP: maximum intensity projection.

sustained regionally increased myocardial ^{18}F-FDG uptake. Maurer et al. have shown that total cardiac uptake activity was suppressed in only 9% of an oncologic patient cohort despite adequate fasting [62]. Additionally, Israel et al. demonstrated that cardiac ^{18}F-FDG uptake was significantly higher in male patients, patients younger than 30 years, patients who had fasted for less than 5 h, patients with heart failure, and patients receiving benzodiazepines [71].

11. Analysis of ^{18}F-FDG PET Image

11.1. Semiquantitative Analysis. Focal myocardial ^{18}F-FDG uptake has been considered a finding suggestive of active CS lesions. Ishimaru et al. visually classified ^{18}F-FDG PET uptake into four patterns—"none," "diffuse," "focal," and "focal on diffuse"—where the latter two patterns were considered to be indicative of CS [32, 35]. Similarly, Langah et al. defined the patterns of ^{18}F-FDG uptake in the heart as "diffuse" or "focal" [36]. Alternatively, Yamagishi et al. divided the left ventricle into nine segments and defined a normal perfusion segment on cardiac ^{13}N-NH3 images as the control region. They then compared ^{18}F-FDG uptake between the segments with increased ^{18}F-FDG uptake and the control segment [38]. ^{18}F-FDG PET is often combined with a perfusion scan and ECG gating to rule out coronary artery disease or to identify resting perfusion defects suggestive of inflammation-induced tissue damage [51]. Normal perfusion and increased focal ^{18}F-FDG uptake represent early CS, whereas abnormal perfusion and increased ^{18}F-FDG uptake more likely represent advanced disease with tissue damage. Scarring, a potential outcome of end-stage disease, may result in abnormal perfusion without ^{18}F-FDG uptake [34]. In regard to segmental analysis, Ohira et al. and Yamagishi et al. used 16-segment and 9-segment models of the left ventricle, respectively (Table 1).

11.2. Quantitative Analysis. The standardized uptake value (SUV) is commonly used as an index of tracer uptake in tumor imaging. The SUV can be obtained using the following equation. SUV = (decay-corrected radiotracer concentration, mCi/mL)/(mCi of tracer injected dose into the patient)(body weight). In CS, a high SUV in the ^{18}F-FDG uptake site has

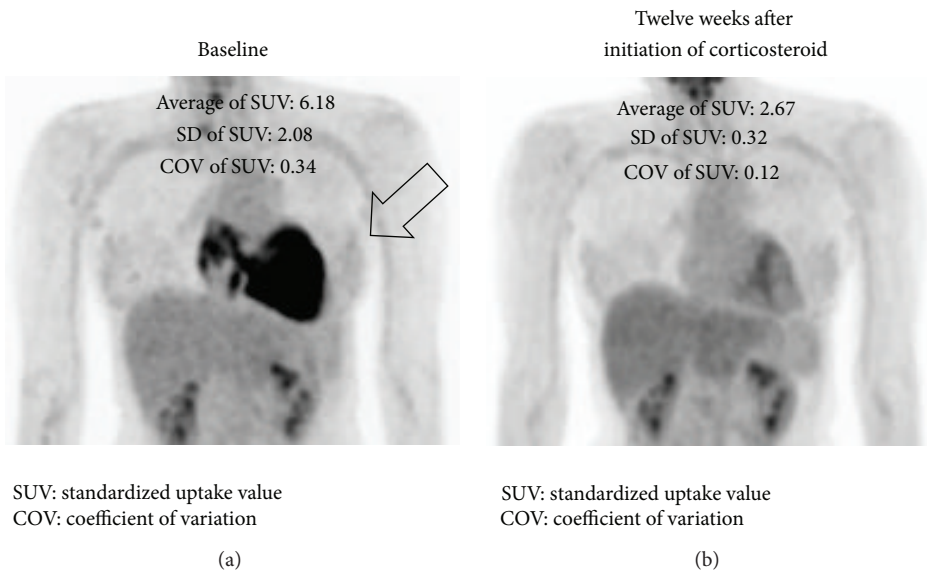

Figure 4: ^{18}F-FDG PET before and after corticosteroid therapy. (a) ^{18}F-FDG PET image (3D maximum intensity projection) before therapy. (b) After administration of 30 mg/day prednisone for 12 weeks, FDG uptake (arrow) has almost disappeared. ^{18}F-FDG PET: ^{18}F-fluoro-2-deoxyglucose positron emission tomography. SUV: standardized uptake value, COV: coefficient of variation.

been reported, consistent with visual determination of the site [34]. Okumura et al. divided the left ventricular cardiac muscle into 13 segments. Patients with CS showed a higher myocardial SUV than did healthy subjects. The diagnostic capability based on the above criterion had a sensitivity of 100% and specificity of 91% [34]. Tahara et al. reported that they utilized visual analysis using ^{18}F-FDG PET images, and the sensitivity and specificity for diagnosing CS were 100% and 46%, respectively, but after the quantitative analysis utilizing the coefficient of variation of SUV for segmental ^{18}F-FDG uptake, they achieved a specificity of 97% (Table 1) [37]. As for the use of SUV in the diagnosis of CS, problems that remain to be solved included unstandardized SUV calculation software and differences in measurement values depending on imaging equipment and imaging conditions.

12. Assessment of Disease Activity during Corticosteroid Treatment

The metabolic signal of inflammation is a marker of disease activity and can be used to guide the need for and response to corticosteroid therapies (Figure 4) [37, 38, 53, 72].

Among the case reports in the literature, Takeda et al. reported a case of CS with third-degree AV block that had markedly increased ^{18}F-FDG uptake in the basal interventricular septum. After corticosteroid therapy, myocardial ^{18}F-FDG uptake disappeared and the complete AV block became a first-degree AV block [53]. Similarly, Tadamura et al. documented a case of reduced regional ^{18}F-FDG uptake in the heart after corticosteroid therapy. In their case, myocardial ^{18}F-FDG uptake decreased, as did the serum level of ACE, a biomarker that reflects the disease activity of sarcoidosis [72]. After steroid therapy, a small study in 17 biopsy-proven CS patients showed a significant decrease in ^{18}F-FDG uptake, while perfusion defects remained stable [38]. Three patients showed improvement on ECG as well. Pandya et al. reported that the recurrence of symptomatic VT was predicted by increased ^{18}F-FDG uptake during corticosteroid tapering [73]. In a recent prospective study of 28 patients with biopsy-proven sarcoidosis, ^{18}F-FDG PET/CT influenced clinical management in 63% [63]. These reports suggest the practical role of ^{18}F-FDG PET in monitoring the disease activity of CS during corticosteroid therapy; however, there are pitfalls in this. First, steroids often induce glucose intolerance along with gluconeogenesis and insulin resistance. Serum glucose and insulin levels elevated by steroid therapy could affect ^{18}F-FDG uptake in target organs including the heart [74, 75]. This may preclude an accurate assessment of the effects of corticosteroid using ^{18}F-FDG PET. Also, ^{18}F-FDG PET has a limited ability in showing fibrous regions, although corticosteroid therapy may facilitate the transition from active inflammatory changes to the fibrotic stage. Fibrous lesions can be a focus of reentrant VT. Therefore, decreased ^{18}F-FDG uptake in the heart should not necessarily be interpreted as a favorable finding.

13. Biomarkers of CS

There are several parameters that can be used to monitor the inflammation of sarcoidosis, including serum ACE, lysozyme, and soluble IL-2 receptor [76–78]. Although ACE is a clinically useful biochemical marker of systemic sarcoidosis, serum levels soon return to the normal range after corticosteroid therapy even when disease activity remains high [79]. ACE inhibitors are often used to treat heart failure

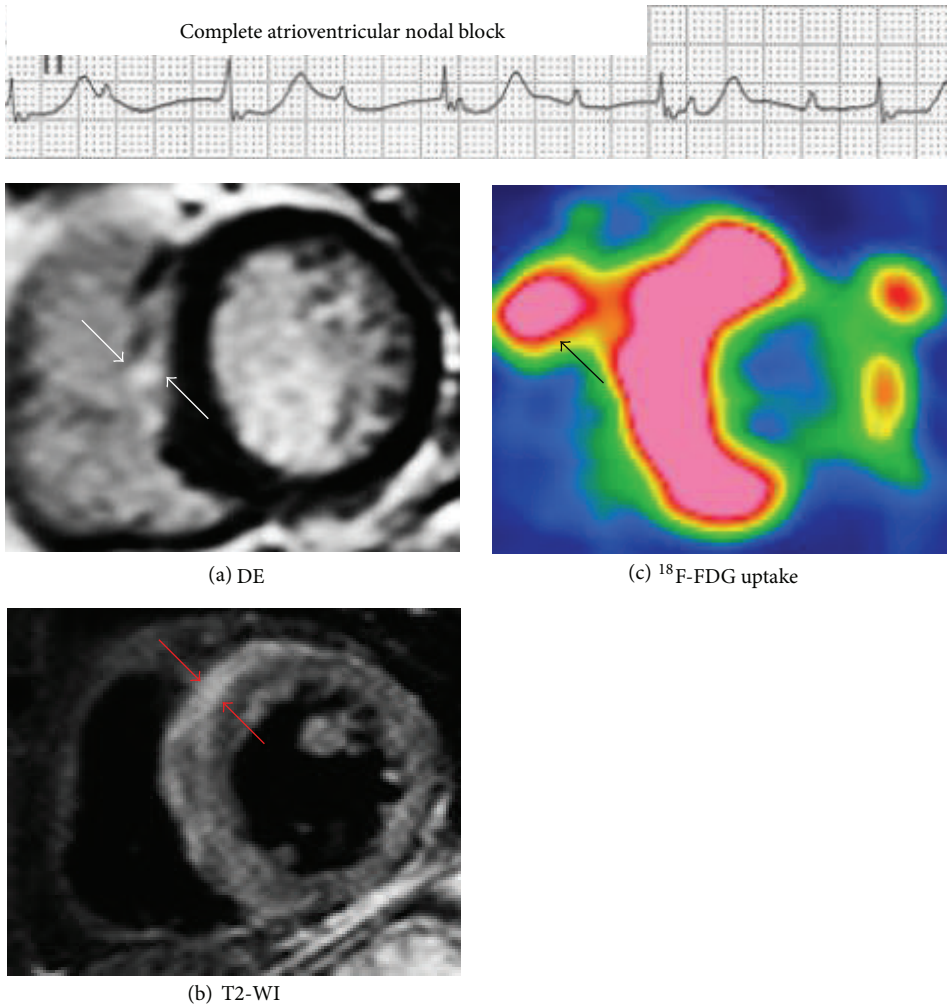

Figure 5: Representative images of cardiac MRI and ^{18}F-FDG PET in a CS patient with complete atrioventricular nodal block. Images of ^{18}F-FDG PET and cardiac MRI in a 66-year-old woman with pathologically proven CS. (a), (b) Cardiac MRI shows areas of DE and increased T2-weighted signal in the anteroseptal wall of the left ventricle (white and red arrows). (c) ^{18}F-FDG PET shows focal ^{18}F-FDG uptake in the anteroseptal of the left ventricle and right ventricle (black arrow). When compared with the ^{18}F-FDG PET image, the distribution of the positive finding on MRI notably differs. CS: cardiac sarcoidosis, DE: delayed enhancement, MRI: magnetic resonance imaging, T2-WI: T2-weighted image, ^{18}F-FDG PET: ^{18}F-fluorodeoxyglucose positron emission tomography.

in CS, and serum ACE levels are therefore likely to be influenced by this treatment.

14. Comparing ^{18}F-FDG PET and Cardiac MRI

^{18}F-FDG PET detects active CS lesions, whereas DE in cardiac MRI primarily detects more advanced fibrotic lesions [32, 35]. Commonly, the two phases overlap, so the mild to moderate correlation between DE in cardiac MRI and ^{18}F-FDG PET is not surprising (Figure 5) [32, 80]. Several studies compared DE in cardiac MRI with ^{18}F-FDG uptake in PET. In a report by Mehta et al., ^{18}F-FDG showed positive findings in 86% of 22 patients with suspected CS, whereas DE in cardiac MRI showed them in only 36% of patients [19]. Ohira et al. similarly reported that ^{18}F-FDG PET (87.5%) was more sensitive than DE in cardiac MRI (75%) [32]. In their study, however, the specificity of ^{18}F-FDG PET (39%) was obviously lower than that of DE in cardiac MRI (88%). When DE in cardiac MRI and ^{18}F-FDG PET were compared against JMHW's criteria, DE in cardiac MRI had a higher specificity but a lower sensitivity [19, 32, 81].

Cardiac MRI has greater spatial and temporal resolution compared with ^{18}F-FDG PET without radiation exposure. It also allows for anatomical and hemodynamic assessment

of cardiac function. However, cardiac MRI is not feasible in patients with implantable devices in the heart, which are often used for CS.

The advantages of ^{18}F-FDG PET include the biologic nature of the imaging signal, the potential for identifying cardiac and extra-cardiac sarcoidosis involvement (Figure 3) [40], and the feasibility of imaging in patients with implantable cardiac devices. Another advantage for therapy or risk stratification may be quantification. According to the European Association of Nuclear Medicine (EANM) and Society of Nuclear Medicine and Molecular Imaging guidelines for ^{18}F-FDG in inflammation, SUV should be used with caution in this setting [48]. However, McArdle et al. found higher quantitative ^{18}F-FDG uptake in CS patients with VT than in those with AV block and asymptomatic controls [40]. Similarly, Blankstein et al. concluded after examining a group of 125 patients that abnormal cardiac PET findings, but not JMHW criteria or the ejection fraction, are associated with a higher risk of death or VT [33].

The disadvantages of ^{18}F-FDG PET include radiation exposure, false-positive result of cardiac uptake, and the inability to detect smaller regions of myocardial damage. Also, a potential source of error in patients with an implantable cardiac device may be hot-spot artifacts at the lead insertion site on attenuation-corrected images. Although some studies have suggested a significant overestimation of SUV [82], others have suggested that images in the presence of metallic leads can be interpreted without correction for metal artifacts [83]. Evaluation of images without attenuation may be used as an adjunct in cases of suspected lead insertion artifacts.

15. Future Directions

The goals for management of patients with CS are to preserve cardiac function and avoid fatal arrhythmia, thereby achieving better quality and longer survival. Advanced imaging such as cardiac MRI and ^{18}F-FDG-PET may be useful for highly accurate early diagnosis, assessment of inflammatory activity, and therapeutic monitoring. Moreover, if optimal risk stratification of CS becomes available in the clinical setting, better prognosis is likely to be achieved in the future. However, a stepwise approach to diagnosing patients with cardiac involvement has not been established. Initial screening in extra-cardiac sarcoidosis usually includes a detailed medical history and physical exam, a surface ECG, and a transthoracic echocardiogram (Figure 6). Significant ECG abnormality such as new AV block or VT and echocardiographic abnormality such as decreased systolic/diastolic LV function should prompt further evaluation, usually with Holter monitoring and additional cardiac imaging [84]. Patients with initially negative screening tests should have repeat evaluations at follow-up visits to improve the sensitivity for detecting cardiac involvement [20]. In patients with initially positive screening tests, cardiac MRI should be performed because of its high specificity. Accordingly, ^{18}F-FDG PET should be considered in patients with positive findings on cardiac MRI to assess inflammatory activity before initiating corticosteroid therapy. On the other hand, ^{18}F-FDG PET-guided myocardial biopsy should be performed in patients with a contraindication to cardiac MRI (Figure 6).

In patients without a prior history of sarcoidosis, cardiac MRI should be considered if they have type II 2nd degree or complete AV block, sustained VT, or unexplained systolic or diastolic LV dysfunction. ^{18}F-FDG PET should be performed in patients with positive findings on cardiac MRI or contraindication to cardiac MRI to detect both cardiac and extra-cardiac sarcoid lesions, and they should undergo ^{18}F-FDG PET-guided biopsy (Figure 7). Clinical benefits and the cost effectiveness of these approaches should be evaluated simultaneously.

In the last decade, ^{18}F-FDG PET has substantially enhanced the detection of CS. However, no noteworthy progress has been made in the treatment of CS, and the prognosis of patients with CS has not notably improved. This means that there are still some problems to be worked out in the use of ^{18}F-FDG PET. First, standardized preparation protocols should be established to suppress physiological ^{18}F-FDG uptake sufficiently in the normal myocardium. This will likely help detect early-stage sarcoid lesions with a favorable sensitivity and specificity. Several protocols have already been introduced, but more easily applicable and reliable preparations are needed. Recently, dual time-point ^{18}F-FDG PET delayed imaging has been reported to be useful, not only for diagnosing malignancies [85], but also for assessing the activity of benign inflammatory disease [86]. In stimulated inflammatory cells, hexokinase, which mediates the phosphorylation of intracellular ^{18}F-FDG and results in its retention within cells, is translocated to the endofacial surface of the glucose transporter and is activated [87, 88]. Therefore, activation of inflammatory cells causes a sustained increase in the accumulation of ^{18}F-FDG over time. In a pulmonary sarcoidosis study, dual time-point ^{18}F-FDG PET was useful over a 1-year observation period for detecting patients with persistent pulmonary disease [89]. However, there has been no data reported on dual time-point ^{18}F-FDG PET delayed imaging in CS. Further studies needed to investigate how we can distinguish inflammatory lesions from physiological ^{18}F-FDG uptake in the myocardium using this method. Second, a standardized methodology that enables quantitative and objective image analysis should be established. The Japanese Society of Nuclear Cardiology has published "Recommendations standardized for ^{18}F-FDG PET imaging for CS" and stated that measurement of SUV in image interpretation may be useful for improving diagnostic capability and quantitative disease activity [90]. Furthermore, adopting a standardized segmentation and nomenclature system of the heart would allow comparison of ^{18}F-FDG PET findings from different institutions [91]. In 2006, EANM launched EANM Research Ltd. (EARL) as an initiative to promote multicenter nuclear medicine and research. In January 2010, EANM published the FDG PET and PET/CT: EANM procedure guidelines for tumour PET imaging: version 1.0 [92] in which quantification of ^{18}F-FDG PET is defined as quantification using SUV. The use of SUV in multicenter oncology PET studies requires

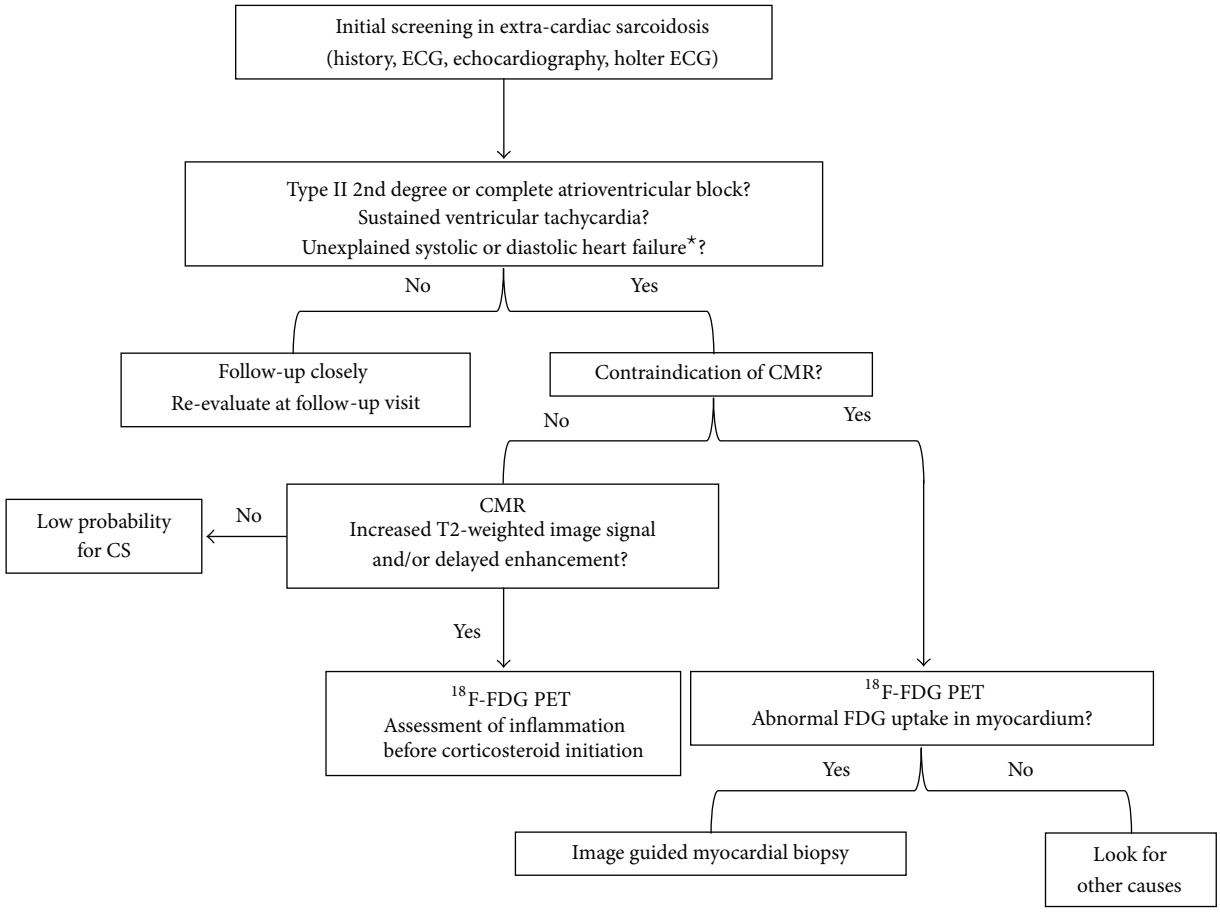

CS: cardiac sarcoidosis
ECG: electrocardiogram
^{18}F-FDG: ^{18}F-fluorodeoxyglucose positron emission tomography
CMR: cardiac magnetic resonance

Figure 6: Diagnostic algorithm for a patient with suspected for cardiac involvement in extra-cardiac sarcoidosis. *Absence of coronary artery disease as determined by selective coronary angiography and the absence of a comorbidity that could explain heart failure. Patients with initially negative screening tests should have repeat evaluations at follow-up visits. Cardiac MRI is the most specific test and ^{18}F-FDG PET is the most sensitive test available for cardiac sarcoidosis. ^{18}F-FDG PET should be considered for patients with positive findings on cardiac MRI to assess inflammatory activity before initiating corticosteroid therapy. ^{18}F-FDG PET-guided myocardial biopsy should be performed in patients with a contraindication to cardiac MRI.

an inter-institution calibration procedure to facilitate the exchangeability of SUVs between institutions. It is important that all participating institutions use a similar methodology To ensure the exchangeability of SUVs, a minimum set of quality-control procedures is recommended; for example, daily quality control, calibration/cross-calibration of PET or PET/CT camera with the institution's own dose calibrator or against another dose calibrator, inter-institution cross-calibration, and determining "activity recovery coefficients." Accurate, reproducible, and quantitative assessment using SUV could be obtained by standardizing the methodology. Further studies are needed to apply the methodology to CS. Third, long-term prospective clinical studies are needed to determine the value of imaging for therapy monitoring and risk stratification. Finally, the use of ^{18}F-FDG PET combined with other imaging modalities is warranted. Hybrid PET/MRI systems have been recently introduced to medical imaging. In the imaging of CS, several case reports have demonstrated the potential of integrated PET/MRI [93, 94]. Cardiac MRI has been shown to provide good diagnostic performance in CS. However, T2-weighted images, which are particularly important for showing inflammatory activity in CS, are prone to artifacts and often do not yield a consistent image quality, especially in patients with arrhythmia and other motion artifacts [95]. In contrast, ^{18}F-FDG PET is useful for assessing inflammatory myocardial disease activity for therapy response evaluation [95]. PET/MRI might emerge as an important modality for the diagnosis of CS and monitoring of its disease activity. Additionally, its lower radiation dose compared with PET/CT will be particularly valuable in the imaging of young patients with potentially curable disease [96].

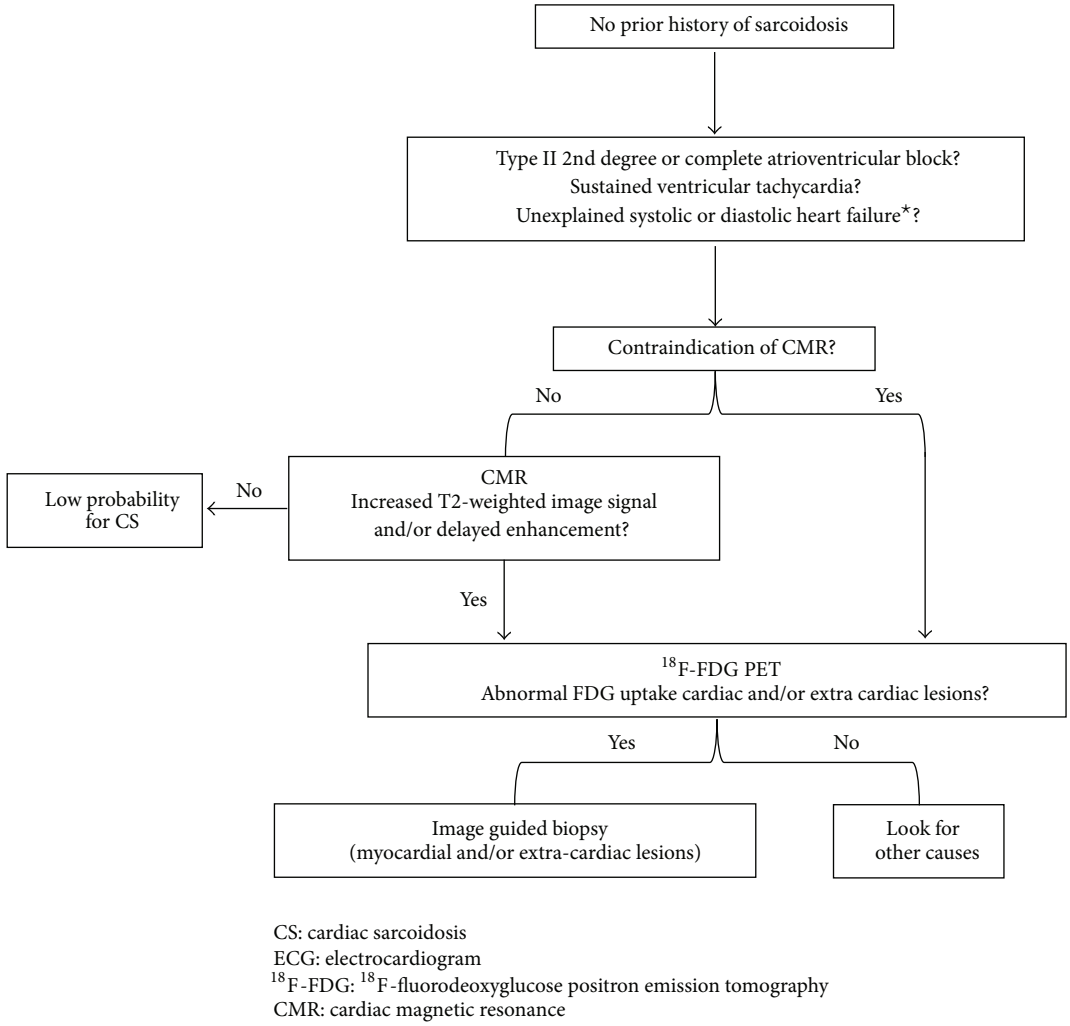

Figure 7: Diagnostic algorithm for a patient with suspected for cardiac sarcoidosis. *Absence of coronary artery disease as determined by selective coronary angiography and the absence of a comorbidity that could explain heart failure. Cardiac MRI is the most specific test and ^{18}F-FDG PET is the most sensitive test available for cardiac sarcoidosis. In patients without a prior history of sarcoidosis, cardiac MRI should be considered if they have type II 2nd degree or complete atrioventricular block, sustained ventricular tachycardia, or unexplained systolic or diastolic LV dysfunction. ^{18}F-FDG PET should be performed in patients with positive findings on cardiac MRI or contraindication to cardiac MRI to detect both cardiac and extra-cardiac sarcoid lesions, and ^{18}F-FDG PET-guided biopsy should be performed.

Conflict of Interests

The authors declare that there is no conflict of interests regarding the publication of this paper.

Acknowledgments

The authors thank Kazuhiro Otani, Kouji Tsuchihashi, and Masaki Terada of Wakayama-Minami Radiology Clinic for their assistance.

References

[1] "Statement on sarcoidosis. Joint Statement of the American Thoracic Society (ATS), the European Respiratory Society (ERS) and the World Association of Sarcoidosis and Other Granulomatous Disorders (WASOG) adopted by the ATS Board of Directors and by the ERS Executive Committee, February 1999," *American Journal of Respiratory and Critical Care Medicine*, vol. 160, no. 2, pp. 736–755, 1999.

[2] W. C. Roberts, H. A. McAllister Jr., and V. J. Ferrans, "Sarcoidosis of the heart: a clinicopathologic study of 35 necropsy patients (group I) and review of 78 previously described necropsy patients (group II)," *The American Journal of Medicine*, vol. 63, no. 1, pp. 86–108, 1977.

[3] M. C. Iannuzzi, B. A. Rybicki, and A. S. Teirstein, "Sarcoidosis," *The New England Journal of Medicine*, vol. 357, no. 21, pp. 2153–2108, 2007.

[4] G. Hillerdal, E. Nou, K. Osterman, and B. Schmekel, "Sarcoidosis: epidemiology and prognosis: a 15-year European study," *American Review of Respiratory Disease*, vol. 130, no. 1, pp. 29–32, 1984.

[5] T. Morimoto, A. Azuma, S. Abe et al., "Epidemiology of sarcoidosis in Japan," *European Respiratory Journal*, vol. 31, no. 2, pp. 372–379, 2008.

[6] L. Varron, V. Cottin, A. Schott, C. Broussolle, and P. Sève, "Late-onset sarcoidosis: a comparative study," *Medicine*, vol. 91, no. 3, pp. 137–143, 2012.

[7] B. A. Rybicki, M. C. Iannuzzi, M. M. Frederick et al., "Familial aggregation of sarcoidosis: a Case-Control Etiologic Study of Sarcoidosis (ACCESS)," *American Journal of Respiratory and Critical Care Medicine*, vol. 164, no. 11, pp. 2085–2091, 2001.

[8] A. Sverrild, V. Backer, K. O. Kyvik et al., "Heredity in sarcoidosis: a registry-based twin study," *Thorax*, vol. 63, no. 10, pp. 894–896, 2008.

[9] R. P. Baughman, E. E. Lower, and R. M. Du Bois, "Sarcoidosis," *The Lancet*, vol. 361, no. 9363, pp. 1111–1118, 2003.

[10] L. S. Newman, C. S. Rose, E. A. Bresnitz et al., "A case control etiologic study of sarcoidosis: environmental and occupational risk factors," *The American Journal of Respiratory and Critical Care Medicine*, vol. 170, no. 12, pp. 1324–1330, 2004.

[11] J. Müller-Quernheim, M. Schürmann, S. Hofmann et al., "Genetics of Sarcoidosis," *Clinics in Chest Medicine*, vol. 29, no. 3, pp. 391–414, 2008.

[12] E. S. Chen and D. R. Moller, "Etiology of Sarcoidosis," *Clinics in Chest Medicine*, vol. 29, no. 3, pp. 365–377, 2008.

[13] Y. Rosen, "Pathology of sarcoidosis," *Seminars in Respiratory and Critical Care Medicine*, vol. 28, no. 1, pp. 36–52, 2007.

[14] G. Zissel, A. Prasse, and J. Müller-Quernheim, "Immunologic response of sarcoidosis," *Seminars in Respiratory and Critical Care Medicine*, vol. 31, no. 4, pp. 390–403, 2010.

[15] E. S. Chen, Z. Song, M. H. Willett et al., "Serum amyloid a regulates granulomatous inflammation in sarcoidosis through toll-like receptor-2," *American Journal of Respiratory and Critical Care Medicine*, vol. 181, no. 4, pp. 360–373, 2010.

[16] A. Uemura, S. Morimoto, S. Hiramitsu, Y. Kato, T. Ito, and H. Hishida, "Histologic diagnostic rate of cardiac sarcoidosis: evaluation of endomyocardial biopsies," *American Heart Journal*, vol. 138, no. 2 I, pp. 299–302, 1999.

[17] L. S. Newman, C. S. Rose, and L. A. Maier, "Sarcoidosis," *The New England Journal of Medicine*, vol. 336, no. 17, pp. 1224–1234, 1997.

[18] K. J. Silverman, G. M. Hutchins, and B. H. Bulkley, "Cardiac sarcoid: a clinicopathologic study of 84 unselected patients with systemic sarcoidosis," *Circulation*, vol. 58, no. 6, pp. 1204–1211, 1978.

[19] D. Mehta, S. A. Lubitz, Z. Frankel et al., "Cardiac involvement in patients with sarcoidosis: diagnostic and prognostic value of outpatient testing," *Chest*, vol. 133, no. 6, pp. 1426–1435, 2008.

[20] C. Chapelon-Abric, D. de Zuttere, P. Duhaut et al., "Cardiac sarcoidosis: a retrospective study of 41 cases," *Medicine*, vol. 83, no. 6, pp. 315–334, 2004.

[21] F. Tavora, N. Cresswell, L. Li, M. Ripple, C. Solomon, and A. Burke, "Comparison of necropsy findings in patients with sarcoidosis dying suddenly from cardiac sarcoidosis versus dying suddenly from other causes," *The American Journal of Cardiology*, vol. 104, no. 4, pp. 571–577, 2009.

[22] K. Banba, K. F. Kusano, K. Nakamura et al., "Relationship between arrhythmogenesis and disease activity in cardiac sarcoidosis," *Heart Rhythm*, vol. 4, no. 10, pp. 1292–1299, 2007.

[23] R. Kandolin, J. Lehtonen, and M. Kupari, "Cardiac sarcoidosis and giant cell myocarditis as causes of atrioventricular block in young and middle-aged adults," *Circulation: Arrhythmia and Electrophysiology*, vol. 4, no. 3, pp. 303–309, 2011.

[24] G. Youssef, R. S. B. Beanlands, D. H. Birnie, and P. B. Nery, "Cardiac sarcoidosis: applications of imaging in diagnosis and directing treatment," *Heart*, vol. 97, no. 24, pp. 2078–2087, 2011.

[25] H. Furushima, M. Chinushi, H. Sugiura, H. Kasai, T. Washizuka, and Y. Aizawa, "Ventricular tachyarrhythmia associated with cardiac sarcoidosis: its mechanisms an outcome," *Clinical Cardiology*, vol. 27, no. 4, pp. 217–222, 2004.

[26] M. Sekiguchi, Y. Numao, M. Imai, T. Furuie, and R. Mikami, "Clinical and histopathological profile of sarcoidosis of the heart and acute idiopathic myocarditis: concepts through a study employing endomyocardial biopsy. I. Sarcoidosis," *Japanese Circulation Journal*, vol. 44, no. 4, pp. 249–263, 1980.

[27] Y. Yazaki, M. Isobe, M. Hiroe et al., "Prognostic determinants of long-term survival in Japanese patients with cardiac sarcoidosis treated with prednisone," *The American Journal of Cardiology*, vol. 88, no. 9, pp. 1006–1010, 2001.

[28] V. Sekhri, S. Sanal, L. J. DeLorenzo, W. S. Aronow, and G. P. Maguire, "Cardiac sarcoidosis: a comprehensive review," *Archives of Medical Science*, vol. 7, no. 4, pp. 546–554, 2011.

[29] H. Hiraga, K. Iwai, and M. Hiroe, *Guidelines for Diagnosis of Cardiac Sarcoidosis, Study Report on Diffuse Pulmonary Diseases*, pp. 23-24, The Japanese Ministry of Health and Welfare, Tokyo, Japan, 1993, (Japanese).

[30] "Diagnostic standard and guidelines for sarcoidosis," *Japanese Journal of Sarcoidosis Granulomatous Disorders*, vol. 27, pp. 89–102, 2007 (Japanese).

[31] K. Soejima and H. Yada, "The work-up and management of patients with apparent or subclinical cardiac sarcoidosis: with emphasis on the associated heart rhythm abnormalities," *Journal of Cardiovascular Electrophysiology*, vol. 20, no. 5, pp. 578–583, 2009.

[32] H. Ohira, I. Tsujino, S. Ishimaru et al., "Myocardial imaging with 18F-fluoro-2-deoxyglucose positron emission tomography and magnetic resonance imaging in sarcoidosis," *European Journal of Nuclear Medicine and Molecular Imaging*, vol. 35, no. 5, pp. 933–941, 2008.

[33] R. Blankstein, M. Osborne, M. Naya et al., "Cardiac positron emission tomography enhances prognostic assessments of patients with suspected cardiac sarcoidosis," *Journal of the American College of Cardiology*, vol. 63, no. 4, pp. 329–336, 2013.

[34] W. Okumura, T. Iwasaki, T. Toyama et al., "Usefulness of fasting18F-FDG PET in identification of cardiac sarcoidosis," *Journal of Nuclear Medicine*, vol. 45, no. 12, pp. 1989–1998, 2004.

[35] S. Ishimaru, I. Tsujino, T. Takei et al., "Focal uptake on 18F-fluoro-2-deoxyglucose positron emission tomography images indicates cardiac involvement of sarcoidosis," *European Heart Journal*, vol. 26, no. 15, pp. 1538–1543, 2005.

[36] R. Langah, K. Spicer, M. Gebregziabher, and L. Gordon, "Effectiveness of prolonged fasting 18f-FDG PET-CT in the detection of cardiac sarcoidosis," *Journal of Nuclear Cardiology*, vol. 16, no. 5, pp. 801–810, 2009.

[37] N. Tahara, A. Tahara, Y. Nitta et al., "Heterogeneous myocardial FDG uptake and the disease activity in cardiac sarcoidosis," *JACC Cardiovascular Imaging*, vol. 3, no. 12, pp. 1219–1228, 2010.

[38] H. Yamagishi, N. Shirai, M. Takagi et al., "Identification of cardiac sarcoidosis with 13N-NH 3/18F-FDG PET," *Journal of Nuclear Medicine*, vol. 44, no. 7, pp. 1030–1036, 2003.

[39] O. Manabe, H. Ohira, K. Yoshinaga et al., "Elevated 18F-fluorodeoxyglucose uptake in the interventricular septum is associated with atrioventricular block in patients with suspected cardiac involvement sarcoidosis," *European Journal of Nuclear Medicine and Molecular Imaging*, vol. 40, no. 10, pp. 1558–1566, 2013.

[40] B. A. McArdle, D. H. Birnie, R. Klein et al., "Is there an association between clinical presentation and the location and extent

of myocardial involvement of cardiac sarcoidosis as assessed by 18F-fluorodoexyglucose positron emission tomography?" *Circulation: Cardiovascular Imaging*, vol. 6, no. 5, pp. 617–626, 2013.

[41] S. Greulich, C. C. Deluigi, S. Gloekler et al., "CMR imaging predicts death and other adverse events in suspected cardiac sarcoidosis," *JACC: Cardiovascular Imaging*, vol. 6, no. 4, pp. 501–511, 2013.

[42] J. Smedema, G. Snoep, M. P. G. van Kroonenburgh et al., "Evaluation of the accuracy of gadolinium-enhanced cardiovascular magnetic resonance in the diagnosis of cardiac sarcoidosis," *Journal of the American College of Cardiology*, vol. 45, no. 10, pp. 1683–1690, 2005.

[43] R. J. Kim, M. R. Patel, P. J. Cawley et al., "Detection of myocardial damage in patients with sarcoidosis," *Circulation*, vol. 120, no. 20, pp. 1969–1977, 2009.

[44] O. Vignaux, R. Dhote, D. Duboc et al., "Clinical significance of myocardial magnetic resonance abnormalities in patients with sarcoidosis: a 1-year follow-up study," *Chest*, vol. 122, no. 6, pp. 1895–1901, 2002.

[45] T. Shimada, K. Shimada, T. Sakane et al., "Diagnosis of cardiac sarcoidosis and evaluation of the effects of steroid therapy by gadolinium-DTPA-enhanced magnetic resonance imaging.," *The American Journal of Medicine*, vol. 110, no. 7, pp. 520–527, 2001.

[46] B. E. Hillner, B. A. Siegel, D. Liu et al., "Impact of positron emission tomography/computed tomography and positron emission tomography (PET) alone on expected management of patients with cancer: initial results from the National Oncologic PET Registry," *Journal of Clinical Oncology*, vol. 26, no. 13, pp. 2155–2161, 2008.

[47] L. K. Shankar, J. M. Hoffman, S. Bacharach et al., "Consensus recommendations for the use of 18F-FDG PET as an indicator of therapeutic response in patients in National Cancer Institute Trials," *Journal of Nuclear Medicine*, vol. 47, no. 6, pp. 1059–1066, 2006.

[48] F. Jamar, J. Buscombe, A. Chiti et al., "EANM/SNMMI guideline for 18F-FDG use in inflammation and infection," *Journal of Nuclear Medicine*, vol. 54, no. 4, pp. 647–658, 2013.

[49] S. Yamada, K. Kubota, R. Kubota, T. Ido, and N. Tamahashi, "High accumulation of fluorine-18-fluorodeoxyglucose in turpentine-induced inflammatory tissue," *Journal of Nuclear Medicine*, vol. 36, no. 7, pp. 1301–1306, 1995.

[50] T. Mochizuki, E. Tsukamoto, Y. Kuge et al., "FDG uptake and glucose transporter subtype expressions in experimental tumor and inflammation models," *Journal of Nuclear Medicine*, vol. 42, no. 10, pp. 1551–1555, 2001.

[51] B. A. Mc Ardle, E. Leung, H. Ohira et al., "The role of F18-fluorodeoxyglucose positron emission tomography in guiding diagnosis and management in patients with known or suspected cardiac sarcoidosis," *Journal of Nuclear Cardiology*, vol. 20, no. 2, pp. 297–306, 2013.

[52] G. Youssef, E. Leung, I. Mylonas et al., "The use of ^{18}F-FDG PET in the diagnosis of cardiac sarcoidosis: a systematic review and metaanalysis including the Ontario experience," *Journal of Nuclear Medicine*, vol. 53, no. 2, pp. 241–248, 2012.

[53] N. Takeda, I. Yokoyama, Y. Hiroi et al., "Positron emission tomography predicted recovery of complete A-V nodal dysfunction in a patient with cardiac sarcoidosis," *Circulation*, vol. 105, no. 9, pp. 1144–1145, 2002.

[54] L. H. Brudin, S. O. Valind, C. G. Rhodes et al., "Fluorine-18 deoxyglucose uptake in sarcoidosis measured with positron emission tomography," *European Journal of Nuclear Medicine*, vol. 21, no. 4, pp. 297–305, 1994.

[55] P. J. Lewis, A. Salama, A. Alavi, C. A. Buchpiguel, A. Loessner, and S. M. Larson, "Uptake of fluorine-18-fluorodeoxyglucose in sarcoidosis," *Journal of Nuclear Medicine*, vol. 35, no. 10, pp. 1647–1649, 1994.

[56] J. P. Smedema, V. Reenaers, and R. Geukens, "Images in cardiology. Cardiac sarcoidosis in a 60 year old woman.," *Heart*, vol. 92, article 688, 2006.

[57] H. Koiwa, I. Tsujino, H. Ohira, K. Yoshinaga, N. Otsuka, and M. Nishimura, "Imaging of cardiac sarcoid lesions using fasting cardiac 18F-fluorodeoxyglucose positron emission tomography: an autopsy case," *Circulation*, vol. 122, no. 5, pp. 535–536, 2010.

[58] M. L. Bartlett, S. L. Bacharach, L. M. Voipio-Pulkki, and V. Dilsizian, "Artifactual inhomogeneities in myocardial PET and SPECT scans in normal subjects," *Journal of Nuclear Medicine*, vol. 36, no. 2, pp. 188–195, 1995.

[59] R. J. Gropler, B. A. Siegel, K. J. Lee et al., "Nonuniformity in myocardial accumulation of fluorine-18-fluorodeoxyglucose in normal fasted humans," *Journal of Nuclear Medicine*, vol. 31, no. 11, pp. 1749–1756, 1990.

[60] M. Orii, K. Hirata, T. Tanimoto et al., "Early abnormality detected by speckle-tracking echocardiography in a patient with suspected cardiac sarcoidosis," *Journal of Echocardiography*, vol. 11, no. 2, pp. 69–71, 2013.

[61] P. Iozzo, P. Chareonthaitawee, M. D. Terlizzi, D. J. Betteridge, E. Ferrannini, and P. G. Camici, "Regional myocardial blood flow and glucose utilization during fasting and physiological hyperinsulinemia in humans," *The American Journal of Physiology: Endocrinology and Metabolism*, vol. 282, no. 5, pp. E1163–E1171, 2002.

[62] A. H. Maurer, M. Burshteyn, L. P. Adler, J. P. Gaughan, and R. M. Steiner, "Variable cardiac 18FDG patterns seen in oncologic positron emission tomography computed tomography importance for differentiating normal physiology from cardiac and paracardiac disease," *Journal of Thoracic Imaging*, vol. 27, no. 4, pp. 263–268, 2012.

[63] V. Ambrosini, M. Zompatori, L. Fasano et al., "18F-FDG PET/CT for the assessment of disease extension and activity in patients with sarcoidosis: results of a preliminary prospective study," *Clinical Nuclear Medicine*, vol. 38, no. 4, pp. e171–e177, 2013.

[64] C. N. B. Harisankar, B. R. Mittal, K. L. Agrawal, M. L. Abrar, and A. Bhattacharya, "Utility of high fat and low carbohydrate diet in suppressing myocardial FDG uptake," *Journal of Nuclear Cardiology*, vol. 18, no. 5, pp. 926–936, 2011.

[65] G. Williams and G. M. Kolodny, "Suppression of myocardial 18F-FDG uptake by preparing patients with a high-fat, low-carbohydrate diet," *The American Journal of Roentgenology*, vol. 190, no. 2, pp. W151–w156, 2008.

[66] J. A. Wisneski, E. W. Gertz, R. A. Neese, and M. Mayr, "Myocardial metabolism of free fatty acids. Studies with 14C-labeled substrates in humans," *The Journal of Clinical Investigation*, vol. 79, no. 2, pp. 359–366, 1987.

[67] K. Yoshinaga and N. Tamaki, "Imaging myocardial metabolism," *Current Opinion in Biotechnology*, vol. 18, no. 1, pp. 52–59, 2007.

[68] Y. Choi, R. C. Brunken, R. A. Hawkins et al., "Factors affecting myocardial 2-[F-18]fluoro-2-deoxy-D-glucose uptake in positron emission tomography studies of normal humans,"

European Journal of Nuclear Medicine, vol. 20, no. 4, pp. 308–318, 1993.

[69] E. Persson, "Lipoprotein lipase, hepatic lipase and plasma lipolytic activity. Effects of heparin and a low molecular weight heparin fragment (Fragmin)," *Acta Medica Scandinavica*, vol. 724, pp. 1–56, 1988.

[70] M. Morooka, M. Moroi, K. Ito, and R. Minamimoto, "Heparin vs. long fasting method: which inhibits the FDG myocardial physiological uptake more strongly?" *Journal of Nuclear Medicine*, vol. 54, supplement, p. 406P, 2013.

[71] O. Israel, M. Weiler-Sagie, S. Rispler et al., "PET/CT quantitation of the effect of patient-related factors on cardiac 18F-FDG uptake," *Journal of Nuclear Medicine*, vol. 48, no. 2, pp. 234–239, 2007.

[72] E. Tadamura, M. Yamamuro, S. Kubo et al., "Multimodality imaging of cardiac sarcoidosis before and after steroid therapy," *Circulation*, vol. 113, no. 20, pp. e771–e773, 2006.

[73] C. Pandya, R. C. Brunken, P. Tchou, P. Schoenhagen, and D. A. Culver, "Detecting cardiac involvement in sarcoidosis: a call for prospective studies of newer imaging techniques," *European Respiratory Journal*, vol. 29, no. 2, pp. 418–422, 2007.

[74] A. Alavi, N. Gupta, J. Alberini et al., "Positron emission tomography imaging in nonmalignant thoracic disorders," *Seminars in Nuclear Medicine*, vol. 32, no. 4, pp. 293–321, 2002.

[75] J. M. Chang, H. J. Lee, J. M. Goo, J. J. Lee, J. Chung, and J. Im, "False positive and false negative FDG-PET scans in various thoracic diseases," *Korean Journal of Radiology*, vol. 7, no. 1, pp. 57–69, 2006.

[76] J. Lieberman, "Elevation of serum angiotension converting enzyme (ACE) level in sarcoidosis," *The American Journal of Medicine*, vol. 59, no. 3, pp. 365–372, 1975.

[77] O. Selroos and C. Gronhagen-Riska, "Angiotensin converting enzyme, III: changes in serum level as an indicator of disease activity in untreated sarcoidosis," *Scandinavian Journal of Respiratory Diseases*, vol. 60, no. 6, pp. 328–336, 1979.

[78] S. Rothkrantz-Kos, M. P. van Dieijen-Visser, P. G. H. Mulder, and M. Drent, "Potential usefulness of inflammatory markers to monitor respiratory functional impairment in sarcoidosis," *Clinical Chemistry*, vol. 49, no. 9, pp. 1510–1517, 2003.

[79] M. W. Ziegenhagen, M. E. Rothe, M. Schlaak, and J. Müller-Quernheim, "Bronchoalveolar and serological parameters reflecting the severity of sarcoidosis," *European Respiratory Journal*, vol. 21, no. 3, pp. 407–413, 2003.

[80] M. Soussan, P. Brillet, H. Nunes et al., "Clinical value of a high-fat and low-carbohydrate diet before FDG-PET/CT for evaluation of patients with suspected cardiac sarcoidosis," *Journal of Nuclear Cardiology*, vol. 20, no. 1, pp. 120–127, 2013.

[81] N. Y. Hamzeh, F. S. Wamboldt, and H. D. Weinberger, "Management of cardiac sarcoidosis in the United States: a Delphi study," *Chest*, vol. 141, no. 1, pp. 154–162, 2012.

[82] F. P. DiFilippo and R. C. Brunken, "Do implanted pacemaker leads and ICD leads cause metal-related artifact in cardiac PET/CT?" *Journal of Nuclear Medicine*, vol. 46, no. 3, pp. 436–443, 2005.

[83] P. Ghafarian, S. M. R. Aghamiri, M. R. Ay et al., "Is metal artefact reduction mandatory in cardiac PET/CT imaging in the presence of pacemaker and implantable cardioverter defibrillator leads?" *European Journal of Nuclear Medicine and Molecular Imaging*, vol. 38, no. 2, pp. 252–262, 2011.

[84] J. Smedema, G. Snoep, M. P. G. Van Kroonenburgh et al., "Cardiac involvement in patients with pulmonary sarcoidosis assessed at two university medical centers in the Netherlands," *Chest*, vol. 128, no. 1, pp. 30–35, 2005.

[85] A. Mavi, M. Urhan, J. Q. Yu et al., "Dual time point 18F-FDG PET imaging detects breast cancer with high sensitivity and correlates well with histologic subtypes," *Journal of Nuclear Medicine*, vol. 47, no. 9, pp. 1440–1446, 2006.

[86] I. Kim, J. S. Lee, S. Kim et al., "Double-phase 18F-FDG PET-CT for determination of pulmonary tuberculoma activity," *European Journal of Nuclear Medicine and Molecular Imaging*, vol. 35, no. 4, pp. 808–814, 2008.

[87] J. Huang, A. L. Kindzelskii, and H. R. Petty, "Hexokinase translocation during neutrophil activation, chemotaxis, and phagocytosis: Disruption by cytochalasin D, dexamethasone, and indomethacin," *Cellular Immunology*, vol. 218, no. 1-2, pp. 95–106, 2002.

[88] K. C. Pedley, G. E. Jones, M. Magnani, R. J. Rist, and R. J. Naftalin, "Direct observation of hexokinase translocation in stimulated macrophages," *Biochemical Journal*, vol. 291, no. 2, pp. 515–522, 1993.

[89] Y. Umeda, Y. Demura, M. Morikawa et al., "Prognostic value of dual-time-point18F-fluorodeoxyglucose positron emission tomography in patients with pulmonary sarcoidosis," *Respirology*, vol. 16, no. 4, pp. 713–720, 2011.

[90] Y. Ishida, K. Yoshinaga, M. Miyagawa et al., "Recommendations for ^{18}F-fluorodeoxyglucose positron emission tomography imaging for cardiac sarcoidosis: Japanese Society of Nuclear Cardiology Recommendations," *Annals of Nuclear Medicine*, vol. 28, no. 4, pp. 393–403, 2014.

[91] M. D. Cerqueira, N. J. Weissman, V. Dilsizian et al., "Standardized myocardial segmentation and nomenclature for tomographic imaging of the heart: a statement for healthcare professionals from the Cardiac Imaging Committee of the Council on Clinical Cardiology of the American Heart Association," *Circulation*, vol. 105, pp. 539–542, 2002.

[92] R. Boellaard, M. J. O'Doherty, W. A. Weber et al., "FDG PET and PET/CT: EANM procedure guidelines for tumour PET imaging: version 1.0," *European Journal of Nuclear Medicine and Molecular Imaging*, vol. 37, no. 1, pp. 181–200, 2010.

[93] S. Schneider, A. Batrice, C. Rischpler, M. Eiber, T. Ibrahim, and S. G. Nekolla, "Utility of multimodal cardiac imaging with PET/MRI in cardiac sarcoidosis : implications for diagnosis, monitoring and treatment," *European Heart Journal*, vol. 35, no. 5, p. 312, 2014.

[94] J. A. White, M. Rajchl, J. Butler, R. T. Thompson, F. S. Prato, and G. Wisenberg, "Active cardiac sarcoidosis first clinical experience of simultaneous positron emission tomography-magnetic resonance imaging for the diagnosis of cardiac disease," *Circulation*, vol. 127, no. 22, pp. e639–e641, 2013.

[95] D. P. Sobic-Saranovic, I. T. Grozdic, J. Videnovic-Ivanov et al., "Responsiveness of FDG PET/CT to treatment of patients with active chronic sarcoidosis," *Clinical Nuclear Medicine*, vol. 38, no. 7, pp. 516–521, 2013.

[96] F. Nensa, K. Beiderwellen, P. Heusch, and A. Wetter, "Clinical applications of PET/MR: current status and future perspectives," *Diagnostic and Interventional Radiology*, 2014.

Hindawi Publishing Corporation
BioMed Research International
Volume 2014, Article ID 867381, 15 pages
http://dx.doi.org/10.1155/2014/867381

Review Article

Antimicrobial Peptides: Their Role as Infection-Selective Tracers for Molecular Imaging

Thomas Ebenhan,[1,2] Olivier Gheysens,[3] Hendrick Gert Kruger,[2] Jan Rijn Zeevaart,[4] and Mike Machaba Sathekge[1]

[1] *Department of Nuclear Medicine, University of Pretoria & Steve Biko Academic Hospital, Corner of Malherbe and Steve Biko Road, Pretoria 0001, South Africa*
[2] *Catalysis and Peptide Research Unit, School of Health Sciences, University of KwaZulu Natal, E-Block 6th Floor, Westville Campus, University Road, Westville, Durban 3630, South Africa*
[3] *Department of Nuclear Medicine, University Hospitals Leuven, Katholieke Universiteit Leuven, Campus Gasthuisberg, Herestraat 49, 3000 Leuven, Belgium*
[4] *Department of Science and Technology, Preclinical Drug Development Platform, North West University, 11 Hoffman Street, Potchefstroom 2520, South Africa*

Correspondence should be addressed to Mike Machaba Sathekge; mike.sathekge@up.ac.za

Received 7 June 2014; Accepted 29 July 2014; Published 27 August 2014

Academic Editor: Filippo Galli

Antimicrobial peptides (AMPs) are a heterogeneous class of compounds found in a variety of organisms including humans and, so far, hundreds of these structures have been isolated and characterised. They can be described as natural microbicide, selectively cytotoxic to bacteria, whilst showing minimal cytotoxicity towards the mammalian cells of the host organism. They act by their relatively strong electrostatic attraction to the negatively charged bacterial cells and a relatively weak interaction to the eukaryote host cells. The ability of these peptides to accumulate at sites of infection combined with the minimal host's cytotoxicity motivated for this review to highlight the role and the usefulness of AMPs for PET with emphasis on their mechanism of action and the different interactions with the bacterial cell. These details are key information for their selective properties. We also describe the strategy, design, and utilization of these peptides as potential radiopharmaceuticals as their combination with nuclear medicine modalities such as SPECT or PET would allow noninvasive whole-body examination for detection of occult infection causing, for example, fever of unknown origin.

1. Introduction

Compared with other conventional technologies, tomographic imaging can evaluate disease processes deep within the body, noninvasively and relatively rapidly. It is therefore not surprising that molecular imaging has powerfully augmented the investigation of various disease processes and has become an essential tool in the field of oncology, for both research and patient care [1]. Another major advantage of imaging is its ability to provide a holistic, three-dimensional assessment of the whole organ or body, less likely to be limited by sampling errors and therefore corelating well with the overall disease process. While continued advances in molecular imaging have provided unparalleled opportunities for more refined methods to monitor diseases, tools for evaluating infection and inflammation remain limited. Two imaging methods, widely used in the clinics currently, include high resolution computed tomography (CT) that measures anatomic (and therefore late) changes or ^{18}F-labeled 2-fluoro-deoxy-D-glucose (^{18}F-FDG)-positron emission tomography (PET), which is a general marker of metabolic activity. As ^{18}F-FDG is also accumulating in sites of infection and inflammation due to the elevated glucose metabolism in these loci [2], thus it is nonspecific for infection. Therefore it became increasingly important to develop more specific and

selective infection imaging agents. Direct, *ex vivo*, labeling of leukocytes is considered the "gold standard" for infection imaging by PET. Unfortunately this process is very laborious and time-consuming and requires the handling of blood products [3–5]. Alternatively, indirectly labeled leukocytes can be achieved using radiolabeled molecules, such as chemotactic peptides or cytokines, that bind to receptors on the leukocytes [3]. Unfortunately the biological effects of some of the leukocyte receptor-targeting compounds have limited their clinical use as infection-specific molecular imaging agents [5]. Although the most commonly labeled leukocytes, neutrophils and lymphocytes, are quite selective for infection, there are cases when they may fail to detect an infection or accumulate in noninfected sites. If the infection fails to elicit an immune response, labeled leukocytes will not accumulate at the infected loci, which may be the case in a severely immune-compromised individual, or in the case of infection by certain pathogens, such as *Mycobacterium tuberculosis* or *Pneumocystis carinii*. Some noninfectious immune conditions, such as rheumatoid arthritis, may also provoke an immune response and accumulate the tracer [3]. Through the use of different tracers, different targeting strategies are possible to image infection using PET.

Tracers that interact directly with the pathogenic microbes responsible for infection are, by nature, highly specific for infection and unlike labeled leukocytes should not accumulate in sterile inflammations. These types of tracers include radiolabeled antibiotics and antimicrobial peptides. Technetium-99m labeled ciprofloxacin (^{99m}Tc-ciprofloxacin) has been the most widely studied antibiotic-based tracer for SPECT infection imaging [6] targeting DNA Gyrase, an enzyme present in all dividing bacteria and is not thought to accumulate in dead bacteria or sterile inflammations. Some problems associated with its use as a tracer in SPECT infection imaging have occurred with regards to poor radiochemical purity and stability [3]. More recently it has been reported that localisation at infected foci takes place primarily through increased extravasation and stasis. This process also occurs at uninfected sites with increased vascular permeability and ^{99m}Tc-ciprofloxacin may accumulate at sites of sterile inflammation thereby reducing its specificity for infection [7].

Antimicrobial peptides (AMP) have attracted interest as potential targeting vectors for the development of PET tracers designed for the detection of infection. These peptides are found in a variety of organisms including humans, and, so far, hundreds have been isolated and characterised. It is believed that these peptides function as broad-spectrum microbicides and form part of the innate immune system of many eukaryotes, including humans. Regardless of their origin, they share many common properties such as having a net positive charge, being amphipathic and, in most cases, are membrane active [8]. Due to their role in the body as a natural microbicide, these antimicrobial peptides are selectively cytotoxic to bacteria, whilst showing minimal cytotoxicity towards cells of the host organism. It is thought that the net cationic nature of the peptides results in a relatively strong electrostatic attraction to negatively charged bacterial cells and a relatively weak attraction to the eukaryote host cells, which are usually less negatively charged than prokaryotes, and is believed to form the basis of this cell-type discrimination [9]. The ability of these peptides to accumulate at sites of infection combined with their almost negligible cytotoxicity or attraction to host cells makes these peptides attractive as targeting vectors for PET imaging of infection [10].

2. Overview of Antimicrobial Peptides

Antimicrobial peptides are evolutionarily conserved biomolecules that form part of the defence mechanisms in many organisms [11], ranging from prokaryotes to multicellular animals such as humans [9]. They form part of the first line of defence against pathogenic microbes in higher animals and in many lower forms of life; they are the only form of defence against pathogenic and saprophytic microbes [12]. The selective cytotoxicity of these peptides, where they attack the pathogenic microbes and leave the host cells unharmed, is due to the fundamental differences in composition and structure of the host cells to those of the pathogenic bacteria and yeasts. Despite some AMPs showing immunomodulatory effects and/or chemotactic behaviour, a common feature of these antimicrobial peptides is that they are amphipathic but possess an overall positive charge [9]. Approximately 1500 antimicrobial peptides have been characterised in a wide range of organisms and classification of these peptides can be complicated due to the high degree of sequence dissimilarity between the various peptides. However, classification has been attempted based on amino acid composition and secondary structures.

Three large groups (Table 1) have been identified, namely, α-helical peptides, cysteine-containing β-sheet peptides, and flexible peptides rich in specific amino acids such as proline, tryptophan, histidine, arginine, and glycine [13].

2.1. α-Helical Antimicrobial Peptides. Approximately 30 to 50% of all antimicrobial peptides identified and studied to date contain predominant α-helical structures. This may be due the relative ease with which these peptides are chemically synthesised, which allows for extensive characterisation in the laboratory. These peptides usually consist of 12–40 amino acid residues and contain an abundance of helix stabilising residues such as alanine, leucine, and lysine but never cysteine. In aqueous solutions these peptides are often unstructured but assume their amphipathic α-helical conformations when associated with a cell membrane or in a membrane mimetic environment. Often these peptides are not strictly α-helices and may contain an internal kink [14].

2.2. β-Sheet Antimicrobial Peptides. The other major group of antimicrobial peptides are those that typically contain two to ten cysteine residues that form one to five interchain disulfide bonds. This bonding interaction allows these peptides to adopt the β-sheet conformation. Most β-sheet antimicrobial peptides are part of the defensin family and these peptides are evolutionarily conserved across plants, fungi, insects, molluscs, and vertebrate animals. Defensins typically consist

Table 1: Representative antimicrobial peptides of different classifications (modified from [13]).

Class	Representatives	Host
α-helical	LL-37	Mammal: human
	Cecropins	Insect: moth
	Melittin	Insect: honey bee
	Magainins	Amphibian: frog
	Fowlicidins	Ave: chicken
β-sheet	Thanatin	Insect: soldier bug
	Tachyplesins	Arthropod: horseshoe crab
	Protegrins	Mammal: pig
	Plant defensin VrD2	Plant: mung bean
	Plectasin	Fungus: ebony cup
	Insect defensin A	Insect: northern blow fly
	α-defensin	Mammal: human
	β-defensin	Mammal: human
	θ-defensin	Mammal: rhesus monkey
Flexible	Indolicidin	Mammal: cow
	Tritrpticin	Mammal: pig
	Histatins	Mammal: human
	PR-39	Mammal: pig

of two to three antiparallel β-sheets stabilized by three to four intramolecular disulfide bonds; however in some cases an α-helical or unstructured segment is found at the N- or C-terminus. Unlike the α-helical antimicrobial peptides, which are unstructured in aqueous solutions, the defensins maintain a compact globular structure under such conditions [12, 13]. Apart from overall similarity in secondary structure, most mammalian-derived α-defensins possess two additional common features, namely, a protruding loop resulting from a conserved arginine/glutamate salt bridge and a β-bulge caused by a conserved glycine-X-cysteine (X: any amino acid) motif between the first and second cysteine residues [13].

2.3. Flexible Antimicrobial Peptides Rich in Specific Amino Acids. A minority of antimicrobial peptides contain a high proportion of certain amino acids such as proline, tryptophan, histidine, arginine, and glycine. Representative members of this class include the tryptophan rich bovine indolicidin and porcine tritrpticin, histidine rich human histatins, and the arginine and proline-rich porcine PR-39. Due to their unusual amino acid compositions, these peptides have highly variable secondary structures. The 13-amino acid indolicidin (ILPWKWPWWPWRR), for example, adopts a largely extended conformation in the presence of zwitterionic micelles composed of substances such as dodecylphosphocholine or anionic sodium-dodecyl sulfate [13].

3. Mechanisms of Cell Specificity and Selectivity of Antimicrobial Peptides

Inherent differences in the microbial versus the host cell membrane composition and architecture aid selectivity of the antimicrobial peptides. Regulation of expression or localisation of the peptides is also thought to prevent unwanted interactions with vulnerable host cells.

3.1. Target Specificity and Selective Cell Toxicity. A biological membrane can be thought of as simply a fluid mosaic consisting of phospholipids interspersed with proteins. In different organisms glycerides and sterols may also contribute to the biochemical architecture and surface topology of such membranes. There are, however, fundamental differences that exist between microbial and animal cell membranes that allow the antimicrobial peptides to distinguish between these cells and selectively target one over the other as sketched in Figure 1 [9].

3.2. Membrane Composition, Charge, and Hydrophobicity. The core component of almost all natural biomembranes is the phospholipid bilayer. These bilayers are amphipathic, meaning they have both hydrophobic and hydrophilic regions. However, eukaryotic and prokaryotic cell membranes differ significantly in terms of exact composition and cell energetics (Figure 2). Phosphatidylcholine (PC) and its analogue sphingomyelin (SM) as well as phosphatidylethanolamine (PE) have no charge under physiological conditions [9]. Cholesterol and other sterols such as ergosterol which are abundantly found in eukaryotic membranes, but very seldom in prokaryotic membranes, are also generally neutrally charged (Figure 2) [15]. Hydroxylated phospholipids such as phosphatidylglycerol (PG), cardiolipin (CL), and phosphatidylserine (PS) possess a net negative charge under physiological conditions. It can be seen how the charge of the membrane is mainly due to the ratio and location of the various phospholipids, with cell membranes comprising mostly PG, CL, and PS, as is the case in most pathogenic bacteria, being very electronegative, whereas those membranes that are rich in PC, PE, or SP tend to have a net neutral charge, as is the case in mammalian cell membranes [15, 16].

3.3. Membrane Asymmetry. Although cellular membranes are neither symmetric nor static, differences between mammalian and microbial phospholipid bilayers can serve as potential targets for antimicrobial peptides. In some cells such as the bovine erythrocyte, only 2% of the total PE content is located on the outer membrane leaflet [13]. Differences in membrane symmetry, saturation of phospholipid bilayers, and compositional stoichiometry will influence the membrane's fluidity and phase transition. In a similar manner, the charge of the inner and outer leaflets of the cellular bilayer may also be different [15].

3.4. Microbial Ligands and Receptors as Targets for Antimicrobial Peptides. Experiments have shown that D-and L-amino acid versions of antimicrobial peptides exhibit similar binding affinities to targets cells, suggesting that stereospecific receptors are not involved in targeting pathogenic cells [9]. However, several studies appear to refute this and suggest that certain proteins located in the microbial cell membrane may serve as binding targets for certain classes of

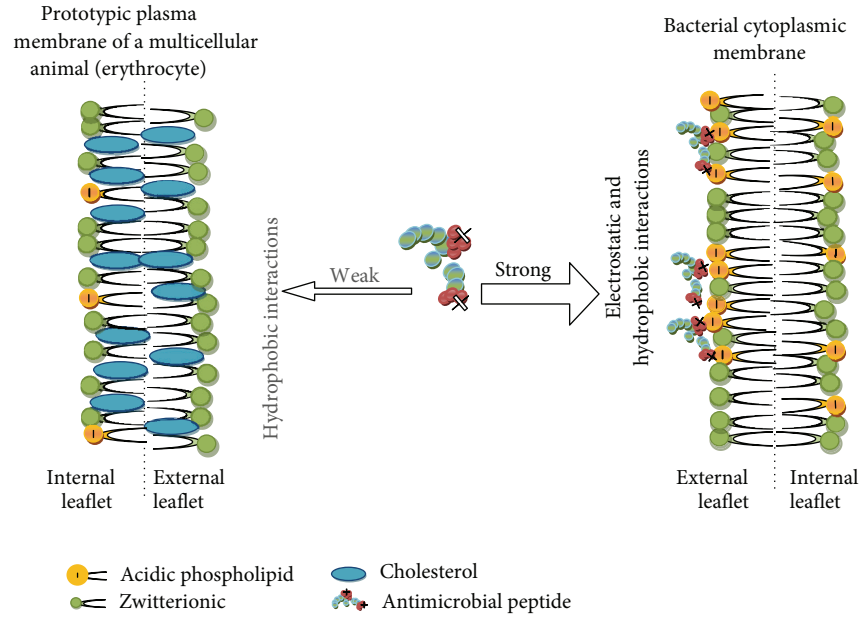

Figure 1: Membrane targeting of antimicrobial peptides and basis of their selectivity (adapted from [45]).

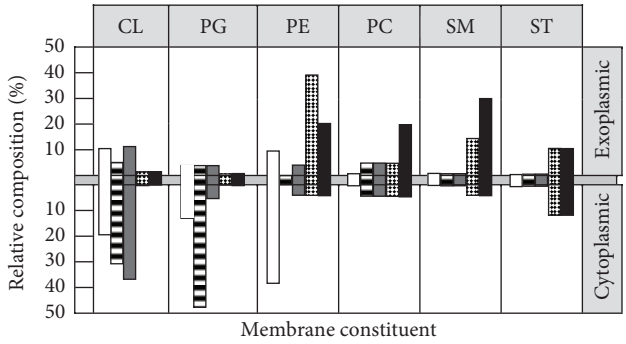

Figure 2: Comparative lipid architecture of microbial and human cytoplasmic membranes. Cytoplasmic membranes of bacterial (*Escherichia coli*, *Staphylococcus aureus*, or *Bacillus subtilis*) and fungal (*Candida albicans*) pathogens are compared with that of the human erythrocyte in relative composition and distribution between inner and outer membrane leaflets. Membrane constituents ranging from anionic (left) to neutral (right) are CL, PG, PE, PC, SM, and sterols (cholesterol or ergosterol, ST). Note the marked difference among microbial pathogens and human erythrocytes resides in the phospholipid composition and asymmetry. These differences are believed to account for the selective antimicrobial peptide affinity for microbial versus host cells to the extent that it exists for a given antimicrobial peptide. Keys: open, *E. coli*; horizontal hatching, *S. aureus*; shaded, *B. subtilis*; checkered, *C. albicans*; solid, human erythrocyte (adapted from [9]).

antimicrobial peptides such as histatins. This would support the findings why histadins are involved in local defence mechanisms with particular type of pathogens and have been recovered in dental or skin wounds. Some researchers also postulate that anionic components of cell membranes, for example, CL, PG, or lipopolysaccharide (LPS), may serve as pseudoreceptors, enabling the initial interaction between the antimicrobial peptide and the microbial cell target [13]. Hence, antimicrobial-binding receptors may be an alternative pathway of AMP interaction with the bacterial cell envelop.

3.5. Transmembrane Potential. The transmembrane potential is yet another way in which microbial and mammalian cells vary and it is in the charge separation that exists between the inner and outer layers of the cytoplasmic membrane. An electrochemical gradient, resulting from the differing rates or proton exchange across the cell membrane, is referred to as the transmembrane potential ($\Delta\psi$). A normal mammalian cell has a $\Delta\psi$ between −90 and −110 mV in range. Pathogenic bacteria, however, generally exhibit $\Delta\psi$ in the −130 to −150 mV range. This significant difference in electrochemical potential may be another factor that allows antimicrobial peptides to distinguish between host and target cells [9].

4. Selective Toxicity Based on Antimicrobial Peptide Design

In the aqueous intercellular environment, many antimicrobial peptides are believed to adopt extended or unstructured conformations, although this may not be the case if there are intramolecular bonds present, which will ensure a specific conformation in a variety of environments due to induced rigidity. Once the antimicrobial peptide binds to the cell membrane of a pathogenic microbe, it may undergo significant conformational change and adopt a specific conformation, such as a α-helix. Studies suggest that dynamic and/or inherent conformations of antimicrobial peptides have an effect on their selective cytotoxicity [9, 17, 18]. Additionally, antimicrobial peptides may undergo conformational transition, self-association, or oligomerization within the target

pathogen membrane, but not the host cell membrane to increase cell-specific toxicity [13]. Zhang and coworkers [16] employed synthetic test peptides that were uniformly cationic but varied in conformation and included extended, cyclic, α-helical, and β-sheet structures. It was determined that all test peptides were able to interact with and penetrate lipid monolayers composed of PG, a negatively charged phospholipid. However, only the α-helical and extended peptides were able to interact with the more neutrally charged PC membrane. In the same study it was also found that β-sheet peptides were able to translocate phospholipids from the inner to the outer leaflet at concentrations that were lower than those that were required to permeabilize the membrane. Similarly, Kol and coworkers [19] showed that peptides with comparable conformation, but rich in histidine and lysine and lacking in tryptophan, were also able to induce significant levels of phospholipid translocation. It can be concluded from these studies that not only do antimicrobial peptides interact with phospholipid membranes of only specific composition and symmetry, but they are also able to affect remodelling of the membranes in specific cells.

4.1. In Vivo Preferential Affinity for Microbial versus Mammalian Cells. Welling and colleagues [20] conducted an *in vivo* experiment where they tested the binding affinity of a radiolabeled fragment of the cationic ubiquicidin antimicrobial peptide ^{99m}Tc-UBI 29–41 for microbial cells as compared to host cells. In the study, animals were infected with *Candida albicans*, *Klebsiella pneumonia,* or *Staphylococcus aureus*. Sterile inflammations were also induced in the thigh muscles of animals through injection of heat-killed microorganisms or purified LPS, to serve as controls. The radiolabeled peptides accumulated to a significant extent in the infected sites relative to sterile or noninfectiously inflamed parts of the body. This *in vivo* experiment demonstrated that the peptides could distinguish between host and microbial cells and also accumulate at the infected sites. Through scintigraphic measurements it was determined that the radiolabeled peptides accumulated in infected tissues at a rapid rate and that there was up to a fivefold increase in rates of accumulation in infected tissues relative to noninfected tissues. This rapid localization was interpreted as the peptides having a higher or preferential affinity for the target cell surface relative to that of the host cell surface.

4.2. Localisation of Cytotoxic Antimicrobial Peptides Limits Exposure of Vulnerable Host Tissues. It is possible that host cell cytotoxicity is reduced in many multicellular organisms due to their localization to tissues that are not vulnerable to their cytotoxic effects. In most animals these peptides are secreted by cells onto relatively inert and robust surfaces such as the epithelia of the intestines or lung, or in amphibians, onto the skin. These localities are most likely to interact with potentially harmful microbes most frequently, and the expression of most of the antimicrobial peptides is either constitutive or rapidly inducible, to allow them to form part of the first defences against pathogens [9]. Another means of protecting sensitive host tissues from antimicrobial peptides is by containing them within granules in the phagocyting leukocytes, which engulf pathogens and expose them to lethal concentrations of antimicrobial peptides and oxidizing agents. The defensin class of antimicrobial peptides is deployed in this way, since they are some of the most toxic and least selective of the host produced antimicrobial peptides. The slightly acidic microenvironment within the mature phagolysosome is also the most effective environment for the defensins, as they exhibit maximum cytotoxicity under these conditions [12].

5. Mechanisms of Antimicrobial Peptide Action

The generally conserved structures of antimicrobial peptides, across a wide variety of organisms, lend some clues as to their mechanisms of action. They are almost exclusively amphipathic and cationic under physiological conditions, and this is believed to aid their target cell selectivity. The ideal antimicrobial peptide should have low host cell cytotoxicity but be toxic to a wide range of pathogenic microbes. The antimicrobial determinants should be easily accessible and should not be prone to change or alteration. In general, antimicrobial peptides have amphipathic structures that allow them to interact with phospholipid membranes, structures that are essential to all pathogens [17]. Parameters such as conformation (X), hydrophobicity (H), hydrophobic moment (M_H), charge (Q), polar angle (θ), and amphipathicity (A) are all important to the functioning of antimicrobial peptides. Furthermore, all these determinants are interrelated and modification of one of these features will lead to alteration of the others [9].

5.1. Conformation (X). Although antimicrobial peptides may be found in a wide range of host organisms and have differing amino acid sequences, they can be classified into a few discrete groups based on their secondary structure. The two largest groups include peptides that possess a β-sheet or α-helical secondary structure. The majority of the remaining antimicrobial peptides are those that have an unusually high proportion of one or more amino acids such as tryptophan or proline and arginine. The α-helical peptides are frequently found in the intercellular fluid of insects and amphibians and generally adopt an unstructured or extended conformation in aqueous solution, only adopting their helical structure upon interaction with a phospholipid membrane [21]. The reason for this is that the intramolecular hydrogen bonding required for an α-helic conformation is disrupted in a polar solvent such as water. In a membrane, the polar hydrogen bonding groups are shielded from lipophilic (apolar) membrane environment through α-helic formation. The helix conformation also exposes the apolar side chains to the neutral lipid environment inside the membrane. Although the primary structure of the β-sheet class of antimicrobial peptides shows a level of dissimilarity in amino acid sequence, they all share common features with regard to amphipathic structure, possessing distinct hydrophilic and hydrophobic domains [9].

5.2. Charge (Q). Most of the antimicrobial peptides are overall cationic and have charges ranging from +2 to +9, with many possessing highly defined negatively charged domains. This positive charge is important for the initial attraction to and interaction with the anionic cellular membranes of bacteria and other pathogenic microorganisms. Likewise the relatively less anionic membranes of the host do not electrostatically attract the antimicrobial peptides and may confer some target cell selectivity to the peptides. Pathogenic bacteria are generally rich in acidic phospholipids such as CL, PG, and PS. Additionally the teichoic and teichuronic acids of the cell walls of *Gram*-positive bacteria and the LPS of *Gram*-negative bacteria confer additional electronegative charge to the bacterial cell surface. It has been determined that the $\Delta\psi$ of bacteria is typically 50% higher than that of mammalian cells and it has been proposed that antimicrobial peptides may be concentrated onto the surface of pathogenic microbes in an electrophoretic manner [22]. Although many studies were able to correlate the cationicity of antimicrobial peptides with their antimicrobial activity, a strictly linear relationship does not exist. Dathe and coworkers [23] demonstrated in studies with analogues of magainin that increasing the cationicity from +3 to +5 resulted in an increase in antibacterial activity against both *Gram*-positive and *Gram*-negative species. They did, however, note that there was a limit to cationicity, after which any increases in positive charge no longer increase antibacterial activity. It is believed that this decrease in antibacterial activity may have been due to the peptides binding so strongly to the negatively charged phospholipid head group that translocation of the peptide into the cell was impossible [9].

5.3. Amphipathicity (A) and Hydrophobic Moment (M_H). Amphipathicity is a nearly universal feature amongst antimicrobial peptides and is achieved through a number of different peptide structures. The amphipathic α-helix is one of the most common and simplest of these features. By alternating anionic and cationic amino acid residues at every three to four positions the peptide is able to adopt a secondary structure that allows for optimal electrostatic interaction with amphipathic phospholipid membranes (Figure 3). This feature allows the peptide to exert cytotoxic activity towards not only negatively charged cell membranes but also those with a neutral charge or amphipathic nature [14].

Amphipathicity of a peptide can be described by its hydrophobic moment (M_H) which can be calculated as the vectorial sum of individual amino acid hydrophobicities, normalized to an ideal helix. An increase in hydrophobic moment correlates to increased permeabilization of the target cell membrane. This is especially significant in interactions with lipid membranes that are neutrally charged, where charge factors are unlikely to bring about the required attraction to and interaction with the target cell membrane [17]. Like the α-helical antimicrobial peptides, the β-sheet host defence peptides also exhibit amphipathicity. This is manifested as varying numbers of β-strands organised to form hydrophobic and hydrophilic surfaces. The β-strands, which are often antiparallel, are stabilised by regularly spaced disulphide bonds or by cyclisation of the peptide backbone. This intramolecular bonding allows β-sheet antimicrobial peptides to maintain a rigid conformation even in aqueous extracellular fluid and also facilitates multimerization, as the hydrophobic surfaces will cluster together to avoid exposure to the aqueous environment. Although the exact mechanisms by which amphipathic antimicrobial peptides bring about membrane disruption in the target cell membrane is undetermined at present, largely because the exact conformation of the peptides in the membranes is not known, studies have shown that segregated amphipathicity in both α-helical and β-sheet antimicrobial peptides has a profound effect on peptide disruption of natural biomembranes [9].

5.4. Hydrophobicity (H). The hydrophobicity of a peptide may be defined as the percentage of hydrophobic amino acid residues making up its primary structure. For most antimicrobial peptides the hydrophobicity is around 50% and is essential for the functioning of the peptide as it allows the peptide to interact with and penetrate into the phospholipid bilayer. Although a certain amount of hydrophobicity is essential for the functioning of the antimicrobial peptide, excessive hydrophobicity will increase its likelihood of destroying the host's cells and reduce its specificity for microbial cells [24]. Wieprecht and coworkers [25] studied the relationship between the hydrophobicity of peptides and their ability to permeabilize biomembranes. Using magainin analogues as model antimicrobial peptides, they were able to keep factors such as hydrophobic moment, helicity, and charge nearly constant, whilst producing analogues of variable hydrophobicity. Their experiments showed that hydrophobicity had little or no effect on the peptide's ability to bind to or permeabilize the membrane when it consisted exclusively of PG. However, in membranes consisting of a 3 : 1 ratio of PC : PG, the peptides with the highest hydrophobicity had an approximately 60-fold higher permeabilizing ability than the least hydrophobic peptide, and in membranes composed of only PC there was a 300-fold difference.

5.5. Polar Angle (θ). A peptide's polar angle refers to the relative proportion of polar to nonpolar facets of the peptide conformed to an amphipathic helix. A helical peptide with one facet composed entirely of polar amino acid residues and the other facet composed entirely of nonpolar residues would have a polar angle of 180°. Less segregation between the domains, or an overabundance of hydrophobic residues, would lead to a lower polar angle. Studies conducted by Uematsu and Matsuzaki [26] on both synthetic and naturally occurring peptides have shown that a lower polar angle and therefore a more hydrophobic facet is more conducive to membrane permeabilization. Polar angle has also been correlated with the stability of peptide induced pores in biomembranes. They also demonstrated that antimicrobial peptides with smaller polar angles were able to induce higher degrees of membrane permeabilization and translocation at higher rates than peptides with greater polar angles. However, the pores formed by the peptides with smaller polar angles were less stable than those formed by peptides with greater

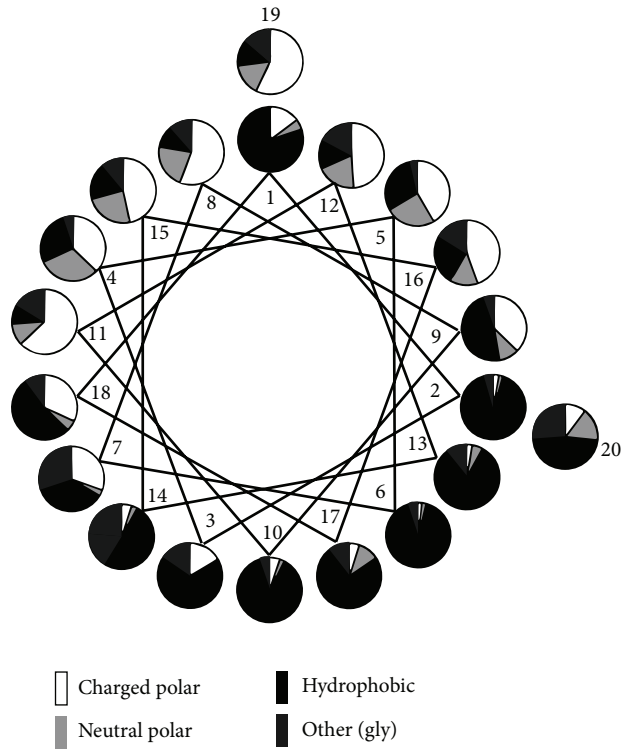

Figure 3: Statistical analysis of residue distribution in the 20-residue N-terminal stretch α-helical AMPs from natural sources. A graphical representation of the frequency of different types of residue at each position on a helical wheel projection is shown. The uneven distribution of hydrophobic and charged peptides contributes to the amphipathic nature of the peptide (adapted from Tossi et al. [17]).

polar angles. Hydrophobic and hydrophilic properties of antimicrobial peptides can be seen to play vital roles in the interactions with and permeabilization of phospholipid cell membranes [18].

5.6. Common Structural Features of Antimicrobial Peptides. Whilst a wide variety of antimicrobial peptides do exist in nature, conservation of key features and secondary structures has been noted. Extremes of features such as amphipathicity, charge, hydrophobic moment, or polar angle are not beneficial since they tend to compromise either antimicrobial activity or lead to increased host cell cytotoxicity. The minimum charge that peptides may possess in order to exert any kind of antimicrobial activity appears to be +2. This minimum cationicity is important because it allows for the initial electrostatic attraction to the bacterial membrane, which is negatively charged. It also allows for the displacement of any other cations that may already be bound to the target cell membrane and for the translocation into the interior of the membrane bilayer. Similarly, the hydrophobicity of the peptide should be moderate, since very hydrophobic antimicrobial peptides would target membranes with a net-neutral charge, such as the host cells, leading to a reduction in target selectivity and damage to the host organism. It can be seen that selective targeting of pathogenic microbes is largely due to a balance between electronegativity and hydrophobicity of the antimicrobial peptides [9].

6. Initial Interactions with the Targeted Cellular Membrane

The initial interaction between the antimicrobial peptide and the cell's phospholipid membrane is important as it determines target cell selectivity and also influences any subsequent interactions with the target cell. The initial interactions are largely determined by physical and chemical features of both the antimicrobial peptide and the target cell membrane [12].

6.1. Electrostatic Interactions. Electrostatic interactions are widely believed to be responsible for the initial targeting of the microbial cell. A study by Matsuzaki [27] correlated antimicrobial peptide cationicity with membrane binding ability, and the fact that cationicity is a conserved feature of almost all antimicrobial peptides in a wide range of organisms further supports this argument. Electrostatic forces act over a long range and the abundance of lysine and arginine residues in antimicrobial peptides, which are attracted to the negatively charged phosphate groups of biomembranes, lends further credibility to the theory that these interactions are responsible for the initial attraction to the target cell membrane [12]. In *Gram*-negative bacteria it is believed that the antimicrobial peptides displace cations that are normally associated with the LPS, since antimicrobial peptides possess a binding affinity for the LPS that is approximately three orders of magnitude greater than the divalent cations usually

associated with this moiety. Strains of bacteria where the LPS is highly substituted with 4-amino-4-deoxy-L-arabinose or is highly acylated show greater resistance to positively charged antimicrobial peptides, lending further credibility to the theory that electrostatic charge is important for interaction with the target cell membrane [28]. *Gram*-positive bacteria lack an LPS or outer cell membrane, but they do have a thick cell wall made up of teichuronic or teichoic acid polymers. These highly anionic structures are ideal targets for the cationic antimicrobial peptides. Strains of *Staphylococcus aureus* where the teichoic acids have been modified, resulting in increased anionic charge, are more susceptible to cationic antimicrobial peptides [29–31]. The fact that most bacteria have a strong electrochemical gradient ($\Delta\psi$) relative to mammalian cells is also thought to increase target selectivity of antimicrobial peptides [9].

6.2. Receptor-Ligand Interactions with the Membrane. Some studies have shown that both naturally occurring and synthetic peptides interact with the membrane equally well regardless of whether D-amino or L-amino acids are used [32, 33]. This would suggest that interactions with biomembranes are not dependant on receptor-ligand mechanisms; however, other studies have shown that this may not be the case with all antimicrobial peptides. Nisin, a naturally occurring, cyclic peptide with powerful antimicrobial action has been found to bind specifically to bacterial membrane bound lipid II [34, 35]. Similarly, tachyplesin has been shown to have a specific affinity for LPS. The data from these studies suggests that receptor mediated binding is important for cell targeting in a small number of antimicrobial peptides [34].

7. Events following Initial Membrane Binding

Experimental determination of initial attraction of peptides to and interaction with cellular membranes is usually simpler than determination of interactions that follow this. A variety of methodologies such as circular dichroism [22, 36], X-ray crystallography, nuclear magnetic resonance [37], reverse phase-high performance liquid chromatography, and surface plasmon resonance [22], amongst other techniques, have been used to elucidate peptide-membrane interactions. However, it is suggested that the antimicrobial efficacy and mechanisms are extremely sensitive to conditions such as pH, osmotic strength, solution viscosity, and temperature, so any data obtained by the above mentioned techniques must be viewed with regard to these conditions [9]. Subsequent to the initial membrane binding, antimicrobial peptides penetrate the outer phospholipid membrane, a phase referred to as threshold concentration, and in doing so is able to exert their cytotoxic effects in the interior of the cell. The entry into the cell by the peptides requires a minimum number, or threshold concentration of antimicrobial peptides to accumulate on the surface of the lipid membrane. This event can be affected by factors other than concentration such as the ability of the peptides to multimerize and also features of the phospholipid membrane itself, such as its lipid composition, head group size, and fluidity [38]. The transmembrane potential of the bilayer may also influence the way in which the peptide enters the membrane, since a highly negative transmembrane potential will facilitate pore formation by drawing the positively charged peptide into the membrane [39].

8. Changes in Peptide Conformation upon Interaction with the Membrane

Many antimicrobial peptides, especially those with α-helical secondary structures undergo significant conformational rearrangement upon entering the nonpolar environment of the inner membrane. The α-helical antimicrobial peptides are normally disordered in the extracellular environment, exhibiting random coil or extended structures, but rapidly conform to a structured α-helix when associated with the biomembrane [18]. Some antimicrobial peptides can only undergo this conformational change in association with a negatively charged bilayer membrane. This may be due to the way the lipids are arranged in such membranes, with the phospholipid head groups inducing optimum periodicity of the cationic amino acid residues in the peptide, which in turn promotes correct conformation into the helical secondary structure [40, 41]. It has been suggested that this feature ensures that the antimicrobial peptides will only be "activated" into the cytotoxic form in the presence of the target cell membrane, in this case a negatively charged bacterium, and will not indiscriminately damage nontarget host cells [17]. The intramolecular disulphide bonds found in β-sheet peptides ensure that they maintain their secondary structure even in aqueous environments, and so they do not undergo the drastic conformational rearrangements seen in α-helical peptides, although quaternary peptide structures may disassociate upon entering the membrane, and this could facilitate selective toxicity [9]. Following the initial interaction with the cell membrane, many peptides may undergo self-association which, when combined with lipid-peptide interactions, may lead to the creation of complex structures that contribute to the cytotoxic effects of the peptide. The antimicrobial peptide's amino acid sequence and conformation in the monomer form will dictate its ability to form these structures. In amphipathic peptides, the hydrophobic domains are able to interact with the nonpolar hydrophobic core region of the lipid bilayer thereby driving the peptide deeper into the membrane. Alternatively they could also interact with the hydrophobic facets of other peptides, promoting multimerization in an attempt to avoid exposure of these facets to the aqueous environment. This type of multimerization and interaction with the interior of the lipid bilayer may result in peptide lined pores or channels being formed in the biomembrane, resulting in loss of integrity and permeabilization. Since biomembranes are highly variable in composition and structure, it is possible that a peptide may behave in a number of different ways when associated with different cellular membranes [9]. Several models have been proposed to describe the pore formation observed in membranes that have been exposed to antimicrobial peptides.

8.1. The Barrel-Stave Model. This mechanism of membrane pore formation is so named because the transmembrane peptides, or peptide complexes, lining the channel are positioned in a barrel-like ring, with the peptides forming transmembrane staves. Amphipathic peptides are oriented so that the hydrophobic domains interact with the nonpolar hydrocarbon tails located in the interior of the lipid membrane, whereas the hydrophilic domains are oriented so that they face the aqueous channel of the pore and form its lining [24]. Initially the monomer peptides accumulate at the cell surface and undergo conformational rearrangement when they contact the membrane (Figure 4). This is thought to force the phospholipid head groups aside and induce thinning of the membrane. This allows the hydrophobic part of the peptide to enter into the nonpolar interior of the membrane, whilst the cationic amino acids of the antimicrobial peptide interact with the negatively charged head groups. When the threshold concentration of the peptides is reached the peptide monomers are able to aggregate to form multimers which further forces the peptides into the hydrophobic centre of the membrane, as the aggregation prevents the hydrophilic parts of the peptide from being exposed to the hydrophobic parts of the inner membrane (Figure 4(a)). As ever increasing numbers of peptide monomers aggregate, the pore in the membrane is expanded [9, 24].

8.2. The Toroidal Pore or Worm-Hole Mechanism. This mechanism of pore formation has been well studied using the α-helical magainin peptides. Upon contacting the charged cellular membrane, the disorganised peptides take on the α-helical structure. Initially the helices orientate themselves so that they are parallel with the surface of the membrane. The polar phospholipid head groups are displaced and the surface of the membrane is weakened, resulting in a positive curvature strain in the membrane. As a result of this strain and thinning, the membrane is destabilised and becomes more susceptible to further peptide interactions. Once a threshold concentration of peptides is reached the peptides reorientate so that they are perpendicular to the membrane and begin to multimerize so that the hydrophilic parts of the peptides are not in contact with the hydrophobic parts of the membrane (Figure 4(b)). The newly formed toroidal pore is unstable and upon disintegration some of the peptides are forced into the inner leaflet of the cell membrane. It is therefore believed that the disintegration step of these transient pores is important as it allows the peptides to translocate into the intracellular space, where they may act on other targets [42].

8.3. The Carpet Model. The carpet model of membrane permeabilization is based on diffuse action by many monomer peptides on the cellular membrane. When sufficiently high concentrations of certain antimicrobial peptides are present on the cell membrane some of the phospholipids of the membrane are displaced which results in changes to the membranes fluidity or brings about weaknesses in the barrier properties of the membrane. The cumulative effect of these displacements is that the membrane is weakened and loses its integrity. As suggested previously, the initial attraction of the antimicrobial peptides to the membrane is through electrostatic attraction forces. No specific channels or pores are formed, and it is believed that permeabilization and loss of membrane integrity are through the unfavourable energetic properties that dispersion of the phospholipids brings about (Figure 4(c)) [22].

9. Impact of Bacterial Infections to Human Health and Traditional Methods of Infection Diagnosis

It is estimated that up to 85% of patients that are critically ill in hospital have a fever but display no other outward sign of infection. Since prolonged episodes of fever can be fatal, it is essential that any underlying infection is detected as soon as possible, so that the correct treatment regime can be initiated [43]. Traditional methods of diagnosis may include examination of tissue biopsies and attempting to culture pathogens, an often inaccurate and time-consuming task which can delay the onset of treatment. Diagnostic imaging procedures are also employed and may include computed tomography (CT) scanning or magnetic resonance imaging (MRI). However, these techniques are generally not able to detect early stage infections as they require morphological changes in the tissues to take place, a feature usually associated with advanced infections [44]. Furthermore, they are generally focussed on specific parts of the body, meaning that it is possible that the infection may be missed, or the true extent of the infection may not be detected. Gallium-radiolabeled antibodies or -immunoglobulins or complexes such as $^{67/68}$Ga-citrate may be employed to highlight regions where leukocyte trafficking is occurring using SPECT or PET scanning. However, these technologies are unable to definitively distinguish between infected tissues and those that are inflamed but sterile, since leukocyte trafficking occurs in both cases [44]. Given the high specific affinity of naturally occurring antimicrobial peptides for pathogenic bacteria or fungi, as opposed to cells of the host organism, it was envisaged that they may be employed to aid the resolution of diagnostic imaging processes [45].

9.1. The Use of Antimicrobial Peptides as Radiopharmaceuticals. Ideally, a radiopharmaceutical employed for infection imaging should allow for rapid detection of bacteria and rapid clearance from the noninfected sites. It should also exhibit high and specific uptake at the infected site, with minimal amounts accumulating in sterile or nontarget tissue. The compound should also have low toxicity and not induce an immune response. Very importantly, it should be able to distinguish between a sterile and an infected inflammation [45]. Since antimicrobial peptides generally show a broad spectrum of activity against a wide range of pathogenic yeasts and bacteria they are ideal targeting molecules for infections where the suspected pathogen has not been identified. Additionally their mode of action requires them to physically associate with the pathogen, and so they would be able to bring a gamma or positron emitting source, such as

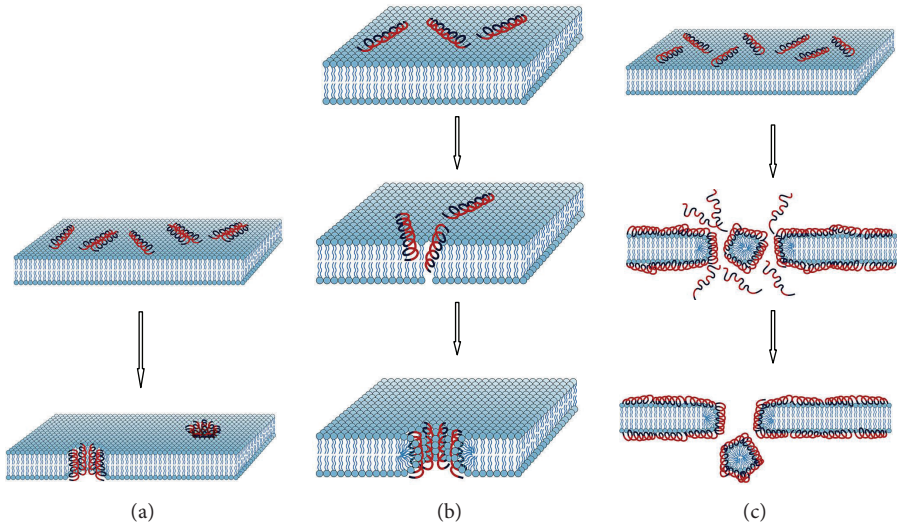

Figure 4: Overview of possible interaction mechanism following peptide interaction with the bacterial cell membrane [53], that is, (a) barrel-stave model (pore formation), (b) toroidal model (pore formation), and (c) carpet model (membrane disruption). Red coloured peptide regions: hydrophilic; blue coloured peptide regions: hydrophobic.

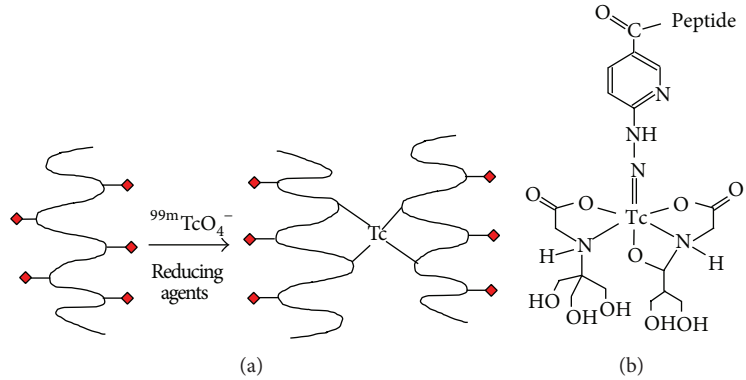

Figure 5: Approaches in radiolabeling of peptides. The direct method (a) where radionuclides are covalently attached to the peptide and the indirect method (b) where radionuclides are attached to targeting peptides by means of bifunctional chelators [8].

technetium-99m (99mTc) or gallium-67 (^{67}Ga), to the exact location of the infection. Their lack of affinity for the host organism's cells also means that they would not accumulate in sterile inflamed tissues. Radiolabeled antimicrobial peptides are also attractive because they are cleared rapidly from the circulatory system and excreted by the body. In addition they are also able to penetrate the extravascular tissues and thereby accumulate at infected sites in a very short space of time [46]. Ideally, the radiolabeling procedure of a targeting molecule should allow for the firm attachment of a radionuclide to the molecule without it adversely affecting its targeting ability or the pharmacokinetics of the molecule. Labelling approaches can either be direct or indirect as follows.

(i) A direct labelling (Figure 5(a)) approach involves incorporation of the radionuclide onto the targeting molecule *via* a covalent bond. In the case of peptide targeting molecules a covalent bond may be formed between the radionuclide and a suitable free amide residue of Lys and Arg [47]. Using the tyrosine residue may cause problems associated with labelling including nonspecific or poor binding, *in vivo* instability of the complex, and unwanted alterations to the peptide structure, such as the cleaving of internal disulphide bonds, which can alter its functioning [8].

(ii) An indirect labelling strategy can be used through addition of chelating agents to the targeting molecule (Figure 5(b)) [8]. Bifunctional chelates have been used to label peptide carrier molecules with radionuclides. The chelating agent may be preloaded with the radionuclide prior to being bonded to the carrier moiety, or it could be firstly attached to the carrier molecule and then exposed to the nuclide for chelation in a process known as postlabelling. Postlabelling has the advantage that the carrier molecule can be stored for a long period of time until needed, and the radionuclide, which undergoes decay, can

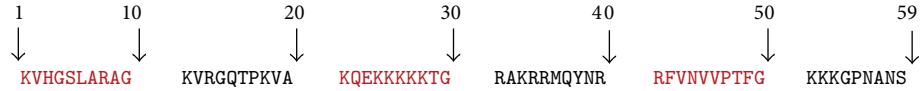

Figure 6: Primary structure of ubiquicidin as originally reported by Hiemstra and coworkers [49].

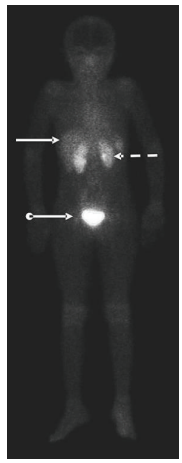

Figure 7: Anterior whole-body image taken at 30 min after tracer injection showing kidneys (dotted arrow), liver (solid arrow), and urinary bladder (ball arrow) (adapted from [52]).

be added shortly before the radiopharmaceutical is administered. This benefits commercialisation of the carrier molecule and makes the technology easier to use in hospitals or clinics [48].

9.2. Ubiquicidin Exemplifies an Approach for Antimicrobial Peptide Derived Radiopharmaceuticals. The 59-amino acid residue antimicrobial peptide ubiquicidin (UBI) is a 6.7 kDa peptide that was first discovered in cytosolic extracts of the murine macrophage (Figure 6). This peptide was shown to exhibit antimicrobial effects against *Salmonella typhimurium* and *Listeria monocytogenes*. It was subsequently found in a wide range of other organisms, including humans [49]. Since it occurs naturally in man, ubiquicidin is not an immunogenic entity, which makes it suitable for administration as a diagnostic tool. It also has high affinity for bacterial cells but does not target mammalian cells, rendering it nontoxic to the patient and selective in that it is unlikely to accumulate at sterile inflammation sites [50]. Several studies have been performed on fragments of ubiquicidin both *in vitro* and *in vivo* to assess its ability to bind to bacterial cells.

Welling and coworkers [51] evaluated the whole ^{99m}Tc labeled ubiquicidin and various radiolabeled fragments of the peptide, including UBI1-18 (KVHGSLARAGKVRGQTPK), UBI29-41 (TGRAKRRMQYNRR), UBI18-29 (KVAKQEKK KKKT), UBI 18–35 (KVAKQEKKKKKTGRAKRR), UBI31-38 (RAKRRMQY), and UBI22-35 (QEKKKKKTGRAKRR) for their ability to bind to bacterial cells and/or human leukocytes *in vitro*. They found that the ubiquicidin peptide fragments UBI 18–35, UBI 31–38, UBI 22–35, and UBI 29–41 showed considerably higher binding affinities for the bacterial cells than they did for the human leukocytes. The *in vivo* results, obtained by scintigraphy of experimentally infected mice following intravenous administration of the various radiolabeled peptides showed that the UBI18-35 and UBI29-41 peptides appeared to be the most promising candidates. After a postadministration period of 2 h and 24 h, the leukocyte to bacteria binding ratios were 1 : 36, 1 : 166, and 1 : 73, 1 : 220 for UBI18-35 and UBI29-41, respectively. The researchers concluded that UBI29-41 and UBI18-35 were the optimal peptides for distinguishing infections from sterile inflammations.

9.3. Human Clinical Trials of ^{99m}Tc-Ubiquicidin 29–41 as an Infection Imaging Agent. Akhtar and coworkers [52] studied the efficacy of ^{99m}Tc-UBI 29–41 as an infection imaging agent in eighteen patients with suspected prosthetic or soft tissue infections. Using scintigraphy to monitor the radiolabeled peptide, the researchers were able to monitor the target to nontarget (T/NT) ratios of the imaging agent. Infection in the patients was confirmed through culture of bacteria from the infected site, or where this was not possible through complete blood examination. The study found that all patients tolerated the radiolabeled peptide well, no significant changes to their vital signs were noted, and no related side effects were seen following the administration of the ^{99m}Tc-UBI 29–41. The T/NT ratio was determined at 30, 60, and 120 minutes, with the 30-minute scan showing the highest mean T/NT value. The anterior whole-body scan (Figure 7) gave information about the biodistribution of the tracer and its routes of elimination by the body. It can be seen that the tracer is mostly eliminated by the urinary system and also some perfusion-dependant liver activity was noted. The imaging agent was found to have a sensitivity of 100% and a specificity of 80%. The researchers concluded that the ^{99m}Tc-UBI 29–41 had a positive predictive value of 92.9%, a negative predictive value of 100%, and an overall diagnostic accuracy of 94.4%. The radiolabeled peptide displayed efficacy against a range of different bacteria, including *Pseudomonas aeruginosa*, *Staphylococcus aureus,* and *Streptococcus pyogenes*. It was the opinion of the researchers that ^{99m}Tc-UBI 29–41 is a highly sensitive and specific imaging agent for detecting soft tissue and bone infections in humans.

10. Discussion and Perspective

The usage of nuclear medicine modalities such as SPECT or PET allows clinicians for noninvasive whole-body examination of physiological processes such as occult infection at cellular level and, apart from being a useful tool for physiological and medical research, these highly sensitive technologies are capable of detection of diseases without, or

prior to, anatomical change (fever of unknown origin). To date, radiolabeled leukocytes, monoclonal antibodies against cytokines/leukocytes, and tracers associated with specific molecular targets or metabolic processes are utilized [54]. Radiolabeled leukocytes have a spectrum of limitations (alteration of leukocyte function due to radiation damage), that is, they have a cumbersome pharmakokinetic and are also relatively nonspecific. Moreover, labeled leukocytes and high molecular weight tracers such as antibodies may also have limited penetration into infected or diseased tissues. The latter presented overview which clarifies the widespread potential of AMPs to be evaluated as imaging probes, given their unique selective involvement with bacteria. A simple literature query, searching for "antimicrobial peptides" resulted in ca. 6000 publications. However, as soon as the query is combined with the term "imaging", it resulted in only 63 publications; only 17 of those have clinical relevance (^{99m}Tc-UBI-29-41 related studies/trials). This is an important observation as this ubiquicidin fragment may represents a near-perfect carrier for targeting molecules for infection detection. The human clinical trials conducted by Akhtar and coworkers [52] with ^{99m}Tc-UBI 29–41 did not find any evidence of cytotoxicity in the patients which supports the findings of the current study. Even though it was stated that the signal to noise ratio is low [46], it has been used successfully for 10 years now. In 2010 the clinical trials to date were justified by de Murphy et al. towards their diagnostic value over the initial 7-year period. ^{99m}Tc-UBI 29–41 meta-analysis returned high values for sensitivity (96.3%), specificity (94.1%), and accuracy (95.3%) with high positive predictive (95.1%) and negative predictive values (95.5%) [54]. From 2011 onwards, seven additional clinical studies (enrolling together over 160 patients) have been successfully carried out and all demonstrated ^{99m}Tc-UBI29-41-SPECT as a highly accurate and selective diagnostic tool for bone infection in diabetic foot [55], hip prostheses [56], or other implant related infections [57, 58]; moreover it also detects osteomyelitis [59, 60] and infective endocarditis [61]. It can be ascertained that this field of applications for ^{99m}Tc-UBI29-41 imaging will keep growing also because research with alternative radioisotopes other than ^{99m}Tc may yield a new group of radiopharmaceutical agents for medical diagnostic imaging using clinical PET/CT or PET/MRI in future. Novel radioisotopes such as ^{68}Ga, ^{82}Rb, or ^{62}Cu can be produced on-demand from a radioisotope generator without the need for an on-site cyclotron and may serve as radionuclides for PET. ^{68}Ga has garnered interest as a positron emitter for molecular imaging due to some of the advantages it offers in a tracer. It has a radioactive half-life of 67.71 minutes which makes it compatible with biokinetics of most low molecular weight radiopharmaceuticals such as peptides, oligonucleotides, aptamers, or antibody fragments. The nuclear decay of the isotope is mainly through positron emission (89%), with average positron energy of 740 keV. Additionally, the coordination chemistry of Ga^{3+} is well understood, which is helpful in designing chelating agents which can be used to link this radionuclide to a targeting vector [62]. Recently, UBI29-41 was conjugated to the macrocycle 1,4,7-triazacyclononane-1,4,7-triacetic acid (NOTA) and subsequently labeled with ^{68}Ga [63]. This approach was initially utilized with 1,4,7,10-tetraazacyclododecane-N′,N″,N‴,N⁗-tetraacetic acid (DOTA) to yield the peptide derivatives such as DOTA-TOC or DOTA-TATE for ^{68}Ga-complexation which subsequently allowed tumor-receptor-based PET imaging. In a preclinical study using ^{68}Ga-NOTAUBI29-41-PET it was shown that the macrocycle conjugation did not compromise the peptide's ability to selectively bind to bacteria *in vivo* [64]. Aside from UBI, there are other compounds evaluated for infection and inflammation imaging [54] but the majority of antimicrobial peptides available remain underinvestigated in terms of infection imaging. In 2000 the human neutrophil peptides (HNP1-3) were considered amongst other peptides as useful agent for targeting infection, as part of the defence mechanism in monocyte/lymphocyte cultures HNPs plays a chemotactic role as mediating molecules. This ambiguous role may be a drawback in developing HNPs for imaging; hence the usage of particular peptides as targeting vectors may have some secondary limitations, despite of their favourable cellular properties [65]. As radiopharmaceuticals are mostly administered by i.v. injection, the peptides can be prone to enzymatic degradation or the destabilisation of the radioisotope as reported for ^{18}F-UBI29-41 [66]. The lactoferrin-derived peptide hLF(1-11) showed great sensitivity as infection agent targeting multidrug-resistant *Acinetobacter baumannii* strains; however binding to *Candida albicans*, a fungus, and the hepatobiliar excretion made it less favourable for imaging [51]. Moreover hLF showed immune-activating or bactericidal effects depending on the dose administered, that is, encountered with a negative feedback mechanism by interleukin-10 modulation [67, 68]. Another example, the AMP Latarcin-2a, extracted from the venom of the Central Asian spider *Lachesana tarabaevi*, has undesirable lytic activity against Gram-positive and Gram-negative bacteria, erythrocytes, and yeast at micromolar concentrations and thus makes it less considered for bacterial detection with PET [69]. Moreover, most bacteria are able to produce both, surface-bound and/or secretory proteases, a defence strategy that can degrade or inactivate AMPs. Consequently, using AMP-derived compounds as imaging agents would result in false-negative diagnostics where a persistent infection might easily be misjudged or overseen entirely. Through understanding these specific bacteria-intrinsic defence mechanisms, it can be avoided to use vulnerable AMP-derived structures as infection imaging agents. It should also be noted that, except for a few structures, research did not reveal a bacteria-specific receptor-like target that complements the potential peptides as a ligands or allosteric modulators. Tumor cells, in contrast, express specific receptors integrin-, bombesin-, or somatostatin ligands or antagonists which are targeted by SPECT or PET tracers [10, 70]. Moreover, the host's immune system, when reacting on infections, has pathologic pathways that can be imaged using PET. Activated macrophages may act as an equivalent host-dependent target which can be visualized by ^{18}F-FDG nonspecifically [3] but

the actual bacterial burden remains overseen. In contrast, AMP-derived peptides are acting in a host-independent mechanism: radiolabeled peptides will bind to free and to cell-adherent but not phagocytised bacteria and hence bacteria become invisible for ^{99m}Tc-UBI29–41-SPECT once they are incorporated by macrophages [71]. The use of this modality potentially allows for the early detection of infection prior to any morphological changes in the body taking place [7]. It also allows for the discrimination of infection from a sterile inflammation which may appear superficially similar as both may present as reddened, swollen, and unusually warm areas. This is due to the increased blood flow, enhanced vascular permeability, and influx of white blood cells which are common in both situations [4]. The latter approach would emphasize a dual tracer imaging regimen in future clinical studies or even dual tracer administration (if the respective radioisotope properties and pharmacokinetic properties are complementing the approach). In summary, the ideal tracer for clinical PET imaging of infection should meet several criteria. (1) It should sustain substantial blood degradation and have a reasonable degree of lipophilicity; (2) it should accumulate and be retained at the site of infection (ideally by internalization and subsequent amplification), with minimal accumulation in noninfected sites; (3) it should have rapid clearance of nonspecific activity uptake from the surrounding regions for high signal-to-noise-ratios; and (4) it should have minimal side effects and should be easy to prepare, at low cost. UBI29-41 has proven its usefulness towards generic infection imaging, and other suitable AMPs based radiopharmaceuticals will follow, undoubtedly.

Abbreviations

AMP: Antimicrobial peptides
B. subtilis: *Bacillus subtilis*
C. albicans: *Candida albicans*
CL: Cardiolipin
CT: Computed tomography
DNA: Deoxyribonucleic acid
E. coli: *Escherichia coli*
FDG: Fluorodeoxyglucose
LPS: Lipopolysaccharide
MRI: Magnetic resonance imaging
PC: Phosphatidylcholine
PE: Phosphatidyl-ethanolamine
PET: Positron emission tomography
PG: Phosphatidyl-glycerol
PS: Phosphatidyl-serine
S. aureus: *Staphylococcus aureus*
SM: *Sphingomyelin*
SPECT: Single photon emission computed tomography
ST: Sterols
T/NT: Target to nontarget ratio
TATE: (Tyrosine^3)octreotate
TOC: (Phenylalanin^1-Tyrosine^3)octreotide
UBI: Ubiquicidin (fragment).

Conflict of Interests

The authors declare that they have no conflict of interests.

Acknowledgments

The work related to this review was funded and kindly supported by National Research Foundation (NRF), the Institute of Cellular and Molecular Medicine and the Nuclear Technologies in Medicine and the Biosciences Initiative (NTeMBI), a national technology platform developed and managed by the South African Nuclear Energy Corporation (Necsa) and funded by the Department of Science and Technology (DST).

References

[1] L. J. Higgins and M. G. Pomper, "The evolution of imaging in cancer: current state and future challenges," *Seminars in Oncology*, vol. 38, no. 1, pp. 3–15, 2011.

[2] S. Basu, T. Chryssikos, S. Moghadam-Kia, H. Zhuang, D. A. Torigian, and A. Alavi, "Positron emission tomography as a diagnostic tool in infection: present role and future possibilities," *Seminars in Nuclear Medicine*, vol. 39, no. 1, pp. 36–51, 2009.

[3] C. J. Palestro, "Radionuclide imaging of infection: In search of the grail," *Journal of Nuclear Medicine*, vol. 50, no. 5, pp. 671–673, 2009.

[4] H. J. J. M. Rennen, O. C. Boerman, W. J. G. Oyen, and F. H. M. Corstens, "Imaging infection/inflammation in the new millennium," *European Journal of Nuclear Medicine*, vol. 28, no. 2, pp. 241–252, 2001.

[5] O. C. Boerman, E. T. M. Dams, W. J. G. Oyen, F. H. M. Corstens, and G. Storm, "Radiopharmaceuticals for scintigraphic imaging of infection and inflammation," *Inflammation Research*, vol. 50, no. 2, pp. 55–64, 2001.

[6] A. Signore, M. Chianelli, C. D'Alessandria, and A. Annovazzi, "Receptor targeting agents for imaging infammatin/infection: where are we now?" *Quarterly Journal of Nuclear Medicine and Molecular Imaging*, vol. 50, no. 3, pp. 236–242, 2006.

[7] S. J. Goldsmith and S. Vallabhajosula, "Clinically proven radiopharmaceuticals for infection imaging: mechanisms and applications," *Seminars in Nuclear Medicine*, vol. 39, no. 1, pp. 2–10, 2009.

[8] C. P. J. M. Brouwer, M. Wulferink, and M. M. Welling, "The pharmacology of radiolabeled cationic antimicrobial peptides," *Journal of Pharmaceutical Sciences*, vol. 97, no. 5, pp. 1633–1651, 2008.

[9] M. R. Yeaman and N. Y. Yount, "Mechanisms of antimicrobial peptide action and resistance," *Pharmacological Reviews*, vol. 55, no. 1, pp. 27–55, 2003.

[10] S. M. Okarvi, "Peptide-based radiopharmaceuticals: future tools for diagnostic imaging of cancers and other diseases," *Medicinal Research Reviews*, vol. 24, no. 3, pp. 357–397, 2004.

[11] E. Guaní-Guerra, T. Santos-Mendoza, S. O. Lugo-Reyes, and L. M. Terán, "Antimicrobial peptides: general overview and clinical implications in human health and disease," *Clinical Immunology*, vol. 135, no. 1, pp. 1–11, 2010.

[12] M. Zasloff, "Antimicrobial peptides of multicellular organisms," *Nature*, vol. 415, no. 6870, pp. 389–395, 2002.

[13] D. Takahashi, S. K. Shukla, O. Prakash, and G. Zhang, "Structural determinants of host defense peptides for antimicrobial activity and target cell selectivity," *Biochimie*, vol. 92, no. 9, pp. 1236–1241, 2010.

[14] I. Zelezetsky and A. Tossi, "Alpha-helical antimicrobial peptides-using a sequence template to guide structure-activity relationship studies," *Biochimica et Biophysica Acta*, vol. 1758, no. 9, pp. 1436–1449, 2006.

[15] R. M. Epand and H. J. Vogel, "Diversity of antimicrobial peptides and their mechanisms of action," *Biochimica et Biophysica Acta*, vol. 1462, no. 1-2, pp. 11–28, 1999.

[16] L. Zhang, A. Rozek, and R. E. W. Hancock, "Interaction of cationic antimicrobial peptides with model membranes," *The Journal of Biological Chemistry*, vol. 276, no. 38, pp. 35714–35722, 2001.

[17] A. Tossi, L. Sandri, and A. Giangaspero, "Amphipathic, alpha-helical antimicrobial peptides," *Biopolymers*, vol. 55, no. 1, pp. 4–30, 2000.

[18] M. Dathe and T. Wieprecht, "Structural features of helical antimicrobial peptides: their potential to modulate activity on model membranes and biological cells," *Biochimica et Biophysica Acta—Biomembranes*, vol. 1462, no. 1-2, pp. 71–87, 1999.

[19] M. A. Kol, A. I. P. M. de Kroon, D. T. S. Rijkers, J. A. Killian, and B. De Kruijff, "Membrane-spanning peptides induce phospholipid flop: a model for phospholipid translocation across the inner membrane of E. coli," *Biochemistry*, vol. 40, no. 35, pp. 10500–10506, 2001.

[20] M. M. Welling, A. Lupetti, H. S. Balter et al., "99mTc-labeled antimicrobial peptides for detection of bacterial and *Candida albicans* infections," *Journal of Nuclear Medicine*, vol. 42, no. 5, pp. 788–794, 2001.

[21] N. Y. Yount and M. R. Yeaman, "Multidimensional signatures in antimicrobial peptides," *Proceedings of the National Academy of Sciences of the United States of America*, vol. 101, no. 19, pp. 7363–7368, 2004.

[22] N. Sitaram and R. Nagaraj, "Interaction of antimicrobial peptides with biological and model membranes: structural and charge requirements for activity," *Biochimica et Biophysica Acta: Biomembranes*, vol. 1462, no. 1-2, pp. 29–54, 1999.

[23] M. Dathe, H. Nikolenko, J. Meyer, M. Beyermann, and M. Bienert, "Optimization of the antimicrobial activity of magainin peptides by modification of charge," *FEBS Letters*, vol. 501, no. 1–3, pp. 146–150, 2001.

[24] Y. Shai, "Mode of action of membrane active antimicrobial peptides," *Biopolymers*, vol. 66, no. 4, pp. 236–248, 2002.

[25] T. Wieprecht, M. Dathe, M. Beyermann et al., "Peptide hydrophobicity controls the activity and selectivity of magainin 2 amide in interaction with membranes," *Biochemistry*, vol. 36, no. 20, pp. 6124–6132, 1997.

[26] N. Uematsu and K. Matsuzaki, "Polar angle as a determinant of amphipathic α-helix-lipid interactions: a model peptide study," *Biophysical Journal*, vol. 79, no. 4, pp. 2075–2083, 2000.

[27] K. Matsuzaki, "Why and how are peptide-lipid interactions utilized for self-defense? Magainins and tachyplesins as archetypes," *Biochimica et Biophysica Acta—Biomembranes*, vol. 1462, no. 1-2, pp. 1–10, 1999.

[28] T. Ganz, "Defensins: antimicrobial peptides of innate immunity," *Nature Reviews Immunology*, vol. 3, no. 9, pp. 710–720, 2003.

[29] L. V. Collins, S. A. Kristian, C. Weidenmaier et al., "Staphylococcus aureus strains lacking D-alanine modifications of teichoic acids are highly susceptible to human neutrophil killing and are virulence attenuated in mice," *The Journal of Infectious Diseases*, vol. 186, no. 2, pp. 214–219, 2002.

[30] M. Gross, S. E. Cramton, F. Götz, and A. Peschel, "Key role of teichoic acid net charge in Staphylococcus aureus colonization of artificial surfaces," *Infection and Immunity*, vol. 69, no. 5, pp. 3423–3426, 2001.

[31] A. Peschel, "How do bacteria resist human antimicrobial peptides?" *Trends in Microbiology*, vol. 10, no. 4, pp. 179–186, 2002.

[32] K. Matsuzaki, "Control of cell selectivity of antimicrobial peptides," *Biochimica et Biophysica Acta*, vol. 1788, no. 8, pp. 1687–1692, 2009.

[33] W. L. Maloy and U. P. Kari, "Structure-activity studies on magainins and other host defense peptides," *Biopolymers*, vol. 37, no. 2, pp. 105–122, 1995.

[34] E. Breukink, I. Wiedemann, C. van Kraaij, O. P. Kuipers, H.-. Sahl, and B. de Kruijff, "Use of the cell wail precursor lipid II by a pore-forming peptide antibiotic," *Science*, vol. 286, no. 5448, pp. 2361–2364, 1999.

[35] I. Wiedemann, E. Breukink, C. van Kraaij et al., "Specific binding of nisin to the peptidoglycan precursor lipid II combines pore formation and inhibition of cell wall biosynthesis for potent antibiotic activity," *The Journal of Biological Chemistry*, vol. 276, no. 3, pp. 1772–1779, 2001.

[36] S. E. Blondelle, K. Lohner, and M. Aguilar, "Lipid-induced conformation and lipid-binding properties of cytolytic and antimicrobial peptides: determination and biological specificity," *Biochimica et Biophysica Acta: Biomembranes*, vol. 1462, no. 1-2, pp. 89–108, 1999.

[37] L. H. Kondejewski, M. Jelokhani-Niaraki, S. W. Farmer et al., "Dissociation of antimicrobial and hemolytic activities in cyclic peptide diastereomers by systematic alterations in amphipathicity," *The Journal of Biological Chemistry*, vol. 274, no. 19, pp. 13181–13192, 1999.

[38] L. Yang, T. M. Weiss, R. I. Lehrer, and H. W. Huang, "Crystallization of antimicrobial pores in membranes: magainin and protegrin," *Biophysical Journal*, vol. 79, no. 4, pp. 2002–2009, 2000.

[39] H. W. Huang, "Action of antimicrobial peptides: two-state model," *Biochemistry*, vol. 39, no. 29, pp. 8347–8352, 2000.

[40] K. A. Henzler Wildman, D. Lee, and A. Ramamoorthy, "Mechanism of lipid bilayer disruption by the human antimicrobial peptide, LL-37," *Biochemistry*, vol. 42, no. 21, pp. 6545–6558, 2003.

[41] J. M. Sanderson, "Peptide-lipid interactions: insights and perspectives," *Organic & Biomolecular Chemistry*, vol. 3, no. 2, pp. 201–212, 2005.

[42] L. Yang, T. A. Harroun, T. M. Weiss, L. Ding, and H. W. Huang, "Barrel-stave model or toroidal model? A case study on melittin pores," *Biophysical Journal*, vol. 81, no. 3, pp. 1475–1485, 2001.

[43] B. Circiumaru, G. Baldock, and J. A. Cohen, "A prospective study of fever in the intensive care unit," *Intensive Care Medicine*, vol. 25, no. 7, pp. 668–673, 1999.

[44] W. Becker and J. Meller, "The role of nuclear medicine in infection and inflammation," *The Lancet Infectious Diseases*, vol. 1, no. 5, pp. 326–333, 2001.

[45] A. Lupetti, P. H. Nibbering, M. M. Welling, and E. K. J. Pauwels, "Radiopharmaceuticals: new antimicrobial agents," *Trends in Biotechnology*, vol. 21, no. 2, pp. 70–73, 2003.

[46] L. Meléndez-Alafort, J. Rodríguez-Cortés, G. Ferro-Flores et al., "Biokinetics of 99mTc-UBI 29-41 in humans," *Nuclear Medicine and Biology*, vol. 31, no. 3, pp. 373–379, 2004.

[47] L. Meléndez-Alafort, F. D. M. Ramírez, G. Ferro-Flores, C. A. de Murphy, M. Pedraza-López, and D. J. Hnatowich, "Lys and Arg in UBI: a specific site for a stable Tc-99m complex?" *Nuclear Medicine and Biology*, vol. 30, no. 6, pp. 605–615, 2003.

[48] D. Blok, R. I. J. Feitsma, P. Vermeij, and E. J. K. Pauwels, "Peptide radiopharmaceuticals in nuclear medicine," *European Journal of Nuclear Medicine*, vol. 26, no. 11, pp. 1511–1519, 1999.

[49] P. S. Hiemstra, M. T. van den Barselaar, M. Roest, P. H. Nibbering, and R. van Furth, "Ubiquicidin, a novel murine microbicidal protein present in the cytosolic fraction of macrophages," *Journal of Leukocyte Biology*, vol. 66, no. 3, pp. 423–428, 1999.

[50] G. Ferro-Flores, C. Arteaga De Murphy, M. Pedraza-López et al., "In vitro and in vivo assessment of 99mTc-UBI specificity for bacteria," *Nuclear Medicine and Biology*, vol. 30, no. 6, pp. 597–603, 2003.

[51] M. M. Welling, A. Paulusma-Annema, H. S. Balter, E. K. J. Pauwels, and P. H. Nibbering, "Technetium-99m labelled antimicrobial peptides discriminate between bacterial infections and sterile inflammations," *European Journal of Nuclear Medicine*, vol. 27, no. 3, pp. 292–301, 2000.

[52] M. S. Akhtar, A. Qaisar, J. Irfanullah et al., "Antimicrobial peptide 99mTc-Ubiquicidin 29-41 as human infection-imaging agent: clinical trial," *Journal of Nuclear Medicine*, vol. 46, no. 4, pp. 567–573, 2005.

[53] K. A. Brogden, "Antimicrobial peptides: pore formers or metabolic inhibitors in bacteria?" *Nature Reviews Microbiology*, vol. 3, no. 3, pp. 238–250, 2005.

[54] C. A. de Murphy, F. Gemmel, and J. Balter, "Clinical trial of specific imaging of infections," *Nuclear Medicine Communications*, vol. 31, no. 8, pp. 726–733, 2010.

[55] S. Saeed, J. Zafar, B. Khan et al., "Utility of ^{99m}Tc-labelled antimicrobial peptide ubiquicidin (29–41) in the diagnosis of diabetic foot infection," *European Journal of Nuclear Medicine and Molecular Imaging*, vol. 40, no. 5, pp. 737–743, 2013.

[56] K. Aryana, A. Hootkani, R. Sadeghi et al., "99mTc-labeled Ubiquicidin scintigraphy: a promising method in hip prosthesis infection diagnosis," *NuklearMedizin*, vol. 51, no. 4, pp. 133–139, 2012.

[57] D. Beiki, G. Yousefi, B. Fallahi et al., "99mtc-Ubiquicidin [29-41], a promising radiopharmaceutical to differentiate orthopedic implant infections from sterile inflammation," *Iranian Journal of Pharmaceutical Research*, vol. 12, no. 2, pp. 347–353, 2013.

[58] B. Nazari, Z. Azizmohammadi, M. Rajaei et al., "Role of99mTc-ubiquicidin 29–41 scintigraphy to monitor antibiotic therapy in patients with orthopedic infection: a preliminary study," *Nuclear Medicine Communications*, vol. 32, no. 8, pp. 745–751, 2011.

[59] M. Assadi, K. Vahdat, I. Nabipour et al., "Diagnostic value of 99mTc-ubiquicidin scintigraphy for osteomyelitis and comparisons with 99mTc-methylene diphosphonate scintigraphy and magnetic resonance imaging," *Nuclear Medicine Communications*, vol. 32, no. 8, pp. 716–723, 2011.

[60] C. Dillmann-Arroyo, R. Cantú-Leal, H. Campa-Núñez, C. López-Cavazos, M. Bermúdez-Argüelles, and J. C. Mejía-Herrera, "Application of the ubiquicidin 29-41 scan in the diagnosis of pyogenic vertebral osteomyelitis," *Acta Ortopédica Mexicana*, vol. 25, no. 1, pp. 27–31, 2011.

[61] A. M. Taghizadeh, M. H. Mandegar, and M. Assadi, "Technetium-99m-ubiquicidin scintigraphy in the detection of infective endocarditis," *Hellenic Journal of Nuclear Medicine*, vol. 17, no. 1, pp. 47–48, 2014.

[62] M. Fani, J. P. André, and H. R. Maecke, "68Ga-PET: a powerful generator-based alternative to cyclotron-based PET radiopharmaceuticals," *Contrast Media & Molecular Imaging*, vol. 3, no. 2, pp. 67–77, 2008.

[63] T. Ebenhan, N. Chadwick, M. M. Sathekge et al., "Peptide synthesis, characterization and ^{68}Ga-radiolabeling of NOTA-conjugated ubiquicidin fragments for prospective infection imaging with PET/CT," *Nuclear Medicine and Biology*, vol. 41, no. 5, pp. 390–400, 2014.

[64] T. Ebenhan, J. R. Zeevaart, J. D. Venter et al., "Preclinical evaluation of 68Ga-labeled 1,4,7-triazacyclononane-1,4,7-triacetic acid-ubiquicidin as a radioligand for PET infection imaging," *Journal of Nuclear Medicine*, vol. 55, no. 2, pp. 308–314, 2014.

[65] B. Agerberth, J. Charo, J. Werr et al., "The human antimicrobial and chemotactic peptides LL-37 and α-defensins are expressed by specific lymphocyte and monocyte populations," *Blood*, vol. 96, no. 9, pp. 3086–3093, 2000.

[66] D. Salber, J. Gunawan, K. J. Langen et al., "Comparison of 99mTc- and 18F-ubiquicidin autoradiography to anti-Staphylococcus aureus immunofluorescence in rat muscle abscesses," *Journal of Nuclear Medicine*, vol. 49, no. 6, pp. 995–999, 2008.

[67] L. Dijkshoorn, C. P. J. M. Brouwer, S. J. P. Bogaards, A. Nemec, P. J. Van Den Broek, and P. H. Nibbering, "The synthetic n-terminal peptide of human lactoferrin, hLF(1-11), is highly effective against experimental infection caused by multidrug-resistant *Acinetobacter baumannii*," *Antimicrobial Agents and Chemotherapy*, vol. 48, no. 12, pp. 4919–4921, 2004.

[68] C. P. J. M. Brouwer, M. Rahman, and M. M. Welling, "Discovery and development of a synthetic peptide derived from lactoferrin for clinical use," *Peptides*, vol. 32, no. 9, pp. 1953–1963, 2011.

[69] A. Won, A. Ruscito, and A. Ianoul, "Imaging the membrane lytic activity of bioactive peptide latarcin 2a," *Biochimica et Biophysica Acta—Biomembranes*, vol. 1818, no. 12, pp. 3072–3080, 2012.

[70] X. Chen, E. Sievers, Y. Hou et al., "Integrin $\alpha v\beta 3$-targeted imaging of lung cancer," *Neoplasia*, vol. 7, no. 3, pp. 271–279, 2005.

[71] P. H. Nibbering, M. M. Welling, A. Paulusma-Annema, C. P. J. M. Brouwer, A. Lupetti, and E. K. J. Pauwels, "99mTc-labeled UBI 29-41 peptide for monitoring the efficacy of antibacterial agents in mice infected with Staphylococcus aureus," *Journal of Nuclear Medicine*, vol. 45, no. 2, pp. 321–326, 2004.

Hindawi Publishing Corporation
BioMed Research International
Volume 2014, Article ID 471971, 8 pages
http://dx.doi.org/10.1155/2014/471971

Review Article

^{18}F-Fluorodeoxyglucose Positron Emission Tomography/CT Scanning in Diagnosing Vascular Prosthetic Graft Infection

Ben R. Saleem,[1] Robert A. Pol,[1] Riemer H. J. A. Slart,[2] Michel M. P. J. Reijnen,[3] and Clark J. Zeebregts[1]

[1] *Division of Vascular Surgery, Department of Surgery, University Medical Center Groningen, University of Groningen, P.O. Box 30 001, 9700 RB Groningen, The Netherlands*
[2] *Nuclear Medicine and Molecular Imaging, University Medical Center Groningen, University of Groningen, P.O. Box 30 001, 9700 RB Groningen, The Netherlands*
[3] *Department of Surgery, Rijnstate Hospital, P.O. Box 9555, 6800 TA Arnhem, The Netherlands*

Correspondence should be addressed to Clark J. Zeebregts; czeebregts@hotmail.com

Received 6 June 2014; Accepted 1 August 2014; Published 19 August 2014

Academic Editor: Francois Rouzet

Vascular prosthetic graft infection (VPGI) is a severe complication after vascular surgery. CT-scan is considered the diagnostic tool of choice in advanced VPGI. The incidence of a false-negative result using CT is relatively high, especially in the presence of low-grade infections. ^{18}F-fluorodeoxyglucose positron emission tomography (^{18}F-FDG PET) scanning has been suggested as an alternative for the diagnosis and assessment of infectious processes. Hybrid ^{18}F-FDG PET/CT has established the role of ^{18}F-FDG PET for the assessment of suspected VPGI, providing accurate anatomic localization of the site of infection. However, there are no clear guidelines for the interpretation of the uptake patterns of ^{18}F-FDG as clinical tool for VPGI. Based on the available literature it is suggested that a linear, diffuse, and homogeneous uptake should not be regarded as an infection whereas focal or heterogeneous uptake with a projection over the vessel on CT is highly suggestive of infection. Nevertheless, ^{18}F-FDG PET and ^{18}F-FDG PET/CT can play an important role in the detection of VPGI and monitoring response to treatment. However an accurate uptake and pattern recognition is warranted and cut-off uptake values and patterns need to be standardized before considering the technique to be the new standard.

1. Introduction

Vascular prosthetic graft infection (VPGI) is an uncommon complication after reconstructive vascular surgery with an incidence ranging between 1 and 6%. The incidence of VPGI varies according to the bypass localization with less than 1% in case of subrenal aortic bypass, 1-2% after aortofemoral bypass, and up to 6% in case of infrainguinal bypass [1–3]. Nevertheless, it is one of the most difficult challenges faced by the vascular surgeon and is associated with devastating complication such as limb amputation (5–25%) and mortality rates as high as 25–88% [1–3]. The first and principal dilemma in clinically suspected VPGI is to obtain definite proof of the graft infection. Positive cultures either from percutaneous aspirated perigraft fluid or from surgically obtained material are considered by many the gold standard for VPGI but in clinical practice are often difficult to obtain. For adequate treatment, it is important to diagnose graft infection at an early stage. Unfortunately, clinical signs are variable and often subtle. They may include recurrent fevers and chills, back or groin pain, erythema, swelling, or a pulsatile mass in the groin, thus making the correct diagnosis sometimes tedious [4]. The commonly used first methods to evaluate and diagnose a VPGI are evaluation of elevated infection parameters in peripheral blood samples (erythrocyte sedimentation rate, white blood cell count, and C-reactive protein (CRP)), duplex ultrasound scanning, computed tomography (CT) scanning, and magnetic resonance imaging (MRI). However, the predictive value for diagnosing VPGI with either one of these diagnostic tools has proven to be relatively low [5]. To date CT is considered the gold standard in diagnosing VPGI because of its high spatial resolution providing a detailed view

Table 1: Summary of literature data regarding the use of ^{18}F-FDG PET imaging requested in suspected vascular graft infection.

Study	Year	Study Design	Number of patient's	Imaging modality	Interpretation criteria	TP[1]	TN[2]	FP[3]	FN[4]	Sens* %	Spec** %
Fukuchi et al. [10]	2005	prospective	33	PET	Semiquantitative[a]	10	14	8	1	91	64
Keidar et al. [13]	2007	prospective	39	PET/CT	Visual	14	22	2	1	93	91
Lauwers et al. [14]	2008	case series	4	PET	Visual	3	0	1	0	—	—
Spacek et al. [15]	2009	prospective	76	PET/CT	Semiquantitative[b]	54	31	10	1	78.2	92.7
Bruggink et al. [16]	2010	retrospective	25	PET and PET/CT	Semiquantitative[c]	15	10	0	0	93†	70†
Tokuda et al. [17]	2013	retrospective	9	PET/CT	Semiquantitative[d]	4	5	0	0	—	—

[1]True positive.
[2]True negative.
[3]False positive.
[4]False negative.
*Sensitivity.
**Specificity.
[a]Five-point scale intensity of FDG uptake.
[b]Three point scale intensity of FDG uptake.
[c]Four point scale intensity of FDG uptake.
[d]SUVmax cut off value.
†Results for both FDG-PET and fused FDG-PET-CT, judged by a nuclear medicine physician.

of the vascular structures and perivascular spaces. Diagnostic signs for VPGI on CT include the presence of local fluid, perigraft retention, pseudoaneurysm formation, and focal bowel thickening and air bubbles [6], though these findings are present in just 50% of VPGI cases and are even considered normal findings in the early postoperative period. Other CT findings suggesting a VPGI include thickening of the graft wall, adjacent blurred fat, and soft tissue swelling. CT scan sensitivity and specificity are claimed to be 95% but this high percentage can only be reached in clinically high suspected VPGI [7–9]. CT scan is much less reliable in case of a low-grade infection, with a sensitivity and specificity of 55% and 100%, respectively [10–12]. In particular, the false-positive results may lead to unnecessary surgery or lengthy antibiotic use while the false-negative results may have life or limb threatening consequences. Since 1996, several studies have evaluated the usefulness of 18-F-Fluoro-D-deoxyglucose positron emission tomography (^{18}F-FDG PET) in the detection of infectious foci and, more specific, the usefulness in the analyses of suspected VPGI (Table 1). This review aims to summarize the accuracy and interpretation of ^{18}F-FDG PET in the detection of VPGI.

2. Search

A literature search was carried out using the following databases: Pubmed, the Cochrane library, Science Direct, and Embase. Two authors (Ben R. Saleem and Robert A. Pol), independently of each other, identified the studies for inclusion based on title or abstract using the following medical subject headings (MeSH): "positron emission tomography," "blood vessel prosthesis," and "infection." These MeSH terms were applied in various combinations using the Booleans operators AND or OR. Papers were included from the start of the databases until January 2014. Reference lists from the selected articles were manually checked for additional relevant studies. In Pubmed, the "related article" algorithm was employed to identify additional articles. Case reports and short case series (number of patients < 4) were excluded from further review. In total, six original studies were selected and listed in Table 1.

3. ^{18}F-FDG PET Imaging in Infectious Diseases

^{18}F-FDG PET imaging is based on uptake of radioactive-labeled glucose (^{18}F-FDG) in metabolically active cells. Activated inflammatory cells, like malignant cells, predominantly metabolize glucose as a source of energy. In the stimulated state, inflammatory cells, such as neutrophils and macrophages, express high concentrations of glucose transporters that facilitate the movement of FDG through the cell membrane. The initial application was designed to diagnose cancer as increased glucose metabolism is often present in tumor cells, resulting in a higher ^{18}F-FDG uptake than in the surrounding tissues [18]. However, it appeared that inflammatory and infectious lesions sometimes caused false-positive results. In the early years of clinical ^{18}F-FDG PET imaging in oncology, cases of false-positive uptake in a wide variety of infections were described [19]. Although initially interpreted as false-positive results and even a disadvantage of the technique, its usefulness in detecting inflammation was further explored with respect to the potential of ^{18}F-FDG PET imaging in different types of infection and inflammation [20, 21] (Figure 1). To increase the sensitivity and specificity FDG-PET can be fused with CT and or MR images. Hybrid PET/CT has been increasingly applied during the last decade [22]. ^{18}F-FDG PET/CT can identify infections and their relation to the surrounding anatomy. Hybrid PET/MR has rapidly increased in interest in daily clinical practice. PET/MR also provides the anatomic information but with much higher soft tissue contrast and without the additional radiation dose from CT [23, 24]. To date the majority of reports on the role of ^{18}F-FDG PET and fused ^{18}F-FDG PET/CT imaging in the diagnosis

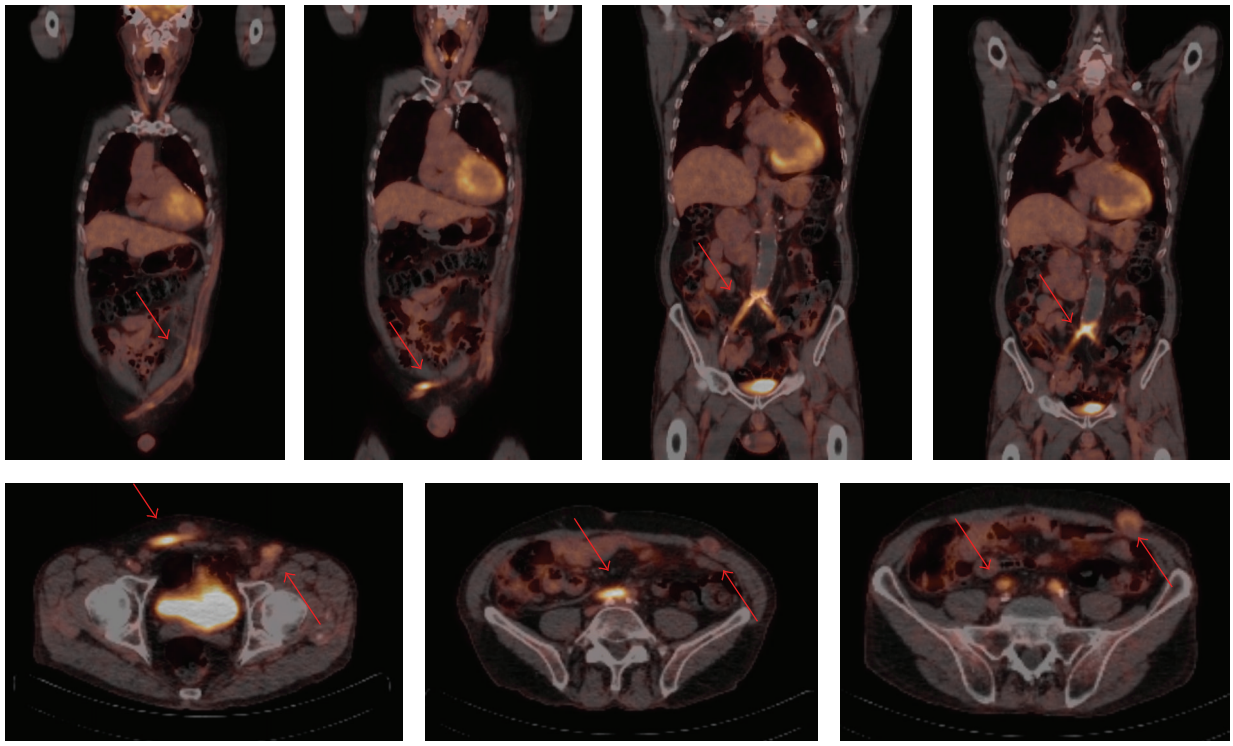

Figure 1: Coronal and axial view of fused ^{18}F-FDG PET/CT images. In this particular case, a 67-year-old male patient underwent an aorto-bi-iliac bypass 16 years ago. After 3 years the bypass was revised because of an occlusion. Five years later the second bypass also occluded and an axillobifemoral bypass was constructed. Unfortunately this bypass also occluded twice. Patient is admitted to the hospital because of pain and redness at the level of the axillobifemoral bypass probably due to infection. ^{18}F-FDG PET/CT scanning showed increased FDG uptake at the level of both occluded bypasses, the aorto-bi-iliac bypass and the axillobifemoral bypass. Arrows are pointing at increased FDG uptake in both bypasses. Ultimately, no bacteria were cultured.

of VPGI are case series and case reports of single patients [10, 13–17, 25, 26].

4. Accuracy of ^{18}F-FDG PET in VPGI

The sensitivity and specificity of ^{18}F-FDG PET vary greatly in current literature. Table 1 summarizes data on the use of ^{18}F-FDG PET and fused ^{18}F-FDG PET/CT imaging in suspected VPGI. In a large case series of 33 patients that compared the feasibility of ^{18}F-FDG PET with CT, the sensitivity and specificity of ^{18}F-FDG PET were, respectively, 91 and 64% [10]. Comparably, if no better results were published by Keidar et al. they prospectively assessed 39 patients (69 vascular prosthetic grafts) with suspected VPGI by ^{18}F-FDG PET fused with CT. ^{18}F-FDG PET/CT results were true positive in 14, false negative in 1, and false positive in 2 cases, resulting in sensitivity and specificity rates of 93% and 91%, respectively [13]. Spacek et al. also evaluated fused ^{18}F-FDG PET/CT images in 76 patients (96 vascular prosthetic grafts) with suspected VPGI [15]. Although in this paper the specificity was similarly high with 93%, the sensitivity of 78% was remarkably low. The most recent study by our group evaluated both ^{18}F-FDG PET and fused ^{18}F-FDG PET/CT imaging. In a retrospective study a sensitivity of 93% and a specificity of 70% of ^{18}F-FDG PET in 25 patients with clinically suspected VPGI were found [16]. We found no differences regarding sensitivity or specificity when fused ^{18}F-FDG PET/CT images were assessed for their accuracy in diagnosing VPGI. Also no differences have been found in the literature yet on accuracy of ^{18}F-FDG PET/CT between abdominal versus thoracic aorta graft infection [17].

5. Interpretation and Grading of the ^{18}F-FDG PET Findings

There is no consensus with respect to the interpretation of the ^{18}F-PET findings in the reviewed studies wherein a visual grading scale was used. Different variants such as a four- or five-point scale were used [10, 16]. The five-point scale was structured as follows: grade 0, FDG uptake similar to that in the background, grade 1, with low FDG uptake, comparable with that by inactive muscles and fat, grade 2, with moderate FDG uptake, clearly visible and higher than the uptake by inactive muscles and fat, grade 3, with strong FDG uptake, but distinctly less than the physiologic uptake by the bladder, and grade 4, with very strong FDG uptake, comparable with the physiologic urinary uptake by the bladder. Using this classification, lesions with grades 3 and 4 uptake are considered infected lesions [20]. The four-point grading scale consists of grade 1, with FDG uptake

similar to that in the background, grade 2, with low FDG uptake, comparable with that by inactive muscles and fat, grade 3, with moderate FDG uptake, clearly visible and higher than the uptake by inactive muscles and fat, but distinctly less than the physiologic uptake by the bladder, and grade 4, with strong FDG uptake, comparable with the physiologic urinary uptake by the bladder. Lesions with grades 3 and 4 uptake were classified as high probability of VPGI. Besides these four- and five-point scales, other interpretations of FDG uptake have also been used. Keidar et al. defined an infectious process if focal increased ^{18}F-FDG uptake in the region of any of the vascular grafts had a higher intensity than the surrounding tissues [13]. Spacek et al. interpreted FDG uptake as intense, inhomogeneous, or no uptake [15]. They considered intense focal FDG uptake as a positive result for VPGI. However, when inhomogeneous uptake was also considered as a positive result, then the sensitivity increased but the specificity decreased. The subgroup of patients with inhomogeneous FDG uptake represents the big challenge, because of nondiagnostic results. Spacek et al. suggested that a mild inhomogeneous FDG uptake might be explained either by infection of very low grade in which only a weak immune reaction might be anticipated or in immunocompromised patients [15]. Hybrid ^{18}F-FDG PET/CT was found as a promising diagnostic tool in patients with inhomogeneous FDG uptake with the morphological appearance of the graft boundary [15]. Because a physiologic uptake is often visible in or around vascular prostheses, patterns of interpretation have been discussed. It is believed that a linear, diffuse, and homogeneous uptake is not likely to represent infection whereas focal or heterogeneous uptake with projection over the vessel on CT is highly suggestive of infection [10]. ^{18}F-FDG PET scans can also be assessed using (semi) qualitative parameters (maximal standardized uptake value (SUVmax) and tissue-to-background ratio (TBR)). The TBR ratio can be calculated by dividing the SUVmax in the graft material by the mean blood-pool activity [16]. More recently, a semi-quantitative method has been suggested for the evaluation of thoracic prosthetic graft infections in which a standard uptake value-max >8 in the perigraft area was considered the cut-off value for distinguishing between an infected graft and a noninfected graft [17]. Until now there are no clear guidelines for the interpretation of the uptake patterns of ^{18}F-FDG as a signal for VPGI. Apparently the interpretation of the images by a visual grading scale is predominantly subjective. Besides visual and semiquantitative analyses, a quantitative analysis can be performed in which it is possible to calculate the curve of the arterial FDG concentration plotted against time (arterial input function). In this way physiological parameters can be measured in absolute units (e.g., glucose metabolic rate in mol min^{-1} g^{-1} or blood flow in ml min^{-1} g^{-1}). Such absolute quantification is usually not performed in the clinical routine. It requires direct sampling of arterial blood with serial measurements and dynamic acquisition. Some noninvasive alternatives have been studied; the input function can be retrieved from the PET images using the aorta or using volumes of interest and partial volume correction.

6. False-Positive Interpretation of Images and Graft Physiological Uptake Patterns

Increased ^{18}F-FDG uptake may occur in postsurgical inflammatory changes, scar tissue, and native vessels [3, 13, 27]. The chronic aseptic inflammation due to the synthetic graft material, mediated primarily by macrophages, fibroblasts, and foreign-body giant cells, constitutes a potential base for ^{18}F-FDG uptake even a long time after surgery, up to 16 years, depending on the used prosthetic material [28–30]. Within the first 6 to 8 weeks after surgery a physiological ^{18}F-FDG graft uptake can result in a false-positive scan [2, 15, 17] (Figure 2). These physiological uptake patterns of ^{18}F-FDG in synthetic vascular graft have been reported in both symptomatic and asymptomatic patients and render a diagnosis of an early VPGI extremely difficult. In a recent study patients who underwent an ^{18}F-FDG PET/CT scan for other reasons than suspected graft infection were analyzed and a 3-grade arbitrary scale was used, high, low, or no uptake, to indicate ^{18}F-FDG accumulation within the graft. Five circular regions of interest were drawn at different levels of the descending and suprarenal abdominal aorta to measure the SUVmean. The TBR was calculated by dividing the maximum SUV in the graft material by the mean blood-pool activity. Elevated ^{18}F-FDG was seen in 10 out of 12 patients with synthetic abdominal aortic grafts after open reconstruction and in 1 out of 4 grafts after endovascular repair. Only 1 patient eventually developed a VPGI and thus the authors concluded that the risk of a false-positive diagnosis of VPGI by ^{18}F-FDG PET/CT shortly after surgery is high [31]. More recently, a retrospective evaluation of the incidence and patterns of ^{18}F-FDG uptake in 107 noninfected vascular grafts was published [32]. A 12-year ^{18}F-FDG PET/CT scan database was searched for cancer patients with a history of vascular surgery with a synthetic graft. Again the SUVmean was measured in each graft and the pattern of uptake for each graft was recorded as focal, diffuse homogeneous, inhomogeneous, or absent. Dacron grafts had a significant higher metabolic activity than Gore-Tex grafts and native vein grafts. Also grafts used for a central reconstruction had a higher ^{18}F-FDG uptake compared to grafts anastomosed in the groin or lower limb, most likely because Dacron is most commonly used during central reconstruction. Furthermore, the authors found a diffuse ^{18}F-FDG uptake in 92% of noninfected vascular prostheses. The intensity of ^{18}F-FDG uptake however was independent of the period after surgery, ranging from 5 months to 16 years with an average of 10 years [32].

7. ^{18}F-FDG Uptake Patterns in Diabetes Mellitus Patients

Diabetes mellitus (DM) or elevated serum glucose levels and its influence on the sensitivity, specificity, and the accuracy of ^{18}F-FDG studies are a controversial issue. Glucose metabolism can be disturbed in DM patients and therefore result in an increased uptake of ^{18}F-FDG. A number of animal and human studies have shown that plasma glucose competes

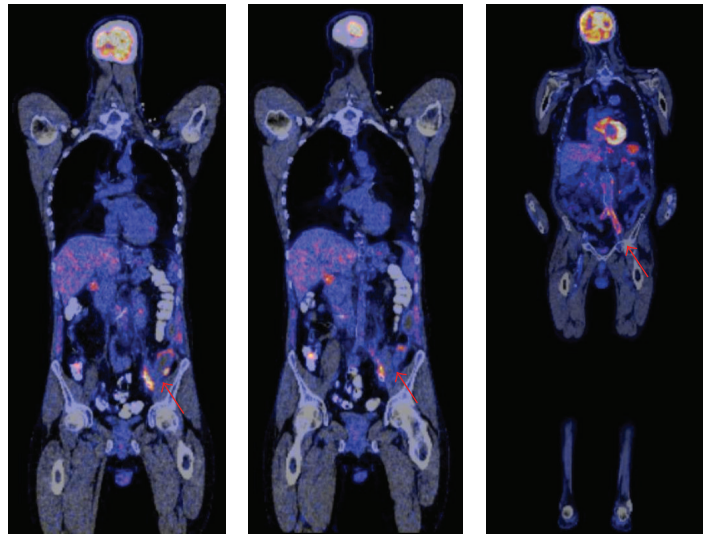

Figure 2: Coronal view of fused ^{18}F-FDG PET/CT image of a culture proven not infected vascular prosthetic graft. In this particular case, a 45-year-old male patient underwent emergency surgery by placement of a Viabahn in the left common iliac artery because of rupture. He was admitted to the hospital 6 weeks later with fever and sepsis. ^{18}F-FDG PET/CT scanning showed increased FDG uptake at the level of the left iliac artery. Ultimately, no bacteria were cultured from the graft under antibiotic therapy.

with ^{18}F-FDG uptake in tumors. It therefore has been postulated that hyperglycemia may reduce and impair ^{18}F-FDG uptake in malignant lesions [33–35]. Only a few studies are available on the role of DM in ^{18}F-FDG uptake in infectious or inflammatory diseases. A recent study concluded that the incidence of false-negative scans in patients assessed for suspicion of an infectious or inflammatory process was not adversely affected between patients with or without DM and with high or normal serum glucose levels at the time of scanning [36]. While not affecting the accuracy when assessing infection, hyperglycemia during ^{18}F-FDG PET scan in the oncology group may lead to higher false-negative rate and should be therefore avoided [36, 37]. For further interpretation, it is pertinent that FDG-PET reflects glucose metabolism not only in pathological conditions but also in various physiological conditions which can cause an increase in ^{18}F-FDG. These issues require further research in order to improve the interpretations of ^{18}F-FDG PET in diagnosing VPGI possible.

8. Uptake Patterns and Causative Organisms

Staphylococcus species are the most common causative organisms of aortic graft infection, mostly due to bacterial contamination at the time of graft placement. *Staphylococcus epidermidis* is a slowly growing, slime-producing organism classically causing a late, indolent VPGI [1, 38, 39]. It is estimated that *Staphylococcus aureus* species account for approximately 25% to 50% of al VPGI [40]. No studies are available about the differences in uptake patterns of ^{18}F-FDG in VPGI caused by different species. The ^{18}F-FDG PET characteristics of *Staphylococcus aureus* osteomyelitis and foreign-body-associated *Staphylococcus epidermidis* infections have been studied in rabbits [41]. *Staphylococcus epidermidis* was found to reflect a low virulence of the pathogen and limited leukocyte infiltration, which was characterized by low ^{18}F-FDG uptake.

9. Monitoring Response to Treatment with ^{18}F-FDG PET/CT

Recently, the combined guidelines from the European Association of Nuclear Medicine (EANM) and the Society of Nuclear Medicine and Molecular Imaging (SNMMI) were published for the use of ^{18}F-FDG PET in inflammation and infection [42, 43]. Based on cumulated reported accuracies, more than 85% of these guidelines state that the major indications for the use of ^{18}F-FDG PET/CT in infection and inflammation are sarcoidosis, peripheral bone osteomyelitis, spondylodiscitis, evaluation of fever of unknown origin, and the primary evaluation of vasculitis [44]. For VPGI, it remains unclear if ^{18}F-FDG PET/CT offers advantages over other imaging techniques yet, based on the available published data [40–44]. However, ^{18}F-FDG PET/CT can not only be used to diagnose VPGI but it could also be used as a monitor of treatment response. ^{18}F-FDG PET/CT seems to be useful for the diagnosis and also for therapy evaluation in vasculitis, sarcoidosis, and spondylodiscitis [44]. Other well-described applications, but without sufficient evidence-based indication, included suspected infection of intravascular devices, pacemakers, and catheters [45–48]. However to date there are no studies which show the benefits of ^{18}F-FDG PET/CT as a monitoring tool for VPGI.

10. Discussion

This review has shown that ^{18}F-FDG PET and ^{18}F-FDG PET/CT may play an important role in the detection of VPGI.

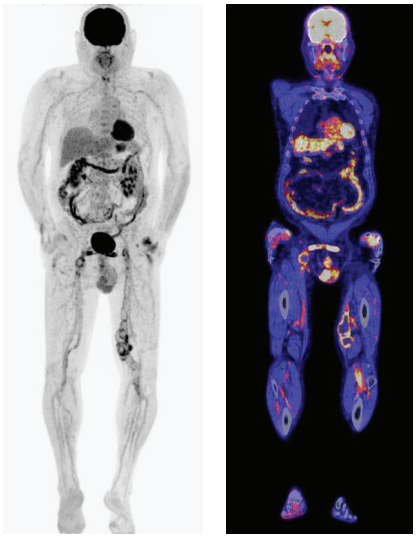

Figure 3: Coronal view of a fused ^{18}F-FDG PET/CT image of a culture proven infected vascular prosthetic graft. In this particular case, a 70-year-old male patient underwent an ileofemoral bypass from the left to right side using Dacron. After 10 years the patient was readmitted with an occlusion of the bypass possibly due to a suture aneurysm. CT scan revealed an occlusion of the bypass with no signs of infection. ^{18}F-FDG PET/CT scanning clearly showed increased FDG uptake at the level of the suture aneurysm. Ultimately, *Escherichia coli* were cultured from the graft.

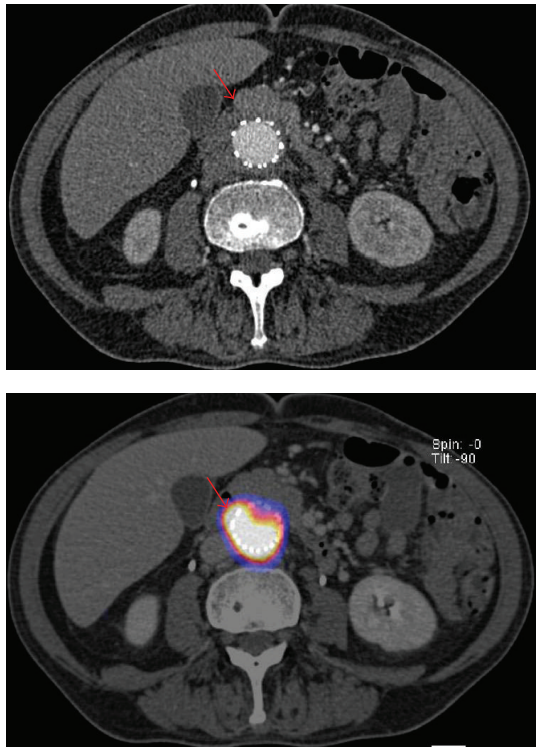

Figure 4: Axial view of a CT scan and fused ^{18}F FDG PET/CT image of a culture proven infected vascular prosthetic graft. In this particular case, a 67-year-old male patient underwent an urgent endovascular procedure of a contained ruptured abdominal aortic aneurysm using a Cook Zenith prosthesis. After 7 months the patient was readmitted with clinical signs of a prosthetic infection. CT scan was assessed as a possible prosthesis infection. An ^{18}F-FDG PET/CT scan confirmed the diagnosis by showing an increased FDG uptake at the level of the endograft. Ultimately, *Escherichia coli* were cultured from the graft.

However, to date, there is only limited information regarding the accuracy of ^{18}F-FDG PET/CT imaging in the detection of these infections. There are no clear guidelines for the interpretation of ^{18}F-FDG PET images made for suspicion of VPGI. Because physiologic uptake is often visible in/around vascular prostheses, the specific patterns of uptake appear to be crucial. Based on the available literature it is suggested that a linear, diffuse, and homogeneous uptake should not be regarded as an infection whereas focal or heterogeneous uptake with a projection over the vessel on CT is highly suggestive of infection (Figures 3 and 4). However, low-grade infection may be presented as mild inhomogeneous of FDG uptake [15]. In case of inhomogeneous FDG uptake, we suggest a follow-up policy. ^{18}F-FDG PET scan can not only be fused with CT scan. Recent studies show the benefits of fusing PET with MR scan. Possible additional advantages of PET/MR over PET/CT are the potential for motion correction, as well as reconstruction driven by anatomic information. The combination of PET radiopharmaceuticals and PET/MR imaging could significantly improve the sensitivity and specificity of the diagnosis and follow-up treatment of infectious and inflammatory diseases. It would allow for more accurate assessment of the extent and exact localization of inflammatory lesions than PET alone or PET/CT, especially in soft tissues that are prone to movement artifacts, for example, in vascular and cardiac infections and inflammatory bowel disease [24]. The development of PET/MR has triggered a shift in the PET detector technology and image correction paradigms. Most of the technical challenges have been solved, but clinical studies are required to show the areas of patient care for which PET/MR has advantages over other diagnostic methods.

With this current knowledge we recommend to further develop semiquantitative and quantitative analysis methods for the assessment of the FDG-PET images. One of the semiquantitative values is SUV. It is suggested in the literature that SUVmax >8 in the perigraft area appears to be the cut-off value for distinguishing infected grafts from noninfected grafts. However, this was based on a small number of patients and probably the SUV measurement was not based on the ENAM and SNMMI guidelines which makes it difficultly reproducible in other centres. ^{18}F-FDG PET is generally assessed using visual criteria, looking for a focally increased uptake that may be compatible with infection. It is unclear if semiquantitative measurements such as SUV will contribute to the assessment, partly because of the considerable variability in the methodology used. This recommendation is an attempt to increase uniformity of ^{18}F-FDG PET investigations in multicentre studies and for routine clinical applications [43]. It is therefore also essential that the used equipment is comparable. Besides the development

of a quantitative analysis and to minimize the false-negative and false-positive interpretations, an experienced department of nuclear medicine is needed to analyze the ^{18}F-FDG PET/CT scan. Hyperglycemia and DM have been previously considered as one of the main reasons for false-negative ^{18}F-FDG PET/CT studies. However, based on the available literature, this appears to be an overestimated problem in which the false-negative rate in patients assessed for VPGI is not statistically significantly different between patients with and without hyperglycemia.

In conclusion,^{18}F-FDG PET and ^{18}F-FDG PET/CT can play an important role in the detection of VPGI and monitoring response to treatment; however, an accurate uptake and pattern recognition is warranted. Standardization of techniques and definitions of the cut-off uptake values and patterns are needed before recommending the technique as the new gold standard.

Conflict of Interests

The authors declare that there is no conflict of interests regarding the publication of this paper.

References

[1] B. R. Saleem, R. Meerwaldt, I. F. J. Tielliu, E. L. G. Verhoeven, J. J. A. M. van den Dungen, and C. J. Zeebregts, "Conservative treatment of vascular prosthetic graft infection is associated with high mortality," *The American Journal of Surgery*, vol. 200, no. 1, pp. 47–52, 2010.

[2] L. Legout, P. V. D'Elia, B. Sarraz-Bournet et al., "Diagnosis and management of prosthetic vascular graft infections," *Medecine et Maladies Infectieuses*, vol. 42, no. 3, pp. 102–109, 2012.

[3] Z. Keidar and S. Nitecki, "FDG-PET in prosthetic graft infections," *Seminars in Nuclear Medicine*, vol. 43, no. 5, pp. 396–402, 2013.

[4] T. W. Swain III, K. D. Calligaro, and M. D. Dougherty, "Management of infected aortic prosthetic grafts," *Vascular and Endovascular Surgery*, vol. 38, no. 1, pp. 75–82, 2004.

[5] R. J. Valentine, "Diagnosis and management of aortic graft infection," *Seminars in Vascular Surgery*, vol. 14, no. 4, pp. 292–301, 2001.

[6] R. N. Low, S. D. Wall, R. B. Jeffrey Jr., R. A. Sollitto, L. M. Reilly, and L. M. Tierney Jr., "Aortoenteric fistula and perigraft infection: evaluation with CT," *Radiology*, vol. 175, no. 1, pp. 157–162, 1990.

[7] D. F. Orton, R. F. LeVeen, J. A. Saigh et al., "Aortic prosthetic graft infections: radiologic manifestations and implications for management," *Radiographics*, vol. 20, no. 4, pp. 977–993, 2000.

[8] R. Kumar, S. Basu, D. Torigian, V. Anand, H. Zhuang, and A. Alavi, "Role of modern imaging techniques for diagnosis of infection in the era of 18F-fluorodeoxyglucose positron emission tomography," *Clinical Microbiology Reviews*, vol. 21, no. 1, pp. 209–224, 2008.

[9] A. Mark, A. A. Moss, R. Lusby, and J. A. Kaiser, "CT evaluation of complications of abdominal aortic surgery," *Radiology*, vol. 145, no. 2, pp. 409–414, 1982.

[10] K. Fukuchi, Y. Ishida, M. Higashi et al., "Detection of aortic graft infection by fluorodeoxyglucose positron emission tomography: comparison with computed tomographic findings," *Journal of Vascular Surgery*, vol. 42, no. 5, pp. 919–925, 2005.

[11] T. A. Macedo, A. W. Stanson, G. S. Oderich, C. M. Johnson, J. M. Panneton, and M. L. Tie, "Infected aortic aneurysms: imaging findings," *Radiology*, vol. 231, no. 1, pp. 250–257, 2004.

[12] E. Sueyoshi, I. Sakamoto, Y. Kawahara, Y. Matsuoka, and K. Hayashi, "Infected abdominal aortic aneurysm: early CT findings," *Abdominal Imaging*, vol. 23, no. 6, pp. 645–648, 1998.

[13] Z. Keidar, A. Engel, A. Hoffman, O. Israel, and S. Nitecki, "Prosthetic vascular graft infection: the role of 18F-FDG PET/CT," *Journal of Nuclear Medicine*, vol. 48, no. 8, pp. 1230–1236, 2007.

[14] P. Lauwers, S. Van Den Broeck, L. Carp, J. Hendriks, P. Van Schil, and P. Blockx, "The use of positron emission tomography with (18)f-fluorodeoxyglucose for the diagnosis of vascular graft infection," *Angiology*, vol. 58, no. 6, pp. 717–724, 2008.

[15] M. Spacek, O. Belohlavek, J. Votrubova, P. Sebesta, and P. Stadler, "Diagnostics of "non-acute" vascular prosthesis infection using ^{18}F-FDG PET/CT: our experience with 96 prostheses," *European Journal of Nuclear Medicine and Molecular Imaging*, vol. 36, no. 5, pp. 850–858, 2009.

[16] J. L. M. Bruggink, A. W. J. M. Glaudemans, B. R. Saleem et al., "Accuracy of FDG-PETeCT in the diagnostic work-up of vascular prosthetic graft infection," *European Journal of Vascular and Endovascular Surgery*, vol. 40, no. 3, pp. 348–354, 2010.

[17] Y. Tokuda, H. Oshima, Y. Araki et al., "Detection of thoracic aortic prosthetic graft infection with 18F-fluorodeoxyglucose positron emission tomography/computed tomography," *European Journal of Cardio-Thoracic Surgery*, vol. 43, no. 6, pp. 1183–1187, 2013.

[18] A. Signore, M. Chianelli, C. D'Alessandria, and A. Annovazzi, "Receptor targeting agents for imaging infammatin/infection: where are we now?" *Quarterly Journal of Nuclear Medicine and Molecular Imaging*, vol. 50, no. 3, pp. 236–242, 2006.

[19] S. M. Bakheet and J. Powe, "Benign causes of 18-FDG uptake on whole body imaging," *Seminars in Nuclear Medicine*, vol. 28, no. 4, pp. 352–358, 1998.

[20] K. D. M. Stumpe, H. Dazzi, A. Schaffner, and G. K. Von Schulthess, "Infection imaging using whole-body FDG-PET," *European Journal of Nuclear Medicine*, vol. 27, no. 7, pp. 822–832, 2000.

[21] F. de Winter, D. Vogelaers, F. Gemmel, and R. Dierckx, "Promising role of 18-F-fluoro-D-deoxyglucose positron emission tomography in clinical infectious diseases," *European Journal of Clinical Microbiology and Infectious Diseases*, vol. 21, no. 4, pp. 247–257, 2002.

[22] J. L. M. Bruggink, R. H. J. A. Slart, J. A. Pol, M. M. P. J. Reijnen, and C. J. Zeebregts, "Current role of imaging in diagnosing aortic graft infections," *Seminars in Vascular Surgery*, vol. 24, no. 4, pp. 182–190, 2011.

[23] J. A. Disselhorst, I. Bezrukov, A. Kolb, C. Parl, and B. J. Pichler, "Principles of PET/MR imaging," *Journal of Nuclear Medicine*, vol. 55, pp. 1–9, 2014.

[24] A. W. Glaudemans, A. M. Quintero, and A. Signore, "PET/MRI in infectious and inflammatory diseases: will it be a useful improvement?" *European Journal of Nuclear Medicine and Molecular Imaging*, vol. 39, no. 5, pp. 745–749, 2012.

[25] B. R. Saleem, P. Berger, C. J. Zeebregts, R. H. Slart, E. L. Verhoeven, and J. J. van den Dungen, "Periaortic endograft

infection due to *Listeria monocytogenes* treated with graft preservation," *Journal of Vascular Surgery*, vol. 47, no. 3, pp. 635–637, 2008.

[26] Z. Keidar and S. Nitecki, "FDG-PET for the detection of infected vascular grafts," *Quarterly Journal of Nuclear Medicine and Molecular Imaging*, vol. 53, no. 1, pp. 35–40, 2009.

[27] G. J. R. Cook, I. Fogelman, and M. N. Maisey, "Normal physiological and benign pathological variants of 18-fluoro-2-deoxyglucose positron-emission tomography scanning: potential for error in interpretation," *Seminars in Nuclear Medicine*, vol. 26, no. 4, pp. 308–314, 1996.

[28] R. D. Hagerty, D. L. Salzmann, L. B. Kleinert, and S. K. Williams, "Cellular proliferation and macrophage populations associated with implanted expanded polytetrafluoroethylene and polyethyleneterephthalate," *Journal of Biomedical Materials Research*, vol. 49, no. 4, pp. 489–497, 2000.

[29] D. L. Salzmann, L. B. Kleinert, S. S. Berman, and S. K. Williams, "Inflammation and neovascularization associated with clinically used vascular prosthetic materials," *Cardiovascular Pathology*, vol. 8, no. 2, pp. 63–71, 1999.

[30] P. H. J. van Bilsen, E. R. Popa, L. A. Brouwer et al., "Ongoing foreign body reaction to subcutaneous implanted (heparin) modified Dacron in rats," *Journal of Biomedical Materials Research A*, vol. 68, no. 3, pp. 423–427, 2004.

[31] J. Wassélius, J. Malmstedt, B. Kalin et al., "High 18F-FDG uptake in synthetic aortic vascular grafts on PET/CT in symptomatic and asymptomatic patients," *Journal of Nuclear Medicine*, vol. 49, no. 10, pp. 1601–1605, 2008.

[32] Z. Keidar, N. Pirmisashvili, M. Leiderman, S. Nitecki, and O. Israel, "^{18}F-FDG uptake in noninfected prosthetic vascular grafts: incidence, patterns, and changes over time," *Journal of Nuclear Medicine*, vol. 55, no. 3, pp. 392–395, 2014.

[33] T. Torizuka, K. R. Zasadny, and R. L. Wahl, "Diabetes decreases FDG accumulation in primary lung cancer," *Clinical Positron Imaging*, vol. 2, no. 5, pp. 281–287, 1999.

[34] M. Gorenberg, W. A. Hallett, and M. J. O'Doherty, "Does diabetes affect [^{18}F]FDG standardised uptake values in lung cancer?" *European Journal of Nuclear Medicine*, vol. 29, no. 10, pp. 1324–1327, 2002.

[35] C. G. Diederichs, L. Staib, G. Glatting, H. G. Beger, and S. N. Reske, "FDG PET: elevated plasma glucose reduces both uptake and detection rate of pancreatic malignancies," *Journal of Nuclear Medicine*, vol. 39, no. 6, pp. 1030–1033, 1998.

[36] Z. Rabkin, O. Israel, and Z. Keidar, "Do hyperglycemia and diabetes affect the incidence of false-negative 18F-FDG PET/CT studies in patients evaluated for infection or inflammation and cancer? A comparative analysis," *Journal of Nuclear Medicine*, vol. 51, no. 7, pp. 1015–1020, 2010.

[37] H. M. Zhuang, A. CortÉs-Blanco, M. Pourdehnad et al., "Do high glucose levels have differential effect on FDG uptake in inflammatory and malignant disorders?" *Nuclear Medicine Communications*, vol. 22, no. 10, pp. 1123–1128, 2001.

[38] H. W. Kaebnick, D. F. Bandyk, T. W. Bergamini, and J. B. Towne, "The microbiology of explanted vascular prostheses," *Surgery*, vol. 102, no. 4, pp. 756–762, 1987.

[39] W. J. Sharp, J. J. Hoballah, C. R. Mohan et al., "The management of the infected aortic prosthesis: a current decade of experience," *Journal of Vascular Surgery*, vol. 19, no. 5, pp. 844–850, 1994.

[40] S. F. FitzGerald, C. Kelly, and H. Humphreys, "Diagnosis and treatment of prosthetic aortic graft infections: confusion and inconsistency in the absence of evidence or consensus," *Journal of Antimicrobial Chemotherapy*, vol. 56, no. 6, pp. 996–999, 2005.

[41] P. Lankinen, K. Lehtimäki, A. J. Hakanen, A. Roivainen, and H. T. Aro, "A comparative ^{18}F-FDG PET/CT imaging of experimental *Staphylococcus aureus* osteomyelitis and *Staphylococcus epidermidis* foreign-body-associated infection in the rabbit tibia," *EJNMMI Research*, vol. 2, no. 1, pp. 1–10, 2012.

[42] F. Jamar, J. Buscombe, A. Chiti et al., "EANM/SNMMI guideline for ^{18}F-FDG use in inflammation and infection," *Journal of Nuclear Medicine*, vol. 54, no. 4, pp. 647–658, 2013.

[43] R. Boellaard, M. J. O'Doherty, W. A. Weber et al., "FDG PET and PET/CT: EANM procedure guidelines for tumour PET imaging: version 1.0," *European Journal of Nuclear Medicine and Molecular Imaging*, vol. 37, no. 1, pp. 181–200, 2010.

[44] A. W. Glaudemans, E. F. de Vries, F. Galli, R. A. Dierckx, R. H. Slart, and A. Signore, "The use of ^{18}F-FDG-PET/CT for diagnosis and treatment monitoring of inflammatory and infectious diseases," *Clinical and Developmental Immunology*, vol. 2013, Article ID 623036, 14 pages, 2013.

[45] M. H. Miceli, L. B. J. Jackson, R. C. Walker, G. Talamo, B. Barlogie, and E. J. Anaissie, "Diagnosis of infection of implantable central venous catheters by [^{18}F]fluorodeoxyglucose positron emission tomography," *Nuclear Medicine Communications*, vol. 25, no. 8, pp. 813–818, 2004.

[46] P. Singh, B. Wiggins, Y. Sun et al., "Imaging of peritoneal catheter tunnel infection using positron-emission tomography," *Advances in Peritoneal Dialysis*, vol. 26, pp. 96–100, 2010.

[47] L. Bensimhon, T. Lavergne, F. Hugonnet et al., "Whole body [^{18}F]fluorodeoxyglucose positron emission tomography imaging for the diagnosis of pacemaker or implantable cardioverter defibrillator infection: a preliminary prospective study," *Clinical Microbiology and Infection*, vol. 17, no. 6, pp. 836–844, 2011.

[48] S. Turpin, R. Lambert, and N. Poirier, "An unusual looking pacemaker infection imaged with 18F-FDG PET/CT," *European Journal of Nuclear Medicine and Molecular Imaging*, vol. 37, no. 7, p. 1438, 2010.

Hindawi Publishing Corporation
BioMed Research International
Volume 2014, Article ID 926203, 8 pages
http://dx.doi.org/10.1155/2014/926203

Review Article

Hepatosplenic Sarcoidosis: Contrast-Enhanced Ultrasound Findings and Implications for Clinical Practice

Claudio Tana,[1] Christoph F. Dietrich,[2] and Cosima Schiavone[1]

[1] *Unit of Internistic Ultrasound, Department of Medicine and Science of Aging, "G. d'Annunzio" University, Via dei Vestini 29, 66100 Chieti, Italy*
[2] *Medizinische Klinik 2, Caritas-Krankenhaus, Uhlandstraße 7, 97980 Bad Mergentheim, Germany*

Correspondence should be addressed to Cosima Schiavone; cschiavone@unich.it

Received 4 June 2014; Accepted 17 July 2014; Published 18 August 2014

Academic Editor: Andor Glaudemans

Sarcoidosis is a complex granulomatous disease that affects virtually every organ and tissue, with a prevalence that varies significantly among the sites involved. The role of conventional imaging, such as computed tomography and magnetic resonance imaging, in the assessment of hepatosplenic sarcoidosis is well established by revealing organ enlargement, multiple discrete nodules, and lymphadenopathy. In this review, we aim to describe contrast-enhanced ultrasound (CEUS) findings in liver and spleen involvement by sarcoidosis, reporting evidence from the literature and cases from our experience, after a brief update on safety profile, cost-effectiveness, and clinical indications of this novel technique. Furthermore, we highlight potential advantages of CEUS in assessing hepatosplenic sarcoidosis that may be useful in the clinical practice.

1. Introduction

Sarcoidosis is a complex granulomatous disease that virtually affects every organ and tissue, with a prevalence that varies significantly among the sites involved. However, it affects most often compartments such as lungs and mediastinal lymph nodes, manifesting as a pulmonary restrictive disorder in up to 65% of patients, and with pulmonary fibrosis in 20–25% of them [1–3]. The value of mediastinal ultrasound in patients with sarcoidosis has been recently shown [4]. The high prevalence of pulmonary disease could be associated with the primary activation of alveolar macrophages by inhaled exogenous agents, such as inorganic particles, insecticides used at work, and those from exposition to moldy environments [1–3]. The formation of typical noncaseating granulomas represents the final product of an incomplete antigens degradation, associated with an exuberant macrophage and T- and B-cell activity due to prolonged antigenaemia [5, 6]. Also genetic factors (both HLA and non-HLA genes) have been associated with an increased risk of sarcoidosis, and the complex interaction between endogenous and exogenous agents may reflect the great variability of clinical manifestations [7].

Organs, such as liver and spleen, are less frequently affected than lungs, and their involvement often shows a benign course but portal hypertension and loss of liver function may occur [8–10]. However, a correct evaluation of these organs represents an important step in patients with sarcoidosis, before starting appropriate treatment.

2. Clinical and Laboratory Findings in Hepatosplenic Sarcoidosis: When to Perform Imaging Studies

Although there are no specific recommendations for hepatosplenic imaging studies in patients with sarcoidosis, it is widely accepted to perform exams such as unenhanced ultrasound, computed tomography (CT), and magnetic resonance imaging (MRI) when an increase of liver function tests is found or when abdominal symptoms, such as nausea, vomiting, and weight loss, are reported.

Liver can be affected in 10–25% of cases, but hepatic involvement is often oligo- or asymptomatic. Various degrees of dysfunction of liver function tests such as alanine aminotransferase (ALT), aspartate aminotransferase (AST),

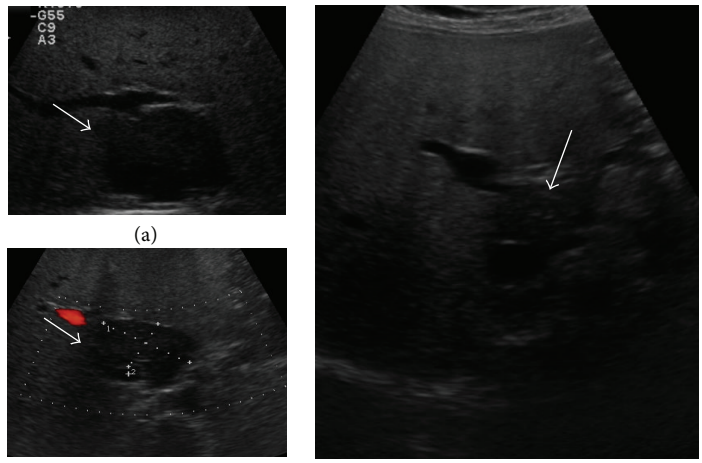

Figure 1: A 51-year-old woman with diagnosis of pulmonary sarcoidosis, who presented with dyspepsia. (a) B-mode US showed diffuse liver hyperechogenicity suggestive of fatty liver disease and a hypoechoic lesion in the hepatic segment I (arrow). The lesion was in close contiguity with inferior vena cava and had a maximum size of 51 mm. Imaging findings were suggestive of focal fatty sparing, but histopathological examination revealed noncaseating granulomas, suggesting liver involvement by sarcoidosis. Spleen was normal. (b) Color Doppler US showed no flow inside the nodule (arrow). (c) After six months of steroid therapy, the lesion was significantly reduced (arrow).

gamma-gt, and alkaline phosphatase can be observed [8]. In a recent study that comprises 837 patients with sarcoidosis, an increase of ALT and AST was found in up to 15% of cases [11]. Hepatic sarcoidosis can manifest with constitutional symptoms such as weight loss, anorexia, fever, and night sweats [1] or, less frequently, with symptoms related to chronic intrahepatic cholestasis, such as pruritus and jaundice. In these cases, laboratory tests reveal an increase of alkaline phosphatases and total and direct bilirubin [12]. Rarely, cholestasis is associated with common bile duct compression by a mass in the pancreatic head or by enlarged perihepatic lymph nodes [13]. Only few cases complicated by cirrhosis and portal hypertension have been reported in the literature, and they present with ascites and/or bleeding from rupture of gastroesophageal varices [14–16].

Splenic involvement is uncommon (5–10% of cases) and usually manifests with asymptomatic and mild splenomegaly. Rarely, the enlargement of the spleen is more pronounced with hypersplenism and pancytopenia [8, 14].

3. Conventional Imaging in the Assessment of Hepatosplenic Sarcoidosis

3.1. B-Mode and Color Doppler Ultrasound Findings. Hepatosplenic sarcoidosis is common in patients with systemic disease, but it is often underestimated on imaging techniques, in particular conventional ultrasound, because granulomatous inflammation of the liver and spleen can be minimal and/or manifest with nonspecific patterns. While granulomas have been found in 60–80% of liver biopsy specimen, sarcoid hepatic nodules are found on imaging in only 5% of cases [17].

The most common finding is represented by hepatomegaly with homogenous distribution of echoes and without evidence of prominent nodules. Sometimes, US can demonstrate an increase of parenchymal liver echogenicity, mimicking fatty liver disease (Figure 1) [18, 19]. A prominent parenchymal inhomogeneity with coarsening pattern can also be found, suggesting an irregular patchy infiltration of the parenchyma by confluent granulomas, associated with various degrees of fibrosis surrounding the coalescing tissue (Figure 2) [20–22]. Hepatic nodules usually appear on US as multiple, discrete, and rounded hypoechoic lesions of various sizes. They may mimic liver cirrhosis or nodular regenerative hyperplasia [23]. They can also manifest as areas of increased or similar echogenicity with respect to the adjacent parenchyma, though these patterns are less frequently reported in the literature [17, 24]. Isoechoic lesions can be missed on conventional US and are found on imaging such as CT or MRI. Usually, the nodules are multiple, have different sizes ranging from 1 to 2 mm to several centimeters, are not associated with mass effect on the surrounding parenchyma, and show hypovascularity on Color Doppler US (Figure 2) [17, 22]. Less frequently, single hypoechoic nodules can be observed, raising problems of differential diagnosis with other focal lesions (Figure 1). In our experience enlarged perihepatic lymph nodes can be encountered in almost all patients with circumscribed focal sarcoid liver infiltration.

Splenomegaly can be observed in either absence or presence of focal splenic lesions, and there is a different prevalence in observing discrete nodules among published studies (6–33%), perhaps reflecting ethnic differences in study populations [17]. Splenic nodules usually appear as multiple and hypoechoic focal lesions; they show different size on US (usually less than 10 mm but larger lesions may occur) and are hypovascular on Color Doppler US (Figure 3) [10]. The nodules can also manifest as hyper or isoechoic lesions with respect to the healthy parenchyma. The different patterns can be related to a different degree of fibrosis in the granulomatous tissue [25].

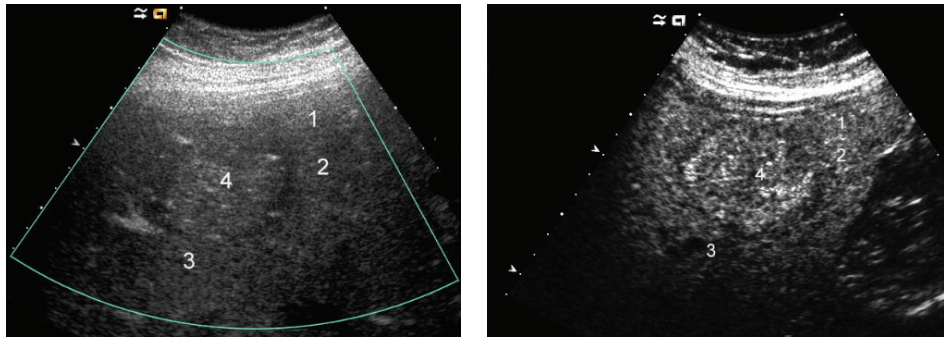

(a) (b)

Figure 2: A 24-year-old female with histopathological diagnosis of hepatic sarcoidosis that resembled advanced stage of cirrhosis on US. (a) The liver was almost completely subverted by multiple more diffuse and also more circumscribed hypoisoechoic nodules (numbers 1 to 4); the lesions did not demonstrate vascularity on Color Doppler US. (b) Contrast-enhanced US in the late phase showed almost isoenhancing lesions.

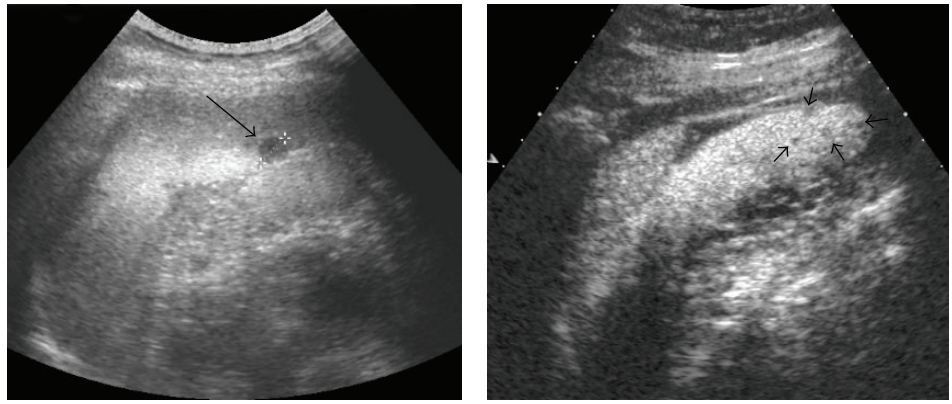

(a) (b)

Figure 3: A 53-year-old male with history of pulmonary sarcoidosis. (a) B-mode US showed a rounded and hypoechoic lesion located in the lower pole of the spleen; the nodule did not show flow on Color Doppler US and had a maximum size of 1 cm (arrow, caliper 1). (b) Contrast-enhanced US confirmed the lesion and showed other progressively hypoenhancing nodules of few mm (in median 5 mm, arrowheads) that were not evident on conventional US. Histopathological examination of the spleen revealed infiltration by sarcoidosis.

Furthermore, enlarged lymph nodes have been observed in up to 76% of cases, both in hepatic and splenic sarcoidosis, and they appear as single or multiple hypoechoic masses that are located most often in periportal, celiac, paracaval, and paraaortic compartments, with sizes between 1 and 2 cm [26]. We generally observed larger perihepatic lymph nodes in advanced liver disease with a lymph node size up to 4–6 cm (Figure 4). In the context of benign diseases such large perihepatic lymph nodes have been observed only in primary biliary cirrhosis (PBC) [27].

Involved abdominal lymph nodes may show inhomogeneous echotexture, with multiple low-level echoes inside [22, 28]. The concomitant enlargement of perihepatic and mediastinal lymph nodes is typical for sarcoidosis but has also been observed in chronic virus hepatitis C [29]. Other not commonly observed findings are represented by punctate calcifications that appear as multiple, small, hyperechoic areas of few millimeters. They can be found in both liver and spleen [20, 26].

Hepatic and splenic involvement by sarcoidosis can be associated with systemic disease or can be isolated. In the latter, the diagnosis is difficult if based only on imaging studies and requires often a biopsy and a histopathological examination of the organs [25–33].

US can also demonstrate some atypical pattern, rarely described in the literature. Some nodules, due to their confluence tendency and irregular appearance, raise the problem of differential diagnosis with neoplastic disorders [10, 34, 35].

Bauones et al. have recently reported a case of incidental finding of multiple hypoechoic and nonvascular splenic nodules that were associated with a significant retraction of the overlying splenic capsule; splenomegaly was not found and no other organ involvement was documented. This atypical finding has mimicked neoplastic disease, and the patient underwent a laparoscopic splenectomy in order to exclude malignancy [25]. In these cases, histopathological examination is required to avoid a misdiagnosis that can lead to a completely different therapeutic approach.

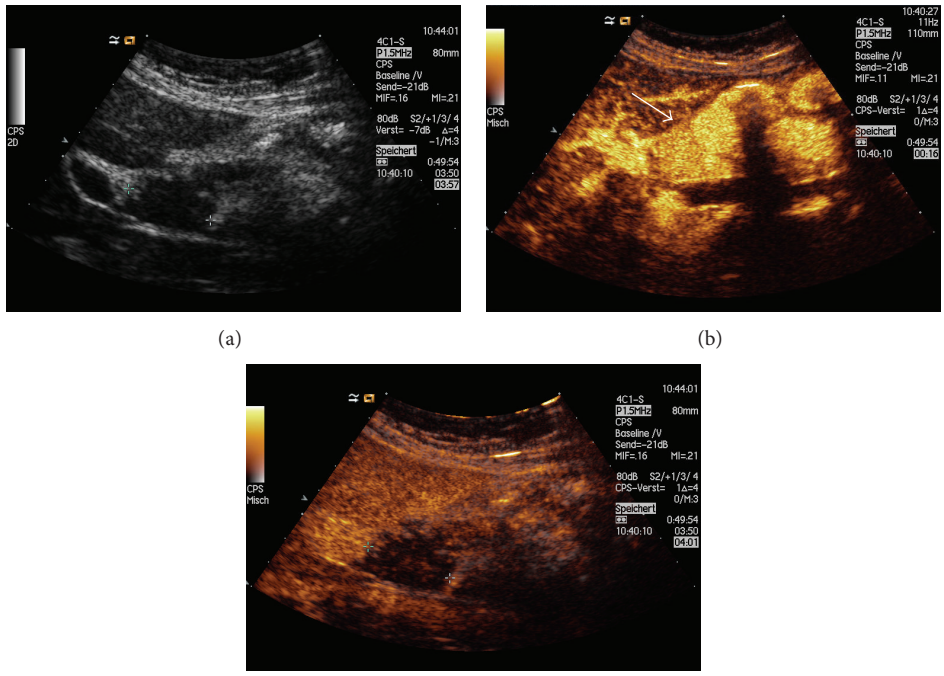

(a) (b)

(c)

Figure 4: A 64-year-old female with sarcoidosis. (a) B-mode US documented typical prominent perihepatic lymphadenopathy (maximum size of 3 cm, caliper). Contrast-enhanced US showed (b) homogenous enhancement during the arterial phase (arrow) and (c) prominent wash-out (caliper).

The diagnosis of sarcoidosis can be suspected on the basis of typical clinical, laboratory, and imaging features but is usually achieved with histopathological findings that confirm the presence of noncaseating granulomas and exclude other causes of granulomatous inflammation [1, 36]. Effort should be made to obtain a sample to analyze from biopsy specimen [1, 37–39].

3.2. The Role of Computed Tomography and Magnetic Resonance Imaging. Other imaging techniques, such as contrast-enhanced CT (CECT) and MRI, are reliable to evaluate the organ involvement in sarcoidosis. CT can confirm hepatosplenomegaly, and, in most cases, the liver appears homogeneous; sometimes, however, the liver appears heterogeneous and a septa-like pattern can be found after contrast agent injection [17]. CECT can be useful to confirm hepatosplenic nodules or to reveal them, for the first time, after a negative US examination. The lesions manifest as hypodense masses relative to the adjacent healthy tissue, without peripheral enhancement [17, 40, 41]. MRI can also serve as an adjunctive diagnostic tool to confirm the presence of both hepatic and splenic nodules that appear hypointense, relative to the adjacent parenchyma on all sequences, without substantial contrast enhancement after gadolinium administration, and appear less evident on delayed imaging, suggesting equilibration. The nodules are best visualized on T2-weighted fat-suppressed and early-phase dynamic contrast-enhanced images [42]. Furthermore, MRI can be useful to reveal nonspecific hepatic findings such as periportal hyperintensity on T2-weighted images; some authors have suggested that this sign could be associated with a greater tendency of granulomas to localize within periportal spaces [17, 22]. Finally, both CT and MRI can be useful to reveal the presence of punctate calcifications and/or lymphadenopathy [26].

4. Contrast-Enhanced Ultrasound (CEUS) in the Assessment of Hepatosplenic Lesions Derived from Sarcoidosis

4.1. The Evolving Role of CEUS. In recent years, the use of ultrasound contrast agents (UCAs) has rapidly increased in the clinical practice. Since the first guidelines regarding the use of CEUS in the assessment of liver lesions, released by European Federation of Societies for Ultrasound in Medicine and Biology (EFSUMB) in 2004 and lastly updated in 2013 [43–45], new fields have been investigated with the evaluation of other organs such as spleen, pancreas, gastrointestinal tract, kidneys, and lungs. EFSUMB released an extensive update on nonhepatic use of CEUS, highlighting the wide range of clinical applications that can be carried out [46]. Comments on the guidelines have been published as well [47, 48]. UCAs perform as blood pool tracers and are constituted by gas surrounded by a membrane that prolongs their half-life and provides stability. The envelope consists of organic materials such as galactose, palmitic acid, albumin, and phospholipids. After intravenous injection, enhancement patterns can be evaluated in real time with a higher temporal resolution than in other imaging techniques [44]. UCAs are

generally safe and have a low incidence of side effects, without heart, liver, and renal toxicity. Incidence of life-threatening anaphylactoid reactions is very low (0.001% among the 23,000 patients examined) and it is not necessary to perform laboratory tests before starting CEUS examination [45].

4.2. CEUS in the Differentiation between Benign and Malignant Focal Hepatosplenic Lesions. CEUS has demonstrated a high overall diagnostic accuracy in the differential diagnosis of focal liver lesions, with similar values of sensitivity and specificity as compared to conventional imaging, such as CT or MRI [49–55]. A recent systematic review and cost-effectiveness analysis found that the pooled estimates of sensitivity and specificity to detect and/or characterize malignant lesions were 95.1% and 93.8% using CEUS, and 94.6% and 93.1% using CECT, respectively [53]. Similar results were obtained by also comparing CEUS and MRI [50]. The use of CEUS is effective in the workup of patients with focal liver lesions, by identifying specific patterns and selecting those who need further diagnostic investigation [56, 57].

Furthermore, several authors have demonstrated that CEUS can provide valuable information in the differential diagnosis of focal splenic lesions with high accuracy [58–62]; Yu et al. have found that the sensitivity, specificity, and accuracy of CEUS in the diagnosis of focal splenic lesions were 91.1%, 95.0%, and 92.0%, respectively. Lower values were obtained using conventional US (75.0%, 84.2%, and 77.3%, resp.) [59]. CEUS can also improve the differentiation between benign vascular and malignant lesions [63] and can be useful when there are no suggestive findings on benign conventional US [64]. The good safety profile, real time evaluation, and absence of radiation exposure are some of the reasons for the wide diffusion of CEUS in the last few years and for the establishment of appropriate indications for its use.

4.3. CEUS Patterns of Hepatosplenic Sarcoidosis. Although there is increasing evidence regarding the usefulness and reliability of CEUS, a broad group of disorders have not been investigated so far with this technique. Actually, there is a lack of ad hoc studies in patients with hepatosplenic sarcoidosis, and most evidence derives from description of single case reports or from findings of small case series [10]. Most of the trials have been conducted with the aim to differentiate benign focal lesions from malignant focal lesions, as discussed above.

It is reasonable to expect this lack of data, first of all because sarcoidosis is an uncommon disease, and demonstration of liver and spleen involvement on imaging is even rarer; then, in most of cases, hepatosplenic sarcoidosis appears homogenous on US without evidence of discrete nodules, and second imaging, such as CT and MRI, is preferred to assess the organ involvement in these cases. However, CEUS has documented accuracy to characterize splenic and hepatic parenchymal inhomogeneity, when found [44, 46].

Even if the evidence is limited, hypoechoic hepatic lesions derived from sarcoidosis appear, after UCA injection, as variably arterial enhancing and progressively hypoenhancing nodules in the portal-venous and late phases [10, 65].

Also hypoechoic lesions of the spleen appear most often as progressive hypoenhancing nodules, in arterial and parenchymal phases, compared to adjacent splenic tissue, with increasing lesion-to-parenchyma contrast diffusion while moving to parenchymal phase (Figure 3) [58, 65]. The pattern of slight enhancement can be diffusely homogenous or heterogeneous in the arterial phase and diffusely homogenous or dotted in parenchymal phase. Furthermore, some peripheral irregular vessels can be found [58]. Other authors have described a complete absence of enhancement in both arterial and parenchymal phases [66]. In one case, we observed a more rim-like enhancement in the arterial phase, followed by hypoenhancement in parenchymal and late phases (Figure 5) [10, 67]. This pattern can overlap with those observed in neoplastic disorders [57], and biopsy with histopathological examination is, therefore, required to exclude malignancy.

CEUS can be useful to identify hepatic or splenic isoechoic nodules that are not otherwise evident on conventional US; these lesions appear as progressively hypoenhancing masses (Figure 3) [24]. Sometimes, they appear as almost isoenhancing nodules in the late phase (Figure 2). CEUS can also confirm the presence of abdominal lymph nodes enlargement with homogeneous enhancement, suggesting a benign inflammatory pattern (Figure 4) [68].

5. Conclusion: Implications for Clinical Practice and Future Perspectives

The limited evidence regarding CEUS findings in hepatosplenic sarcoidosis raises the need for further studies that evaluate the role of CEUS in this uncommon disease. Although the most observed pattern is characterized by absence or less enhancement of the nodules with respect to the healthy parenchyma, no studies have reported CEUS findings in hyperechoic lesions derived from hepatosplenic sarcoidosis. It would be interesting to explore these patterns and to see if there is a different behavior after UCA administration; however, we expect similar findings for hyperechoic nodules on CEUS to that of hypo- and isoechoic lesions, because of their similar hypodense appearance on CECT [17, 24]. CT and MRI are often preferred to evaluate organ involvement in sarcoidosis, because lesions with similar echogenicity to the healthy parenchyma cannot be found on conventional US. CEUS can overcome these limitations and reveal hepatic and splenic nodules. In our experience, we observed that conventional ultrasound may be also useful to show treatment response and a significant reduction in the size of hepatosplenic lesions after steroid therapy. Further studies should evaluate any change of contrast enhancement pattern after treatment of focal lesions and perihepatic lymphadenopathy [27]. CEUS could be useful to follow up the lesions over time, thus avoiding unnecessary radiation exposure associated with CT imaging and kidney damage in patients at risk, after administration of iodine contrast or gadolinium.

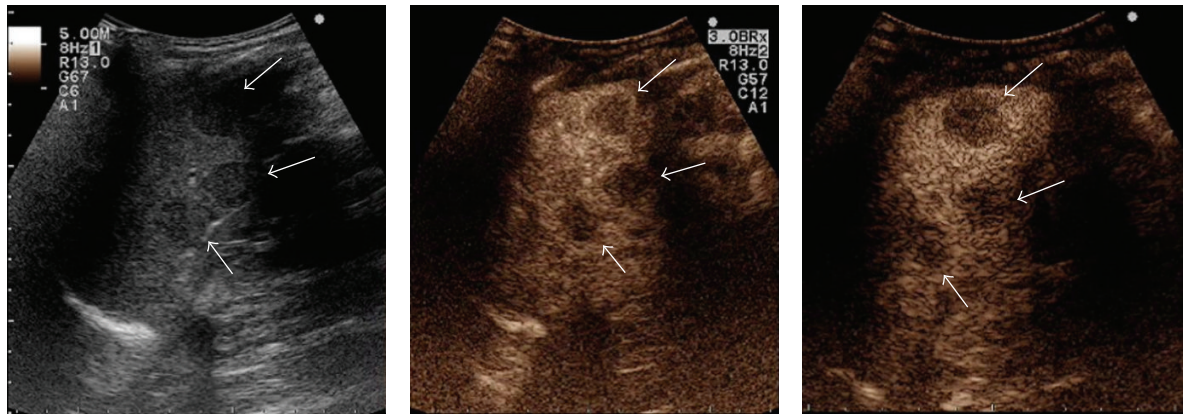

(a) (b) (c)

Figure 5: A 45-year-old woman with history of colon cancer, polycystic ovary syndrome, and migraine, who presented with fatigue, weight loss, and headache. No changes in bowel habits were reported. Physical examination revealed only laterocervical lymphadenopathy. (a) B-mode US documented splenomegaly, with parenchyma subverted by multiple and rounded hypoechoic lesions (arrows). The nodules had maximum size of 22 mm and showed no flow on Color Doppler US. Contrast-enhanced US documented (b) rim-like enhancement of the lesions in the arterial phase (7 seconds, arrows) and hypoenhancement in the parenchymal (c) (1 min 20 sec, arrows) and late phases. In view of the patient history, this pattern was first suggestive of malignancy. However, other organs were normal on second imaging, and histopathological examination revealed noncaseating granulomas, suggesting the diagnosis of splenic sarcoidosis (reprinted with permission from [10]).

In conclusion, hepatosplenic sarcoidosis remains so far a challenging diagnosis [69, 70]. Imaging findings are often nonspecific, and, in cases of isolated abdominal organ involvement, a diagnosis of sarcoidosis can be achieved only by revealing noncaseating granulomas in tissue specimens and excluding other causes of granulomatous inflammation [36, 71, 72]. The role of conventional imaging, such as ultrasound, CT, and MRI, can be reserved in the staging of the disease and not for diagnostic purposes, because isolated hepatosplenic sarcoidosis can be misdiagnosed with disorders such as lymphoma or metastasis that manifest with similar findings and may raise an erroneous suspicion, especially if the patients have a history of malignancy. CEUS has potential in the assessment of hepatosplenic sarcoidosis, but there is need of prospective, controlled trials that aim to explore CEUS patterns in comparison with conventional imaging and biopsy, before drawing definite conclusions.

Conflict of Interests

The authors declare that there is no conflict of interests regarding the publication of the paper.

References

[1] M. C. Iannuzzi, B. A. Rybicki, and A. S. Teirstein, "Sarcoidosis," *The New England Journal of Medicine*, vol. 357, no. 21, pp. 2153–2165, 2007.

[2] M. C. Iannuzzi and J. R. Fontana, "Sarcoidosis: clinical presentation, immunopathogenesis, and therapeutics," *Journal of the American Medical Association*, vol. 305, no. 4, pp. 391–399, 2011.

[3] D. Valeyre, A. Prasse, H. Nunes, Y. Uzunhan, P. Y. Brillet, and J. Müller-Quernheim, "Sarcoidosis," *The Lancet*, vol. 383, no. 9923, pp. 1155–1167, 2014.

[4] T. O. Hirche, H. Hirche, X. W. Cui, T. O. Wagner, and C. F. Dietrich, "Ultrasound evaluation of mediastinal lymphadenopathy in patients with sarcoidosis," *Medical Ultrasonography*, vol. 16, no. 3, pp. 194–200, 2014.

[5] C. Tana, M. A. Giamberardino, M. Di Gioacchino, A. Mezzetti, and C. Schiavone, "Immunopathogenesis of sarcoidosis and risk of malignancy: a lost truth?" *International Journal of Immunopathology and Pharmacology*, vol. 26, no. 2, pp. 305–313, 2013.

[6] D. G. James, "A clinicopathological classification of granulomatous disorders," *Postgraduate Medical Journal*, vol. 76, no. 898, pp. 457–465, 2000.

[7] B. A. Rybicki and M. C. Iannuzzi, "Epidemiology of sarcoidosis: recent advances and future prospects," *Seminars in Respiratory and Critical Care Medicine*, vol. 28, no. 1, pp. 22–35, 2007.

[8] H. Nunes, D. Bouvry, P. Soler, and D. Valeyre, "Sarcoidosis," *Orphanet Journal of Rare Diseases*, vol. 2, no. 1, article 46, 2007.

[9] J. P. Cremers, M. Drent, R. P. Baughman, P. A. Wijnen, and G. H. Koek, "Therapeutic approach of hepatic sarcoidosis," *Current Opinion in Pulmonary Medicine*, vol. 18, no. 5, pp. 472–482, 2012.

[10] C. Tana, G. Iannetti, P. D'Alessandro, M. Tana, A. Mezzetti, and C. Schiavone, "Pitfalls of contrast-enhanced ultrasound (CEUS) in the diagnosis of splenic sarcoidosis," *Journal of Ultrasound*, vol. 16, no. 2, pp. 75–80, 2013.

[11] J. Cremers, M. Drent, A. Driessen et al., "Liver-test abnormalities in sarcoidosis," *European Journal of Gastroenterology and Hepatology*, vol. 24, no. 1, pp. 17–24, 2012.

[12] C. J. Kahi, R. Saxena, M. Temkit et al., "Hepatobiliary disease in sarcoidosis," *Sarcoidosis Vasculitis and Diffuse Lung Diseases*, vol. 23, no. 2, pp. 117–123, 2006.

[13] R. J. Schauer, U. Völker, and A. Kreuzmayr, "An unorthodox pancreatic lesion in a young man presenting with jaundice," *Gastroenterology*, vol. 141, no. 5, pp. 1563–1949, 2011.

[14] E. C. Ebert, M. Kierson, and K. D. Hagspiel, "Gastrointestinal and hepatic manifestations of sarcoidosis," *American Journal of Gastroenterology*, vol. 103, no. 12, pp. 3184–3192, 2008.

[15] D. R. Moller, "Rare manifestations of sarcoidosis," *European Respiratory Monograph*, vol. 10, pp. 233–250, 2005.

[16] N. Ara, K. Iijima, J. Honda et al., "Endoscopically proven case of rapid esophagogastric variceal progression and rupture as a result of portal hypertension with liver sarcoidosis," *Digestive Endoscopy*, 2013.

[17] D. M. Warshauer and J. K. T. Lee, "Imaging manifestations of abdominal sarcoidosis," *American Journal of Roentgenology*, vol. 182, no. 1, pp. 15–28, 2004.

[18] S. Sartori, R. Galeotti, N. Calia et al., "Sonographically guided biopsy and sonographic monitoring in the diagnosis and follow-up of 2 cases of sarcoidosis with hepatic nodules and inconclusive thoracic findings," *Journal of Ultrasound in Medicine*, vol. 21, no. 9, pp. 1035–1039, 2002.

[19] M. Giovinale, C. Fonnesu, A. Soriano et al., "Atypical sarcoidosis: case reports and review of the literature," *European Review for Medical and Pharmacological Sciences*, vol. 13, no. 1, pp. 37–44, 2009.

[20] A. Kessler, D. G. Mitchell, H. L. Israel, and B. B. Goldberg, "Hepatic and splenic sarcoidosis: ultrasound and MR imaging," *Abdominal Imaging*, vol. 18, no. 2, pp. 159–163, 1993.

[21] C. Hoeffel, C. Bokemeyer, J. C. Hoeffel, H. Gaucher, M. Galanski, and P. Fornes, "CT hepatic and splenic appearances with sarcoidosis," *European Journal of Radiology*, vol. 23, no. 2, pp. 94–96, 1996.

[22] D. M. Warshauer, P. L. Molina, S. M. Hamman et al., "Nodular sarcoidosis of the liver and spleen: analysis of 32 cases," *Radiology*, vol. 195, no. 3, pp. 757–762, 1995.

[23] D. Faust, C. Fellbaum, S. Zeuzem, and C. F. Dietrich, "Nodular regenerative hyperplasia of the liver: a rare differential diagnosis of cholestasis with response to ursodeoxycholic acid," *Zeitschrift fur Gastroenterologie*, vol. 41, no. 3, pp. 255–258, 2003.

[24] P. Grzelak, L. Augsburg, A. Majos et al., "Use of contrast-enhanced ultrasonography in hepatosplenic sarcoidosis: report of 2 cases," *Polish Journal of Radiology*, vol. 77, no. 3, pp. 60–63, 2012.

[25] S. Bauones, T. Le Corroller, O. Durieux et al., "Splenic sarcoidosis mimicking neoplastic disease," *Journal of Clinical Ultrasound*, vol. 42, no. 1, pp. 38–41, 2014.

[26] S. J. Folz, C. D. Johnson, and S. J. Swensen, "Abdominal manifestations of sarcoidosis in CT studies," *Journal of Computer Assisted Tomography*, vol. 19, no. 4, pp. 573–579, 1995.

[27] C. F. Dietrich, M. S. Leuschner, S. Zeuzem et al., "Peri-hepatic lymphadenopathy in primary biliary cirrhosis reflects progression of the disease," *European Journal of Gastroenterology and Hepatology*, vol. 11, no. 7, pp. 747–753, 1999.

[28] C. F. Dietrich, M. Hocke, and C. Jenssen, "Ultrasound for abdominal lymphadenopathy," *Deutsche Medizinische Wochenschrift*, vol. 138, no. 19, pp. 1001–1018, 2013.

[29] C. F. Dietrich, K. Viel, B. Braden, W. F. Caspary, and S. Zeuzem, "Mediastinal lymphadenopathy: an extrahepatic manifestation of chronic hepatitis C?" *Zeitschrift fur Gastroenterologie*, vol. 38, no. 2, pp. 143–152, 2000.

[30] C. Jöst, C. Aiginger, and H. Prosch, "Isolated sarcoidosis of the spleen and liver as incidental ultrasound findings," *RöFo*, vol. 182, no. 4, pp. 353–354, 2010.

[31] W. Gul, K. Abbass, R. J. Markert, and S. Akram, "Case of isolated hepatic sarcoidosis," *European Review for Medical and Pharmacological Sciences*, vol. 15, no. 1, pp. 107–108, 2011.

[32] V. Vardhanabhuti, N. Venkatanarasimha, G. Bhatnagar et al., "Extra-pulmonary manifestations of sarcoidosis," *Clinical Radiology*, vol. 67, no. 3, pp. 263–276, 2012.

[33] D. M. Warshauer, "Splenic sarcoidosis," *Seminars in Ultrasound, CT and MRI*, vol. 28, no. 1, pp. 21–27, 2007.

[34] Z. V. Fong, J. Wong, W. R. Maley et al., "Sarcoid-reaction mimicking metastatic malignant hepatopancreatobiliary tumors: report of two cases and review of the literature," *Journal of Gastrointestinal Surgery*, vol. 16, no. 6, pp. 1245–1250, 2012.

[35] G. Jung, N. Brill, L. W. Poll, J. A. Koch, and M. Wettstein, "MRI of hepatic sarcoidosis: large confluent lesions mimicking malignancy," *The American Journal of Roentgenology*, vol. 183, no. 1, pp. 171–173, 2004.

[36] Y. Rosen, "Pathology of sarcoidosis," *Seminars in Respiratory and Critical Care Medicine*, vol. 28, no. 1, pp. 36–52, 2007.

[37] G. Tchernev, C. Tana, C. Schiavone, J. C. Cardoso, J. Ananiev, and U. Wollina, "Sarcoidosis versus sarcoid-like reactions: the two sides of the same Coin?" *Wiener Medizinische Wochenschrift*, 2014.

[38] G. Tchernev, "Cutaneous sarcoidosis: the "great imitator": etiopathogenesis, morphology, differential diagnosis, and clinical management," *The American Journal of Clinical Dermatology*, vol. 7, no. 6, pp. 375–382, 2006.

[39] G. Tchernev and U. Wollina, "Sarcoidosis, cancer and molecular mimicry," *International Journal of Immunopathology and Pharmacology*, vol. 26, no. 3, pp. 753–755, 2013.

[40] G. C. Scott, J. M. Berman, and J. L. Higgins Jr., "CT patterns of nodular hepatic and splenic sarcoidosis: a review of the literature," *Journal of Computer Assisted Tomography*, vol. 21, no. 3, pp. 369–372, 1997.

[41] L. Thanos, A. Zormpala, E. Brountzos, A. Nikita, and D. Kelekis, "Nodular hepatic and splenic sarcoidosis in a patient with normal chest radiograph," *European Journal of Radiology*, vol. 41, no. 1, pp. 10–11, 2002.

[42] D. M. Warshauer, R. C. Semelka, and S. M. Ascher, "Nodular sarcoidosis of the liver and spleen: appearance on MR images," *Journal of Magnetic Resonance Imaging*, vol. 4, no. 4, pp. 553–557, 1994.

[43] T. Albrecht, M. Blomley, L. Bolondi et al., "Guidelines for the use of contrast agents in ultrasound: January 2004," *Ultraschall in der Medizin*, vol. 25, no. 4, pp. 249–256, 2004.

[44] M. Claudon, D. Cosgrove, T. Albrecht et al., "Guidelines and good clinical practice recommendations for contrast enhanced ultrasound (CEUS)—Update 2008," *Ultraschall in der Medizin*, vol. 29, no. 1, pp. 28–44, 2008.

[45] M. Claudon, C. F. Dietrich, B. I. Choi et al., "Guidelines and good clinical practice recommendations for contrast enhanced ultrasound (CEUS) in the liver—update 2012: a WFUMB-EFSUMB initiative in cooperation with representatives of AFSUMB, AIUM, ASUM, FLAUS and ICUS," *Ultraschall in der Medizin*, vol. 34, no. 1, pp. 11–29, 2013.

[46] F. Piscaglia, C. Nolsøe, C. F. Dietrich et al., "The EFSUMB guidelines and recommendations on the clinical practice of contrast enhanced ultrasound (CEUS): update 2011 on non-hepatic applications," *Ultraschall in der Medizin*, vol. 33, no. 1, pp. 33–59, 2012.

[47] C. F. Dietrich, "Liver tumor characterization—comments and illustrations regarding guidelines," *Ultraschall in der Medizin*, vol. 33, pp. S22–S30, 2012.

[48] C. F. Dietrich, X. W. Cui, and A. Ignee, "EFSUMB Guidelines 2011: comments and illustrations," *Ultraschall in der Medizin*, vol. 33, pp. S11–S21, 2012.

[49] D. Strobel, K. Seitz, W. Blank et al., "Contrast-enhanced ultrasound for the characterization of focal liver lesions—diagnos-

tic accuracy in clinical practice (DEGUM multicenter trial)," *Ultraschall in der Medizin*, vol. 29, no. 5, pp. 499–505, 2008.

[50] K. Seitz, T. Bernatik, D. Strobel et al., "Contrast-enhanced ultrasound (CEUS) for the characterization of focal liver lesions in clinical practice (DEGUM Multicenter Trial): CEUS vs. MRI aprospective comparison in 269 patients," *Ultraschall in der Medizin*, vol. 31, no. 5, pp. 492–499, 2010.

[51] I. G. Molins, J. M. Font, J. C. Alvaro, J. L. Navarro, M. F. Gil, and C. M. Rodríguez, "Contrast-enhanced ultrasound in diagnosis and characterization of focal hepatic lesions," *World Journal of Radiology*, vol. 2, no. 12, pp. 455–462, 2012.

[52] Y. Guang, L. Xie, H. Ding, A. Cai, and Y. Huang, "Diagnosis value of focal liver lesions with SonoVue- enhanced ultrasound compared with contrast-enhanced computed tomography and contrast-enhanced MRI: a meta-analysis," *Journal of Cancer Research and Clinical Oncology*, vol. 137, no. 11, pp. 1595–1605, 2011.

[53] M. Westwood, M. Joore, J. Grutters et al., "Contrast-enhanced ultrasound using SonoVue (sulphur hexafluoride microbubbles) compared with contrast-enhanced computed tomography and contrast-enhanced magnetic resonance imaging for the characterisation of focal liver lesions and detection of liver metastases: A systematic review and cost-effectiveness analysis," *Health Technology Assessment*, vol. 17, no. 16, pp. 1–243, 2013.

[54] C. F. Dietrich, M. Sharma, R. N. Gibson, D. Schreiber-Dietrich, and C. Jenssen, "Fortuitously discovered liver lesions," *World Journal of Gastroenterology*, vol. 19, no. 21, pp. 3173–3188, 2013.

[55] I. Sporea, R. Badea, A. Popescu et al., "Contrast-enhanced ultrasound (CEUS) for the evaluation of focal liver lesions—a prospective multicenter study of its usefulness in clinical practice," *Ultraschall in der Medizin*, vol. 35, no. 3, pp. 259–266, 2014.

[56] M. Friedrich-Rust, T. Klopffleisch, J. Nierhoff et al., "Contrast-enhanced ultrasound for the differentiation of benign and malignant focal liver lesions: a meta-analysis," *Liver International*, vol. 33, no. 5, pp. 739–755, 2013.

[57] D. D. Cokkinos, M. J. Blomley, C. J. Harvey, A. Lim, C. Cunningham, and D. O. Cosgrove, "Can contrast-enhanced ultrasonography characterize focal liver lesions and differentiate between benign and malignant, thus providing a one-stop imaging service for patients?" *Journal of Ultrasound*, vol. 10, no. 4, pp. 186–193, 2007.

[58] A. Stang, H. Keles, S. Hentschke et al., "Differentiation of benign from malignant focal splenic lesions using sulfur hexafluoride-filled microbubble contrast-enhanced pulse-inversion sonography," *American Journal of Roentgenology*, vol. 193, no. 3, pp. 709–721, 2009.

[59] X. Yu, J. Yu, P. Liang, and F. Liu, "Real-time contrast-enhanced ultrasound in diagnosing of focal spleen lesions," *European Journal of Radiology*, vol. 81, no. 3, pp. 430–436, 2012.

[60] W. Li, G. Liu, W. Wang et al., "Real-time contrast enhanced ultrasound imaging of focal splenic lesions," *European Journal of Radiology*, vol. 83, no. 4, pp. 646–653, 2014.

[61] A. Ignee, X. Cui, T. Hirche et al., "Percutaneous biopsies of splenic lesions—a clinical and contrast enhanced ultrasound based algorithm," *Clinical Hemorheology and Microcirculation*, 2014.

[62] H. X. Xu, "Contrast-enhanced ultrasound: the evolving applications," *World Journal of Radiology*, vol. 1, no. 1, pp. 15–24, 2009.

[63] A. Von Herbay, A. Barreiros, A. Ignee et al., "Contrast-enhanced ultrasonography with SonoVue: differentiation between benign and malignant lesions of the spleen," *Journal of Ultrasound in Medicine*, vol. 28, no. 4, pp. 421–434, 2009.

[64] A. Stang, H. Keles, S. Hentschke et al., "Incidentally detected splenic lesions in ultrasound: does contrast-enhanced ultrasonography improve the differentiation of benign hemangioma/hamartoma from malignant lesions?" *Ultraschall in der Medizin*, vol. 32, no. 6, pp. 582–592, 2011.

[65] M. Stryckers, D. Voet, D. Vogelaers, M. Afschrift, K. Verstraete, and S. van Belle, "Contrast-enhanced ultrasonography in hepatosplenic sarcoidosis," *Acta Clinica Belgica*, vol. 66, no. 6, pp. 429–431, 2011.

[66] M. J. Pérez-Grueso, A. Repiso, R. Gómez et al., "Splenic focal lesions as manifestation of sarcoidosis: characterization with contrast-enhanced sonography," *Journal of Clinical Ultrasound*, vol. 35, no. 7, pp. 405–408, 2007.

[67] C. Tana, G. Iannetti, A. Mezzetti, and C. Schiavone, "Splenic sarcoidosis remains a diagnostic challenge," *Journal of Clinical Ultrasound*, vol. 42, no. 3, p. 156, 2014.

[68] X. W. Cui, C. Jenssen, A. Saftoiu, A. Ignee, and C. F. Dietrich, "New ultrasound techniques for lymph node evaluation," *World Journal of Gastroenterology*, vol. 19, no. 30, pp. 4850–4860, 2013.

[69] F. Robertson, P. Leander, and O. Ekberg, "Radiology of the spleen," *European Radiology*, vol. 11, no. 1, pp. 80–95, 2001.

[70] A. Karagiannidis, M. Karavalaki, and A. Koulaouzidis, "Hepatic sarcoidosis," *Annals of Hepatology*, vol. 5, no. 4, pp. 251–256, 2006.

[71] A. P. Barreiros, B. Braden, C. Schieferstein-Knauer, A. Ignee, and C. F. Dietrich, "Characteristics of intestinal tuberculosis in ultrasonographic techniques," *Scandinavian Journal of Gastroenterology*, vol. 43, no. 10, pp. 1224–1231, 2008.

[72] C. Tana, M. Tana, A. Mezzetti, and C. Schiavone, "Sarcoidosis: old certainties and new perspectives," *Italian Journal of Medicine*, vol. 6, no. 3, pp. 186–194, 2012.

Hindawi Publishing Corporation
BioMed Research International
Volume 2014, Article ID 687608, 13 pages
http://dx.doi.org/10.1155/2014/687608

Review Article

The Role of ^{18}F-FDG PET/CT in Large-Vessel Vasculitis: Appropriateness of Current Classification Criteria?

H. Balink,[1] R. J. Bennink,[2] B. L. F. van Eck-Smit,[2] and H. J. Verberne[2]

[1] *Department of Nuclear Medicine, Medical Center Leeuwarden, P.O. Box 850, 8901 BR Leeuwarden, The Netherlands*
[2] *Department of Nuclear Medicine, Academic Medical Center, 1105 AZ Amsterdam, The Netherlands*

Correspondence should be addressed to H. Balink; hans.balink@znb.nl

Received 22 May 2014; Accepted 20 July 2014; Published 14 August 2014

Academic Editor: Filippo Galli

Patients with clinical suspicion of large-vessel vasculitis (LVV) may present with nonspecific signs and symptoms and increased inflammatory parameters and may remain without diagnosis after routine diagnostic procedures. Both the nonspecificity of the radiopharmaceutical ^{18}F-FDG and the synergy of integrating functional and anatomical images with PET/CT offer substantial benefit in the diagnostic work-up of patients with clinical suspicion for LVV. A negative temporal artery biopsy, an ultrasonography without an arterial halo, or a MRI without aortic wall thickening or oedema do not exclude the presence of LVV and should therefore not exclude the use of ^{18}F-FDG PET/CT when LVV is clinically suspected. This overview further discusses the notion that there is substantial underdiagnosis of LVV. Late diagnosis of LVV may lead to surgery or angioplasty in occlusive forms and is often accompanied by serious aortic complications and a fatal outcome. In contrast to the American College of Rheumatology 1990 criteria for vasculitis, based on late LVV effects like arterial stenosis and/or occlusion, ^{18}F-FDG PET/CT sheds new light on the classification of giant cell arteritis (GCA) and Takayasu arteritis (TA). The combination of these observations makes the role of ^{18}F-FDG PET/CT in the assessment of patients suspected for having LVV promising.

1. Introduction

This paper focuses on the role of ^{18}F-FDG PET/CT in patients with symptoms possibly related with large vessel vasculitis (LVV) and the pathophysiologically associated polymyalgia rheumatica (PMR). Patients with clinical suspicion of LVV may present with nonspecific signs and symptoms like fatigue, malaise, weight loss, anorexia, subfebrile temperatures or night sweats, and increased C-reactive protein (CRP) levels or erythrocyte sedimentation rate (ESR). This patient population may remain without a diagnosis after routine diagnostic procedures. Both the nonspecificity of the radiopharmaceutical ^{18}F-FDG and the synergy of integrating functional and anatomical images with hybrid PET/CT may offer substantial benefit in the diagnostic work-up of patients with clinical suspicion for LVV. An important feature of ^{18}F-FDG PET imaging is the ability to reveal increased metabolism and functional alterations that precede the morphological changes. In addition this paper discusses whether the specific characteristics of ^{18}F-FDG PET/CT may shed new light on the American College of Rheumatology (ACR) classification of LVV in giant cell arteritis (GCA) and Takayasu arteritis (TA).

2. Background

Vasculitides are a heterogeneous group of syndromes; the 1990 American College of Rheumatology (ACR) established criteria designed to differentiate among patients with 7 types of vasculitis [1]. Historically, TA and GCA have been considered distinct diseases based on differences in age at onset, ethnic distribution, and clinical features, including predilection for involvement of certain arterial territories [2, 3].

The goals of the first International Chapel Hill Consensus Conference on the Nomenclature of Systemic Vasculitides (CHCC1994) were to reach consensus on names for the most

common forms of vasculitis and furthermore to construct a specific definition for each form [4]. The CHCC1994 classification organized vasculitis according to vessel size:

(i) large vessels: giant cell arteritis (GCA), Takayasu arteritis (TA);

(ii) medium vessels: periarteritis nodosa, Kawasaki's arteritis, primary CNS vasculitis, and Buerger's disease (thromboangiitis obliterans);

(iii) small vessels: Wegener's disease, Churg-Strauss syndrome, microscopic polyangiitis, Henoch-Schonlein purpura, and essential cryoglobulinaemic vasculitis.

Because of advances in understanding the pathophysiology of vasculitis, another International Chapel Hill Consensus Conference (CHCC2012) was convened. With respect to LVV, changes in definition were made. Criteria for TA based on late effects of arterial lumen narrowing or occlusion were removed: "claudication of an extremity, decreased brachial artery pulse, difference in systolic blood pressure between arms, a bruit over the subclavian arteries or the aorta, arteriographic evidence of narrowing or occlusion of the entire aorta." Furthermore, the previous existing gap in age between the onset of <40 years for TA of age and ≥50 years of age for GCA was closed. The following definitions were formulated.

(i) *Giant cell arteritis*: arteritis, often granulomatous, usually affecting the aorta and/or its major branches, with a predilection for the branches of the carotid and vertebral arteries. Often involving the temporal artery. Onset usually in patients older than 50 years and often associated with polymyalgia rheumatica.

(ii) *Takayasu arteritis*: arteritis, often granulomatous, predominantly affecting the aorta and/or its major branches. Onset usually in patients younger than 50 years.

The term "temporal arteritis" was not regarded as a suitable alternative for GCA because not all patients have temporal artery involvement, and other categories of vasculitis can affect the temporal arteries. The CHCC2012 made notation that in patients with LVV large arteries may not be the predominant type of vessel affected because especially medium size arteries may be affected as well, or even smaller arteries, for example, ciliary and retinal arteries [5, 6]. It was recognized that the histopathological features of Takayasu arteritis and giant cell arteritis are indistinguishable, but the CHCC2012 participants did not seek to resolve the important question whether or not CGA and TA are the same disease [5].

3. Giant Cell Arteritis and Takayasu Arteritis

The idea that GCA and TA are part of a spectrum of conditions of a single disease was first proposed by Hall in 1973, who suggested that polymyalgia rheumatica (PMR), GCA, and TA constitute an "unholy trinity" of a single disease [7].

GCA is characterised by arterial injuries affecting the smooth muscle cells located in the media with fragmentation of the internal elastic lamina and also lymphocyte-monocyte transmural infiltration with the presence of macrophages [8]. GCA is associated with polymyalgia rheumatica (PMR) in approximately 40% of patients [9, 10]. GCA involvement of the aorta and/or its major branches may be asymptomatic or induce non-specific clinical complaints, which explains why it is often overlooked. This is underlined by the fact that late effects/complications of extracranial GCA may only be discovered after life-threatening events such as stroke, myocardial infarction, ruptured aortic aneurysm, or aortic dissections [11–14].

TA is a pan-arteritis with mononuclear infiltrates and giant cells, mostly located in the adventitia and the media [15]. TA has an estimated incidence of only 2 cases per 1 million persons. The mean age at onset is 35 years, and prevalence of the disease in women is 2–25 times higher than that in men. During the course of the disease, stenoses, occlusions, and aneurysms may occur [16]. TA is reported to be potentially life-threating, reflected in mortality rates as high as 35% at 5 years after diagnosis, similar to that seen in malignancies [17].

The pathogenesis of both GCA and TA is unknown. Both are thought to be antigen-driven cell-mediated autoimmune processes, although the specific antigenic stimulus and or stimuli have not been identified [18]. Interleukin-6 (IL-6) may be a key mediator in GCA, TA, and PMR. Patients with GCA, TA, and PMR have elevated concentrations of IL-6 in both their peripheral circulation and their inflamed tissues, and serum levels of IL-6 correlate with disease activity. IL-6 receptor blockade with tocilizumab led to clinical and serologic improvement in patients with refractory or relapsing GCA, TA, and PMR [19].

Recent observations have shown that the histopathology of arterial lesions in GCA and TA is difficult to distinguish [18, 20]. On angiography strong similarities and subtle differences in these lesions were observed between GCA and TA [21].

4. Temporal Artery Biopsy

Temporal artery biopsy is considered the cornerstone of the diagnosis of GCA, which explains why review articles were published under the title "Large-Vessel Vasculitis" but dealt almost entirely with the problems of interpreting laboratory results and the results of ultrasonography and temporal artery biopsy [22]. Temporal artery biopsyis invasive and can be false negative, due to, for example, skip lesions, in 15–70% of the cases, which may considerably delay the diagnosis [23].

Large-vessel arteritis may occur in isolation, without classical features such as headache and scalp tenderness, making a clinical diagnosis difficult. In a recent study of 74 patients with subclavian/axillary GCA diagnosed by angiography and 74 control patients with temporal artery biopsy-proven GCA and without large-vessel involvement at angiography were matched for the date of first diagnosis. PMR occurred with similar frequency in both patient groups and temporal artery biopsy findings were negative in 42% of patients with large-vessel GCA. Large-vessel GCA was associated with higher

concentrations of interleukin-2 gene transcripts in arterial tissue and overrepresentation of the HLA-DRB1*0404 allele, indicating differences in pathogenetic mechanisms. GCA is apparently not a single entity but may comprise several variants of the same disease. In the spectrum of clinical manifestations it often occurs without involvement of the cranial arteries [24].

This interpretation is supported by the variable phenotypes in patients at different ages that are reported in analyses of other autoimmune diseases, including systemic lupus erythematosus, rheumatoid arthritis, systemic sclerosis, and dermatomyositis [20].

5. Underestimation of the Prevalence/Incidence of LVV

The incidence of LVV generally mentioned in the literature is 20–30/100.000 persons (0.02%) [26]. Based on the largest retrospective series, the prevalence of involvement of extracranial vessels in GCA is around 15% [27]. The notion that there is substantial underdiagnosis of LVV is supported by several autopsy observations.

A small study from 1968 of six autopsy cases revealed involvement of the aorta and other arteries in patients with coexisting giant cell arteritis, as well in patients with PMR in whom a temporal artery biopsy was negative or clinical signs of vasculitis were absent [28]. Most convincing is a retrospective study (from 1973!) of arterial changes in 20,591 autopsy subjects in Sweden, which revealed that PMR with signs of aortic involvement is far more common than is diagnosed clinically; arteritis was found in 0.4% and only half of them had temporal arteritis [29]. The often asymptomatic course of LVV was demonstrated by a retrospective review of 1,204 aortic surgical specimens that were gathered over a period of 20 years; 52 (4.3%) were clinically and pathologically classified as idiopathic aortitis. In 31%, aortitis was associated with a remote patient history of vasculitis and a variety of other systemic disorders [30].

The heterogeneity of LVV was substantiated in a report on 72 cases of, during life, documented GCA with aortic and extracranial large vessel involvement. The disease process affected the entire aorta in 35 of 72 cases, the head and neck or upper limb arteries in 24/72 cases, and the lower limb arteries in 13/72 cases [31].

6. Importance of Early Diagnosis of LVV

Additionally, a late diagnosis of LVV leading to surgery or angioplasty in occlusive forms (with higher frequency in patients classified as TA) is often accompanied by serious aortic complications and a fatal outcome [32]. Manifestations are very polymorphous, with presentations that range from asymptomatic to neurologic complications. LVV has also been reported to manifest as isolated involvement of renal arteries (for which renal revascularization was required), or pulmonary arteries resulting in occlusion, and of coronary arteries, requiring bypass surgery [33–37]. Particularly in older patients visual loss in one eye was reported to be prevalent in 16–18% of patients at initial diagnosis [38, 39]. In Great Britain visual loss in patients diagnosed with temporal arteritis occurs in as much as 20% of patients [40].

Abdominal aortic aneurysms (AAA) are a substantial burden on health care. Recent studies may bridge a gap between the clinical signs and diagnosis of AAA and immune-mediated large-vessel vasculitis. Serum levels of IL-1β, TNF-α, and IL-6 were proven to be elevated in AAA patients. In AAA tissue samples, levels of TNF-α were found to be higher in small-sized AAAs than in large-sized AAAs and may be related to infiltration of macrophages [41, 42]. In a follow-up of 96 GCA patients that all fulfilled the ACR criteria, and of which 88 had artery biopsy specimens showing GCA (87 temporal, 1 occipital), it was found that these patients were 17 times more likely to develop a thoracic aneurysm and 2.4 times more likely to develop an AAA compared with the general population [27]. In the same cohort of 96 patients (diagnosed between January 1950 and December 1999) the median time from diagnosis of GCA to detection for AAA was 6.3 years and for thoracic aortic aneurysms 10.9 years [43].

7. Utility of ^{18}F-FDG PET/CT in the Diagnosis of LVV, PMR, and Temporal Arteritis

7.1. LVV. In a review from 2003 and later in 2009 it was stated that in patients presenting with a prolonged inflammatory syndrome with nonconclusive signs and symptoms, the presence of diffuse increased ^{18}F-FDG uptake in the wall of the aorta and its main branches may efficiently guide to the diagnosis of LVV [44, 45].

To further substantiate this statement, ^{18}F-FDG PET/CT was recently performed in a series of 140 patients with inflammation of unknown origin (IUO). IUO was defined as repeated CRP values more than 20 mg/L or ESR more than 20 mm/h, with nonspecific signs and complaints, body temperature below 38.3°C (100.9°F), and without a diagnosis after conventional diagnostic procedures. The final diagnosis was related to infection in 35 patients, malignancy in 18 patients, noninfectious inflammatory disease (NIID) in 44 patients, and a variety of uncommon conditions in 7 patients. NIID was the main category with PMR in 18 patients as the first main diagnosis and LVV in 12 patients as the second most established diagnosis. Signs of PMR were seen in 3 patients with LVV, and vice versa LVV signs on the PET images in 4 patients with PMR. None of the 12 patients with LVV had clinical signs or symptoms of temporal arteritis; nevertheless biopsy was positive for GCA in 1 patient and another patient with LVV had wall thickening with ultrasonography of the temporal artery [25]. Another recent study on IUO included 88 patients aged 50 years or older with nonspecific complaints and an ESR of more than 50 mm/h for which routine evaluation revealed no diagnosis. Of the 88 included patients 18 were diagnosed with LVV and 6 with PMR, with only one of these patients eventually diagnosed with temporal arteritis [46]. In both IUO studies parameters like the proportion of patients with disease, the contribution of ^{18}F-FDG PET/CT to the diagnosis, and the distribution of diseases in infection,

NIID, and malignancy were similar to "fever of unknown origin" (FUO) patient populations [47–52].

In the literature reports on LVV—with the presence of diffuse and mildly intense ^{18}F-FDG uptake in the wall of the aorta and its main branches—are numerous and mostly comprise large patient numbers (Figure 1). The reported initial response to immunosuppressive therapy is better in LVV patients with nonspecific symptoms at the time of diagnosis, compared to patients that comply to the ACR 1990 criteria with measurable effects of arterial stenosis [49, 53–61].

Reports on patients with LVV limited to the aortic arch or only in isolated arteries; for example, the carotid or vertebral arteries are scarce (only case reports) and the images display a more intense ^{18}F-FDG in the aortic or arterial wall, compared to patients with LVV in the entire wall of the aorta and its main branches. A relatively high number of patients have symptoms at the time of diagnosis due to arterial occlusion and both relapse and progression (metabolic and angiographic) despite immunosuppressive therapy are reported [34–37, 62–64].

7.2. Polymyalgia Rheumatica. ^{18}F-FDG PET/CT images of patients with PMR reveal a characteristic pattern of pathologic ^{18}F-FDG uptake in the soft tissue and ligaments (perisynovitis or enthesitis) around the shoulders and hips, lumbar (and in many cases cervical) spinous processes, and ischial tuberosities (Figure 2) [65, 66]. ^{18}F-FDG PET/CT may show 2 different patterns of interspinous uptake: focal and diffuse. Diffuse uptake may reflect interspinous ligament inflammation; focal interspinous uptake may represent interspinous bursitis [66]. After chronic ligamentous interspinous inflammation, interspinous bursae may develop, leading to interspinous bursitis [67]. MRI is widely used to detect bone marrow edema and enthesitis in patients with spondyloarthritides (SpA). ^{18}F-FDG PET/CT may provide an alternative diagnostic method and will likely contribute to the early diagnosis of SpA in PMR [68]. Both LVV and PMR may be detected, in the early onset of the disease, by ^{18}F-FDG PET/CT. In some patients LVV is associated with PMR and vice versa [69, 70].

7.3. Temporal Arteritis. The first introduced stand-alone PET cameras provided a spatial resolution of 10 mm; a study from 2004 concluded, as a consequence, that stand-alone ^{18}F-FDG PET was not yet suitable for the diagnosis of temporal arteritis and therefore could not replace invasive biopsy [71]. Ongoing improvements in technology created an evolution in spatial resolution from 6 mm to 4 mm. In recent years increased ^{18}F-FDG uptake is visualized in patients with arteritis temporalis [72]. The most recently introduced PET/CT cameras claim a 2.5 mm spatial resolution for the PET component under optimal conditions. It is therefore to be expected that pathologic ^{18}F-FDG uptake in temporal arteritis will be reported more frequently. However, in patient populations with prolonged inflammatory parameters and nonspecific complaints and a positive ^{18}F-FDG PET/CT result for the diagnosis of LVV, temporal artery biopsy was negative in 50% [49, 73].

8. Specificity and Differential Diagnosis of Pathologic ^{18}F-FDG Uptake in the Arterial Wall

Many patients, assessed for malignant disease but without a history of vasculitis, may show some uptake of ^{18}F-FDG in, for example, the walls of the aorta, the subclavian arteries, and are with highest incidence in the iliofemoral arteries [74, 75]. Therefore, nuclear medicine physicians and other PET/CT practitioners have to be aware of the clinical significance of the different vascular patterns. As ^{18}F-FDG accumulates in macrophage-rich areas, it cannot distinguish between sterile inflammation—such as large vessel vasculitis—and infectious inflammation. In the differential diagnosis, the pattern and the localisation of the vascular involvement as well as the intensity of ^{18}F-FDG vascular uptake in the arterial wall should be taken into account for interpretation and especially differentiated from blood pool activity.

The differentiation of atherosclerosis from large vessel vasculitis is considered less problematic with PET/CT compared to a stand-alone PET [76]. Atherosclerosis usually displays a patchwork of partially normal vessel wall, focal inflammation, and calcifications. In terms of patient age, arterial inflammation precedes calcification; a study from 2005 with ^{18}F-FDG PET/CT showed that inflammation and calcification only had overlap in <2% of cases, suggesting that calcification and focal arterial inflammation represent different stages in the evolution of atheroma (Figure 4) [44, 77]. Future studies will tell if this simple interpretation of the images holds true; the possible link between vasculitis, inflammation, and atherosclerosis was already suggested more than a decade ago [78–80]. Subsequent studies showed that waist circumference and atherogenic risk factors were the strongest determinants of a patchy ^{18}F-FDG arterial uptake pattern, and for that reason "metabolic syndrome" was associated [74, 81].

In addition to GCA and Takayasu arteritis, other rheumatologic disorders, including rheumatoid arthritis, systemic lupus erythematosus, Wegener granulomatosis, Behçet's disease, polyarteritis nodosum, and microscopic polyangiitis, may lead to aortitis. In the case of rheumatoid associated aortitis, rheumatoid nodules are reported in the aortic wall in up to 50% of pathological specimens [82]. Furthermore, aortitis was reported in the HLA-B27-associated seronegative spondyloarthropathies, Reiter's syndrome, and ankylosing spondylitis [83]. Case reports exist on aortitis associated with sarcoidosis [84]. Cogan's syndrome is an unusual disorder characterized by episodes of interstitial keratitis and vestibuloauditory dysfunction (i.e., eye and ear symptoms); aortitis occurs in up to 10% of cases of Cogan's syndrome [62, 85]. Syphilitic aortitis, localized in only the wall of the ascending aorta, is reported in several recent case reports [86–88]. Aortitis also occurs in association with idiopathic retroperitoneal fibrosis (Ormond's disease), inflammatory

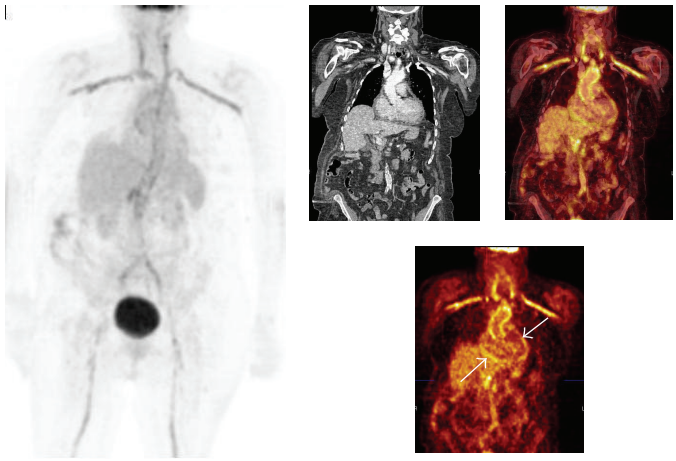

Figure 1: Patient history: lack of appetite and pain between the shoulder blades. Cardiologic evaluation and gastroscopy negative. CRP 224 mg/L. Increased ^{18}F-FDG uptake in the aorta and its main branches and less intense FDG uptake in the distal abdominal aortic wall; corresponding CT slices show calcifications here. The mild increased perisynovial ^{18}F-FDG uptake at both shoulders, which might be indicative of associated PMR. The increased ^{18}F-FDG uptake at the pericardium is suggestive of pericarditis (white arrows). Note: patient had a carbohydrate restricted diet for 2 days before the ^{18}F-FDG PET/CT investigation to decrease the ^{18}F-FDG uptake in the myocardium. Patient had a TIA one year earlier and subsequent carotid artery desobstruction. LVV was not suspected at that time; no immunosuppressive therapy was given. After the diagnosis of LVV patient was in remission during 4 years with Prednisolon orally tapered from 10 to 7.5 and later 5 mg daily. Due to relapse Prednisolon was increased to 15 mg daily. Patient died 5 years after the diagnosis of LVV after a severe CVA.

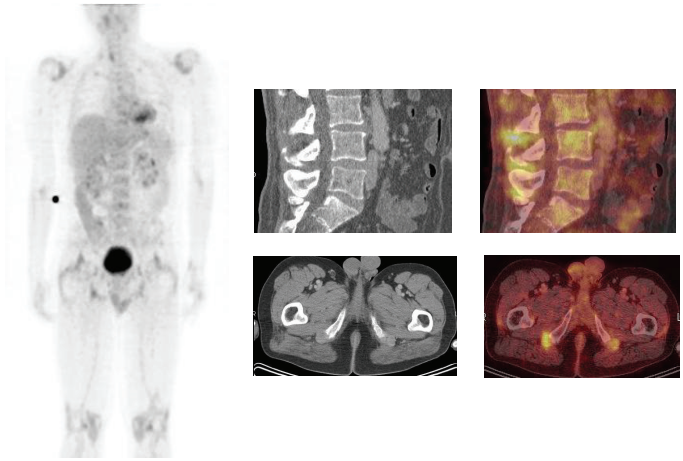

Figure 2: A 48-year-old man presented with initial painful calves followed by progressive painful arms and legs, shoulders, and knees. No hydrops or other clinical signs of arthritis. Normal body temperatures; CRP level, 84 mg/L; ESR, 41 mm/h; normal routine laboratory values; rheumatoid factor negative; cyclic citrullinated peptide antibody test negative; serum angiotensin-converting enzyme, 10.3 units/L; antinuclear antibody test negative; and anticytoplasmic autoantibodies negative. Urine sediment: albumin trace. Glomerular basal membrane antibody test negative. Viral serology negative. Chest X-ray and abdominal ultrasonography without abnormalities. X-ray of hands, feet, and knees revealed no erosive changes. Ultrasonography of the hips revealed no abnormalities. Also ^{18}F-FDG PET/CT showed pathological perisynovial uptake at the major joints, as well as pathological lumbar interspinous uptake in the soft tissue (bursae) lateral to both of the greater trochanters and dorsal to both of the tuber ischii. The diagnosis of PMR was made; after treatment with steroids, the patient became pain free, and the CRP values remained less than 10 mg/L [25].

abdominal aortic aneurysm, and perianeurysmal retroperitoneal fibrosis, a group of clinical disorders now categorized as chronic periaortitis [89].

However, the above-mentioned disease entities are different from LVV in that the inflammation is limited to the aorta and periaortic tissues rather than a manifestation of a widespread vasculitis of the aorta and its main branches.

As ^{18}F-FDG PET/CT will be more frequently used as a screening tool in more complex diagnostic settings like fever and inflammation of unknown origin, a routine investigator-independent strategy for establishing the diagnosis of LVV is needed. In this respect semiquantification might be helpful: a ratio of the ^{18}F-FDG maximal standardized uptake values (SUVmax) of the aorta-to-liver

Table 1: Definitions for large vessel vasculitis according to the American College of Rheumatology (ACR) 1990 criteria for the classification of giant cell arteritis and Takayasu's arteritis and the definitions revised by the 2012 International Chapel Hill Consensus Conference on the Nomenclature of Vasculitides (CHCC2012).

	ACR 1990 criteria	CHCC2012 definition
Large-vessel vasculitis (LVV)		Vasculitis affecting large arteries more often than other vasculitides Large arteries are the aorta and its major branches
Giant cell arteritis (GCA)	Age at onset of disease ≥ 50 yr New headache Temporal artery abnormality Elevated erythrocyte sedimentation rate Abnormal findings on biopsy of temporal artery Diagnosis: at least 3/5 criteria	Arteritis, often granulomatous, usually affecting the aorta and/or its major branches, with a predilection for the branches of the carotid and vertebral arteries Often involves the temporal artery Onset usually in patients older than 50 years and often associated with polymyalgia rheumatica Arteritis, often granulomatous, predominantly affecting the aorta and/or its major branches
Takayasu arteritis (TA)	Age at onset of disease ≤ 40 yr Onset usually in patients younger than 50 years Claudication of an extremity Arteritis, often granulomatous, Decreased brachial artery pulse predominantly affecting the aorta and/or its major Difference in systolic blood pressure between arms branches A bruit over the subclavian arteries or the aorta Arteriographic evidence of narrowing or occlusion of the entire aorta Diagnosis: at least 3/6 criteria	Onset usually in patients younger than 50 years Arteritis, often granulomatous, predominantly affecting the aorta and/or its major branches

appeared more reliable compared to the SUVmax of the aorta-mediastinum ratios for the diagnosis of LVV and was not affected by minor inflammation-associated changes in hepatic metabolism [56].

9. Sensitivity and Specificity of ^{18}F-FDG-PET/CT in Comparison to Other Imaging Modalities

In the knowledge that ultrasonography, MRI, arteriography, and PET/CT have proven useful image techniques in the diagnostic approach of LVV or suspicion of LVV, it remains difficult to compare the different imaging modalities. Results have to be interpreted with caution as metabolic changes in the arterial wall usually precede the anatomic changes [90–94]. Furthermore, the instigating inflammatory process may have subsided in arterial stenosis or aortic aneurysm. Problems rise therefore in the interpretation of ^{18}F-FDG PET/CT results in the many reports that describe patient populations that met the ACR 1990 classification criteria for GCA (i.e., with temporal artery abnormalities and/or a positive biopsy for arteritis) and TA (i.e., with clinical and measurable effects of arterial stenosis) (Table 1). Furthermore, in the majority of studies, patients were already receiving steroids, which negatively influences the sensitivity of ^{18}F-FDG PET for inflammatory processes, while sequelae like oedema and aortic/arterial wall thickening (CT or MRI) need more time to respond to therapy.

Reported discrepancies in ^{18}F-FDG PET/CT results, disease activity measured by inflammatory parameters, and radiologic evaluation with MRI may very well be caused by interpreting monitoring immunosuppressive therapy response with ^{18}F-FDG PET/CT as an initial staging procedure [54, 58, 64].

The active phases of recruitment, activation, migration, and infiltration of T cells, macrophages, and leucocytes usually precede the appearance of inflammatory oedema; ^{18}F-FDG PET/CT may therefore be positive at an earlier stage than an MRI scan [95]. Also angiography is suboptimal for the diagnosis of LVV because it detects only the late anatomical changes such as arterial wall abnormalities, arterial stenosis, or aortic aneurysm [96]. However, the chronic inflammation in asymptomatic AAAs was not sufficiently metabolically active to result in detection with ^{18}F-FDG PET/CT. Despite that histologic examination of large asymptomatic AAAs (range 52–66 mm) and small AAAs (range 34–40 mm) showed residual inflammatory cell infiltration with T cells and macrophages [97].

In addition the lack of a gold standard creates problems in the calculation of sensitivity and specificity; in some reports LVV diagnosed by ^{18}F-FDG PET/CT was confirmed by histology (of the temporal artery while patients with LVV have

Table 2: Sensitivity and specificity of different imaging modalities for LVV with their pathognomonic/typical imaging findings. (data on US and MRI from [111]).

	Pathognomonic/typical findings	Sensitivity/specificity
(Color-doppler) ultrasonography	(i) Edema, halo around the (temporal) artery (ii) Stenosis, increased blood flow velocities (iii) Occlusion, absent colour signal	Sens. 87%, Spec. 96% (for late effects of arteritis temporalis)
MRI	(i) Wall thickening (ii) Increased mural gadolinium contrast enhancement	Sens. 81%, Spec. 97% (for late effects of LVV)
^{18}F-FDG PET/CT	Increased ^{18}F-FDG uptake in walls of aorta and main cervical and thoracic branches	(i) Able to detect early inflammation without (late) effects like oedema, wall thickening, or arterial stenosis or aortic dilatation (ii) How to calculate sensitivity and specificity in lack of a gold standard?

involvement of the temporal artery in only approximately 50% of the cases!) or MRI angiography [61] (Table 2).

Or the diagnostic accuracy and sensitivity/specificity of an international expert panel was calculated and compared to computer calculated logistic regression models as a reference to assess the impact on clinical management with and without ^{18}F-FDG PET results [55].

Because GCA and TA were considered as two independent distinct diseases, patients with Takayasu arteritis (i.e., patients younger than 50 years) were excluded in reports and reviews [98].

In conclusion, a negative temporal artery biopsy, an ultrasonography without an arterial halo, or an MRI without aortic wall thickening or oedema do not exclude the presence of LVV and should therefore not exclude the use of ^{18}F-FDG PET/CT when LVV is clinically suspected.

10. Cost-Efficacy

In the "new" era of health care technology assessment (HTA), the costs of a diagnostic procedure should be weighed against its effectiveness in daily clinical practice. ^{18}F-FDG PET/CT has the ability to visualize the early onset of inflammatory processes within a whole body scan; positive findings correlate well with clinical and laboratory markers of inflammation, in particular C-reactive protein. The level of ^{18}F-FDG uptake may also provide prognostic information in LVV [96]. The intensity of thoracic aortic wall ^{18}F-FDG uptake at the time of diagnosis correlated with later increased aortic diameter (as measured by CT) after a mean of 46.7-month follow-up (adjusted for age, sex, hypertension, diabetes, cholesterol levels, erythrocyte sedimentation rate, and CRP). On multivariate analysis, only ^{18}F-FDG uptake at baseline remained significantly associated with increased thoracic aortic diameter ($P = 0.039$) [59].

Repeated ^{18}F-FDG PET/CT procedures involve expenses and radiation exposure to patients with vasculitis [99]. On the other hand, in patients diagnosed with PMR and without signs of LVV, an additional ^{18}F-FDG PET/CT will probably offer no advantage over the traditional follow-up of PMR patients, based on clinical evaluation and periodic determination of inflammatory laboratory parameters [100]. However, in patients diagnosed with LVV and treated with steroids, both normalization of laboratory data and symptomatic improvement of the patient correlated well with normalization of ^{18}F-FDG uptake in the large-vessel walls. CT and MRI frequently show residual abnormal findings even after symptoms have completely resolved and with discrepancies concerning ESR and CRP laboratory data [101, 102].

Patients diagnosed with LVV probably need to be classified in different risk groups, as already suggested in 1999 [24]. ^{18}F-FDG PET/CT is able to diagnose patients with LVV without cranial or cervical artery involvement, which is clinically relevant as patients with arteritis temporalis are probably more prone to develop thoracic aortic dilatation or arterial occlusion, and therefore need a more intensive treatment and close monitoring as compared to patients with isolated LVV or PMR [100, 103]. Those patients with localized and more intense ^{18}F-FDG uptake limited to only one artery or, for example, in the cervical arteries need even more close monitoring due to a higher risk of relapse and vascular complications; for example, aortitis in Cogan's syndrome is indistinguishable from TA. During the course of Cogan's syndrome aortic insufficiency may develop that may require valve replacement. Reports describe relapse and progression (both metabolic and angiographic) despite immunosuppressive therapy (Figure 3) [62, 104–106].

11. ACR Classification Criteria of LVV in Clinical Practices Using ^{18}F-FDG-PET/CT

The ACR vasculitis classification criteria were never intended for diagnostic purposes, as pointed out by Hunder and colleagues [1]. Nevertheless, clinicians often use these criteria to diagnose LVV. The ACR 1990 criteria for GCA and TA were based on the diagnosis of advanced cases. The criteria for GCA were developed at a time when involvement of the

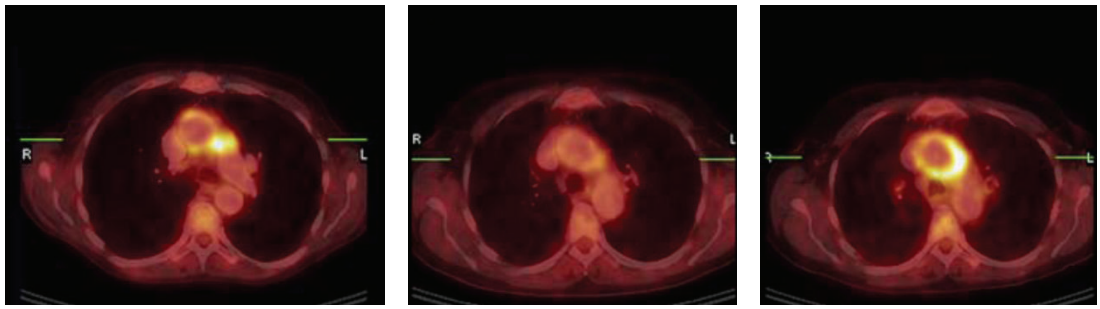

(a) (b) (c)

Figure 3: Aortitis in Cogan's syndrome. (a) Transverse hybrid PET/CT slice; pathological uptake in the wall of the aortic arch, more intense in the lateral wall and perivascular space adjacent to the truncus pulmonalis. (SUVmas 12, ESR 52 mm/h, CRP53 mg/L). (b) Follow-up PET/CT showed clearly decreased uptake in the aortic arch after 3 weeks treatment with methyl-Prednisolon i.v. and Prednisolon orally. (SUVmax 4, ESR 11 mm/h, and CRP < 2 mg/L). (c) Second follow-up PET/CT 6 months later (patient was in a stable condition with methotrexate and low-dose prednisone) with again high uptake in the wall of the aortic arch, with higher intensity in the lateral wall and perivascular space adjacent to the truncus pulmonalis. Methotrexate and prednisone were both increased to 20 mg/day (SUVmax 13, ESR 24 mm/h, and CRP 14 mg/L).

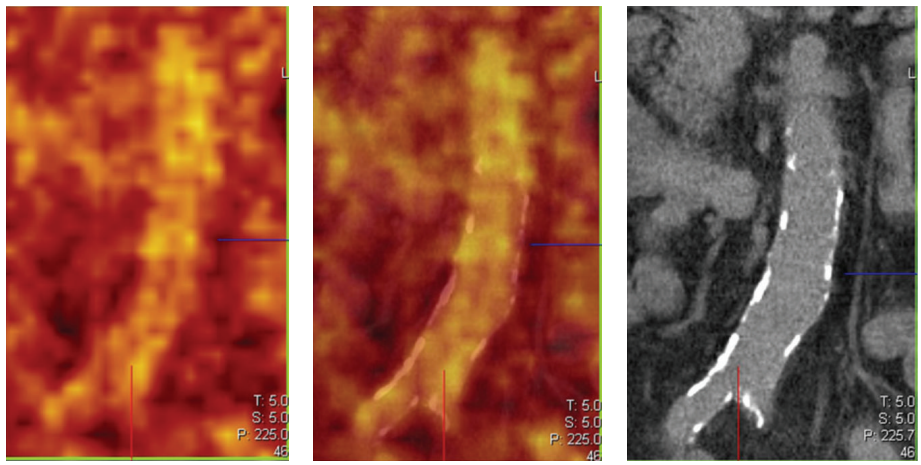

(a) (b) (c)

Figure 4: From left to right: PET, PET/CT, and CT coronal slices of atherosclerosis of the lower abdominal aorta. The focal and patchy increased FDG uptake representing inflammation and calcifications do not show overlap.

aorta and its main branches was not a well-recognized feature of GCA, and instead there was a focus on the involvement of cranial arteries of the disease. Already in 1998 it was concluded that the ACR 1990 classification criteria function poorly in the diagnosis of the specific vasculitides. Patients who do not have a vasculitis syndrome may meet very well the ACR criteria, and on the other hand patients who have a specific type of vasculitis may meet criteria for more than one of the vasculitides as specified by the ACR criteria [107].

A retrospective review of 75 patients with TA and 69 patients with GCA (as defined by the ACR 1990 criteria) compared the signs and symptoms of disease. Patients with GCA had a greater prevalence of jaw claudication (GCA 33%, TA 5%), blurred vision (GCA 29%, TA 8%), diplopia (GCA 9%, TA 0%), and blindness (GCA 14%, TA 0%). The perception of clinicians that the widely recognized classic manifestations are distinct for GCA and TA may have led to bias in history taking, physical examination, and selection of diagnostic studies. This bias might have impaired the recognition of similarities between GCA and TA [20].

The strict implementation of the ACR criteria in combination with ^{18}F-FDG PET/CT may create a significant source of confusion in the statistics and a significant bias in how the data are gathered in the classification of LVV. This is, for example, illustrated as patients with isolated and intense pathologic ^{18}F-FDG uptake in the vertebral arteries and with neurologic symptoms were diagnosed TA in one case report and as GCA in another, given an age of more or less than 50 years at the onset of disease [34, 35]. It is also puzzling that patients with a homogeneous pattern of increased ^{18}F-FDG uptake in the aorta and its main branches and no arterial wall abnormalities on the corresponding CT slices

are diagnosed as either TA or GCA, with only their age (≤ or ≥ 50 years) as the discriminating parameter [54, 55, 58, 60, 98, 108, 109]. TA is reported to be potentially life-threating, reflected in high mortality rates related to arterial stenoses, occlusions, and aortic aneurysms. Notwithstanding, complicated courses of GCA (mean age 66 years) were reported, with persistent inflammatory markers, arterial stenoses, and aortic aneurysms despite immunosuppressive therapy and ^{18}F-FDG PET showing signs of active vasculitis [92].

To further describe the confusion that ^{18}F-FDG PET/CT results may create in LVV classification, patients older than 50 years with a homogeneous pattern of increased ^{18}F-FDG uptake in the wall of the aorta and its main branches were erroneously reported as having TA instead of GCA [54, 58, 101, 110].

12. Conclusions and Future Perspectives

This review illustrates the usefulness of ^{18}F-FDG PET/CT in the heterogeneity of the large vessel vasculitides. In patients with a clinical suspicion for LVV, ^{18}F-FDG PET/CT is able to diagnose LVV especially at the early onset of disease. In contrast to the ACR 1990 criteria for vasculitis, based on late LVV effects like arterial stenosis and/or occlusion, ^{18}F-FDG-PET/CT sheds new light on the classification of GCA and TA and strengthens the notion that GCA and TA are more likely to be different expressions of a common histopathological entity. ^{18}F-FDG PET/CT is a powerful metabolic imaging tool that may help to improve the current classification system, based on the intensity of the ^{18}F-FDG uptake and its distribution pattern:

(i) isolated polymyalgia rheumatica (PMR) with pathologic ^{18}F-FDG uptake in the soft tissue and ligaments (perisynovitis or enthesitis) around the shoulders/hips and other major joints, lumbar/cervical spinous processes, and ischial tuberosities;

(ii) diffuse and mildly intense ^{18}F-FDG uptake in the wall of the aorta and its main branches and without arteritis temporalis, PMR, or anatomic arterial wall abnormalities;

(iii) diffuse and mildly intense ^{18}F-FDG uptake in the wall of the aorta and its main branches with arteritis temporalis, PMR, or anatomic arterial wall abnormalities;

(iv) intense and focal ^{18}F-FDG uptake in the aortic arch or intense ^{18}F-FDG uptake in isolated arteries.

In our opinion it is redundant to classify patients with a positive ^{18}F-FDG PET/CT for LVV in ≤50 years or ≥50 years of age.

An unintended problem that arises from the diagnosis of the early onset of LVV with ^{18}F-FDG PET/CT is the longer time period patients will be exposed to the adverse effects of glucocorticoids resulting in more pressure on the major need for more specific drugs to induce and maintain remission and to reduce the cumulative adverse effects of long-term glucocorticoid exposure. However, ^{18}F-FDG PET/CT may be useful in the increasing need for therapy monitoring resulting in better treatment planning and possibly reducing long-term adverse treatment effects.

Conflict of Interests

No conflict of interests and sources of funding were declared.

References

[1] G. G. Hunder, W. P. Arend, D. A. Bloch et al., "The American College of Rheumatology 1990 criteria for the classification of vasculitis: introduction," *Arthritis and Rheumatism*, vol. 33, no. 8, pp. 1065–1067, 1990.

[2] W. P. Arend, B. A. Michel, D. A. Bloch et al., "The American College of Rheumatology 1990 criteria for the classification of Takayasu arteritis," *Arthritis and Rheumatism*, vol. 33, no. 8, pp. 1129–1134, 1990.

[3] G. G. Hunder, D. A. Bloch, B. A. Michel et al., "The American College of Rheumatology 1990 criteria for the classification of giant cell arteritis," *Arthritis and Rheumatism*, vol. 33, no. 8, pp. 1122–1128, 1990.

[4] J. C. Jennette, R. J. Falk, K. Andrassy et al., "Nomenclature of systemic vasculitides: proposal of an international consensus conference," *Arthritis and Rheumatism*, vol. 37, no. 2, pp. 187–192, 1994.

[5] J. C. Jennette, R. J. Falk, P. A. Bacon et al., "2012 revised international Chapel Hill consensus conference nomenclature of vasculitides," *Arthritis & Rheumatology*, vol. 65, no. 1, pp. 1–11, 2013.

[6] S. S. Hayreh, P. A. Podhajsky, and B. Zimmerman, "Ocular manifestations of giant cell arteritis," *American Journal of Ophthalmology*, vol. 125, no. 4, pp. 509–520, 1998.

[7] G. H. Hall, "Giant cell arteritis-an unholy trinity," *The American Heart Journal*, vol. 85, no. 6, pp. 835–837, 1973.

[8] W. L. Gross, A. Trabandt, and E. Reinhold-Keller, "Diagnosis and evaluation of vasculitis," *Rheumatology*, vol. 39, no. 3, pp. 245–252, 2000.

[9] D. Blockmans, S. Stroobants, A. Maes, and L. Mortelmans, "Positron emission tomography in giant cell arteritis and polymyalgia rheumatica: evidence for inflammation of the aortic arch," *The American Journal of Medicine*, vol. 108, no. 3, pp. 246–249, 2000.

[10] D. Ernst, N. T. Baerlecken, R. E. Schmidt, and T. Witte, "Large vessel vasculitis and spondyloarthritis: coincidence or associated diseases?" *Scandinavian Journal of Rheumatology*, vol. 43, no. 3, pp. 246–248, 2014.

[11] G. Liu, R. Shupak, and B. K. Y. Chiu, "Aortic dissection in giant-cell arteritis," *Seminars in Arthritis and Rheumatism*, vol. 25, no. 3, pp. 160–171, 1995.

[12] G. M. Greene, D. Lain, R. M. Sherwin, J. E. Wilson, and B. M. McManus, "Giant cell arteritis of the legs. Clinical isolation of severe disease with gangrene and amputations," *The American Journal of Medicine*, vol. 81, no. 4, pp. 727–733, 1986.

[13] R. G. Klein, G. G. Hunder, A. W. Stanson, and S. G. Sheps, "Large artery involvement in giant cell (temporal) arteritis," *Annals of Internal Medicine*, vol. 83, no. 6, pp. 806–812, 1975.

[14] E. Nordborg and B.-A. Bengtsson, "Death rates and causes of death in 284 consecutive patients with giant cell arteritis confirmed by biopsy," *British Medical Journal*, vol. 299, no. 6698, pp. 549–550, 1989.

[15] M. Hotchi, "Pathological studies on Takayasu arteritis," *Heart and Vessels*, vol. 7, no. 7, pp. 11–17, 1992.

[16] H. L. Gornik and M. A. Creager, "Aortitis," *Circulation*, vol. 117, no. 23, pp. 3039–3051, 2008.

[17] E. Y. Kissin and P. A. Merkel, "Diagnostic imaging in Takayasu arteritis," *Current Opinion in Rheumatology*, vol. 16, no. 1, pp. 31–37, 2004.

[18] M. B. Gravanis, "Giant cell arteritis and Takayasu aortitis: morphologic, pathogenetic and etiologic factors," *International Journal of Cardiology*, vol. 75, supplement 1, pp. S21–S33, 2000.

[19] S. Unizony, L. Arias-Urdaneta, E. Miloslavsky et al., "Tocilizumab for the treatment of large-vessel vasculitis (giant cell arteritis, Takayasu arteritis) and polymyalgia rheumatica," *Arthritis Care and Research*, vol. 64, no. 11, pp. 1720–1729, 2012.

[20] K. Maksimowicz-Mckinnon, T. M. Clark, and G. S. Hoffman, "Takayasu arteritis and giant cell arteritis: a spectrum within the same disease?" *Medicine*, vol. 88, no. 4, pp. 221–226, 2009.

[21] P. C. Grayson, K. Maksimowicz-McKinnon, T. M. Clark et al., "Distribution of arterial lesions in Takayasu's arteritis and giant cell arteritis," *Annals of the Rheumatic Diseases*, vol. 71, no. 8, pp. 1329–1334, 2012.

[22] P. Seo and J. H. Stone, "Large-vessel vasculitis," *Arthritis Care and Research*, vol. 51, no. 1, pp. 128–139, 2004.

[23] S. S. Hayreh, P. A. Podhajsky, R. Raman, and B. Zimmerman, "Giant cell arteritis: validity and reliability of various diagnostic criteria," *The American Journal of Ophthalmology*, vol. 123, no. 3, pp. 285–296, 1997.

[24] A. Brack, V. Martinez-Taboada, A. Stanson, J. J. Goronzy, and C. M. Weyand, "Disease pattern in cranial and large-vessel giant cell arteritis," *Arthritis & Rheumatology*, vol. 42, no. 2, pp. 311–317, 1999.

[25] H. Balink, R. J. Bennink, N. J. Veeger, B. L. van Eck-Smit, and H. J. Verberne, "Diagnostic utility of 18F-FDG PET/CT in inflammation of unknown origin," *Clinical Nuclear Medicine*, vol. 39, no. 5, pp. 419–425, 2014.

[26] C. Salvarani, F. Cantini, and G. G. Hunder, "Polymyalgia rheumatica and giant-cell arteritis," *The Lancet*, vol. 372, no. 9634, pp. 234–245, 2008.

[27] J. M. Evans, W. M. O'Fallon, and G. G. Hunder, "Increased incidence of aortic aneurysm and dissection in giant cell (temporal) arteritis: a population-based study," *Annals of Internal Medicine*, vol. 122, no. 7, pp. 502–507, 1995.

[28] B. Hamrin, N. Jonsson, and S. Hellsten, ""Polymyalgia arteritica". Further clinical and histopathological studies with a report of six autopsy cases," *Annals of the Rheumatic Diseases*, vol. 27, no. 5, pp. 397–405, 1968.

[29] G. Ostberg, "On arteritis with special reference to polymyalgia arteritica," *Acta Pathologica et Microbiologica Scandinavica, Supplement*, vol. 237, pp. 1–59, 1973.

[30] F. Rojo-Leyva, N. B. Ratliff, D. M. Cosgrove, and G. S. Hoffman III, "Study of 52 patients with idiopathic aortitis from a cohort of 1,204 surgical cases," *Arthritis & Rheumatology*, vol. 43, no. 4, pp. 901–907, 2000.

[31] J. T. Lie, "Aortic and extracranial large vessel giant cell arteritis: a review of 72 cases with histopathologic documentation," *Seminars in Arthritis and Rheumatism*, vol. 24, no. 6, pp. 422–431, 1995.

[32] T. Quéméneur, É. Hachulla, M. Lambert et al., "Takayasu arteritis," *Presse Medicale*, vol. 35, no. 5, pp. 847–856, 2006.

[33] F. A. Weaver, S. R. Kumar, A. E. Yellin et al., "Renal revascularization in Takayasu arteritis-induced renal artery stenosis," *Journal of Vascular Surgery*, vol. 39, no. 4, pp. 749–757, 2004.

[34] A. L. Bartels, C. J. Zeebregts, M. Bijl, R. A. Tio, and R. H. J. A. Slart, "Fused FDG-PET and MRI imaging of Takayasu arteritis in vertebral arteries," *Annals of Nuclear Medicine*, vol. 23, no. 8, pp. 753–756, 2009.

[35] A. M. Goedhart-de Haan, S. J. Pans, K. D. Lensen, M. R. Meijerink, E. F. Comans, and Y. M. Smulders, "Vasculitis revealed by posterior stroke," *Netherlands Journal of Medicine*, vol. 70, no. 2, pp. 81–83, 2012.

[36] B. Kaku, T. Higuchi, H. Kanaya et al., "Usefulness of flourine-18-flourodeoxyglucose positron emission tomography in a patient with Takayasu's arteritis associated with antiphospholipid syndrome," *International Heart Journal*, vol. 47, no. 2, pp. 311–317, 2006.

[37] K. Miyagawa, J. Shiraishi, M. Nasu et al., "Usefulness of ultrasonography in carotid arteries and combined positron emission tomography/computed tomography for diagnosis of Takayasu arteritis with unusual presentation as acute myocardial infarction: a case report," *Journal of Cardiology*, vol. 50, no. 5, pp. 317–324, 2007.

[38] A. N. Ezeonyeji, F. A. Borg, and B. Dasgupta, "Delays in recognition and management of giant cell arteritis: results from a retrospective audit," *Clinical Rheumatology*, vol. 30, no. 2, pp. 259–262, 2011.

[39] C. Mukhtyar, L. Guillevin, M. C. Cid et al., "EULAR recommendations for the management of large vessel vasculitis," *Annals of the Rheumatic Diseases*, vol. 68, no. 3, pp. 318–323, 2009.

[40] B. Dasgupta, "Concise guidance: diagnosis and management of giant cell arteritis," *Clinical Medicine*, vol. 10, no. 4, pp. 381–386, 2010.

[41] K. Hamano, T. S. Li, M. Takahashi et al., "Enhanced tumor necrosis factor-α expression in small sized abdominal aortic aneurysms," *World Journal of Surgery*, vol. 27, no. 4, pp. 476–480, 2003.

[42] M. Schirmer, C. Duftner, R. Seiler, C. Dejaco, and G. Fraedrich, "Abdominal aortic aneurysms: an underestimated type of immune-mediated large vessel arteritis?" *Current Opinion in Rheumatology*, vol. 18, no. 1, pp. 48–53, 2006.

[43] D. M. Nuenninghoff, G. G. Hunder, T. J. H. Christianson, R. L. McClelland, and E. L. Matteson, "Incidence and predictors of large-artery complication (aortic aneurysm, aortic dissection, and/or large-artery stenosis) in patients with giant cell arteritis: a population-based study over 50 years," *Arthritis and Rheumatism*, vol. 48, no. 12, pp. 3522–3531, 2003.

[44] T. Belhocine, D. Blockmans, R. Hustinx, J. Vandevivere, and L. Mortelmans, "Imaging of large vessel vasculitis with 18FDG PET: illusion or reality? A critical review of the literature data," *European Journal of Nuclear Medicine and Molecular Imaging*, vol. 30, no. 9, pp. 1305–1313, 2003.

[45] B. E. Schreiber, H. H. C. Tam, C. Carvalho, W. L. Wong, A. I. Russell, and C. S. Higgens, "F-18 PET-CT showing large vessel vasculitis in a patient with high inflammatory markers and no localizing symptoms," *Clinical Nuclear Medicine*, vol. 34, no. 11, pp. 785–787, 2009.

[46] K. D. F. Lensen, A. E. Voskuyl, C. J. van der Laken et al., "18F-Fluorodeoxyglucose positron emission tomography in elderly patients with an elevated erythrocyte sedimentation rate of unknown origin," *PLoS ONE*, vol. 8, no. 3, Article ID e58917, 2013.

[47] S. Vanderschueren, E. Del Biondo, D. Ruttens, I. van Boxelaer, E. Wauters, and D. D. C. Knockaert, "Inflammation of unknown origin versus fever of unknown origin: two of a kind," *European Journal of Internal Medicine*, vol. 20, no. 4, pp. 415–418, 2009.

[48] H. Balink, J. Collins, G. A. Bruyn, and F. Gemmel, "F-18 FDG PET/CT in the diagnosis of fever of unknown origin," *Clinical Nuclear Medicine*, vol. 34, no. 12, pp. 862–868, 2009.

[49] G. A. Hooisma, H. Balink, P. M. Houtman, R. H. J. A. Slart, and K. D. F. Lensen, "Parameters related to a positive test result for FDG PET(/CT) for large vessel vasculitis: a multicenter retrospective study," *Clinical Rheumatology*, vol. 31, no. 5, pp. 861–871, 2012.

[50] J. F. Sheng, Z. K. Sheng, X. M. Shen et al., "Diagnostic value of fluorine-18 fluorodeoxyglucose positron emission tomography/computed tomography in patients with fever of unknown origin," *European Journal of Internal Medicine*, vol. 22, no. 1, pp. 112–116, 2011.

[51] J. Ferda, E. Ferdová, J. Záhlava, M. Matějovič, and B. Kreuzberg, "Fever of unknown origin: a value of ^{18}F-FDG-PET/CT with integrated full diagnostic isotropic CT imaging," *European Journal of Radiology*, vol. 73, no. 3, pp. 518–525, 2010.

[52] Z. Keidar, A. Gurman-Balbir, D. Gaitini, and O. Israel, "Fever of unknown origin: the role of ^{18}F-FDG PET/CT," *Journal of Nuclear Medicine*, vol. 49, no. 12, pp. 1980–1985, 2008.

[53] M. A. Walter, R. A. Melzer, C. Schindler, J. Müller-Brand, A. Tyndall, and E. U. Nitzsche, "The value of [18F]FDG-PET in the diagnosis of large-vessel vasculitis and the assessment of activity and extent of disease," *European Journal of Nuclear Medicine and Molecular Imaging*, vol. 32, no. 6, pp. 674–681, 2005.

[54] K. Lee, A. Cho, Y. Choi et al., "The role of 18F-fluorodeoxyglucose-positron emission tomography in the assessment of disease activity in patients with takayasu arteritis," *Arthritis and Rheumatism*, vol. 64, no. 3, pp. 866–875, 2012.

[55] M. Fuchs, M. Briel, T. Daikeler et al., "The impact of 18F-FDG PET on the management of patients with suspected large vessel vasculitis," *European Journal of Nuclear Medicine and Molecular Imaging*, vol. 39, no. 2, pp. 344–353, 2012.

[56] H. Hautzel, O. Sander, A. Heinzel, M. Schneider, and H. W. Müller, "Assessment of large-vessel involvement in giant cell arteritis with 18F-FDG PET: introducing an ROC-analysis-based cutoff ratio," *Journal of Nuclear Medicine*, vol. 49, no. 7, pp. 1107–1113, 2008.

[57] M. Bruschi, F. de Leonardis, M. Govoni et al., "18FDG-PET and large vessel vasculitis: preliminary data on 25 patients," *Reumatismo*, vol. 60, no. 3, pp. 212–216, 2008.

[58] L. Arnaud, J. Haroche, Z. Malek et al., "Is 18F-fluorodeoxyglucose positron emission tomography scanning a reliable way to assess disease activity in Takayasu arteritis?" *Arthritis and Rheumatism*, vol. 60, no. 4, pp. 1193–1200, 2009.

[59] D. Blockmans, W. Coudyzer, S. Vanderschueren et al., "Relationship between fluorodeoxyglucose uptake in the large vessels and late aortic diameter in giant cell arteritis," *Rheumatology*, vol. 47, no. 8, pp. 1179–1184, 2008.

[60] G. Treglia, M. V. Mattoli, L. Leccisotti, G. Ferraccioli, and A. Giordano, "Usefulness of whole-body fluorine-18-fluorodeoxyglucose positron emission tomography in patients with large-vessel vasculitis: a systematic review," *Clinical Rheumatology*, vol. 30, no. 10, pp. 1265–1275, 2011.

[61] P. Lehmann, S. Buchtala, N. Achajew et al., "18F-FDG PET as a diagnostic procedure in large vessel vasculitis—a controlled, blinded re-examination of routine PET scans," *Clinical Rheumatology*, vol. 30, no. 1, pp. 37–42, 2011.

[62] H. Balink and G. A. W. Bruyn, "The role of PET/CT in Cogan's syndrome," *Clinical Rheumatology*, vol. 26, no. 12, pp. 2177–2179, 2007.

[63] J. Andrews and J. C. Mason, "Takayasu's arteritis—recent advances in imaging offer promise," *Rheumatology*, vol. 46, no. 1, pp. 6–15, 2007.

[64] K. Ahmadi-Simab, B. Hellmich, K. Holl-Ulrich, C. Fleischmann, O. Dourvos, and W. L. Gross, "Acute coronary syndrome in Takayasu arteritis without elevation of acute phase parameters," *Rheumatology*, vol. 46, no. 3, pp. 554–555, 2007.

[65] A. Toriihara, Y. Seto, K. Yoshida et al., "F-18 FDG PET/CT of polymyalgia rheumatica," *Clinical Nuclear Medicine*, vol. 34, no. 5, pp. 305–306, 2009.

[66] H. Adams, P. Raijmakers, and Y. Smulders, "Polymyalgia rheumatica and interspinous FDG uptake on PET/CT," *Clinical Nuclear Medicine*, vol. 37, no. 5, pp. 502–505, 2012.

[67] C. Salvarani, L. Barozzi, F. Cantini et al., "Cervical interspinous bursitis in active polymyalgia rheumatica," *Annals of the Rheumatic Diseases*, vol. 67, no. 6, pp. 758–761, 2008.

[68] Y. Taniguchi, K. Arii, Y. Kumon et al., "Positron emission tomography/computed tomography: a clinical tool for evaluation of enthesitis in patients with spondyloarthritides," *Rheumatology*, vol. 49, no. 2, pp. 348–354, 2009.

[69] Z. Rehak and P. Szturz, "Comment on: FDG PET in the early diagnosis of large-vessel vasculitis," *European Journal of Nuclear Medicine and Molecular Imaging*, vol. 41, no. 3, pp. 579–580, 2014.

[70] F. Moosig, N. Czech, C. Mehl et al., "Correlation between 18-fluorodeoxyglucose accumulation in large vessels and serological markers of inflammation in polymyalgia rheumatica: a quantitative PET study," *Annals of the Rheumatic Diseases*, vol. 63, no. 7, pp. 870–873, 2004.

[71] M. Brodmann, R. W. Lipp, A. Passath, G. Seinost, E. Pabst, and E. Pilger, "The role of 2-18F-fluoro-2-deoxy-D-glucose positron emission tomography in the diagnosis of giant cell arteritis of the temporal arteries," *Rheumatology*, vol. 43, no. 2, pp. 241–242, 2004.

[72] K. Samejima, K. Nakatani, M. Sioyama et al., "Case of temporal arteritis: FDP-PET (18F-fluorodeoxyglucose- positron emission tomography) was useful for early diagnosis and treatment," *Nihon Rinsho Meneki Gakkai Kaishi*, vol. 33, no. 6, pp. 324–328, 2010.

[73] S. P. Janssen, E. H. Comans, A. E. Voskuyl, W. Wisselink, and Y. M. Smulders, "Giant cell arteritis: heterogeneity in clinical presentation and imaging results," *Journal of Vascular Surgery*, vol. 48, no. 4, pp. 1025–1031, 2008.

[74] M. Yun, S. Jang, A. Cucchiara, A. B. Newberg, and A. Alavi, "18F FDG uptake in the large arteries: a correlation study with the atherogenic risk factors," *Seminars in Nuclear Medicine*, vol. 32, no. 1, pp. 70–76, 2002.

[75] T. Belhocine, D. Blockmans, R. Hustinx, J. Vandevivere, and L. Mortelmans, "Imaging of large vessel vasculitis with (18)FDG PET: illusion or reality? A critical review of the literature data," *European Journal of Nuclear Medicine and Molecular Imaging*, vol. 30, no. 9, pp. 1305–1313, 2003.

[76] H. Balink, P. M. Houtman, and J. Collins, "18F-FDG PET versus PET/CT as a diagnostic procedure for clinical suspicion of large vessel vasculitis," *Clinical Rheumatology*, vol. 30, no. 8, pp. 1139–1141, 2011.

[77] M. P. Dunphy, A. Freiman, S. M. Larson, and H. W. Strauss, "Association of vascular 18F-FDG uptake with vascular calcification," *Journal of Nuclear Medicine*, vol. 46, no. 8, pp. 1278–1284, 2005.

[78] T. J. Reape and P. H. E. Groot, "Chemokines and atherosclerosis," *Atherosclerosis*, vol. 147, no. 2, pp. 213–225, 1999.

[79] J. N. Wilcox and N. A. Scott, "Potential role of the adventitia in arteritis and atherosclerosis," *International Journal of Cardiology*, vol. 54, pp. S21–S35, 1996.

[80] F. Numano, Y. Kishi, A. Tanaka, M. Ohkawara, T. Kakuta, and Y. Kobayashi, "Inflammation and atherosclerosis: atherosclerotic lesions in Takayasu arteritis," *Annals of the New York Academy of Sciences*, vol. 902, pp. 65–76, 2000.

[81] N. Tahara, H. Kai, S. Yamagishi et al., "Vascular inflammation evaluated by [18F]-fluorodeoxyglucose positron emission tomography is associated with the metabolic syndrome," *Journal of the American College of Cardiology*, vol. 49, no. 14, pp. 1533–1539, 2007.

[82] A. P. Burke and R. Virmani, "Localized vasculitis," *Seminars in Diagnostic Pathology*, vol. 18, no. 1, pp. 59–66, 2001.

[83] S. H. Morgan, R. A. Asherson, and G. R. V. Hughes, "Distal aortitis complicating Reiter's syndrome," *British Heart Journal*, vol. 52, no. 1, pp. 115–116, 1984.

[84] V. Weiler, S. Redtenbacher, C. Bancher, M. B. Fischer, and J. S. Smolen, "Concurrence of sarcoidosis and aortitis: case report and review of the literature," *Annals of the Rheumatic Diseases*, vol. 59, no. 11, pp. 850–853, 2000.

[85] B. F. Haynes, M. I. Kaiser-Kupfer, P. Mason, and A. S. Fauci, "Cogan syndrome: studies in thirteen patients, long-term follow-up, and a review of the literature," *Medicine*, vol. 59, no. 6, pp. 426–441, 1980.

[86] H. Balink, A. Spoorenberg, P. M. Houtman, A. Brandenburg, and H. J. Verberne, "Early recognition of aortitis of the aorta ascendens with ^{18}F-FDG PET/CT: syphilitic?" *Clinical Rheumatology*, vol. 32, no. 5, pp. 705–709, 2013.

[87] K. Kösters, C. P. Bleeker-Rovers, R. van Crevel, W. J. G. Oyen, and A. J. A. M. van der Ven, "Aortitis diagnosed by F-18-fluorodeoxyglucose positron emission tomography in a patient with syphilis and HIV coinfection," *Infection*, vol. 33, no. 5-6, pp. 387–389, 2005.

[88] G. Treglia, S. Taralli, F. Maggi, A. Coli, L. Lauriola, and A. Giordano, "Usefulness of 18F-FDG PET/CT in disease extent and treatment response assessment in a patient with syphilitic aortitis," *Clinical Nuclear Medicine*, vol. 38, no. 4, pp. e185–e187, 2013.

[89] M. Kuwana, S. Wakino, T. Yoshida, and M. Homma, "Concise communication: retroperitoneal fibrosis associated with aortitis," *Arthritis and Rheumatism*, vol. 35, no. 10, pp. 1245–1247, 1992.

[90] D. Blockmans, T. Bley, and W. Schmidt, "Imaging for large-vessel vasculitis," *Current Opinion in Rheumatology*, vol. 21, no. 1, pp. 19–28, 2009.

[91] S. Förster, F. Tato, M. Weiss et al., "Patterns of extracranial involvement in newly diagnosed giant cell arteritis assessed by physical examination, colour coded duplex sonography and FDG-PET," *Vasa*, vol. 40, no. 3, pp. 219–227, 2011.

[92] M. Both, K. Ahmadi-Simab, M. Reuter et al., "MRI and FDG-PET in the assessment of inflammatory aortic arch syndrome in complicated courses of giant cell arteritis," *Annals of the Rheumatic Diseases*, vol. 67, no. 7, pp. 1030–1033, 2008.

[93] N. Pipitone, A. Versari, and C. Salvarani, "Role of imaging studies in the diagnosis and follow-up of large-vessel vasculitis: an update," *Rheumatology*, vol. 47, no. 4, pp. 403–408, 2008.

[94] F. Tatò and U. Hoffmann, "Giant cell arteritis: a systemic vascular disease," *Vascular Medicine*, vol. 13, no. 2, pp. 127–140, 2008.

[95] J. Meller, F. Strutz, U. Siefker et al., "Early diagnosis and follow-up of aortitis with [18F]FDG PET and MRI," *European Journal of Nuclear Medicine and Molecular Imaging*, vol. 30, no. 5, pp. 730–736, 2003.

[96] A. Clifford, S. Burrell, and J. G. Hanly, "Positron emission tomography/computed tomography for the diagnosis and assessment of giant cell arteritis: when to consider it and why," *Journal of Rheumatology*, vol. 39, no. 10, pp. 1909–1911, 2012.

[97] G. Tegler, K. Ericson, J. Sörensen, M. Björck, and A. Wanhainen, "Inflammation in the walls of asymptomatic abdominal aortic aneurysms is not associated with increased metabolic activity detectable by 18-fluorodeoxglucose positron-emission tomography," *Journal of Vascular Surgery*, vol. 56, no. 3, pp. 802–807, 2012.

[98] F. L. Besson, J. Parienti, B. Bienvenu et al., "Diagnostic performance of 18F-fluorodeoxyglucose positron emission tomography in giant cell arteritis: a systematic review and meta-analysis," *European Journal of Nuclear Medicine and Molecular Imaging*, vol. 38, no. 9, pp. 1764–1772, 2011.

[99] R. A. Luqmani, "Treat-to-target in vasculitis: Is this a sensible approach?" *Clinical and Experimental Rheumatology*, vol. 30, supplement 73, no. 4, pp. S149–S153, 2012.

[100] D. Blockmans, L. de Ceuninck, S. Vanderschueren, D. Knockaert, L. Mortelmans, and H. Bobbaers, "Repetitive 18-fluorodeoxyglucose positron emission tomography in isolated polymyalgia rheumatica: a prospective study in 35 patients," *Rheumatology*, vol. 46, no. 4, pp. 672–677, 2007.

[101] M. Iwabu, Y. Yamamoto, H. Dobashi, T. Kameda, K. Kittaka, and Y. Nishiyama, "F-18 FDG PET findings of takayasu arteritis before and after immunosuppressive therapy," *Clinical Nuclear Medicine*, vol. 33, no. 12, pp. 872–873, 2008.

[102] H. Otsuka, N. Morita, K. Yamashita, and H. Nishitani, "FDG-PET/CT for diagnosis and follow-up of vasculitis," *The Journal of Medical Investigation*, vol. 54, no. 3-4, pp. 345–349, 2007.

[103] A. Daumas, P. Rossi, F. Bernard-Guervilly et al., "Clinical, laboratory, radiological features, and outcome in 26 patients with aortic involvement amongst a case series of 63 patients with giant cell arteritis," *Revue de Medecine Interne*, vol. 35, no. 1, pp. 4–15, 2014.

[104] K. Raza, D. Karokis, and G. D. Kitas, "Cogan's syndrome with Takayasu's arteritis," *British Journal of Rheumatology*, vol. 37, no. 4, pp. 369–372, 1998.

[105] A. C. Ho, M. I. Roat, A. Venbrux, and D. B. Hellmann, "Cogan's syndrome with refractory abdominal aortitis and mesenteric vasculitis," *Journal of Rheumatology*, vol. 26, no. 6, pp. 1404–1407, 1999.

[106] M. Covelli, G. Lapadula, and V. Pipitone, "Cogan's syndrome: unsuccessful outcome with early combination therapy," *Clinical and Experimental Rheumatology*, vol. 17, no. 4, pp. 479–483, 1999.

[107] J. K. Rao, N. B. Allen, and T. Pincus, "Limitations of the 1990 American College of Rheumatology classification criteria in the diagnosis of vasculitis," *Annals of Internal Medicine*, vol. 129, no. 5, pp. 345–352, 1998.

[108] I. Zerizer, K. Tan, S. Khan et al., "Role of FDG-PET and PET/CT in the diagnosis and management of vasculitis," *European Journal of Radiology*, vol. 73, no. 3, pp. 504–509, 2010.

[109] H. Balink, P. M. Houtman, and H. J. Verberne, "Reassessing classification criteria for Takayasu arteritis: comment on the article by Lee et al," *Arthritis and Rheumatism*, vol. 64, no. 11, pp. 3818–3819, 2012.

[110] Q. Liu, Z. Chang, and M. Qin, "Diagnosis of a 65-year-old male patient with Takayasu's arteritis by 18F-FDG PET/CT," *Rheumatology International*, vol. 31, no. 3, pp. 391–394, 2011.

[111] D. Blockmans, T. Bley, and W. Schmidt, "Imaging for large-vessel vasculitis," *Current Opinion in Rheumatology*, vol. 21, no. 1, pp. 19–28, 2009.